Seismological studies at the hengill geothermal area SW Iceland

Gillian Rose Foulger

ABSTRACT

Iceland is a sub-aerial part of the mid-Atlantic Ridge which has formed above an E migrating ridge centred hotspot. The Hengill area is a ridge-ridge-transform triple point that contains a central volcano-fissure swarm system and a large geothermal area. A seismological study of this triple point was conducted with the main emphasis on natural earthquake studies. The aims were to study the geothermal prospect and tectonic structure and to evaluate the passive seismic method as a geothermal prospecting tool.

The area exhibits continuous small magnitude earthquake activity that correlates positively with surface geothermal displays, and negatively with surface faulting. The log (cumulative frequency) : magnitude relationship is linear and indicates a b value of 0.74 ± 0.06. Focal mechanisms for 178 events indicated both shear and tensile crack type movements, the latter being confined to the high temperature geothermal area. Teleseismic and explosion data indicate a low velocity body beneath the central volcano in the depth range 0 - 10 km, flanked by higher velocity bodies to the W and E.

Two volcanic systems occupy the Hengill area : the presently active Hengill system and the extinct Grensdalur system. The ongoing seismicity of the area is attributed to contraction cracking due to the action of cool groundwater fluids on hot rock, which, in a tensile stress regime, results in tensile crack formation. The high temperature area is fuelled by two heat sources associated with the two volcanic systems and may be divided into two separate fields that exhibit

contrasting reservoir characteristics.

Local seismicity studies may be applied to other Icelandic high temperature geothermal areas as a tool to map those volumes of rock that are fueling the geothermal reservoirs. The continuous formation of small tensile cracks on accretionary plate boundaries offers an explanation for the mechanism of dyke injection.

SEISMOLOGICAL STUDIES AT THE HENGILL GEOTHERMAL AREA, SW ICELAND

by

Gillian Rose Foulger

a thesis submitted for the degree of
Doctor of Philosophy at the University of Durham

Department of Geological Sciences November 1984

To

D.J.D.

who put me back on my feet again.

Þá kom maðr laupandi, ok sagði at jarðeldr var upp kominn í Ölfusi, ok mundi hann laupa á bæ Þórodds goða. Þá tóku heðnir menn til orðs: "eigi er undr í at guðin reiðist tölum slíkum." Þá mælti Snorri goði: "Um hvat reiddust guðin, þá, er hér brann raunit, er nú stöndu vér á."

Kristnisaga

Þá tók Skaði eitrorm ok festi upp yfir Loka, svá at eitrit skyldi drjúpa ór orminum í andlit honum, en Sigyn, kona hans, stendr hjá honum ok heldr mundlaugu undir eitrdropa; en þá er full er mundlaugin, þá gengr hon ok slær út eitrinu, en meðan drýpr eitrit í andlit honum; þá kippisk hann svá hart við, at jörð öll skelfr - þat kallið þér landskjálpta - þar liggr hann í böndum til ragna-rökrs.

Snorra Edda

En hvatki er missagt er í fræðum þessum, þá er skylt at hafa þat heldr, er sannara reynist.

Íslendingabók

CONTENTS

LIST OF FIGURES

LIST OF TABLES

DECLARATION

I declare that this thesis, which I submit for the degree of Doctor of Philosophy at the University of Durham, is my own work and is not substantially the same as any which has previously been submitted for a degree at this or another university.

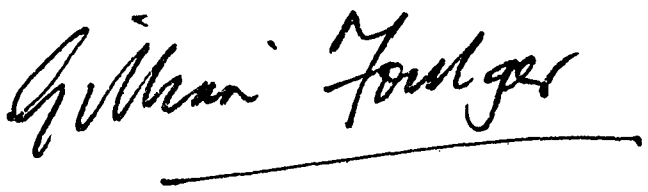

Gillian R. Foulger
University of Durham
November, 1984

CHAPTER 1

1. THE NORTH ATLANTIC AND ICELAND: STRUCTURE AND TECTONIC EVOLUTION

1.1 The North Atlantic: structure and kinematics

The initial opening of the N Atlantic dates from the early Tertiary (approx. -60Ma), and is intimately related to the activity of the Iceland hotspot. It has been proposed that this hotspot lay beneath central Greenland prior to the early Tertiary, but volcanism did not break surface because of the thick cratonic crust (Vogt, 1983). Volcanism became possible when the eastward migrating hotspot intersected a line of Mesozoic basins. Eruption of the west Greenland and British Tertiary/Rockall Plateau volcanics occurred simultaneously and the sum total of all these influences was sufficient to initiate plate separation. The synchronisation of these events may have been due to some mantle "event" of at least continental dimension, e.g. a convective overturn (Bott, 1973; Vogt, 1983). The N Atlantic has since opened and widened over the last 60Ma or so as a result of the crustal accretion process. That the history of this opening has been complex is reflected in the complex nature of the topography and ocean floor magnetic lineations (Fig. 1.1). A considerable amount has been published (data, interpretations and reviews) concerning the structure and tectonic evolution of the N Atlantic, including works of Bott (1973), Bott (1974), Featherstone et al. (1977), Bott and Gunnarsson (1980), Nunns (1983), Bott, (1983a, b) and Bott (1984).

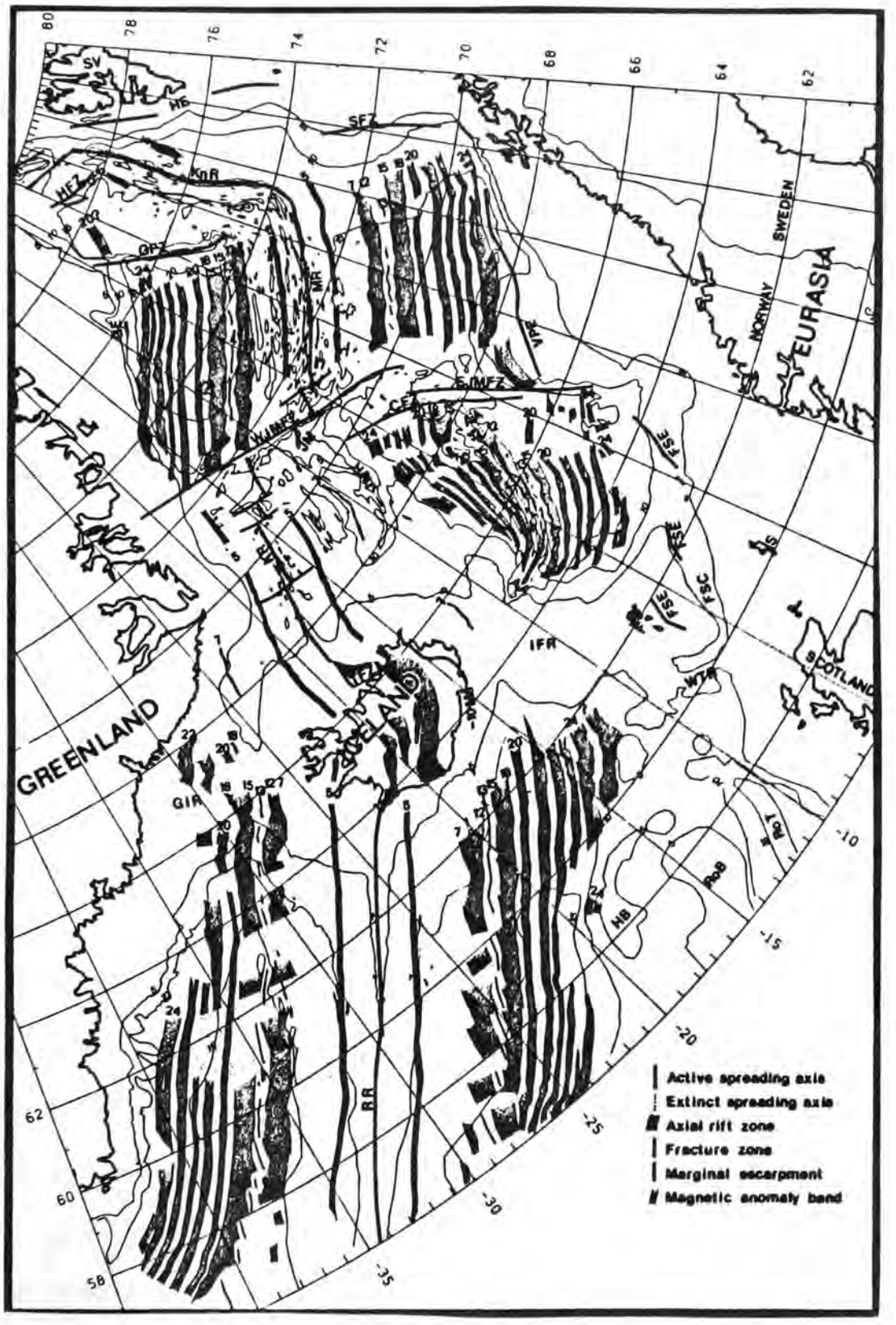

Fig. 1.1 Present configuration of Iceland and the N Atlantic area showing bathymetry, spreading axes, transform faults and magnetic anomalies. AA = Aegir Axis, RR = Reykjanes Ridge, JM = Jan Mayen, KR = Kolbeinsey Ridge. From Nunns, 1983

The summary presented below draws extensively upon these publications. It should be borne in mind, however, that the history of the N Atlantic in the Iceland region is that of a ridge-centred hotspot migrating eastwards with respect to the ridge at a rate of 1.65 cm a^{-1} (Vogt, 1983). The presence of the hotspot may thus not only affect the amount of volcanic activity, but also, locally, the position of the plate boundary. In addition the linear volcano-tectonic system associated with the spreading plate boundary of the N Atlantic is modified by the radial system associated with the hot spot resulting in a structure that varies in 3 dimensions (Bjornsson, 1984).

Plate tectonic reconstructions of the N Atlantic are critically dependent on the accepted nature of the crust beneath the Greenland-Scotland Ridge. Indeed the evolution of the N Atlantic is difficult to envisage unless it is accepted that the Greenland-Scotland Ridge is oceanic, formed by the crustal accretion process, contemporaneously with the ocean basins to its N and S.

The exceptional thickness of the crust (30-35 km) and lack of well developed magnetic lineations led Beloussov and Milanovsky (1977) to regard it as continental. However, drilling has revealed oceanic tholeiitic basalts, and long refraction profiles shot along the crest of the ridge reveal a velocity structure of oceanic type. The anomalous thickness of the crust was found to be due to an unusually thick layer 3, with normal oceanic upper mantle velocities detected below that. Additionally magnetic lineations that traverse the Greenland-Scotland Ridge, albeit poorly developed, have now been recognised. In the light of these data, an oceanic origin is

assumed for the Greenland-Scotland Ridge by Nunns (1983) whose plate tectonic reconstructions are summarised below.

From -56 to -44 Ma, spreading proceeded symmetrically about the Mid Atlantic Ridge, offset dextrally to the Norway basin by a major transform fault. N of this fault, spreading proceeded about the Aegir axis and S of it about the Reykjanes Ridge. From -44 to -26 Ma the Jan Mayen microcontinent broke off from Greenland, forming a ridge-ridge-transform triple junction on the Greenland-Scotland ridge. Spreading N of this triple junction proceeded along both the Aegir axis, and the new Kolbeinsey axis, resulting in the formation of complementary fan-shaped magnetic anomalies. The Greenland-Scotland Ridge developed continuously on the migrating plates as a result of enhanced volcanic activity in the neighbourhood of the hot spot. It probably formed subaerially during these first two periods with the Iceland insular platform beginning to form during the second. From -26 Ma to the present time the Aegir axis has been extinct, superseded by the Kolbeinsey Ridge. The spreading axis formed an eastward arc where it crossed the Greenland-Scotland Ridge in response to the E migrating hotspot. The Iceland insular platform built up over this arc and the present day surface tectonic features developed. The current spreading direction is about N 100° E in the Iceland region (Bjornsson, 1983).

1.2 Iceland: structure and dynamics

1.2.1 Geology

Comprehensive reviews of the geologic structure of Iceland are given by Saemundsson (1978, 1979). The exposed volcanic pile reveals vertical sections of up to 1500 m of extrusives, below which lie at least another 2-5 km if the top of seismic layer 3 is taken to be the base of the extrusives. A thickness of several kilometres for the extrusive lava pile has also been confirmed by mapping and drilling in E Iceland (Gibson et al., 1979; Walker, 1974). The exposed rocks range in age from ~16 Ma to present (Moorbath et al., 1968). They are conventionally divided into four stratigraphic series. These are:

Postglacial:	~10,000 a to present
Upper Pleistocene:	~0.7 Ma to ~10,000 a
Plio-Pleistocene:	~3.1 to ~0.7 Ma
Tertiary:	older than ~3.1 Ma

A regional geological map of Iceland is shown in Fig. 1.2 and the reader is referred to this figure for place names.

It can be seen that the geology of Iceland is dominated by the so-called Neovolcanic Zones that traverse the country from the Reykjanes Peninsula in the SW to Axarfjordur in the NE. These zones are defined by the extent of the upper Pleistocene and Postglacial rocks. They are flanked by Plio-Pleistocene rocks. Outside of these areas the E, N and W of Iceland and the NW Peninsula regions are capped by near horizontal Tertiary

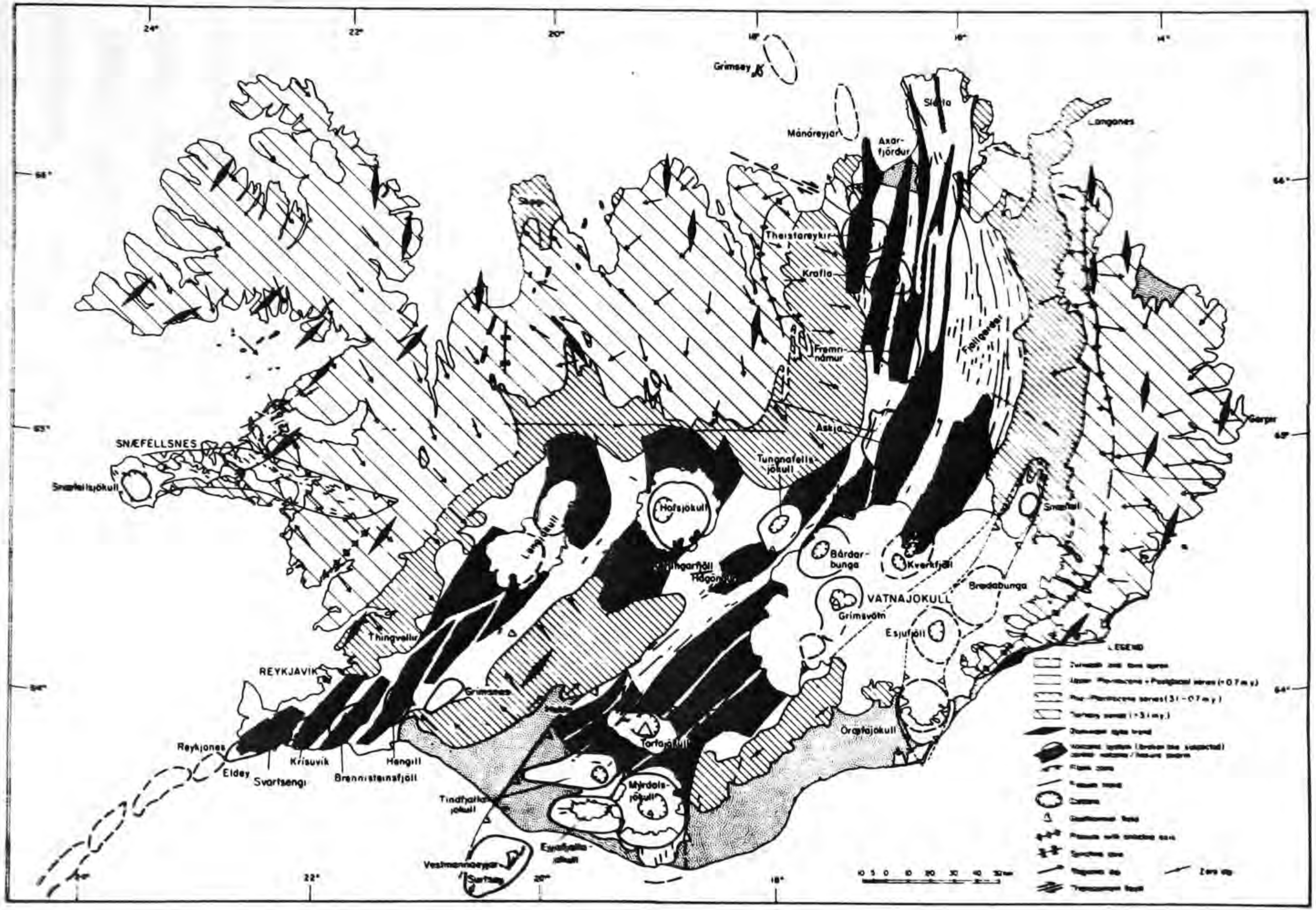

Fig. 1.2 Tectonic map of Iceland. (from Saemundsson, 1979).

lavas.

The structure of the Neovolcanic Zones is dominated by fissure swarms and central volcanoes. The trends of the fissure swarms tend to be uniform within each branch of the Neovolcanic Zone, but they are typically arranged in en echelon arrays which may be dextral or sinistral depending on the trend of the fissures relative to the direction of plate motion. They are typically about 10 km wide, and their length varies from 30 to 100 km. Most of them pass through central volcanoes about half of which exhibit calderas. These central volcanoes mark the sites of maximum lava production within the swarm and are also associated with subordinate acid and intermediate volcanism and high temperature geothermal fields. Hengill is such a central volcano, lacking a caldera. Tholeiitic basalt is erupted along the central part of the Neovolcanic Zones, with transitional to alkali basalts being erupted on their flanks where spreading is negligible (Jakobsson, 1972).

The Neovolcanic Zones are subdivided into axial zones and flank volcanic zones by Saemundsson (1978) on the basis of petrochemistry and tectonics. The axial zones are thought to mark the trace of the plate boundary where active accretion is taking place, and well developed tensional tectonics are observed. The flank volcanic zones are those seen to lie unconformably on older piles of volcanics, and display poorly developed tensional features.

Three flank volcanic zones are recognised. These are the Snaefellsnes, the Torfajokull-Vestmannaeyja and the Oraefajokull-Snaefell Zones. Their structure is dominated by large stratovolcanoes e.g. Snaefellsjokull, Hekla, Oraefa-

jokull. They are characterised by transitional to alkali lavas and exhibit poorly developed tensional features; fissures and graben structures are inconspicuous. The rate of volcanic production is very variable, and is not balanced by graben subsidence in associated fissure swarms. Extreme topography is therefore a feature of these zones. In the case of the Vestmannaeyja and the Oraefajokull-Snaefell Zones a regional thickening of layer 2 is found (Palmason, 1971) that compensates for the extra load.

Saemundsson (1978) considers the Reykjanes-Langjokull-Axafjordur zone to be the single continuous axial rift zone crossing Iceland. Intense fissure swarms and graben structures are commonly associated with central volcanoes and the depth to layer 3 is shallow - generally 2.5-4.5 km (Palmason, 1971; Flovenz, 1980). Tholeiitic basalts are erupted, and the volcanic production rate is highest in the centre of Iceland, which is also its topographic culmination. Towards the SW and NE, gradual lowering of the topography accompanies a decrease in the volcanic production rate and the disappearance of silicic volcanism and central volcanoes. In addition a geochemical trend was reported by Sigvaldason et al. (1974) with high K, P and Ti content of the post glacial basalts of central Iceland, progressively decreasing for 700 km along the plate boundary to the SW. They proposed that the Iceland hotspot is presently centred below Kverkfjoll.

Knowledge of the structure of the older parts of the lava pile comes mostly from the work of Walker in E Iceland (see Walker, 1974 for summary). The pile is mostly built up of tholeiitic lavas and small amounts of volcanic sediments. Some

stratigraphical units can be traced for many kilometers. Local concentrations of acid and intermediate rocks have been interpreted as fossil central volcanoes, and also associated with copious basaltic volcanism and dyke swarms that cut through the lava pile (Fig. 1.3). Dyke swarms have also been mapped that are not associated with central volcanoes. The dimensions of the dyke swarms are similar to those of the present day fissure swarms seen in the Neovolcanic Zone, and so it is considered likely that these are in fact the surface expression of dyke swarms in the upper crust that have been exposed by erosion in E Iceland. The strike of the dyke swarms changes from N-S in the northern part of the area to NE-SW in the south - a similar variation in trend exhibited by the E Neovolcanic Zone and the eastward arc of the accretion zone hypothesised by Bott (1984) to account for the shape of the E edge of the Icelandic insular shelf.

It has been shown that the regional dip of the lavas increases gradually from near zero in the highest exposed levels, to 5-10^{o} at sea level. Also the stratigraphic units thicken down dip. Saemundsson (1978) concluded that the lava pile has grown as lenticular units, each associated with a central volcano - fissure swarm system of limited life span that became extinct as it migrated away from the central axial zone. Downsagging is greatest in the centre of the accretion zone where the lava pile is thickest.

Bearing this principle in mind, another feature of the Tertiary lava shields may be used to infer the positions of extinct accretionary zones. A number of shallow synclines and low anticlines are observed. The synclines are interpreted as

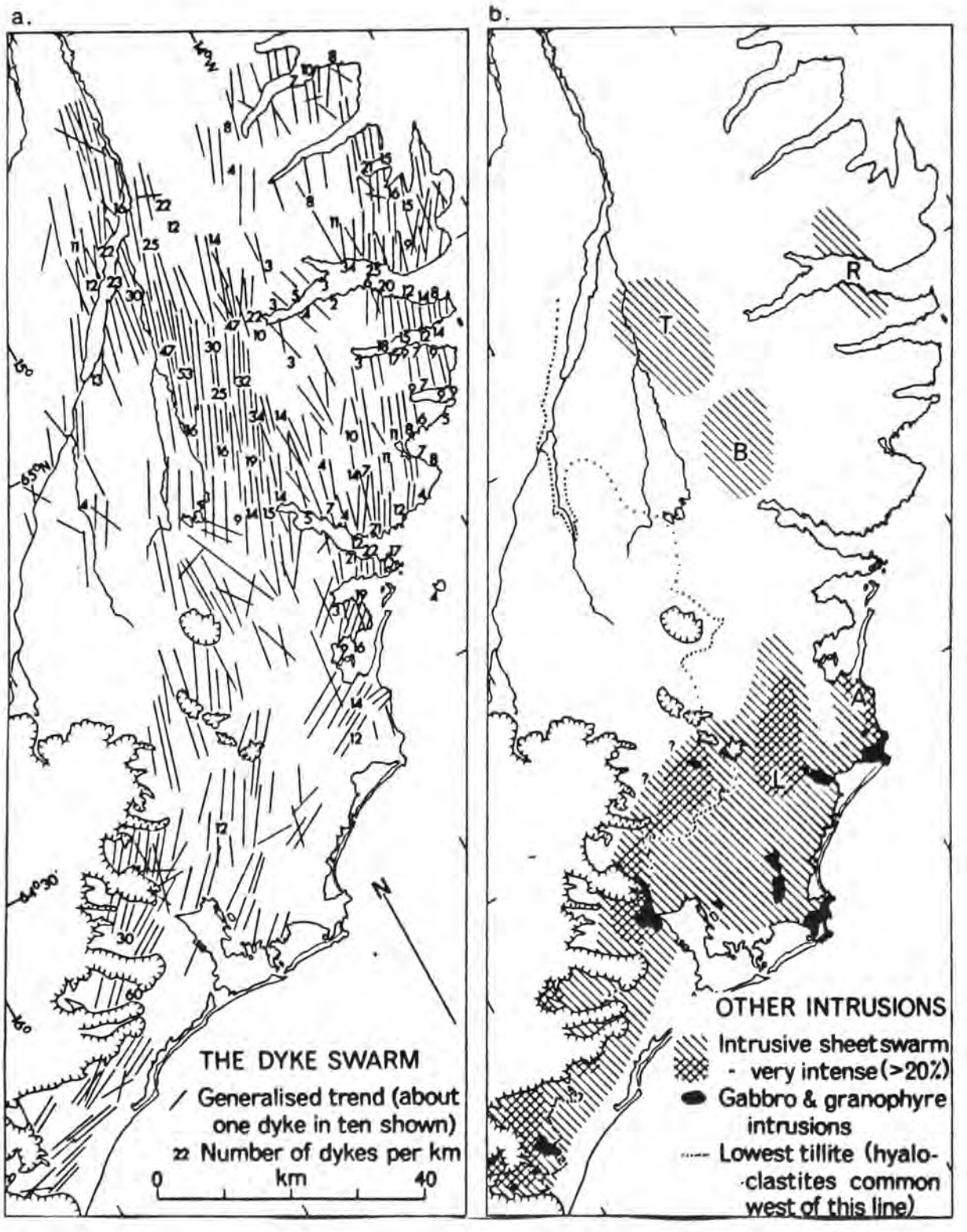

Fig. 1.3 The distribution of dykes and intrusive sheets in eastern Iceland; (b) also shows the known intrusions of gabbro and granophyre. (from Walker, 1974)

being caused by downsagging in the central part of an accretionary plate boundary, hence marking the positions of extinct accretionary zones. Two such extinct accretionary zones are indicated - one in the Snaefellsnes Zone and another in the Langjokull-Skagi zone. Both became extinct at -6 to -7 Ma at which time they were replaced by the presently active zones of Reykjanes-Langjokull and Kverkfjoll-Axafjordur (Saemundsson, 1974, 1978, 1979; Johannesson, 1980). Mean lava extrusion rates have been estimated for W and E Iceland and correspond to a vertical accumulation rate of 700 m/Ma.

1.2.2 The trace of the plate boundary

Magnetic anomalies can be traced clearly on the ocean floor to the N and S of Iceland (Talwani and Eldholm, 1977) but their continuation onto Iceland is problematical. Fig. 1.4 is a summary diagram of the present status of knowledge. With the exception of western anomaly 5, which is traced continuously across Iceland, the picture is clearly a complex one.

The Reykjanes Ridge comes onshore at Reykjanes in SW Iceland and from there the plate boundary is considered to follow the trace of the axial rift zone NE along the Hengill-Langjokull zone, WE along the Langjokull-Kverkfjoll zone and N to Axafjordur. Volcanism is not confined to these zones, however, (see above) and explanations of the nature of the plate boundary in Iceland must be able to account for this. Two major fracture zones are recognised. These are the South Iceland Seismic Zone (Fig. 1.5), that forms a continuation of the Reykjanes Peninsula zone east to connect it with the southern

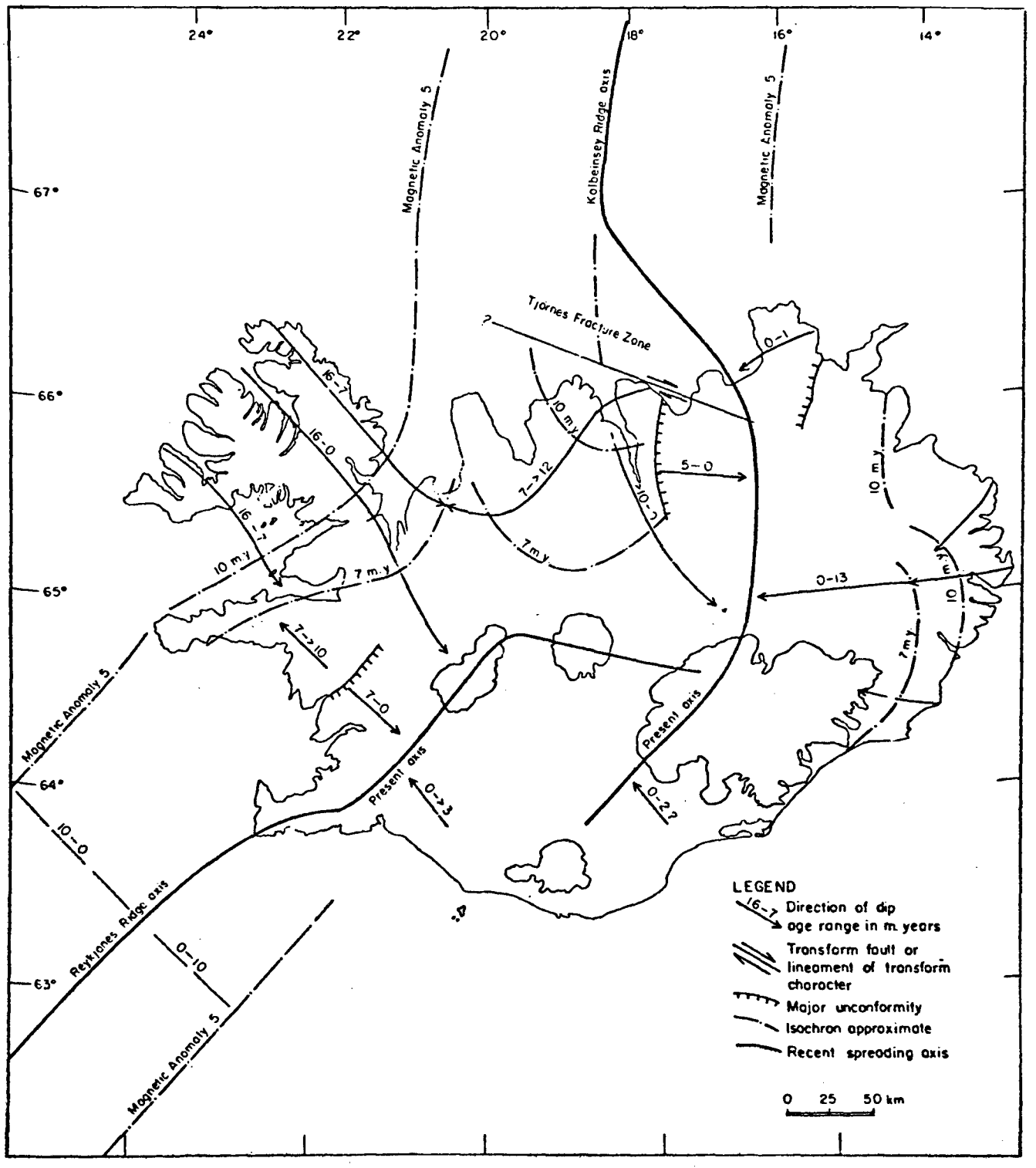

Fig. 1.4 Development of the present geometry of the tectonically active zones in Iceland. Magnetic anomalies and ridge axes are from Talwani and Eldholm (1977). Traces of extinct rift zones are left as structural synclines in the Tertiary areas. Major unconformities developed between sequences produced within extinct rift zones and those produced from the presently active ones. Note assymetric position of Reykjanes Ridge axis relative to anomaly 5. This is not necessarily due to asymmetric spreading but rather a result of eastward displacement of the ridge axis nearest to Iceland. This scheme should be regarded as preliminary since many more dating studies and stratigraphic mapping have to be done before the trace of isochrons on land can be plotted more accurately. (from Saemundsson, 1979)

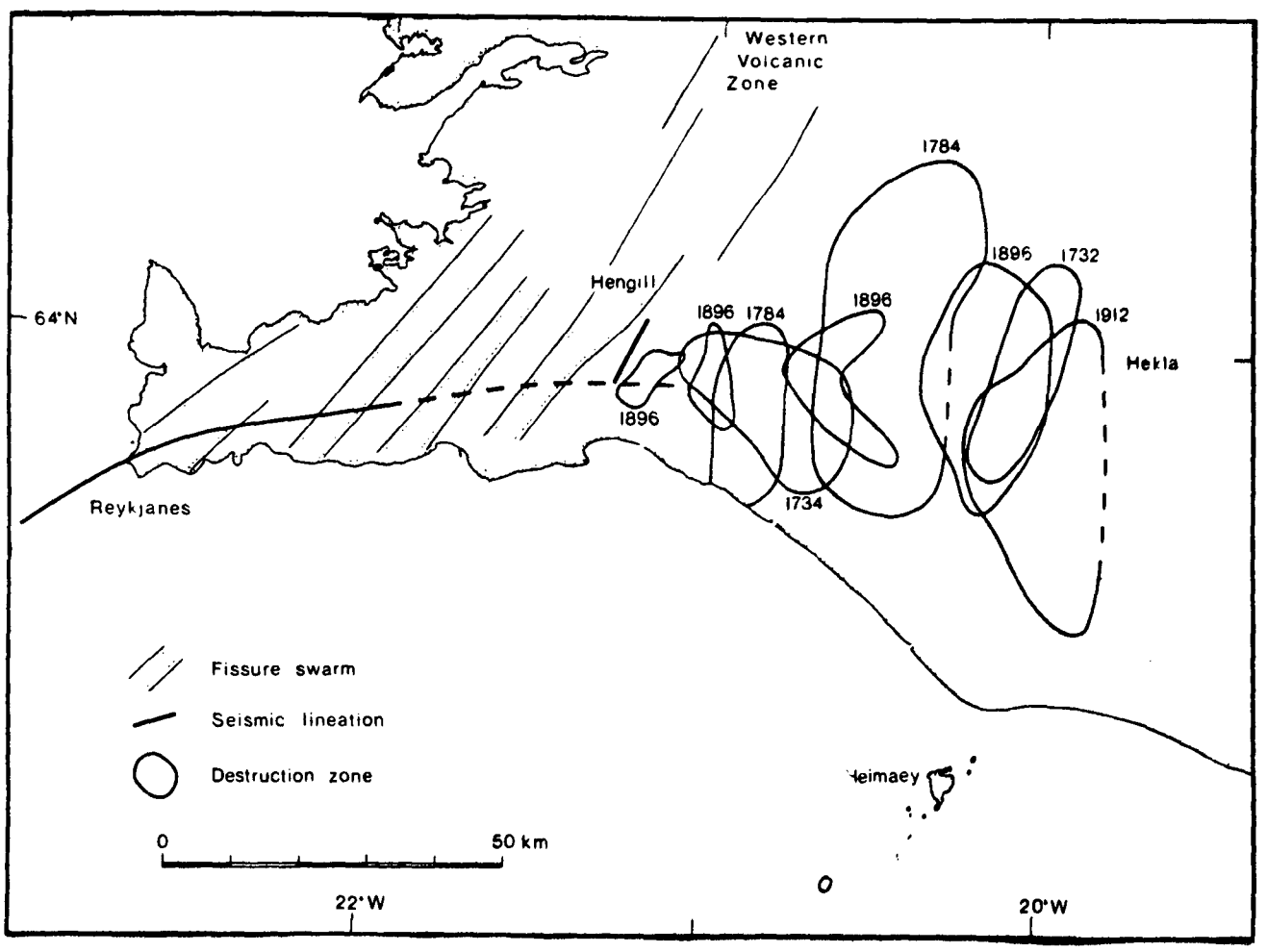

Fig. 1.5 Map of the seismic zones of SW-Iceland showing some of the tectonic features of the Reykjanes Peninsula and the South Iceland Seismic Zone. The seismic lineaments are taken from Klein et al. (1973 and 1977) and Foulger and Einarsson (1980). The destruction zones of the historic earthquakes of 1732-34, 1784, 1896 and 1912 are shown. Within these zones more than 50% of houses at each farm were ruined. Corresponding intensity is MM VIII-IX. (from Einarsson and Bjornsson, 1979)

part of the SE Neovolcanic Zone, and the Tjornes fracture zone (Fig. 1.4) that connects the NE Neovolcanic Zone to the Kolbeinsey Ridge.

The South Iceland Seismic Zone is defined by a belt of severe historical earthquakes (Fig. 1.5). The magnitude of these events may exceed 7 (Einarsson and Bjornsson, 1979). Surface breaks indicate right lateral movement on NS striking faults, which is also the direction of elongation of the destruction zones. The trend of the entire zone, however, and consideration of plate movement, would imply left lateral movement on one or more WE trending faults. It seems that seismic energy is released along planes conjugate to the main deformation zone. A single teleseismic focal mechanism solution is consistent with movement of either type.

Seismicity occurs more frequently in the Tjornes Fracture Zone (Fig. 1.6). Here transform motion is thought to be accommodated along two or more NW striking fault zones (Einarsson and Bjornsson, 1979). Topographically the Tjornes Fracture Zone exhibits a complicated structure of en echelon grabens and fissure swarms (Saemundsson, 1974). Teleseismic focal mechanism solutions are consistent with right lateral strike-slip movement on NW striking planes which is also consistent with inferred plate motions.

The seismicity of Iceland during the period 1962-77, depicted in Fig. 1.6, is generally confined to the Neovolcanic Zone and the two fracture zones described above.

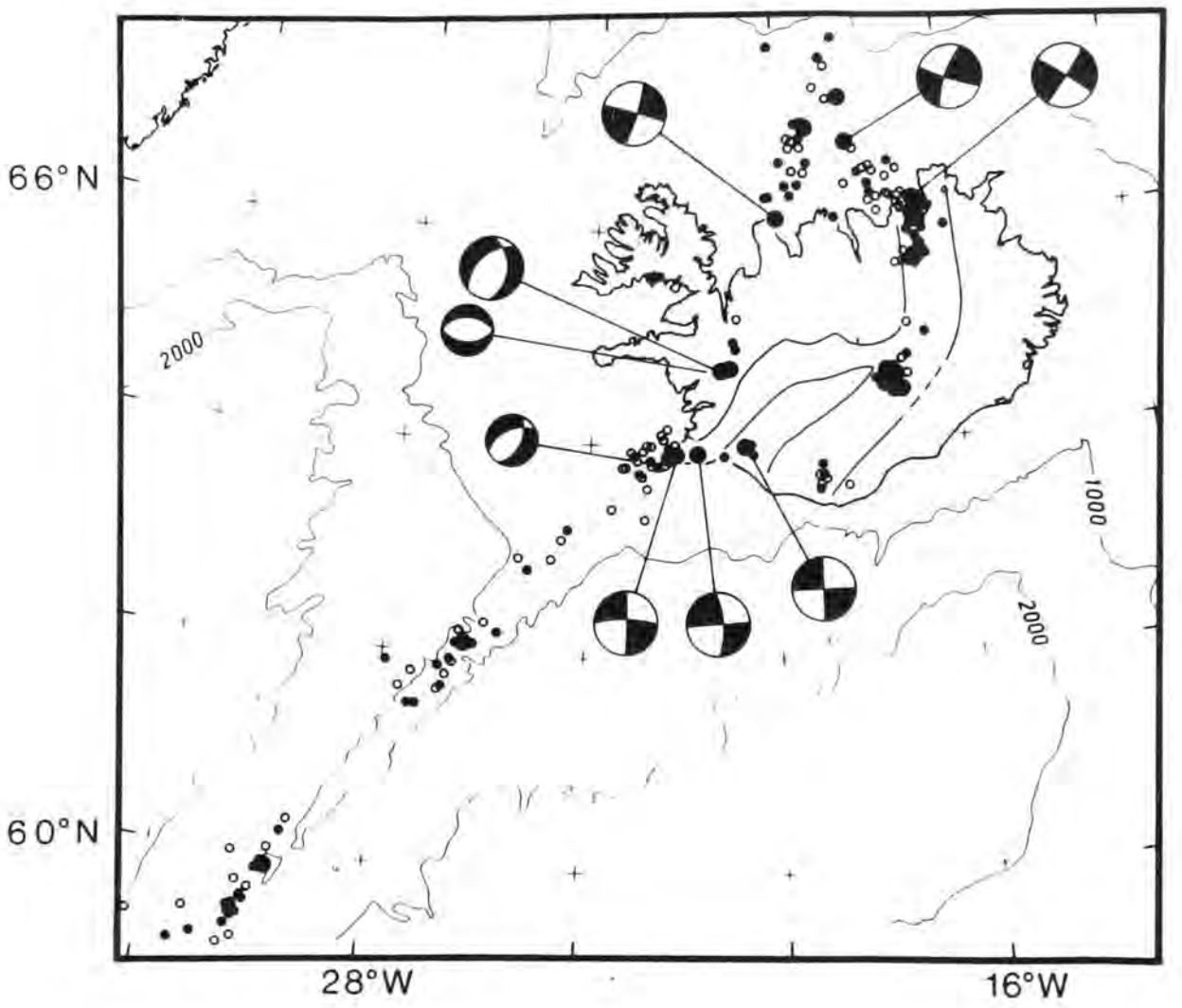

Fig. 1.6 Epicentres and focal mechanisms of earthquakes in Iceland and the northern part of the Reykjanes Ridge. Epicentres are taken from the PDE lists of USCGS, later NOAA and USGS, for the period 1962-1977. Open circles denote epicentres determined with fewer than ten P-wave readings or epicentres of earthquakes smaller than m_b =4.5. Dots are epicentres of events of m_b=4.5 and larger that are determined with ten or more readings. Large dots are epicentres of events of m_b = 5.0 and larger. The focal mechanisms are shown schematically as lower hemisphere equal area projections. The compressional quadrants (containing the least compressive stress axis) are shown black. The bathymetry is taken from a map by the Icelandic Hydrographic Service, Reykjavik, 1975. Depths are in meters. The volcanic rift zones of Iceland are shown. (from Einarsson and Bjornsson, 1979)

1.2.3 The dynamics of crustal accretion

A steady state plate tectonic kinematic model of crustal accretion in Iceland has been presented by Palmason (1973, 1980, 1981). Crustal accretion is considered to proceed both by dyke intrusion, concurrent with lateral movements of the plates, and lava extrusion, which results in loading of the crust and downwarping. Both of these processes are assumed to have a Gaussian distribution with distance from the plate boundary. The model describes the time averaged trajectories of solid crustal elements (Fig. 1.7) with respect to a steady-state crust. Accretion parameters such as width of the deposition zone, total lava production rate, horizontal crustal strain rate, spreading velocity and normal faulting can be calculated using structural properties measured in the Tertiary lava pile, such as the relative dyke volume fraction and the regional dip and deposition rate of lavas. Estimates of the width of ancient accretion zones, plate velocities and volcanic production rates using measurements made in the E and W Iceland Tertiary lava piles were found to be in good agreement with estimates of these parameters for the present day accretion zones. This indicates uniform intensity of volcanism over the last 10-15 Ma. The model also permits calculation of the thermal state of the crust, and isotherms are indicated in Fig. 1.7. It can be seen that some remelting of extruded materials is implied.

A study of the variation in regional heat flow rates is described by Palmason (1974). Thermal gradients are seen to be highest beneath the axial accretion zones, decreasing with increasing distance from the rift. The rate of falling off of

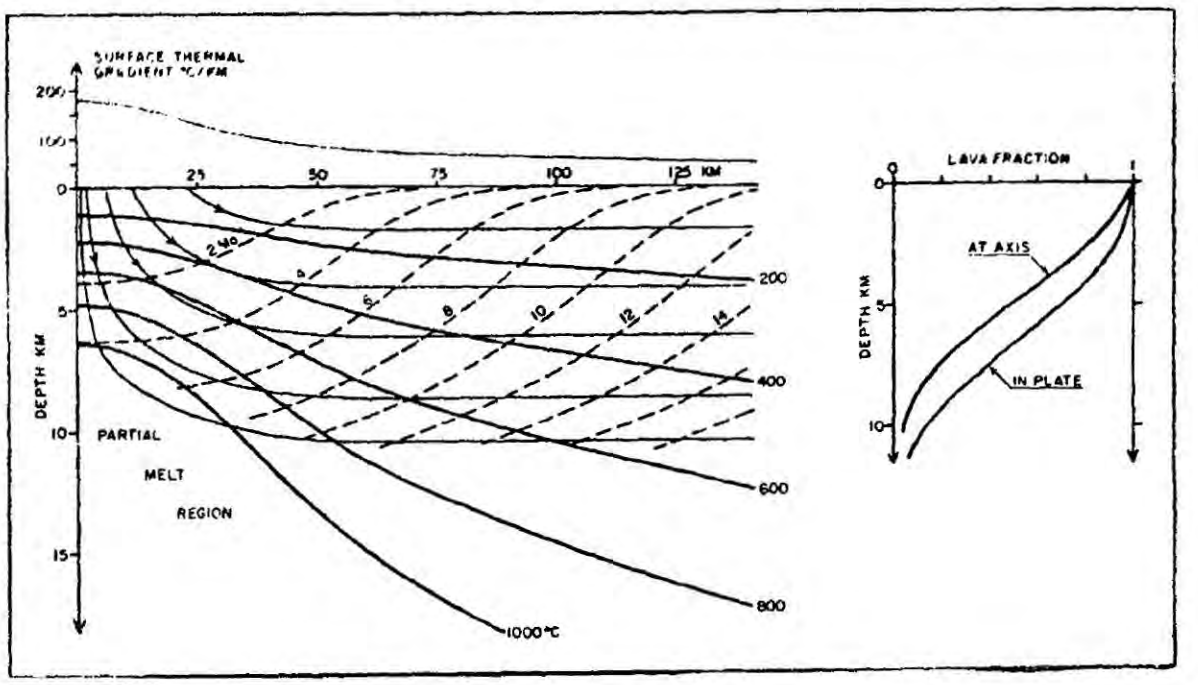

Fig. 1.7 Section through the lithosphere according to the accretion model of Palmason (1973, 1980). Trajectories (arrows) and isochrons (dashed) of lava elements are shown together with isotherms and surface gradient. The lava fraction at the axis and in the distant lithosphere is shown on the right. The model parameters used are: spreading velocity 1 cm a^{-1} ; lava production rate 1.3×10^{-4} km^2 a^{-1} ; crustal strain rate, standard deviation 15 km; lava deposition rate, standard deviation 20 km; normal fault parameters, $\varepsilon = 0.75$ and $\eta_0 = 1$. (from Palmason, 1981)

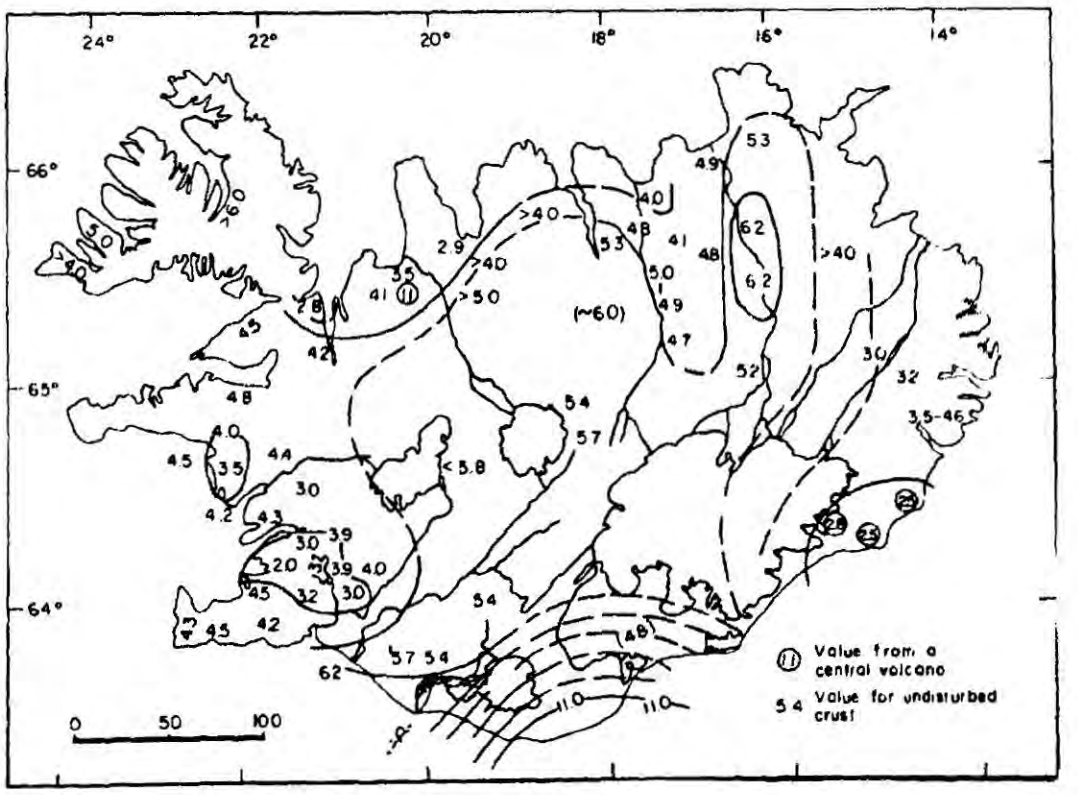

Fig. 1.8 Depth to the lower crust (layer 3) in Iceland. (from Flovenz, 1980)

the heat flow was found to be generally compatible with model calculations based on conductive cooling of lithospheric plates.

During the period 1975-1984 a volcano-tectonic rifting episode occurred in the Krafla system of NE Iceland (Bjornsson et al., 1977; Einarsson, 1978; Bjornsson et al., 1979; Brandsdottir and Einarsson, 1979; Moller and Ritter, 1980; Spickernagel, 1980; Torge and Kanngieser, 1980; Johnsen et al., 1980; Tryggvason, 1980; Sigurdsson, 1980; Einarsson and Brandsdottir, 1980; Bjornsson, 1984). A shallow magma chamber with centre at approximately 3 km depth was continually inflated by magma inflow at a rate of 5 m^3 sec^{-1}. Periodically it catastrophically deflated and magma was injected below surface into the fissure swarm to the N or S of the Krafla volcano. These injection events were accompanied by seismicity that rarely exceeded magnitude 4. Towards the end of the rifting episode, the lava erupted from the fissures, and almost no earthquakes were recorded. Subsidence and several metres of widening were observed across the central part of the fissure swarm, and uplift and contraction on the flanks.

These events are interpreted as demonstrating crustal accretion by lateral dyke injection and lava eruption. Tensional strain is built up by plate movements during inter-episodic periods of quiescence and when this has been released by fissure widening and dyke injection the mobilised magma spills out onto the surface. Only the dyke injection events were accompanied by seismicity since when the magma broke surface, further fracturing of rock was not required to make a passage for the migrating magma. Volume calculations indicate that in total the magma injected into the crust corresponds to

the formation of a dyke 2 km high and up to 6 m wide. It has been suggested that the crust in fact rifted down to its base, at about 8 km depth, and that magma ascending directly from the upper mantle formed the lower part of dyke (Bjornsson, 1984).

This rifting episode demonstrated that central volcanoes can play a key role in the linear accretion process in Iceland, and that dyke injection may occur horizontally. Lavas can travel long distances (in this case up to 60 km) horizontally before eruption. With this in mind, several other fissure eruptions have been linked to central volcanoes relatively distant along their strike (Sigurdsson and Sparks, 1978 a, b).

1.2.4 Geophysical constraints on subsurface structure

Several seismic refraction surveys of the Icelandic crust have been described (Bath, 1960; Tryggvason and Bath, 1961; Palmason, 1963, 1971; Flovenz, 1980; Angenheister et al., 1980). The seismic structure of the crust is found to be oceanic, but of greater thickness than normal oceanic crust. The P-velocity increases rapidly with depth down to an isovelocity surface of 6.5 km sec^{-1} below which the P-wave velocity is nearly constant. On this basis the Icelandic crust is divided into an upper crust, where velocities increase continuously with depth, and a lower crust with an almost constant velocity of 6.5 km sec^{-1}. The top of the 6.5 km sec^{-1} layer is usually considered to be the base of the extrusives (see for example, Saemundsson, 1979) although there is also evidence that it may be a metamorphic boundary (Christensen and Wilkens, 1982). Its depth is generally 3-6 km, but may be shallower in the neighbourhood of

central volcanoes, and deeper in SE Iceland (Fig. 1.8).

Combined reflection-refraction measurements carried out on profiles crossing the axial rift zone in NE and SW Iceland reveal reflecting horizons of average length 1-2 km down to 15 km depth (Zverev et al., 1980 a, b). They generally dip at angles of up to 30^{o} towards the axial rift zone. Volumes were identified beneath the axial rift zones where no refractors occurred, which may be zones of partial melting.

Beneath the crust a layer with seismic velocity of about 7.0 km sec^{-1} has been detected, which is interpreted as anomalous upper mantle. It lies at approximately 8 km depth in SW and W Iceland, but at 14 km in N and SE Iceland. Combining these data and heat flow measurements indicates that the temperature of the top of the anomalous mantle is in or above the melting range for basalts (Palmason, 1971).

An 800 km long profile measured from the SE flank of the Reykjanes Ridge across Iceland, along the E Neovolcanic Zone explored the structure of the crust and upper mantle at great depth, and also the transition from oceanic to Icelandic structure (Angenheister et al., 1980). The oceanic crustal layers were found to continue uninterrupted into Iceland but with increased thickness. In contrast the oceanic upper mantle (Vp = 7.8-8.6 km sec^{-1}) terminates abruptly near the insular shelf and the Icelandic subcrustal velocities range from 7.0-7.6 km sec^{-1} down to 50 km. Other profiles shot in the E and W of Iceland confirm that this layer, extends beneath Iceland outside the Neovolcanic Zone (Bath, 1960).

It has been observed that S waves are in general transmitted through the Icelandic crust and Neovolcanic Zone

down to depths of at least 10 km (Sanford and Einarsson, 1982), although small isolated volumes have been identified as magma pockets on the basis of their seismic properties (Klein et al., 1977; Einarsson, 1978; Zverev et al., 1980 a, b). However, attenuation and progressive slowing with respect to P waves has been observed for explosion generated S waves penetrating the anomalous upper mantle layer (Gebrande et al., 1980). It was concluded that a fundamental change occurs at the top of this layer.

A regional survey of magnetotelluric measurements was carried out in NE Iceland, and a profile traversing the Neovolcanic Zone in SW Iceland (Beblo and Bjornsson, 1978, 1980; Beblo et al., 1983; Hersir et al., 1984). In both cases a low resistivity layer was identified (resistivity 10Ωm) imbedded between layers of higher resistivity. The depth to the top of this layer is about 10 km beneath the axial rift zones but increases to about 20 km below the Tertiary basalts to the E and W. Comparing these results with temperature-resistivity laboratory data and observed near surface temperature gradients, it was concluded that the low resistivity layer is a partially molten basaltic layer at temperature about 1100^{o} C. The higher resistivities below this were interpreted as ultramafic upper mantle at a temperature of about 1100^{o} C. These results have been used to estimate that the degree of partial melt is 5-20% at the top of the mantle. It has been suggested that the partially molten layer occurs at the crust/mantle boundary. It decouples the crust from the mantle, accounts for the instability of the accretionary axis and enables high mobility of the crust during rifting episodes (Bjornsson, 1984). Its

depth is thus an indication of crustal thickness. Bjornsson (1984) presented a regional map of crustal thickness for NE Iceland using the results of MT soundings, and showed that crustal thickness varies from 8-10 km beneath the axial rift zone to 20-30 km in the older Tertiary areas to the W and E.

The depth to the base of the crust in Iceland is still inadequately mapped seismically, but there is some evidence, and several authors have argued, that it thickens with age from perhaps 10 km to 20 km as a result of underplating. (Evans and Sacks, 1979, 1980; Keen et al., 1980; Hermance, 1981).

The depth extent of the anomalous low velocity mantle beneath Iceland has been explored using teleseismic delays and gravity data. Tryggvason (1964) calculated a depth to the base of the anomalous mantle of about 240 km using teleseismic P wave arrival delays. Long and Mitchell (1970) measured a teleseismic delay of 1.4 sec at two Icelandic stations relative to stations in Scotland, Greenland and Sweden, and concluded that the anomalous mantle layer must extend to at least 200 km depth. Tryggvason et al. (1983) modelled the velocity structure beneath Iceland using the Icelandic seismograph network and concluded that the anomalous mantle extends to 375 km.

A bowl-shaped Bouguer anomaly centred on central Iceland is observed to coincide with the topographic anomaly of Iceland (Einarsson, 1954). A low density mantle extending to depths of several hundred kilometers, compensating for the excess mass of the dome would explain these observations. The free air anomaly is approximately constant at +60 mgal and extends over the whole of Iceland (G. Palmason, pers. comm.). This indicates that the structure causing the gravity anomaly must have an aerial

extent of several times the extent of Iceland.

1.3 Summary

1.3.1 The structure of Iceland

The opening of the N Atlantic commenced at about -60 Ma when the E migrating Iceland hotspot intersected a line of weakness in the overlying continental crust, and subaerial volcanism became possible. From -60 Ma to about -26 Ma the Greenland-Scotland Ridge and the Icelandic insular shelf formed in response to hotspot activity. The ocean basins to the N and S formed contemporaneously by linear accretion along spreading ridges, the north having a more complex history than the south.

Regional geological mapping in Iceland indicates that the oldest exposed rocks are 16 Ma old, but that the extrusive Icelandic pile probably dates back to before -20 Ma. The plate boundary is traced across Iceland along the axial Neovolcanic Zone and the South Iceland and Tjornes fracture zones. Off-boundary volcanism also occurs in so-called flank volcanic zones that are thought to be unassociated with active rifting.

Mapping of the Tertiary in Iceland has revealed that the volcanic pile is built up of near horizontal lava flows dissected by dyke swarms and punctuated by central volcano complexes. In the light of these results, a kinematic model of crustal accretion in Iceland has been developed, which can be used to calculate spreading velocities and other parameters from measurements made in old lava successions. The model also explains the interplay of intrusion and extrusion at the plate boundary, and, when correlated with heat flow data, predicts a mechanism for remelting in the crust. The present

volcano-tectonic rifting episode at the Krafla volcano in NE Iceland is demonstrating the dynamics of the crustal accretion process and also the role played by central volcanoes. Synclinal structures in the Tertiary lava pile indicate the positions of extinct accretionary plate boundaries.

Seismic studies indicate that Iceland, the adjoining ocean basins and the Greenland Iceland Ridge are all underlain by oceanic crust, thickest beneath the Greenland-Scotland Ridge, and of intermediate depth below Iceland. Extensive zones of partial melting have not been observed in the Icelandic crust, neither is their existence predicted by heat flow measurements, but small isolated zones of partial melting exist in some places. The depth to the base of the Icelandic crust has not been mapped in detail by seismic studies.

Beneath Iceland the crust is underlain by a partially molten, low resistivity layer which is the top of a mantle exhibiting anomalously low P-wave velocity and high S-wave attenuation. The upper mantle beneath the Greenland-Scotland Ridge and the ocean basins to the N and S exhibit normal P-wave velocities. The partially molten layer beneath Iceland may decouple the crust from the mantle and thus account for its high mobility. Shallowing of the partially molten layer beneath the Neovolcanic Zones indicates that the crust is thinnest beneath the accretionary plate boundary, and progressively thickens away from it.

Teleseismic delays and gravity data indicate that this anomalous mantle extends to at least 200 km depth.

1.3.2 Evolution of the plate boundary in Iceland

The culmination of geochemical, gravity and topographic data indicate that the present position of the hotspot is beneath central east Iceland, in the Kverkfjoll area. The present day distribution of volcanic zones in Iceland may be understood in a plate tectonic context if lateral flow from the hotspot is accepted, preferentially longitudinally along old zones of weakness.

From at least -16 Ma to - 6 or 7 Ma the trace of the plate boundary crossed Iceland in a zone connecting Snaefellsnes and Skagi. The boundary then jumped eastwards and is now represented by the Reykjanes-Langjokull-Axafjordur zone, which joins with the Kolbeinsey Ridge through the Tjornes Fracture Zone (Saemundsson, 1974). Most of the seismicity of Iceland occurs along the boundary, and in the Tjornes Fracture Zone and the South Iceland Seismic Zone. The WE Langjokull-Kverkfjoll Zone of recent volcanism and high topography marks the trajectory of the migrating hotspot.

The Reykjanes-Langjokull Zone is at present becoming replaced by a zone further E. The S part of the E Neovolcanic Zone (the Kverkfjoll-Torfajokull Zone) is a southward propagating accretionary plate boundary that started forming at about -2 Ma. It connects with the Reykjanes Peninsula Zone by the South Iceland Seismic Zone, which is usually interpreted as an EW transform fault. That this EW "transform fault" has no surface topographic expression, and that older surface fault breaks are observed N of its supposed position indicates that this zone may be propagating south along with the tip of the

Kverkfjoll-Torfajokull Zone (Einarsson and Eiriksson, 1982). The fact that ridge jumps have occurred in the past implies the existance of remnant old blocks of crust between the extinct and active spreading axes. The presence of such a block in the N of Iceland is supported by radiometric dating but no such evidence is availible from the S.

The eastwards migration of the plate boundary south of the hot spot has hence "lagged behind" that to the north. It is proposed here that this is because the plate boundary north of the hotspot has been normal to the trajectory of the migrating hotspot. Thus longitudinal flow NS along the Langjokull-Skagi Zone from the hotspot ceased quickly after it migrated off axis. South of the hotspot, however, the opening of the Atlantic has had a different history (see Section 1.1) and the plate boundary is oblique to the hotspot trajectory, permitting longitudinal flow from the hotspot to be maintained for longer. It is also proposed that the Snaefellsnes volcanic zone, a remnant accretionary axis, is a weak zone which is maintained active by lateral flow from the hotspot, made possible by its colinearity with the trace of the hotspot.

CHAPTER 2

2. THE STRUCTURE OF THE HENGILL AREA

2.1 Regional Setting

2.1.1 The triple point

The area herein referred to as the "Hengill area" is the 700 km^2 rectangular area that lies between 63°N55′ - 64°N10′ and 21°W00′ 21°W30′. All local place names within this area referred to in the text are marked in Fig 2.3. It forms a triple junction where three branches of the trace of the plate boundary in Iceland meet (Fig. 2.1). The natures of these three branches are very different and they are described in brief individually below.

2.1.2 The Reykjanes Peninsula

This zone exhibits high seismicity and recent volcanism. Twelve historic eruptions have been documented (Jonsson, 1983). The trace of the plate boundary is defined by a belt of seismicity, less than 2 km wide in most places that comes onshore at the SW tip of the Peninsula and runs in an easterly direction (Einarsson and Bjornsson, 1979). The earthquakes occupy the depth range 1-8 km. Strain built up by plate movements thus appears to be released by brittle deformation of the crust down to 8 km depth, and by aseismic deformation below this. Small scale structures within the zone have been resolved by the seismicity (Klein et al., 1977). Focal mechanism

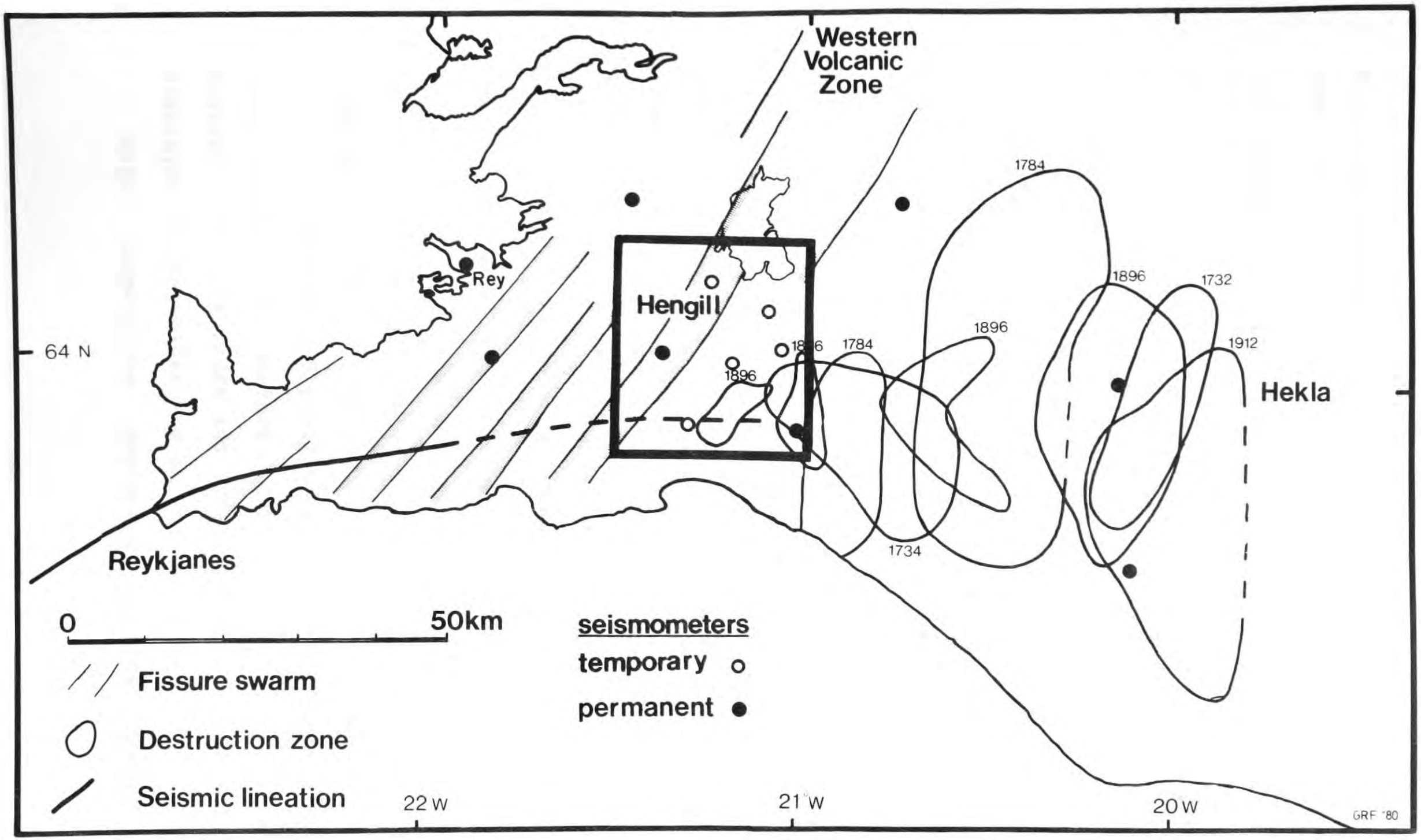

Fig. 2.1 Regional map of SW-Iceland showing the main tectonic features of the 3 branches of the plate boundary that meet in the Hengill triple point. The Hengill area is enclosed by a box. The drum seismograph network is also shown.

solutions obtained for small earthquakes on temporary networks, and two teleseismic solutions consistently indicate a horizontal, NW trend for the direction of minimum compressive stress (Klein et al., 1977; Bjornsson, 1975; Einarsson, 1979) . The direction of maximum compressive stress varies from vertical to NE. Thus fault movements vary between normal dip slip movements on NE striking fault planes, to strike slip movements on N or E striking fault planes. The nature of strain release varies along the seismic zone. To the extreme west, swarm activity and normal faulting predominate. Further to the east, mainshock-aftershock sequences and strike-slip faulting become more common. The zone has not been traced as it approaches the Hengill area because the level of activity has been low in recent years.

The seismic zone is crossed by a series of discrete NE trending en echelon fissure swarms exhibiting normal faults, open fissures and eruptive fissures. Tryggvason (1968) interpreted these features as being indicative of a deep seated left lateral transcurrent fault with a small tensional component (a "leaky" transform fault). Nakamura (1970) pointed out that the NE striking open fissures are evidence of tensional tectonics and hypothesised that the Reykjanes Peninsula is an obliquely spreading ridge with equal shear and tensional components. The surface geologic formations of the Peninsula are mainly glacial and postglacial volcanics, and obscure to some extent, the surface tectonic features. It is clear, however, that both ridge and transform fault characteristics are displayed in the seismicity of the Peninsula.

High temperature geothermal fields occur at the

intersections of the fissure swarms and the seismic trace of the plate boundary. These are, from west to east, the Reykjanes, Svartsengi, Krisuvik and Brennisteinsfjoll geothermal areas. The volcano-tectonic province of the Reykjanes Peninsula is terminated in the east by the largest fissure swarm of all, that transects the Hengill area, contains the 803 m high central volcano Hengill and continues beyond L. Thingvallavatn to merge with the Western Volcanic Zone. The Hengill geothermal area, associated with this fissure swarm, is also the largest of the geothermal areas of this series.

2.1.3 The Western Volcanic Zone

This is a 120 km long rift zone extending from Langjokull in central Iceland to Hengill in the south (Fig. 1.2). The surface rocks are recent eruptives forming single or fissure aligned lava shields and hyaloclastite ridges (Saemundsson, 1978). The rift is moderately seismic, activity occurring mainly as periodic swarms. Structure near the southern end is dominated by a swarm of fissures and normal faults with a NE strike that continues S through the Hengill central volcano (Foulger and Einarsson, 1980). Lateral extension in the lavas has been calculated to be about 0.5 cm a^{-1} (Saemundsson, 1967) or 25% of that estimated for the Reykjanes Ridge.

2.1.4 The South Iceland Seismic Zone

This EW orientated zone connects the Hengill area to the Eastern Volcanic Zone at Hekla (Fig. 2.1). The level of

seismicity is low at the time of writing, but many large destructive earthquakes are documented, which have a recurrence time of 50-100 years (Einarsson et al., 1981). The whole seismic zone has an EW orientation at about 63°N58′, but there is no surface indication of such a fault. Individual earthquakes are accompanied by NS trending surface breaks, and their destruction zones are also aligned NS. En echelon features of these surface breaks imply a least compressive stress in a NW-SE direction and a maximum compressive stress in a NE-SW direction. These data may be interpreted as indicative of an EW trending deep seated deformation zone, which also conforms with a transform fault interpretation for this zone. The brittle crust responds to this motion by fracturing on the conjugate plane (Einarsson and Bjornsson, 1979).

2.2 The Hengill area

2.2.1 Surface research

The area that forms the meeting point of the three contrasting volcano-tectonic zones described above is itself a self-contained tectonic unit. The geology has been described in detail by Saemundsson (1967) (Fig. 2.2) and several additions have been made since then (Saemundsson and Bjornsson, 1970; Saemundsson, 1978; Torfason et al., 1983). The area is dominated by an 803 m high central volcano which is dissected by an intense swarm of normal faults and open fissures that crosses the area with a strike of N 25°E. To the N of the central volcano the fissure swarm has the structure of nested grabens. An inner graben of 4-5 km width is nested within an outer graben of 15-20 km width. The whole graben system is continuous with the fissure zone of the Langjokull Volcanic Zone. Contained within the fissure swarm are both normal faults and open fissures with and without vertical offset. Geological observations in this part of the graben indicate a subsidence rate of 5-8 mm a^{-1} over the past 8000 years. Precision levelling over a 5 year period revealed subsidence at a rate of only 2.5 mm a^{-1} (Tryggvason, 1974). The subsidence is hence probably episodic with most of the movement occurring during short periods of high activity. Such an episode is known to have occurred in 1789, when the whole of the fissure swarm was seismically activated and 60 cm of subsidence was observed in the Thingvellir graben, 20 km N of Hengill (Thoroddsen, 1899).

The surface materials are mostly basaltic hyaloclastites

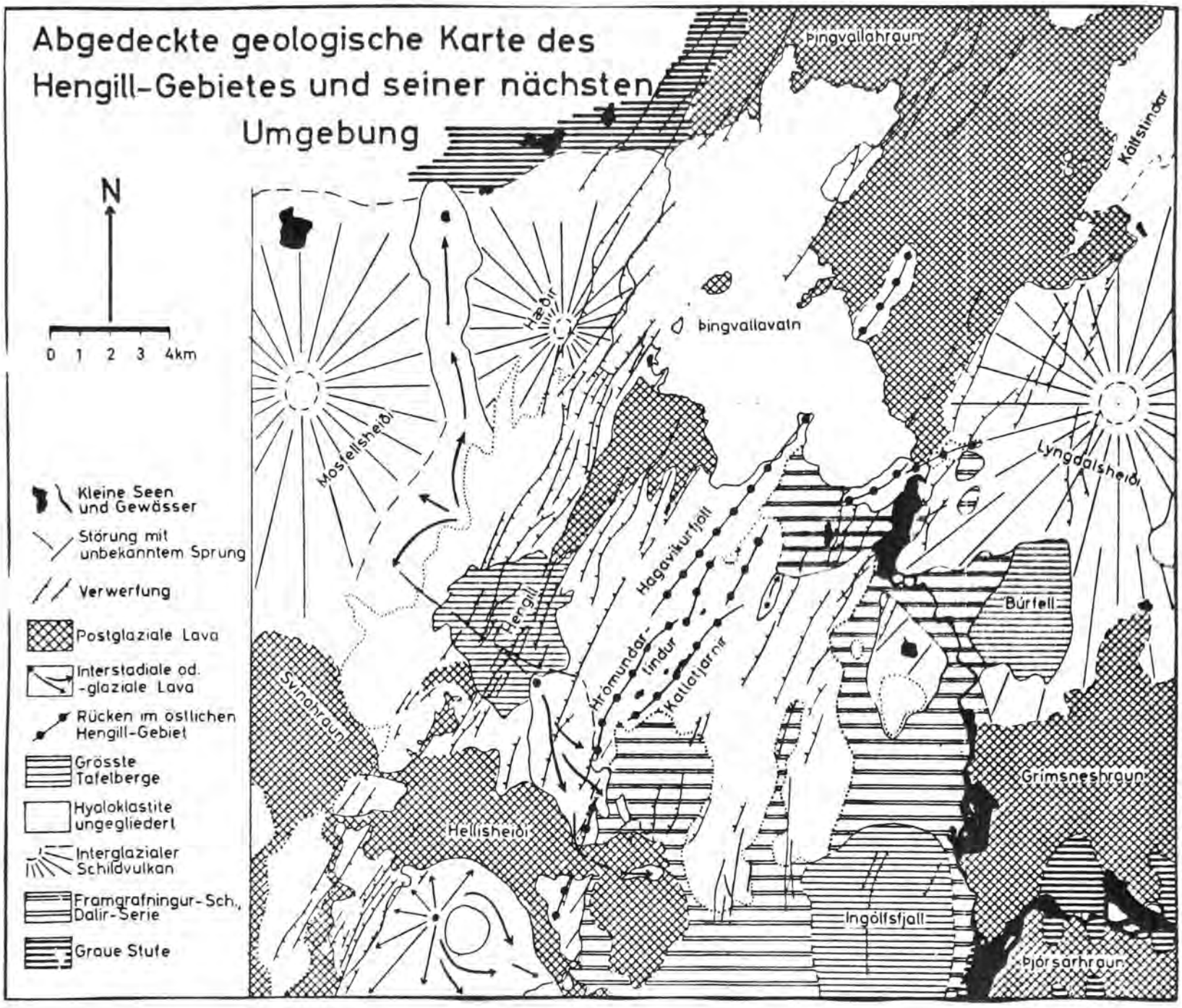

Fig. 2.2 A simplified geological map of the N part of the Hengill area. (from Saemundsson, 1967).

(erupted under ice) and subaerial lavas. Elongated hyaloclastite ridges characterise the area and are thought to be a result of subglacial fissure eruptions. Cone shaped mountains also occur, e.g. Tjarnahnukur, and these were probably formed by eruption through a single circular orifice. Subglacially erupted material and pillow lavas are the most common rock types, and Pleistocene and postglacial lava flows are secondary in importance. A knowledge of the extent of post glacial eruptive sites, and the quantity of material extruded is an indication of the position of the currently active zone and the volcanic production rate over the last 10,000 years. In general the youngest rocks of the area are to be found in and around the fissure swarm and the rocks become progressively older the more easterly one travels. Six postglacial lavas have been mapped, all of which were erupted within the fissure swarm except for one, an early postglacial lava that erupted from Tjarnahnukur, a volcanic cone 4 km SE of Hengill (Fig. 2.3). The most recent eruption, and the only historically documented one occurred in the year 1000 (the Kristnitokuhraun - the Christianity lava). According to the sagas, it erupted whilst debate was in progress in the Althingi as to whether Christianity should be adopted as the official religion of Iceland. The opponents of the motion declared the eruption to be a sign of the anger of the Gods.

Small outcrops of intermediate and acid rocks occur SW of Hengill. The intermediate rocks are andesites, and the acid rocks rhyolites. Intermediate rocks have also been found in Maelifell, NE of Hengill (Fig. 2.3) (V. Hardardottir, pers. comm.).

A large geothermal field, 70 km^2 in area encompasses

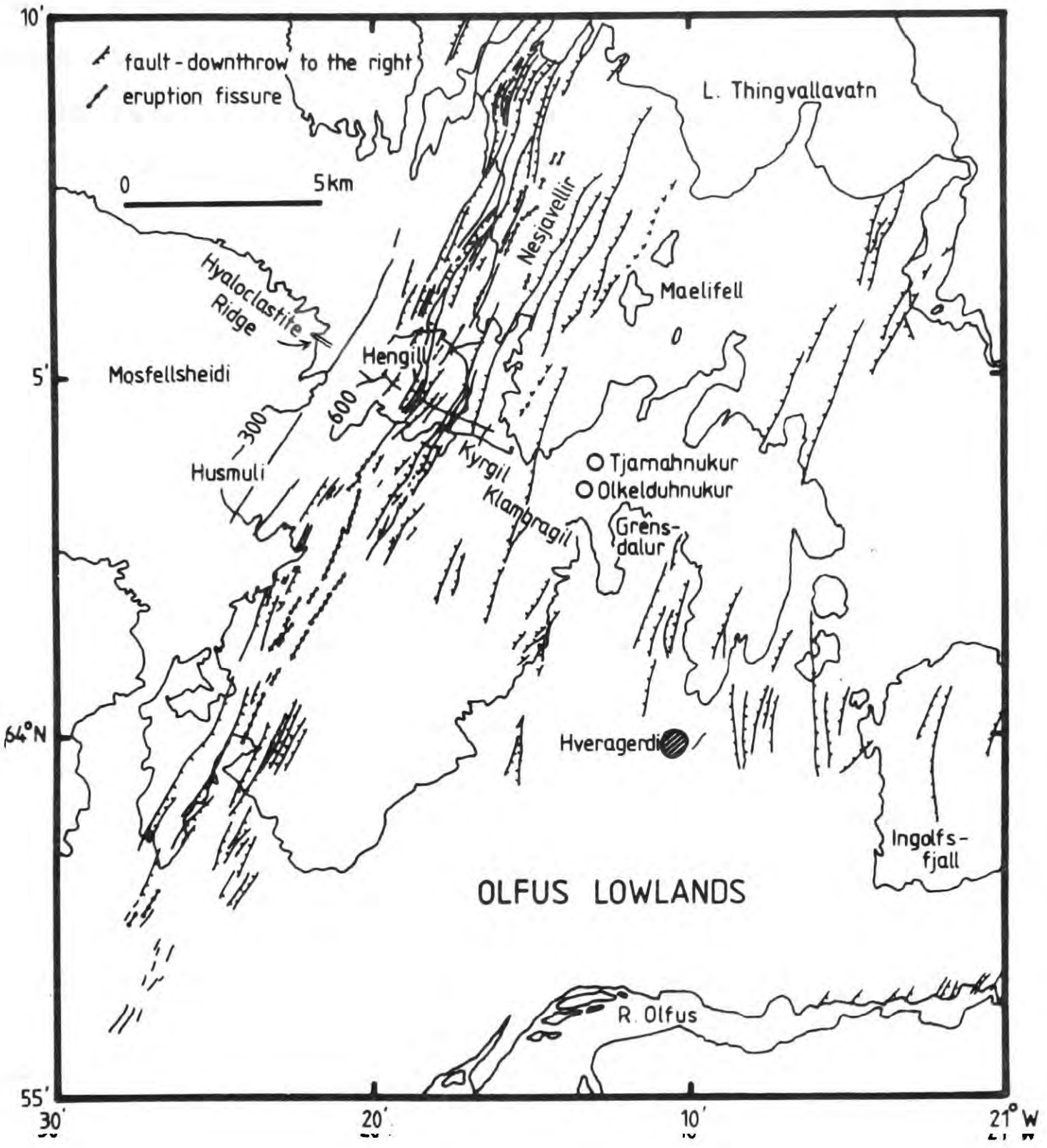

Fig. 2.3 Map of the Hengill area showing surface faulting and fissuring (mapped by Saemundsson, 1967 and Eiriksson, 1973), the 300 m and 600 m contour lines and place names mentioned in the text.

Hengill and surface displays extend over a large area to the SE of the volcano (Fig. 2.4). No corresponding surface displays exist to the W of Hengill. The surface expression of the geothermal field is hence highly asymmetric with respect to the central volcano. Many hot springs lie inside the fissure swarm and close to Hengill. From the E side of Hengill a SE trend may be discerned in the hot spring distribution that subsequently widens to form a diffuse scatter of high temperature displays many of which occupy an eroded topographic low just N of the village Hveragerdi.

This depression also contains the deepest sections in the oldest rocks of the area. They display highly altered dykes and intrusions. The thin soil cover of this area has been highly altered locally around the hot springs.

The picture that emerges from these observations is summarised by Bjornsson et al., (1974). The Hengill area has contained a central volcano and been volcanically active since the early Matuyama geomagnetic epoch. At some time during the early Bruhnes (~ 0.7 Ma to present) the original volcanic centre became extinct and a new one formed to the W of it. The old volcanic centre was first buried by lavas and hyaloclastites, but was later deeply eroded and its roots are now exposed in the area N of Hveragerdi. For convenience, hereafter the present volcanic centre and associated features will be referred to as the "Hengill system" and the extinct volcanic centre and associated features as the "Grensdalur system" (Grensdalur = Earth Valley).

The topography of the area is everywhere very rough except in the Olfus lowlands to the SE (Fig. 2.3). The region of

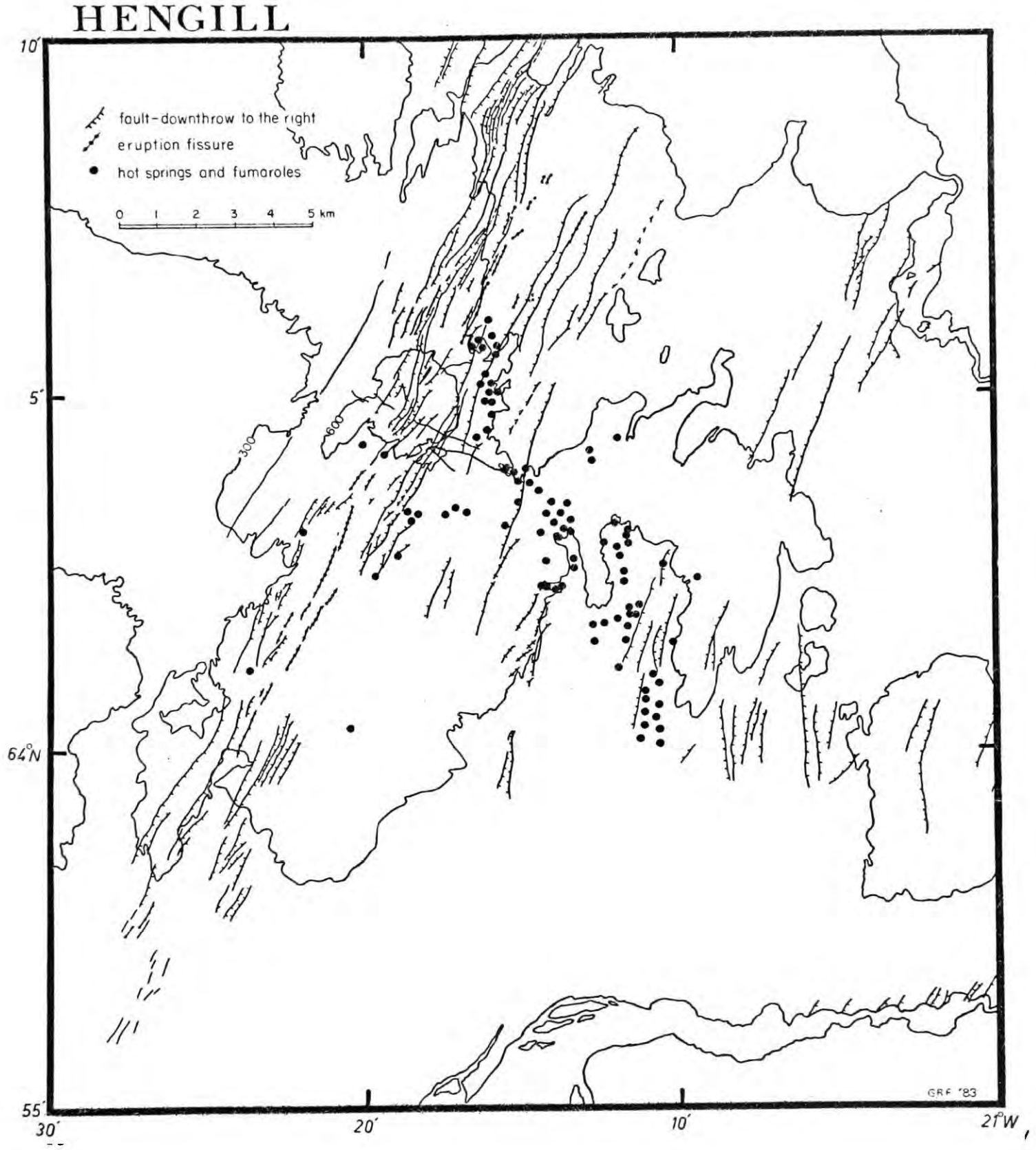

Fig. 2.4 Hot springs and fumaroles in the Hengill area (mapped by Saemundsson, 1967).

Hengill and the fissure swarm is characterised by high hills, deep subsidence valleys, sheer cliffs and NNE elongated features. E of the fissure swarm and N of the 64° parallel the topography is intense, but lower, and accessibility is difficult over much of the geothermal field. A transverse structure is apparent in the topography, that strikes normal to the fissure swarm and runs from Hengill, ESE to Ingolfsfjall. Other features also delineate a structure of this nature. They are, from WNW to ESE:

a) A WNW trending hyaloclastic ridge on Mosfellsheidi, W of Hengill.
b) WNW trending fracture lines that dissect Hengill.
c) The topographic ridge mentioned above. This ridge is a water shed - streams to the N flow NNE, parallel to the fissure swarm, and to topographic features, to empty into L. Thingvallavatn. S of the water shed streams flow direotly S, also following the trend of topographic features.
d) Faults N of the transverse structure trend NNE, parallel to the fissure swarm. Many of those to the S trend NS. Some faults crossing the SE part of the transverse structure change strike in the middle.
e) The valleys Kyrgil, in the E side of Hengill and Klambragil are intense topographic features on the transverse structure with WNW/ESE trend. The N boundary of the topographic depression occupied by the easternmost part of the geothermal field also has a WNW/ESE trend.
f) A WNW/ESE trend is clearly visible in the surface distribution of the hot springs immediatly SE of Hengill.

2.2.2 Geophysical research

The Hengill area is 35 km E of Reykjavik and its suburbs, which contain half of Iceland's population. For this reason there has long been interest in exploiting the geothermal resource either for hot water or electricity generation, and several geophysical methods have been applied in the area with a view to researching the geothermal area. The results of these studies generally confirm the broad picture described above. A brief resume of recent work is given below.

Electrical methods have been extensively applied and the results described by Stefansson (1973), Bjornsson et al. (1974), Stefansson (1975), Hersir (1980) and Bjornsson and Hersir (1981). In the period 1970-1977, 66 Schlumberger and 18 dipole-dipole resistivity soundings were made. The two data groups correlate well, and the picture that emerges is of a conductive layer (resistivity 15Ωm) at variable depth underlying the area (Fig. 2.5). The layer is limited in the W by the western border of the fissure swarm. Around Hveragerdi and the site of the extinct volcano this layer occurs only at shallow depths but it extends much deeper beneath Hengill and the fissure swarm. It is not clear whether the area Nesjavellir to the N of Hengill is connected to the main conductive layer or not. The dipole-dipole soundings indicate an increase in resistivity at 500-700 m b.s.l. under Hengill, which might indicate a change from liquid to two phase conditions in the reservoir at these depths, or a greater percentage of intrusives. S of the high temperature area, in the Olfus lowlands, resistivity measurements and drilling indicate the

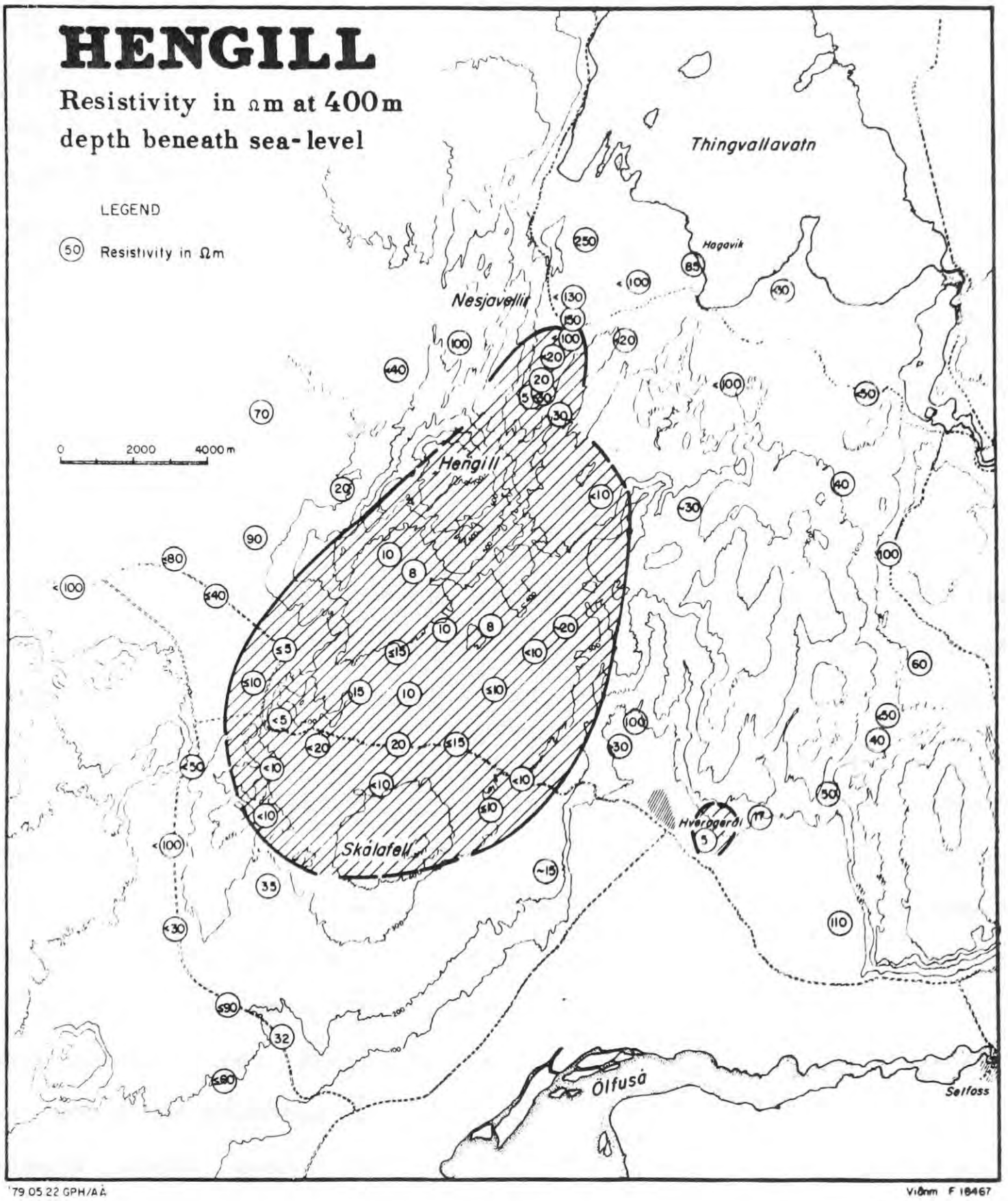

Fig. 2.5 A map showing the resistivity in Ωm at 400 m b.s.l. The hatched area shows the anomalous conductive layer at that depth. (from Hersir, 1980).

presence of low temperature geothermal resources (< 160° C).

In 1976 a 100 km long magnetotelluric profile was measured across the Western Volcanic Zone to the N of L. Thingvallavatn (Fig. 2.6) and 7 soundings were made within and around the Hengill high temperature area (Hersir et al., 1984). The main result that emerged was the detection of an anomalous high conductivity layer present under all stations. The layer is about 2 km thick, and was seen to shallow from 50 km beneath a station distant from the Neovolcanic Zone, to 8 km beneath the centre of the zone (Fig. 2.7). The resistivity of the layer was also seen to increase from 2.5Ωm to 50Ωm with increasing distance from the centre of the zone. This anomalous conducting layer is detected elsewhere in Iceland (Beblo and Bjornsson, 1978, 1980; Beblo et al., 1983) and is interpreted as a highly mobile zone of magma accumulation at the crust/mantle interface with a temperature of about 1100° C and a melt phase fraction of 5-20% (Beblo and Bjornsson, 1978, 1980; Hermance, 1981; Bjornsson, 1984).

A gravity survey was completed in 1983 and the preliminary results are available (Thorbergsson et al., 1984). The Bouguer anomaly map (Fig. 2.8) displays several lows along the fissure swarm, and a high over the topographical depression that marks the site of the extinct Grensdalur central volcano. These data have not as yet been modelled but the features displayed are what would be expected if partial melt exists at shallow depth beneath light hyaloclastics in the fissure swarm, and dense, cool dykes and intrusions characterise the near surface structure of the Grensdalur system.

The results of an aeromagnetic survey of the Hengill area

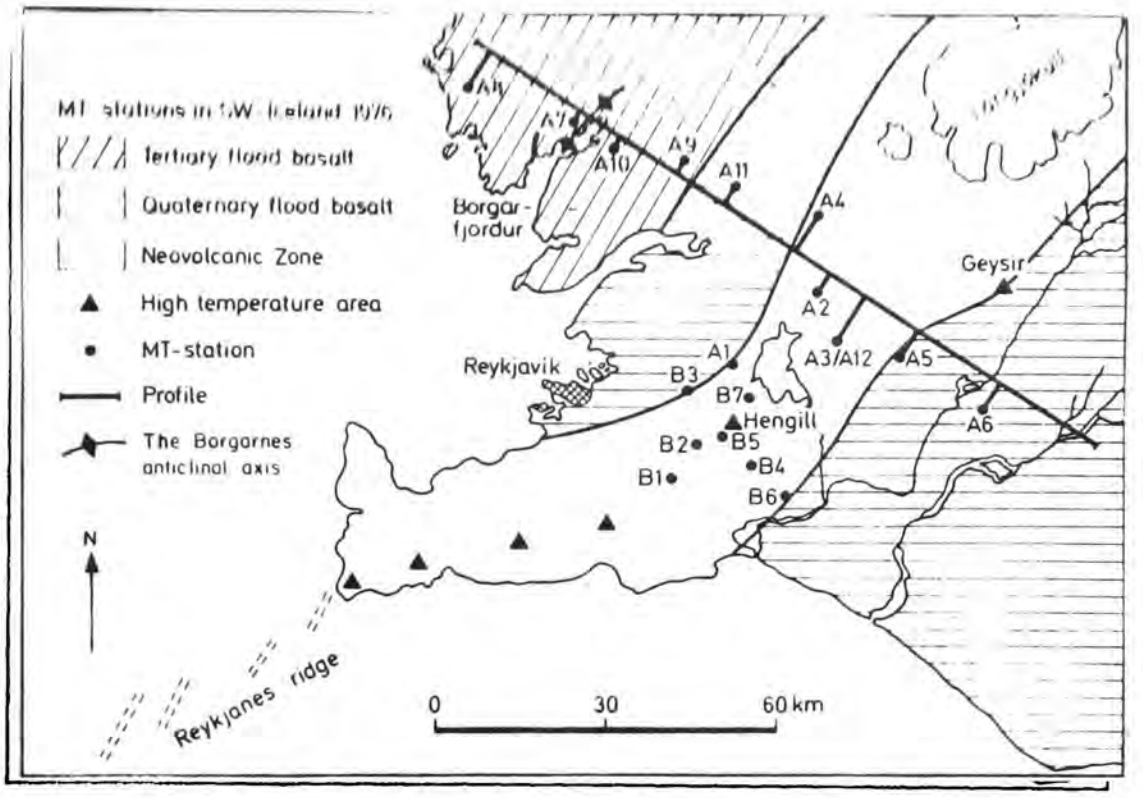

Fig. 2.6 Regional map showing the location of the magnetotelluric profile (Fig. 2.7) and soundings within the Hengill area (from Hersir et al., 1984)

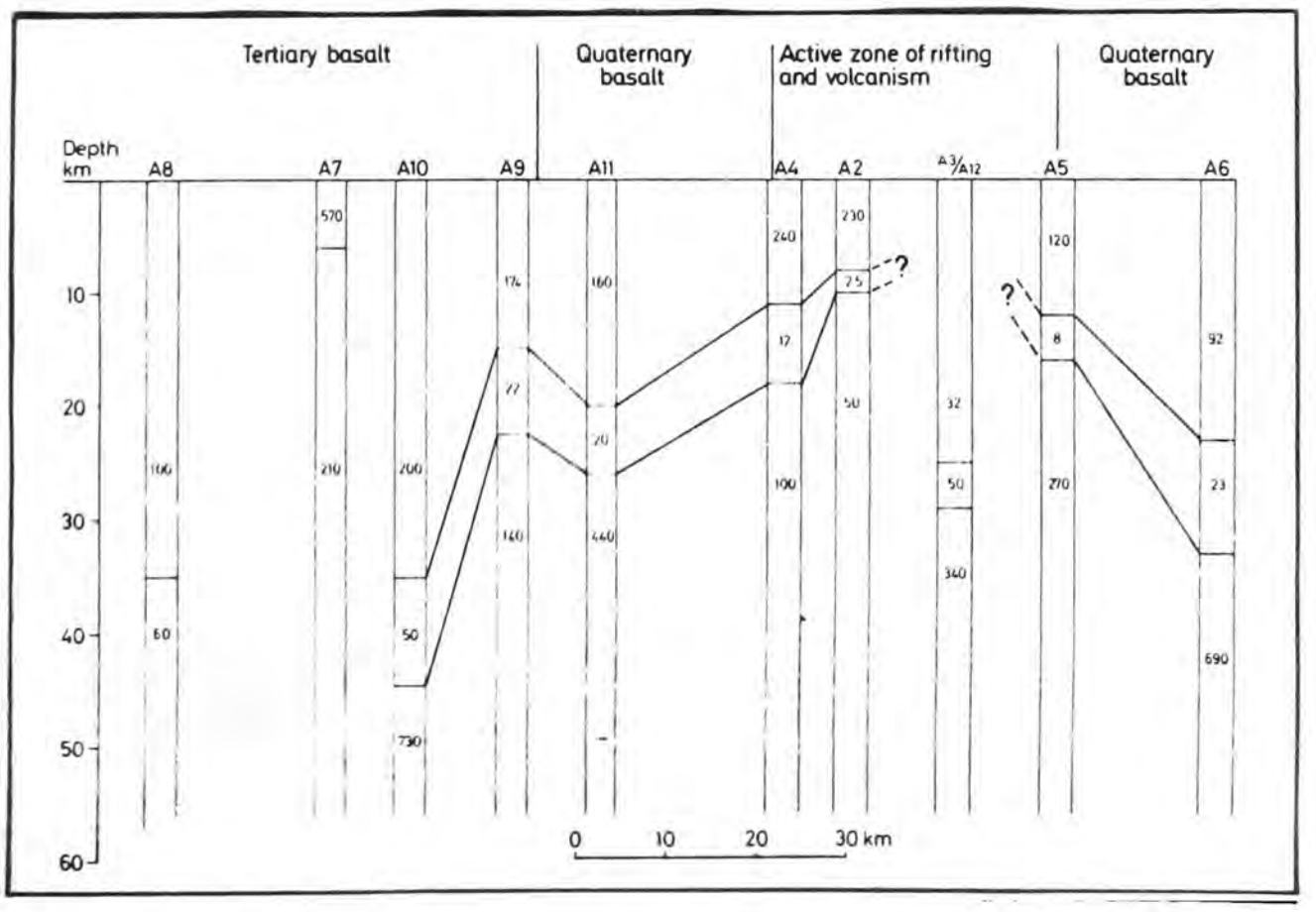

Fig. 2.7 A magnetotelluric resistivity cross section of SW-Iceland measured transversely across the Western Volcanic Zone, 10 km north of L. Thingvallavatn (for location see Fig. 2.6). Resistivities are in Ωm (from Hersir et al., 1984).

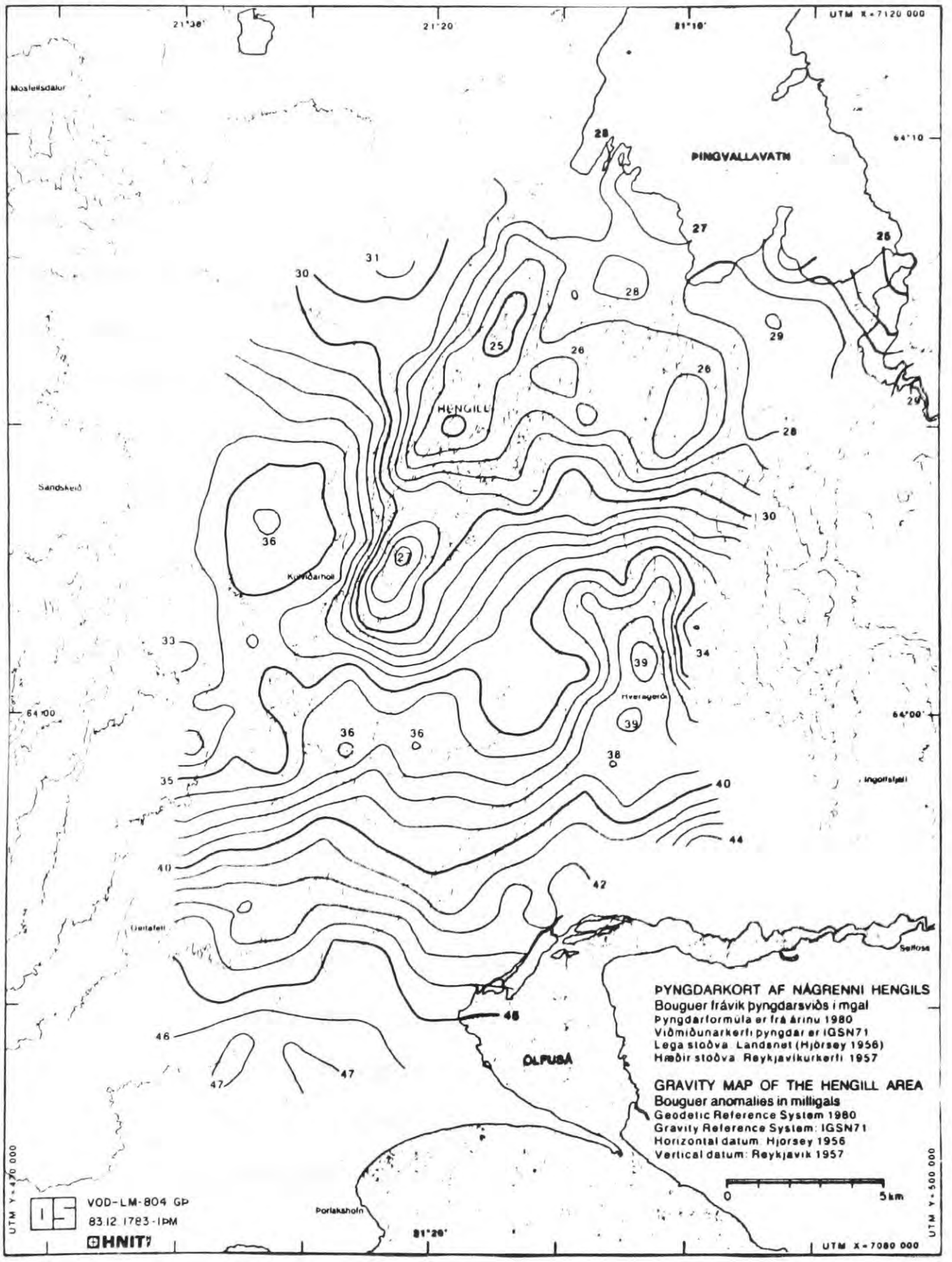

Fig. 2.8 Bouguer gravity map of the Hengill area. Rock density used - 2.6 g cm^{-3}. (from Thorbergsson et al., 1984)

conducted at 800 m altitude in 1975 were compiled by Bjornsson (1976) (Fig. 2.9) and briefly discussed by Hersir (1980). The magnetic polarity of the Hengill-fissure swarm area is normal and is associated with the present Bruhnes epoch. Outside the fissure swarm the polarity is reversed indicating that the field is dominated by material intruded and extruded prior to 0.7 Ma yrs ago, during the Matuyama epoch of reversed magnetism. Three anomalous features may be distinguished:

a) A general magnetic high occupying the fissure swarm,

b) A SE orientated zone of low magnetic intensity crossing the fissure swarm to the S of Hengill and widening to the E to encompass the area of hot springs.

c) A strong magnetic high associated with the mountain Skalafell.

The magnetic high over the fissure swarm is probably a result of the fact that there has been a very large production of material in this zone during the Brunhes normal geomagnetic epoch (0.7 M yrs ago - present) and that the magnetisation of this material dominates the measured field. The transverse magnetic low over much of the geothermal area is thought to be caused by extensive demagnetisation of the rocks by thermal effects. The strong magnetic high over Skalafell can be explained by topography and strongly magnetised rocks in the mountain.

The hydrology and borehole studies which will be described next are almost totally based on data from Nesjavellir, on the N perimeter of the Hengill system, and Hveragerdi, on the S perimeter of the Grensdalur system, since these are the only two sites where deep drill holes have been made.

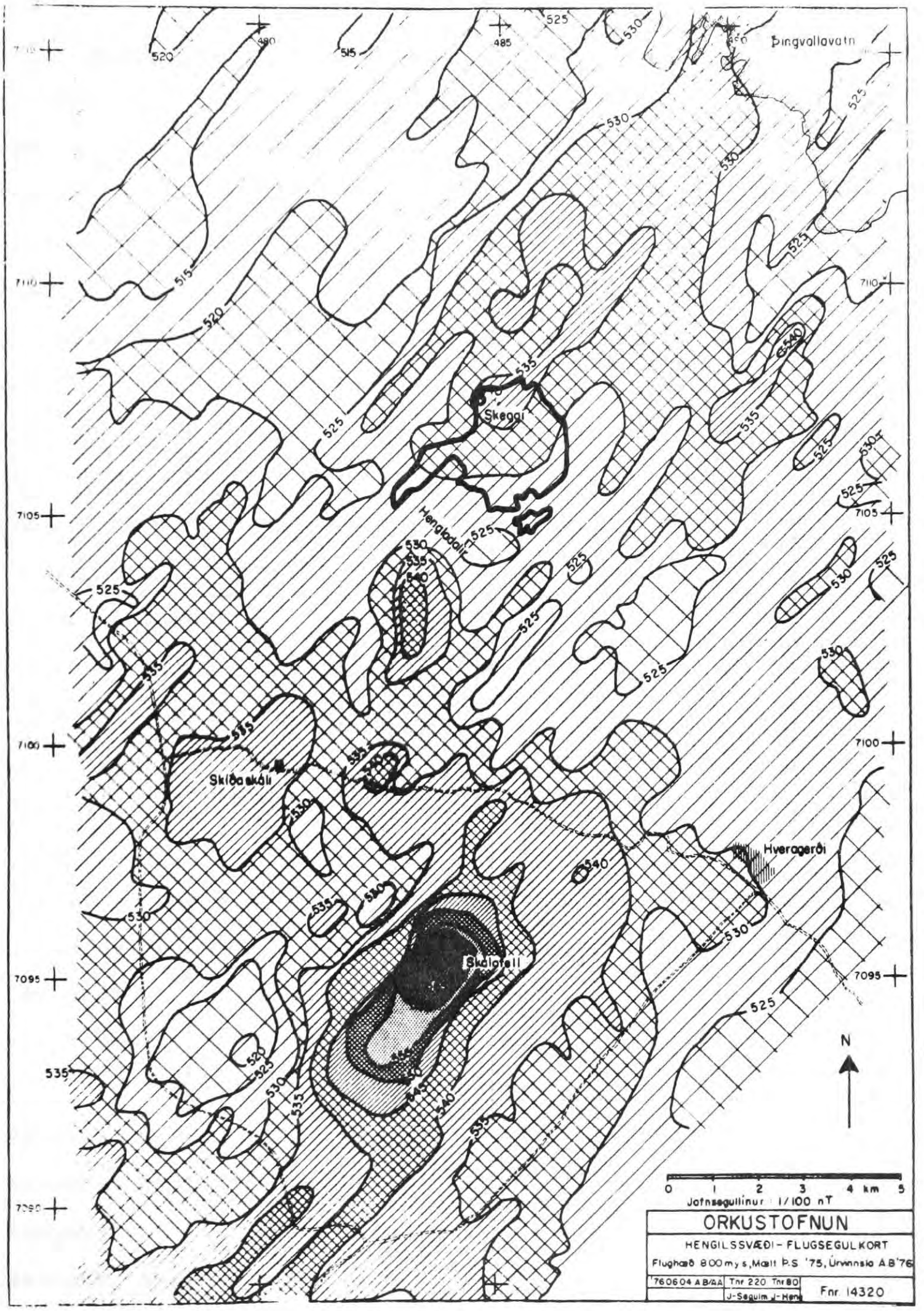

Fig. 2.9 An aeromagnetic map of the Hengill area measured at 800 m u.s.l. Isomagnetic lines labelled in multiples of 100 gammas, and drawn at 500 gamma intervals (compiled by Bjornsson, 1976).

Hydrological investigations are described by Arnason et al. (1969) and Arnason (1976). The results indicate two deep groundwater systems. One is detected in samples taken from a depth of over 800 m in the Nesjavellir drill holes. This water has a deuterium concentration similar to that precipitated over the S part of the Langjokull glacier, so it probably flowed SE along the volcanic zone. Samples taken from Hveragerdi indicate that the deep groundwater system that reaches the surface there derives its water from a mountainous area 35 km NE of Hveragerdi. The deuterium concentration is similar to the water of L. Thingvallavatn. These results show that a double hydrological system in the Hengill area mirrors the double volcanic system. Hot springs at higher elevations are likely to have originated from local precipitation that was heated up by steam and gases ascending from the deeper thermal systems.

The drilling of deep boreholes in the Nesjavellir area has been in progress since 1965 (Steingrimsson and Stefansson, 1979). A preliminary conceptual model is presented by Stefansson et al. (1983) (Fig. 2.10). The main reservoir is found below 800 m depth. In the southern part of the well field the reservoir is boiling at a temperature near 300°C. Pressure and temperature decrease northward.

A short distance to the N of Hveragerdi 8 wells have been drilled (G1-G8) into the S border of the Grensdalur system. The temperature profiles of these wells show that a maximum temperature is reached below which temperature decreases. The maximum temperatures were 184-233° C at 100-600 m depth (Fig. 2.11). The wells are located roughly on a N/S line, and it is found that both the maximum temperature measured and the

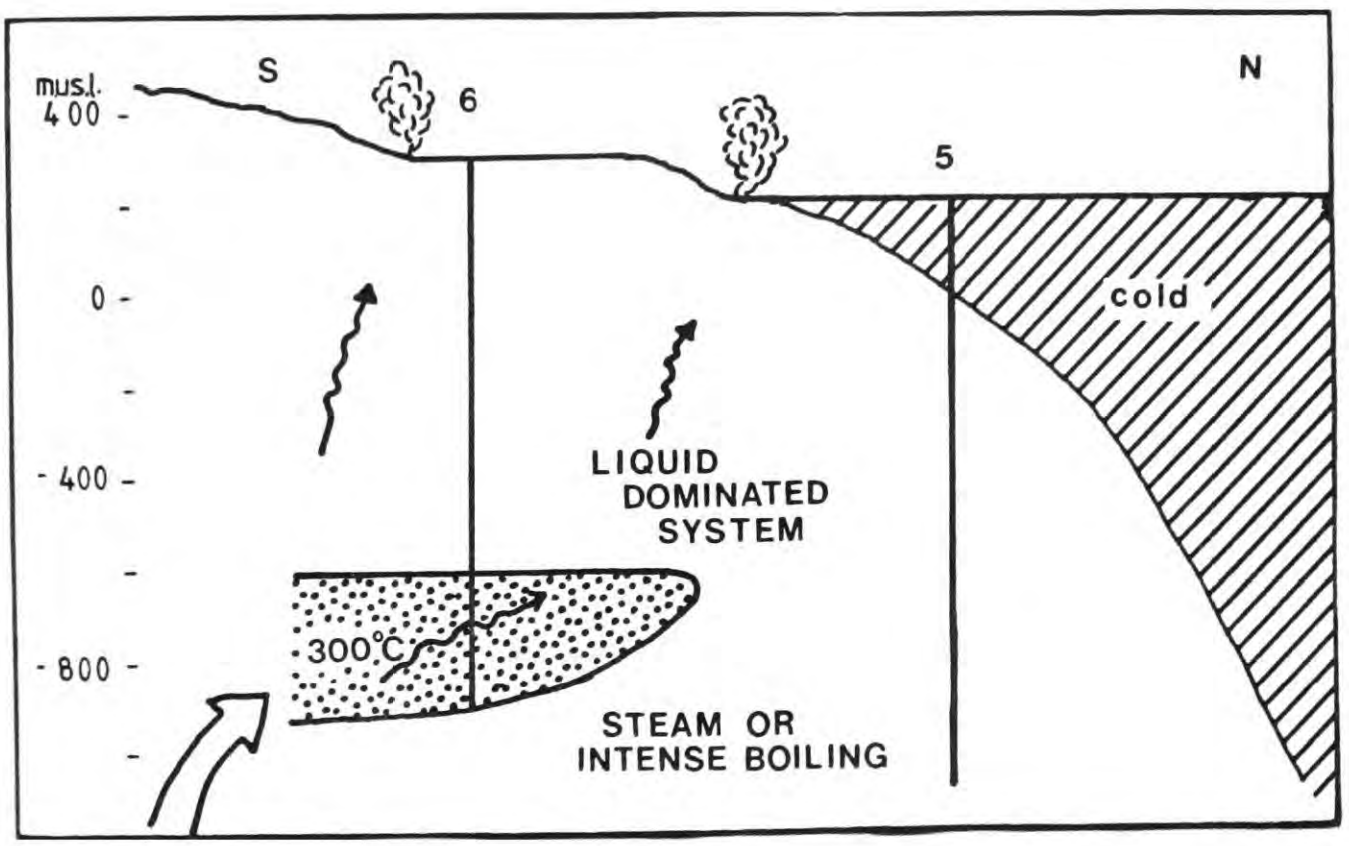

Fig. 2.10 Conceptual model of the geothermal reservoir beneath Nesjavellir (adapted from Stefansson et al., 1983)

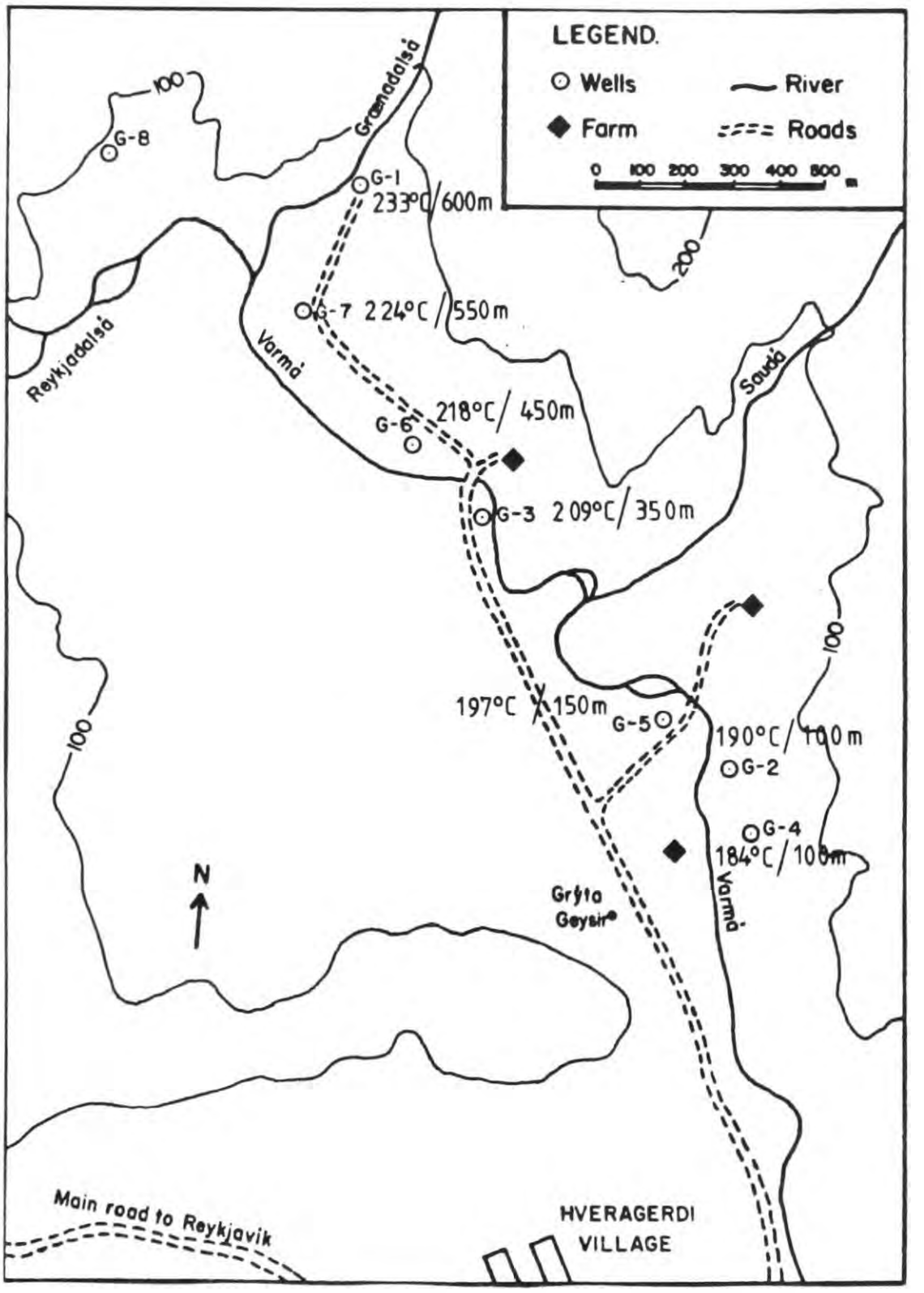

Fig. 2.11 Map showing the relative positions of boreholes G1-G7, N of Hveragerdi. Rivers are marked and contours in metres u.s.l. The maximum temperature measured in each borehole, and the depth at which it was reached is marked for each borehole. (from Xi-Xiang, 1980).

depth to it increased to the N, (Ragnars et al., 1979; Xi-Xiang, 1980). Linear extrapalotion of this trend to the N indicates that temperatures of about 300° C would be expected at 850 m depth about 2 km N of G1.

Extensive sampling of the hot springs and fumaroles of the geothermal area has been conducted in the last 2 or 3 years, with the intention of performing chemical analyses. A brief description of the preliminary results is given by Torfason et al. (1983). The concentration of several gases in fumaroles has been shown to be related to the temperature of the water from which the steam boiled off and thus is an indication of the temperature of the deep geothermal reservoir (see Arnorsson and Gunnlaugsson, 1984 for summary). This applies only if the mineralogy of the rock matrix is in temperature equilibrium in the geothermal system. Several "gas thermometers" have been empirically scaled, e.g. the CO_2, H_2S, H_2, CO_2/H_2 and H_2S/H_2 thermometers. However, their application to geothermal prospecting has so far been restricted because the concentrations of these substances can be subject to alteration by processes that occur in between the steam boiling off and reaching the surface, e.g. partial condensation of the steam and oxidation of the hydrogen and hydrogen sulphide. In the Hengill area, though, good agreement has been demonstrated between the deep temperatures measured in the boreholes and the gas temperatures measured in nearby fumaroles. Fig. 2.12 illustrates the deep temperature distribution over the Hengill geothermal area according to the CO_2 gas thermometer. Three temperature highs are contoured:

a) The most extensive high (max. temp › 310° C) is centred on

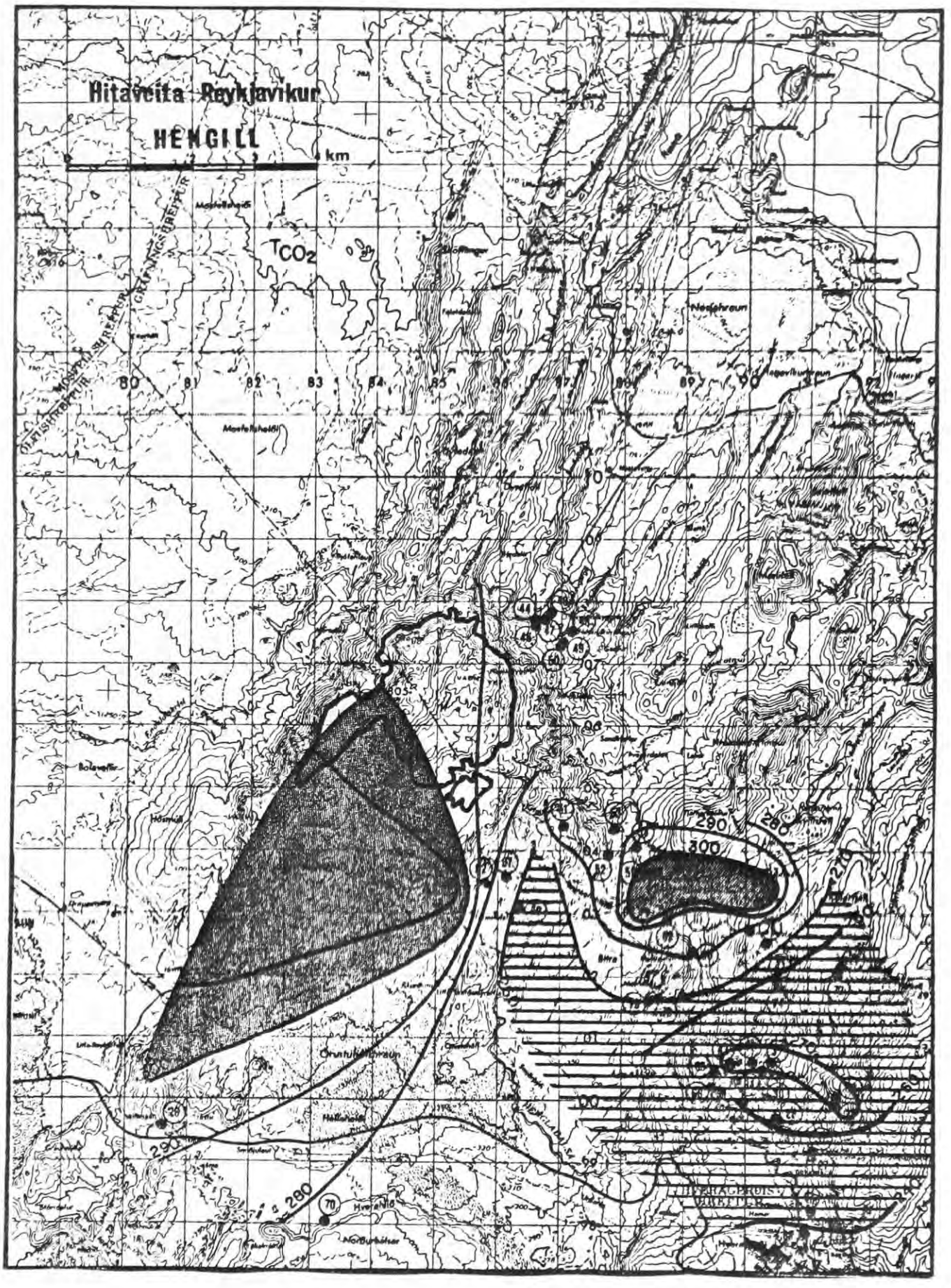

Fig. 2.12 The temperature of the deep geothermal reservoir according to the CO_2 "thermometer". Dots are sampling sites and temperature contours are in °C. (from Torfason et al., 1983). Shaded area is where $T_{CO_2} > 300°C$, cross hatched area is where $T_{CO_2} < 270°C$.

the area to the S of Hengill and is confined to the fissure swarm. Its W boundary is not defined.

b) A second, cooler and less extensive high (max. temp. 300-310°C) lies just S of Tjarnahnukur.

c) A third, even cooler and less extensive temperature high (max. temp. 270-280° C) is centred on the Grensdalur system.

Similar results are reported by Torfason et al. (1983) for the H_2S and H_2 gas thermometers. These results should be considered to be preliminary and uncorrected.

2.2.3 Summary

The suggestion of Bjornsson et al. (1974) that the Hengill area contains both an active central volcano (Hengill) and an extinct one in the area N of Hveragerdi is largely supported by more recent results. It will now be reviewed in the light of these results. It should be borne in mind that in the case of borehole measurements and the hydrological study, little or no data are available except from Nesjavellir and Hveragerdi. Conclusions drawn about the Hengill and Grensdalur systems on the basis of these data are thus extrapolations.

The surface geology and appearance of the geothermal manifestations in the topographic low immediately N of Hveragerdi are consistent with the suggestion that this area is the site of an extinct volcano and a relativly cool part of the geothermal area. At some time during the Bruhnes geomagnetic epoch volcanic activity was transferred to a site W of this volcano and large quantities of material were extruded building

up the 803 m high hyaloclastic pile Hengill. Hengill is relatively inactive compared with other Icelandic central volcanoes and only 5 postglacial eruptions are attributed to it. A 6th eruption occurred in the early post glacial period from Tjarnahnukur. The geothermal area is hottest in the proximity of Hengill and is still being replenished. Other investigations that give results consistent with this picture are as follows:

a) Resistivity studies indicate that the geothermal area is hottest beneath Hengill and in the fissure swarm to the N and S, but extends E beneath the Grensdalur area at shallow depths. Magnetotelluric studies indicate that a molten basaltic layer at the crust/mantle interface is shallowest beneath the fissure swarm.

b) The raw results of a gravity and an aeromagnetic survey indicate that distinct anomalies of opposite sign are associated with the Hengill and the Grensdalur systems.

c) Hydrological studies indicate that the deep circulation system in the area of the Grensdalur volcanic system is distinct and independent of that of the Hengill volcanic system.

d) Borehole measurements indicate that the geothermal field at Nesjavellir is hot, though peripheral, and has been subject to recent heating up. Near Hveragerdi the field is also peripheral, but cooler, and with a temperature gradient to the N.

e) The preliminary results of geochemical studies indicate that the geothermal area may display three separate temperature maximums, one associated with each of the Hengill and the Grensdalur systems and a third just S of Tjarnahnukur.

Recent geophysical work thus supports the theory that two central volcanoes occupy the Hengill area and also suggest that they may be associated with separate hydrological systems.

CHAPTER 3

3. PROGRAMME STRUCTURE, DATA COLLECTION AND PROCESSING

3.1 Programme structure

3.1.1 The aims of the programme

The aims were twofold:

1. To research the geothermal prospect and tectonic structure of the Hengill area using natural earthquake data augmented by explosions, and
2. To evaluate the utility of natural earthquake (passive seismic) studies as a geothermal prospecting tool.

3.1.2 Structuring passive seismological research programmes in geothermal areas

A literature survey of passive seismic studies in geothermal fields was conducted in order to assess the "state of the art" (Foulger, 1982) a copy of which may be found in the pocket at the back of this thesis. It emerged that many studies have been reported, using recordings of local, regional and teleseismic earthquakes made in areas of interest, sometimes augmented by explosions. Various different project designs and processing methodologies for dealing with different types of data were described. Much of the work, however, was of the "pilot project" type, involving small numbers of stations deployed for very short periods, sometimes with little or no foreknowledge of the seismicity of the area of interest. It was

concluded that much of the work done had suffered from poor programme design, but that in a number of instances natural earthquake studies had given useful information about geothermal prospects. No one "composite" study had been reported, designed to collect diverse data and apply the full spectrum of processing methodologies.

It is clear that a meaningful passive seismological research programme in a geothermal area should consist of four phases:

Phase 1 Survey of all pre-existing seismic data from the area.
Phase 2 Pilot field project, reduction of data.
Phase 3 Main field project, reduction of data.
Phase 4 Ongoing monitoring.

The design of each phase and indeed whether or not it is undertaken should be decided on the basis of the results of the previous phase(s). Field projects should be structured to optimise the collection of data of various types to enable the application of as many different processing techniques as possible. Continual comparison should be made with the results of other geoscientific investigations.

Following this plan should ensure that any investment made in this type of research is based on a clear understanding of the expected returns, an aspect important to consider in natural earthquake studies, and that those returns be maximised.

The seismological research programme of the Hengill area followed the plan outlined above closely. It was hoped that by running a programme such as this, based on sound theoretical and

practical background research, and specifically aimed at geothermal research, the value of the method as a prospecting tool could finally be fairly evaluated.

3.1.3 The structure of the Hengill seismological research programme

Phase 1 1978 - 1979

All data available were examined, including reports of historic destructive events and data recorded on the regional seismograph network. The locations of the instruments of this network are shown in Fig. 3.1 and tabulated in Appendix 3. A broad picture of the spatial and temporal nature of the local seismicity emerged (Foulger and Einarsson, 1980).

Phase 2 1979 - 1981

On the basis of the results from Phase 1 a short (4 month) pilot field project was designed and conducted in 1979. Four additional temporary drum seismographs were deployed to augment the two permanent stations in the area. They were located in and around the most seismically active part of the area in order to enable accurate hypocentral determinations (HN, HG, HH, HB, Fig. 3.1). These 4 temporary stations were later made permanent. With the addition of the results from this phase the pattern of activity in the Hengill area became fairly clear (Foulger, 1981).

Phase 3 1981 - 1984

On the basis of the results of Phases 1 and 2 the main field project was designed involving the deployment of a dense seismometer network for a 4 month period in 1981.

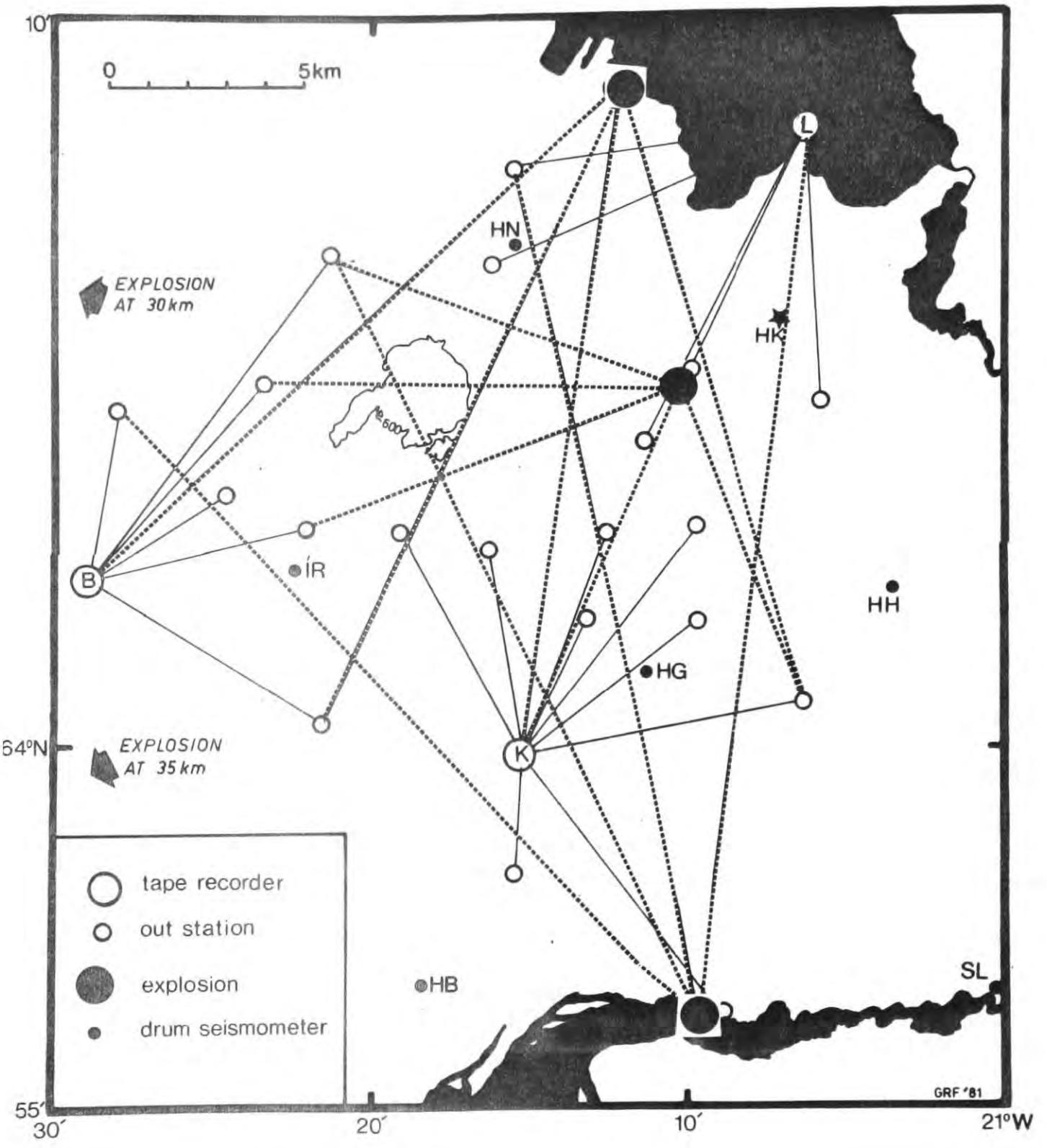

Fig. 3.1 Map of the Hengill area showing locations of the stations of the radio telemetered network and explosions. Ray paths from the explosions to the stations of the fan arrays are shown, and also radio transmission beams. Tape recorder stations are Blakollur (B), Kambar (K) and Lambhagi (L).

A radio telemetered network of 23 stations recording on magnetic tape (geostore equipment) was made available to the programme by the NERC, U.K. It was calculated that the deployment of a network of this size for one summer would provide data sufficient for a study of the spatial and temporal distribution of local earthquakes, frequency-magnitude relationships, focal mechanisms and teleseismic delay times. Local and regional explosions were also planned that would provide data for a study of lateral and vertical velocity variations. This network augmented the network of 7 stations that was already installed in the area (Fig. 3.1). Station locations are tabulated in Appendix 3.

The network was centred on the most seismically active part of the area and its diameter made about three times the expected average hypocentral depth. Station coverage was fairly uniform but slightly denser in the middle. This network geometry enabled accurate locations to be calculated, especially hypocentral depths, and gave good constraint for focal mechanism solutions. Whilst maintaining this broad design, deviations were made for the following reasons:

1. 13 of the stations were deployed to form equidistant fan arrangements around the shot points. Such arrangements would yield arrival time delay and spectral data that would not have to be corrected for distance.
2. Line of sight had to be maintained between the transmitting and receiving aerials, therefore station coverage was poor in the neighbourhood and to the NE of Hengill and in the E, SE and SW of the area.

Phase 4 1984 -

Further monitoring.

3.2 Data collection

3.2.1 The entire data set

The study of local earthquake activity presented in Chapters 4-5 is based on data available concerning the seismicity of the Hengill area since the year 1700. The data are grouped as follows:

1. 1700-1983	historic macroseismic data
2. 1930-1983	data recorded at the regional station REY (Reykjavik) (Fig. 2.1)
3. Aug.1974-June 1981	data recorded on the regional seismograph network, which was occasionally augmented by additional temporary local instruments (the "drum data" set) (Fig. 2.1)
4. July.12-Oct.9 1981	data recorded on the radio telemetered network which augmented the regional seismograph network, (the "tape data" set) (Fig. 3.1)

Data groups 1-3 are "inhomogeneous" i.e. detection threshold and location accuracy did not remain constant (but usually improved) throughout the recording periods.

The teleseismic and explosion data discussed in Chapter 7 were collected on the radio telemetered network.

3.2.2 Historic macroseismic data

These were assessed by Sv. Bjornsson (pers. comm.). Documentation, and hence location and magnitude assessment, improved with time. The data group is considered to be complete for $M_{REY} \geq 6.0$ for the 283 year period studied (see Section 5.2.2.1 for definition of M_{REY} [$M_{REY} \simeq M_s$]).

Location of events in this group are based on reports of felt intensities and are only accurate to within ten km. The data set contains 3 or 4 events.

3.2.3 Data recorded at the regional station REY (Reykjavik)

The station REY has response characteristics similar to the WWSSN stations. It is a 2 component set. The N instrument is a Sprengnether set at $T_s = T_g = 1.5$ sec and the Z instrument is a Willmore set at $T_s = 1$ sec, $T_g = 0.25$ sec. Recording is analogue on light sensitive paper at speeds of 30 and 60 mm min^{-1} respectively.

Event locations were obtained from the station bulletins, from Tryggvason (1978a, b; 1979) and from Ragnar Stefansson and Thorunn Skaftadottir (pers. comm.) of the Icelandic Meteorological Office. The instrumentation at REY was occasionally modernised during the period 1930-1983. Sensitivity and hence detection threshold thus progressively improved. The data set is probably complete for $M_{IL} \geq 3$ for the 53 year period considered (see Section 5.2.2.1 for definition of M_{IL} [$M_{IL} \simeq M_s$]). The data set contains 116 events.

3.2.4 Data recorded on the regional seismograph network

The instruments comprising this network consist of vertical, short-period geophones (natural frequency 2-3 Hz) and paper drum recorders inscribing with pen and ink at a speed of 90 mm min^{-1}. Arrival times were read by hand from the seismograms to an accuracy of 0.1 sec.

The whole network consists of about 40 stations at the time of writing. Of these about 25 provided data for this programme, and 4 lie within the study area. The stations IR (IR skali) and SL (Selfoss) were operational for the whole programme period (Fig. 3.1). In addition four temporary stations were available and were deployed intermittently at HG (Gufudalur), HH (Stori-Hals), HN (Nesjavellir) and HB (Bjarnastadir at Hjalli). These stations were first occupied for 4 months in the summer of 1979 during the pilot field project. In late 1980 semi-permanent stations were installed at these locations (Fig. 3.1). In addition to these drum recorders, a station was operated at HK (Krokur) for part of the time. It consisted of a 3 component set of Willmore Mk II seismometers with natural period adjusted to 1 sec. Recording was analogue on 1/4" magnetic tape. This station was loaned by Dept. of Geological Sciences, University of Durham, U.K. Tapes were played back on the processing system at Durham and paper records of events were written using a 16 channel Siemens ink jet pen. Arrival times were read by hand to an accuracy of 0.01 sec and contributed to the computer locations.

Detection threshold and location accuracy is very variable within this data group because of the variability in station

coverage. Fig. 3.2 illustrates the station coverage that was achieved within the Hengill area. The data set is complete for $M_{IL} \geq 2.0$ for the whole period, but a location threshold as low as $M_{IL} = 0.3$ was achieved when 7 stations were operated within the area.

Computer locations were calculated for this data set (see Section 3.3.1). Both P- and S-wave arrival times were used. S-wave and poor P-wave arrival times were given half weight since they could typically be read to an accuracy of only 0.2 sec. These computer locations typically involve 5-10 arrival times, and are likely to be accurate to 1-2 km. The data set contains 1040 events.

3.2.5 Data recorded on the radio telemetered network

3.2.5.1 Instrumentation

Tape Recorders

Three "Geostores" were used, recording analogue signals on 14 channel 1/2" magnetic tape at a speed of 15/320 in sec^{-1}. This gave an upper cut-off frequency of 32 Hz. One channel recorded time code generated by an internal crystal clock, flutter compensation signals were recorded on two channels, and the MSF radio time signal was recorded on a fourth channel. The remaining 10 channels were available on each recorder for recording seismic signals.

Seismometers

23 Willmore Mk III vertical seismometers were used, with natural period adjusted to 1 second. Each was paired with an

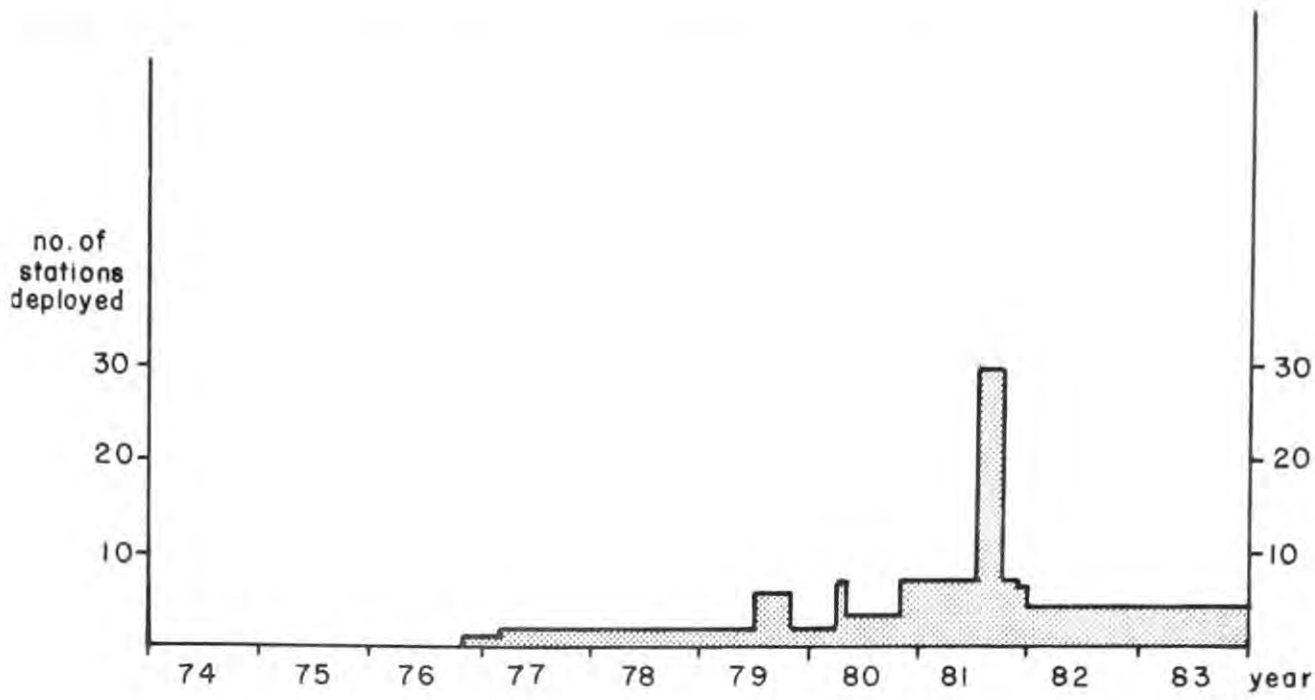

Fig. 3.2 Station coverage achieved in the Hengill area 1974-1983

amplifier-modulator and calibrated in the U.K. before shipment. The instruments were not calibrated for frequency response in the field.

Radio links

20 radio links were deployed. They transmitted on 458-459 MHz at 0.025 MHz intervals. Each consisted of a transmitter, a receiver and a pair of UHF aerials.

Test Boxes

Two types were used. The Mk I type had both audio and visual (paper playout) displays, and was heavy. The Mk II type had audio display only but was light. The test boxes could be connected to the amplifier-modulator, the radio receiver or the tape recorder, to check the functioning of particular stations.

Replay equipment

A 7 channel Siemens ink jet pen inscriber, a 14 channel "store 14" playback tape recorder, an automatic time code

decoder and a stereo audio playback set were used to monitor recording throughout the field season.

3.2.5.2 Field logistics

A detailed description of the fieldwork is given in Appendix 1 and summarised here.

20 radio telemetering outstations and 3 recording stations were established, all seismometers being housed in holes dug down to bedrock. 1.5 m high masts accomodated the radio aerials and power was supplied by portable lead acid batteries.

Amplifier-modulator gains of 6 or 7 were used, depending on the ambient noise conditions at each site. Tape recorders were housed in waterproof aluminium boxes.

Accessibility was difficult in the area and many stations were installed by foot. In these cases the equipment was transported either in rucksacks or by pack horse. Equipment installation took 2 people 1 month.

After commencement of recording tapes were changed at 3 day intervals and played back immediately in order to detect malfunctions as quickly as possible. Three local and two regional dynamite explosions were fired in lakes, at shot-reciever distances of 0 - 55 km. Recording was conducted for 90 days, and equipment malfunction resulted in the loss of 14% of the data.

3.2.5.3 Data playback

The tapes were played back at the University of Durham

using similar equipment to that used to monitor the tapes, but with a 16 channel jet pen. A playback speed of 3.75" sec^{-1} was used and paper records were produced on the scale 60 mm : 1 sec. About 15,000 individual paper records were made, and about 150,000 arrival times read, a process that took about 1 year.

Arrival times were read by hand to an accuracy of 0.01 sec. Station coverage during the recording period was constant, except for a few breakdowns of short duration, and hence detection threshold and location acuracy may be considered to be uniform for this data set. The data set is complete for $M_{IL} \geq -0.9$ (see Section 5.2.2.1).

P-wave arrival times only were used for the computer locations, which typically involve 10-20 readings. The reading accuracy of these data is such that the error in the locations is probably chiefly dependent on the accuracy of the crustal model used. Relocation of the local explosions indicates that epicentral locations are probably accurate to within 400 m (Section 7.2.2). The data set contains 1918 events.

The teleseismic arrival times were also read from paper records, using the wave matching technique (see Section 7.1.2) That data set contains 21 events for which 328 arrival times were measured.

3.3 Data processing

3.3.1 The hypocentre locator and plot computer system

Earthquake locations were calculated using the programme HYPOINVERSE (Klein, 1978). This programme calculates hypocentres and origin times by minimising the root mean square of the P- and S-wave travel time residuals. It uses a velocity structure which involves layers with linear velocity gradients (see Appendix 4).

HYPOINVERSE is installed in the University of Iceland VAX/VMS machine, and is used in conjunction with the earthquake Hypocenter Locator and Plot System (HLPS). HLPS is a system of user utilities that facilitates file editing, data handling, the running of Fortran programmes and data archiving. It also contains plotting utilities (EMAP, DMAP, TMAP) that plot epicentral maps and depth and temporal profiles, and the utility BVALUE that plots magnitude-frequency diagrams and calculates b-values. HLPS was designed by G. Foulger. It was originally written by M. Olafsson and G. Foulger for a PDP 11/60 RT-11 computer (Foulger and Olafsson, 1980a, b). The present version is an adaption made by M. Olafsson of this original version for a VAX/VMS computer. EMAP, DMAP and TMAP were written by T. Gunnlaugsson and G. Foulger and BVALUE was written by B. Skulason. HLPS is documented in a HELP facility in the Universty of Iceland VAX/VMS computer, and briefly here in Appendix 2.

3.3.2 The teleseism computer utilities

The programme HYPERMAP, supplied by Dr. D.H. Tarling, University of Newcastle, was used to plot a map of world coastlines and teleseism locations in Mercator projection centred on Hengill (Fig. 7.1).

The programme MANETA (Savage, 1979) was used to calculate theoretical arrival times for the P- and PKP-waves of the teleseisms at the Hengill stations. This programme reads in station and hypocentral co-ordinates, references the Herrin travel time tables (Herrin, 1968) and applies corrections for the earths ellipticity and the stations height above datum.

The programme SEPD (Savage, 1979) was used to calculate individual station delays from the raw delay times measured for a number of teleseisms. This programme solves, in a least squares sense, the set of overdetermined simultaneous equations relating delay times to station delays and error terms (see Section 7.1.2).

These three programmes are currently installed in the NUMAC IBM system at Durham University.

CHAPTER 4

4. LOCAL EARTHQUAKES: SPATIAL DISTRIBUTION

4.1 The historic macroseismic data

The events in this group may be listed (Tryggvason, 1973; Sv. Bjornsson, pers. comm.):

M_{REY}	Year	Day	Latitude	Longitude
6-6.5	1706	20.4	63° 58.1′	21° 13.6′
(6-6.5	1789	10.6	64° 00.0′	21° 26.6′)
6.0	1896	6.9	63° 58.1′	21° 13.6′
6.0	1935	9.10	64° 00.0′	21° 30.0′

The event of 1789 was a large earthquake swarm that activated at least 30 km of the fissure swarm passing through Hengill, and not a single large shock (Thoroddsen, 1899). The energy release of the whole sequence was equivalent to one magnitude 6 - 6.5 event (Tryggvason, 1973).

The events of 1706 and 1896 are located in the centre of the Olfus lowlands, where population was dense enough to definitely constrain the epicentres to be south of 64° N. The event of 1935 is less well constrained because it occurred in an area of sparse population. The location quoted above for this event was calculated using data from 86 world wide stations (Tryggvason, 1978a).

The main point that emerges, however, is that all 3(4) of these events are located on or south of the 64° line of

latitude, and are hence probably not related to the geothermal field. As will be seen below, this picture is in stark contrast to that which emerges from a short-term study of small magnitude events.

4.2 Data recorded at the regional station REY

This station is about 35 km from the centre of the Hengill area. Events in this group were rarely recorded at any other station, and epicentres cannot be located more accurately than to permit association with the Hengill area. Study of this data group was hence limited to magnitudes and temporal distribution, which are discussed in Chapter 5.

4.3 The computer locations

4.3.1 Presentation of the data

Computer hypocentral locations were calculated for events recorded on the regional seismograph network and the radio telemetered network. These two data sets will be discussed together in this Chapter.

The natures of these two data sets are very different. The tape data set is far superior to the drum data set in terms of number and accuracy, and represents a low magnitude range (mostly $-3 \leq M_{IL} \leq 2.2$) and short recording period (3 months). The drum data set, on the other hand, represents a much longer recording period (7 years) and contains events of higher magnitude (mostly $0 \leq M_{IL} \leq 4.2$). The tape data set thus contains events that correspond to movements on fault lengths of the order of metres whereas the drum data set contains events that correspond to movements on fault lengths of the order of tens of metres. For these reasons they will be presented separately in the Figures. They will be referred to as the "drum data" and the "tape data" respectively.

These two data sets together contain almost 3000 events. The data are 6-dimensional (space, time, magnitude and accuracy) and are presented in Figs. 4.1 - 4.15 as a series of 2-dimensional plots. In order to produce these plots it was necessary to qualitatively decide the plotting constraints. This implies an inherent difficulty encountered in interpreting the data i.e. are the features delineated by the data being enhanced by the constraints used, or are they being produced by

them? As a rule series of plots were made, progressively constraining the data. Spurious epicentral and hypocentral patterns were identified as those that were heavily dependent on the selection criteria.

The spatial constraints imposed are indicated in Figs. 4.1 - 4.15. No time or magnitude constraints were imposed inside the tape or drum data sets: the presentation of them seperately may to some extent be regarded as the presentation of different magnitude groups and time periods (see above). Events were selected for location accuracy within the two data sets, however. The following parameters were constrained:

GAP: The largest azimuthal gap between azimuthally adjacent stations.

ERH: The horizontal error in km, defined as the greatest length of the horizontal projection of the 32% error ellipsoid. (The earthquake has a statistical probability of 32% of lying inside this ellipsoid of error).

RMS: The final root mean square traveltime residual, computed after residual weighting.

ERZ: The vertical error in km, defined as the greatest length of the vertical projection of the 32% error ellipsoid.

To obtain accuracy in the hypocentral depth of an event, comparable to that in the horizontal plane, stations very close to the epicentre are required. Hence additional parameters were constrained in selecting the hypocentral data. These were:

no. arrival times: minimum number of arrival times used for the location

dist/depth: the ratio of the horizontal distance to the nearest station used in the location to the hypocentral depth. Constraining this parameter limits possible selected locations to cone shaped zones beneath each station. However examination of the total data set showed that very few hypocentres were located outside these cones.

These constraints were selected on a trial basis. The aim was to have the effect of "focusing" a picture that would otherwise be "blurred" by a scatter of poorly located events.

In order to make some distinction between data of differing accuracy, the drum and tape data sets were each divided into "epicentral data" and "hypocentral data", the latter being selected for accuracy in the depth determination, and the former for accuracy in the epicentral determination only.

The constraints imposed were:

<u>epicentral data</u>:

	drum data	tape data
GAP	$\leq 180^{\circ}$	$\leq 180^{\circ}$
ERH	$\leq$ 2.5 km	$\leq$ 1.0 km
RMS	$\leq$ 0.15 sec	$\leq$ 0.10 sec
ERZ	$\leq$ 99.0 km	$\leq$ 99.0 km

hypocentral data:

	drum data	tape data
GAP	$< 180^{\circ}$	$< 180^{\circ}$
ERH	< 1.3 km	< 1.0 km
RMS	< 0.15 sec	< 0.10 sec
ERZ	< 2.2 km	< 2.0 km
no. arrival times	> 8	> 12
dist/depth	< 2.0 km	< 2.0 km

4.3.2 The seismicity in detail

4.3.2.1 The central cluster

The main epicentral area of activity lies approximately 5 km NW of Hveragerdi (64°N00′, 21°W10′), and coincides with the area most abundant in hot springs and fumaroles (Figs. 4.1 - 4.4, 2.4). A topographic low formed by three NS trending river valleys (the Grensdalur low - see Fig. 2.3) occupies a large portion of the area of the cluster. The activity does not extend as far south as Hveragerdi.

Examination of the drum data epicentral distribution (Fig. 4.1) shows that activity in this area exhibits two trends:

1. NW striking trend.
2. NE striking trend. These trends intersect at an angle of about 90°. As is seen with other features, this tendency becomes clearer if the most accurately located events are selected. (Fig. 4.3).

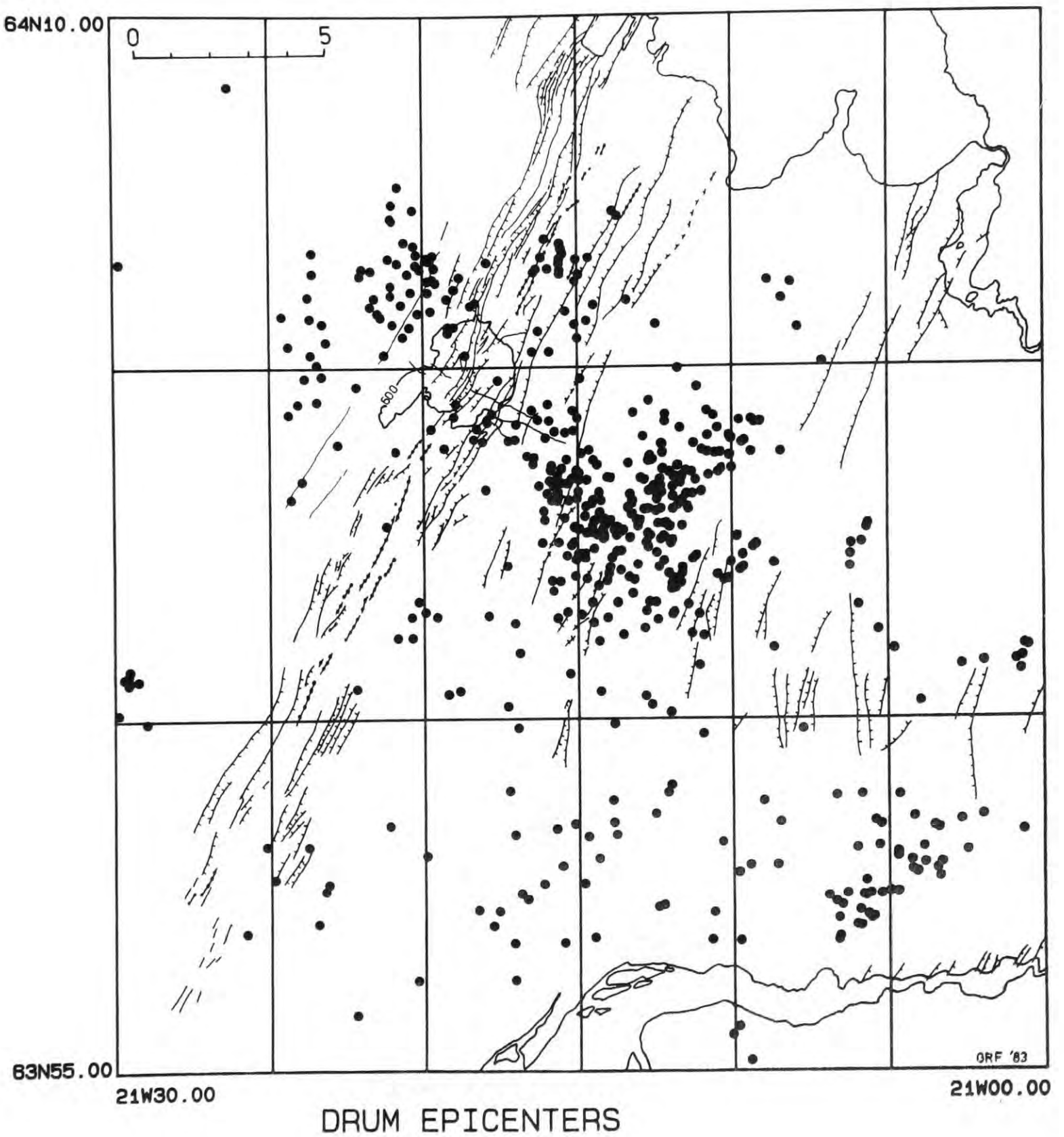

Fig. 4.1 Drum data epicentres.

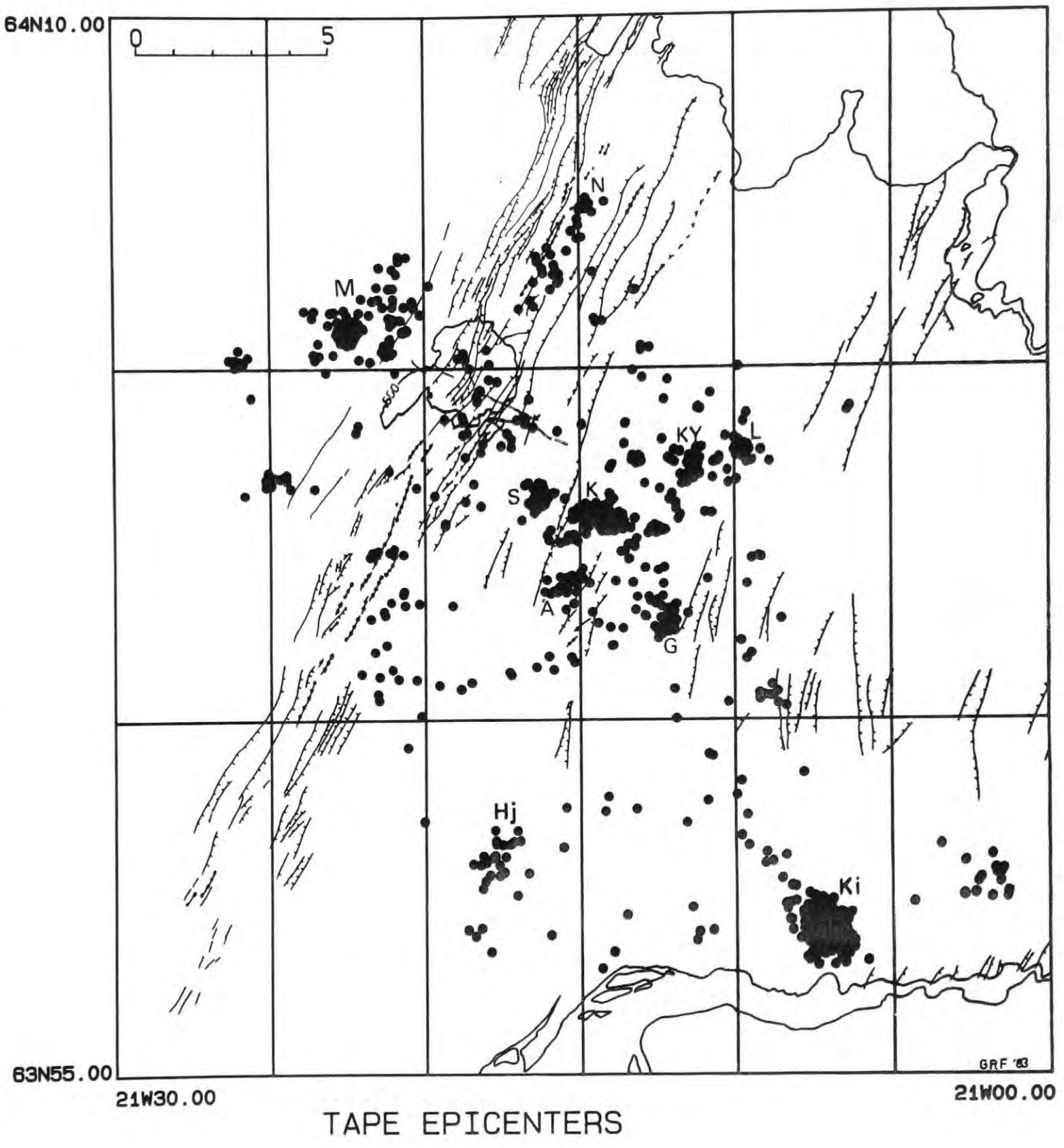

Fig. 4.2 Tape data epicentres. Subclusters discussed in the text are labelled.

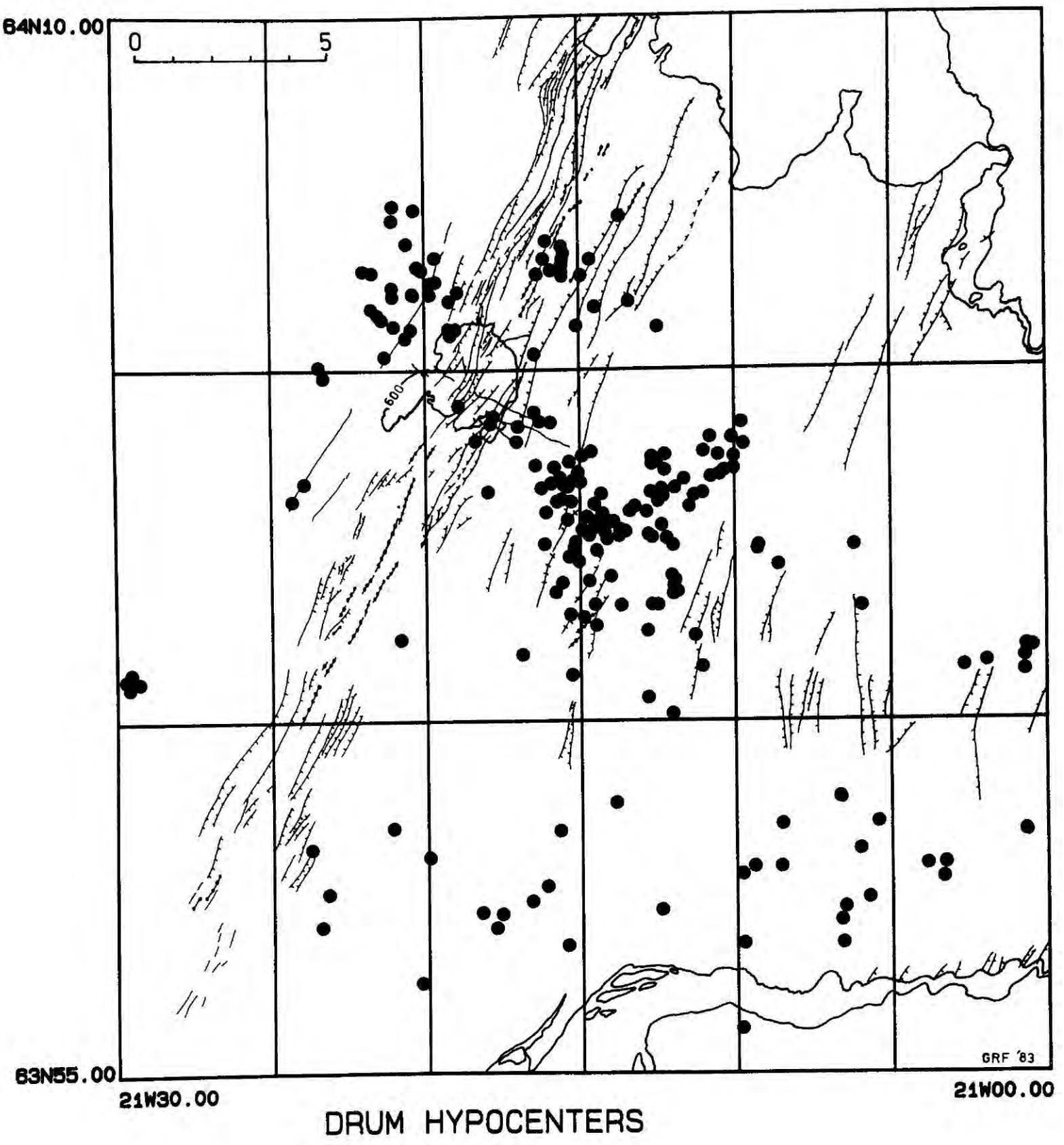

Fig. 4.3 Drum data hypocentres.

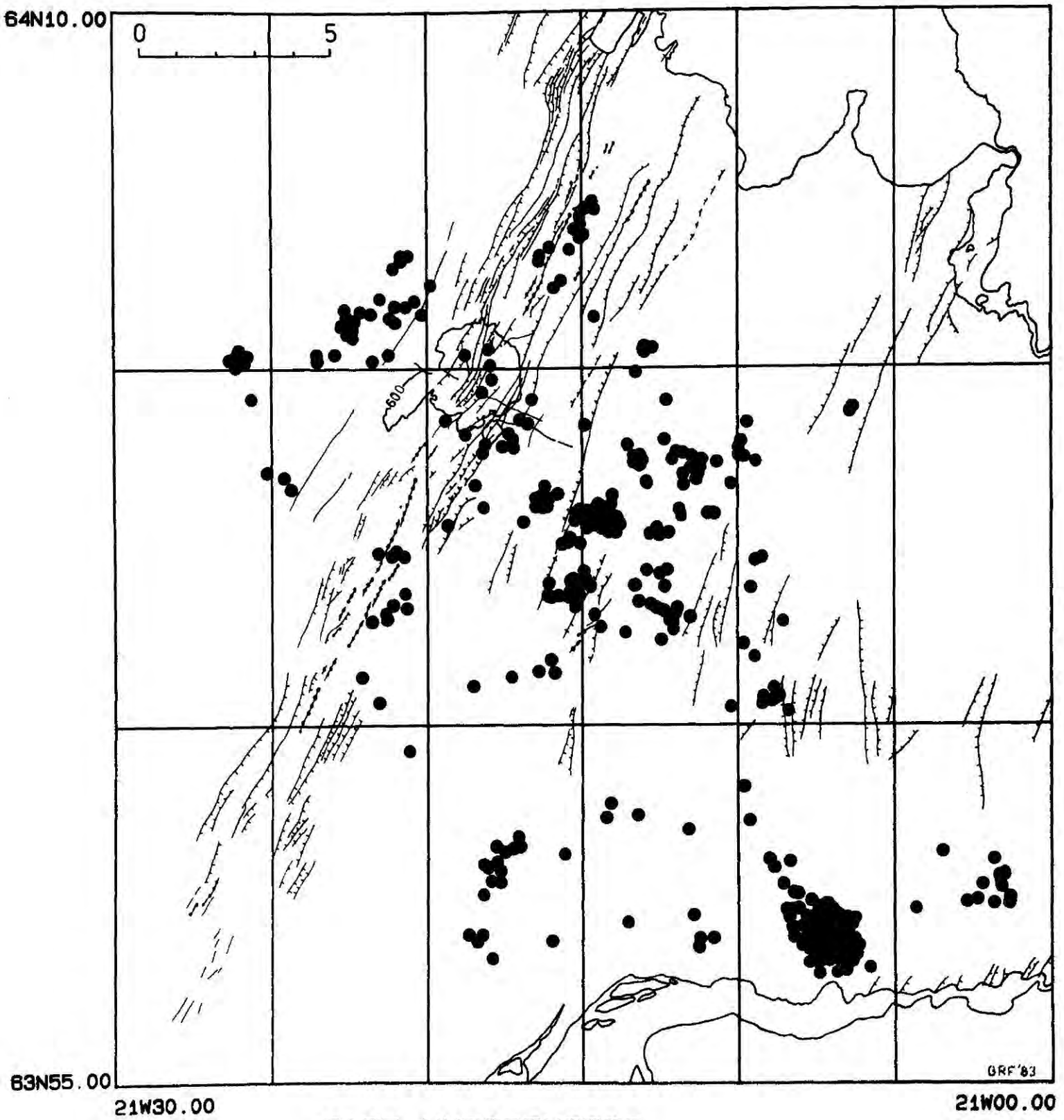

Fig. 4.4 Tape data hypocentres.

In the tape data set (Fig. 4.2) the central cluster appears to divide up into about 6 subclusters, some of which were formed by single swarms, and others by continuous low level activity:

Single swarms	Continuous Activity
Svinahlid (S)	Grensdalur (G)
Astadafjall (A)	Kyllisfell (KY)
Laxadalur head (L)	Klambragil (K)

The Klambragil (K) subcluster is by far the largest and 90 events were located within it. The events were not grouped in time; activity stayed at a consistent level over the whole recording period. A tendency may also be observed in the drum data set (Figs. 4.1 and 4.3) for activity to be locally higher in this vicinity.

In the following discussion, cross sections are as illustrated in Fig. 4.5.

Figs. 4.6 and 4.7 are cross sections colinear with the NW striking trend observed in the epicentral distribution (MOS - REY, Fig. 4.5). These cross sections illustrate the progressive shallowing of the minimum hypocentral depth and the increase in activity as one passes from NW to SE along this trend. The hypocentres are shallowest at a distance of approximately 13 km along the sections in both data sets, i.e. in the region of the Grensdalur (G) subcluster. Some doming of the seismically active zone in the central cluster is thus displayed. A shallowing of the maximum depth of activity is also apparent in the drum data of Fig. 4.6. On the tape section of Fig. 4.7 the dominant Klambragil (K) subcluster, about 10 km along the

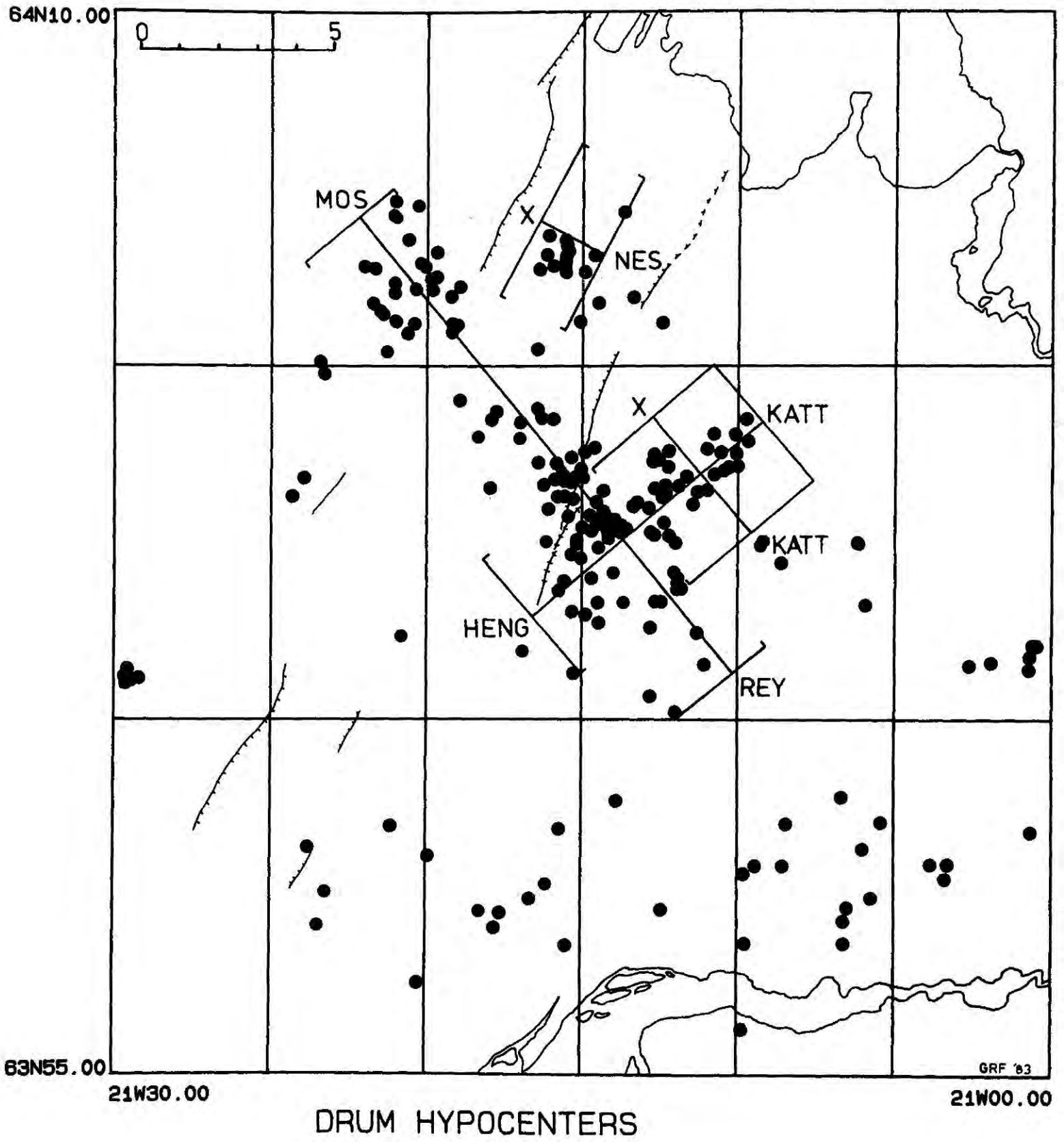

Fig. 4.5 Drum data hypocentral map showing the locations of cross sections presented in Figs. 4.6 - 4.11 and 4.13. Brackets indicate the width of the cross sections.

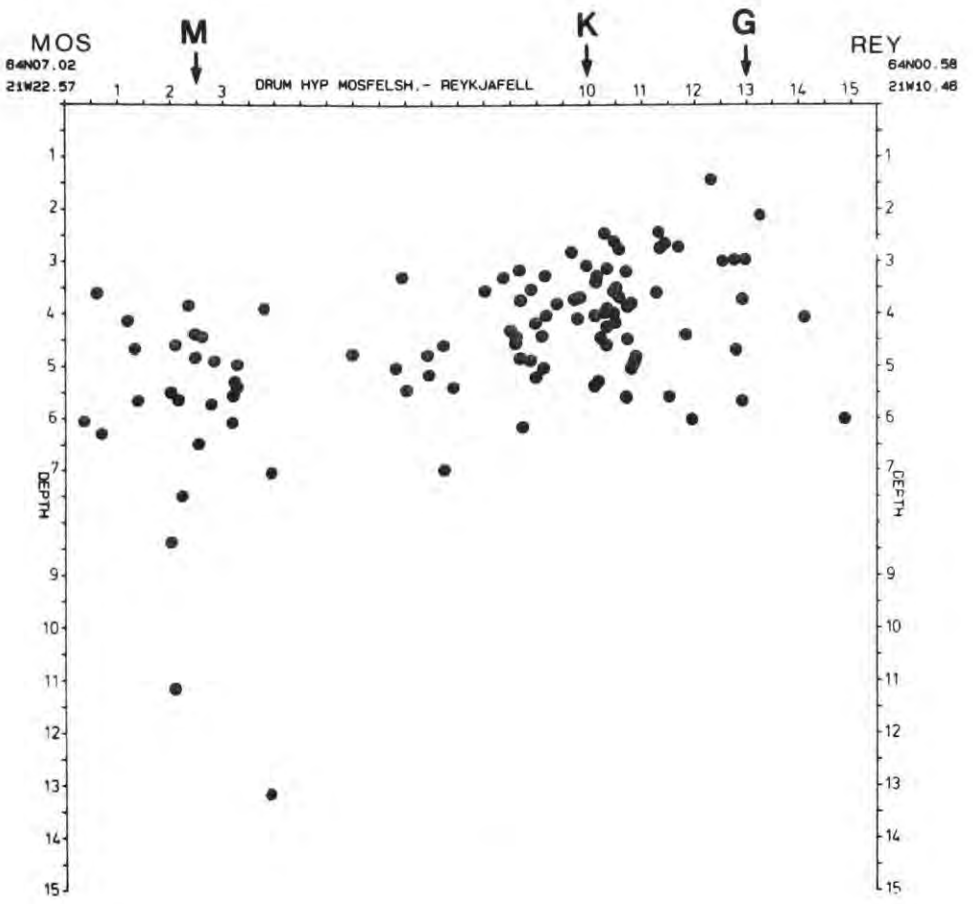

Fig. 4.6 NW-SE cross section Mosfellsheidi Reykjafell. Drum data. Letters correspond to subclusters discussed in the text.

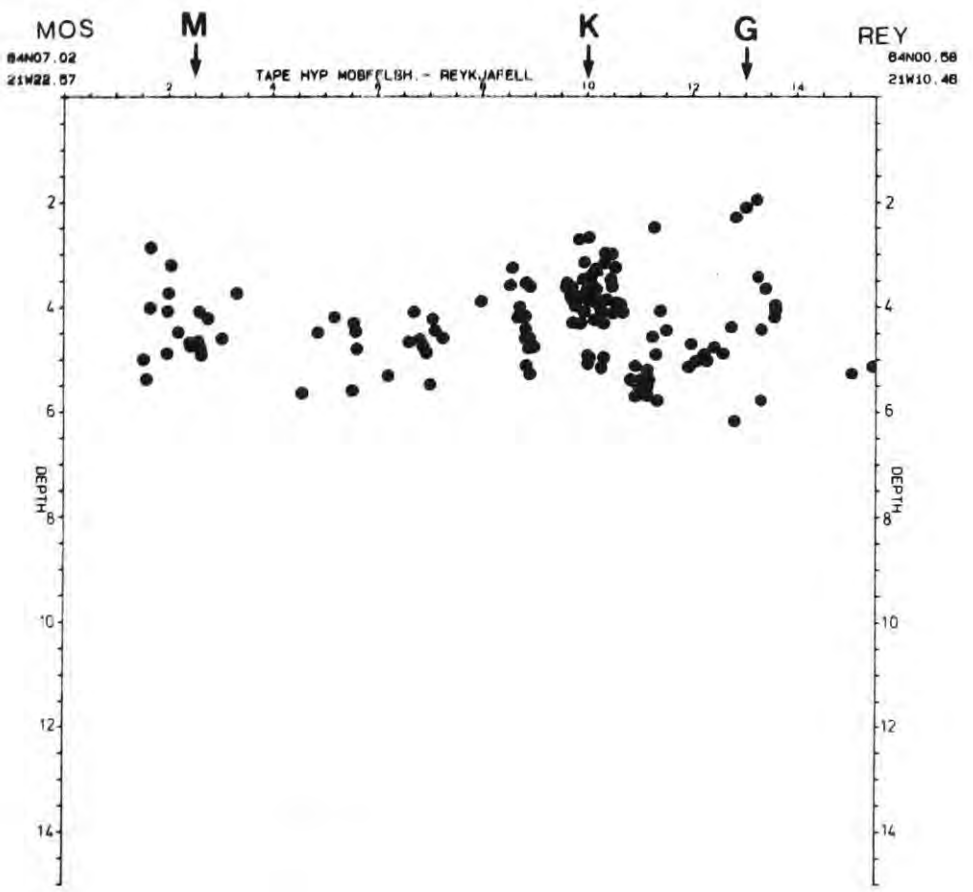

Fig. 4.7 NW-SE cross section Mosfellsheidi - Reykjafell. Tape data. Letters correspond to subclusters discussed in the text.

section, is very obvious, and enhanced activity is also visible in this region on the drum data cross section (Fig. 4.6).

Figs. 4.8 and 4.9 are corresponding SW-NE cross sections across the central cluster (HENG - KATT, Fig. 4.5). It may be noted that the left hand parts of these cross sections are transverse sections of the NW-SE trend, and the right hand parts are longitudinal sections of the SW-NE trend. Both sections show a higher level of activity in the region of the NW-SE trend than in the SW-NE trend. There is also some slight suggestion in the data that the NW-SE trend of hypocentres displays a zone with a SE dip. The doming of the seismic zone noted in Figs. 4.6 and 4.7 is also apparent in Figs. 4.8 and 4.9. Activity is shallowest about 3 km along the profiles, at the location of the Klambragil (K) subcluster.

Figs. 4.10 and 4.11 are NW-SE cross sections (X-KATT, Fig. 4.5) across the SW-NE trend. These sections indicate that the events occupy the depth range 2 - 6 km and that the dip of the active zone is less than 10^{o}.

4.3.2.2 Nesjavellir

The epicentral distribution of events in Nesjavellir (Fig. 2.3), N of Hengill, clearly displays a linear trend (Fig. 4.12). The fault dissected hills to the E and W of the epicentral trend were not very active in the recording period. The trend strikes at N 25^{o} E, is parallel to the fissure swarm, and forms a continuation of a row of hot springs that extends up onto the E slopes of Hengill.

Fig. 4.13 is a WE cross section of these events (Section X

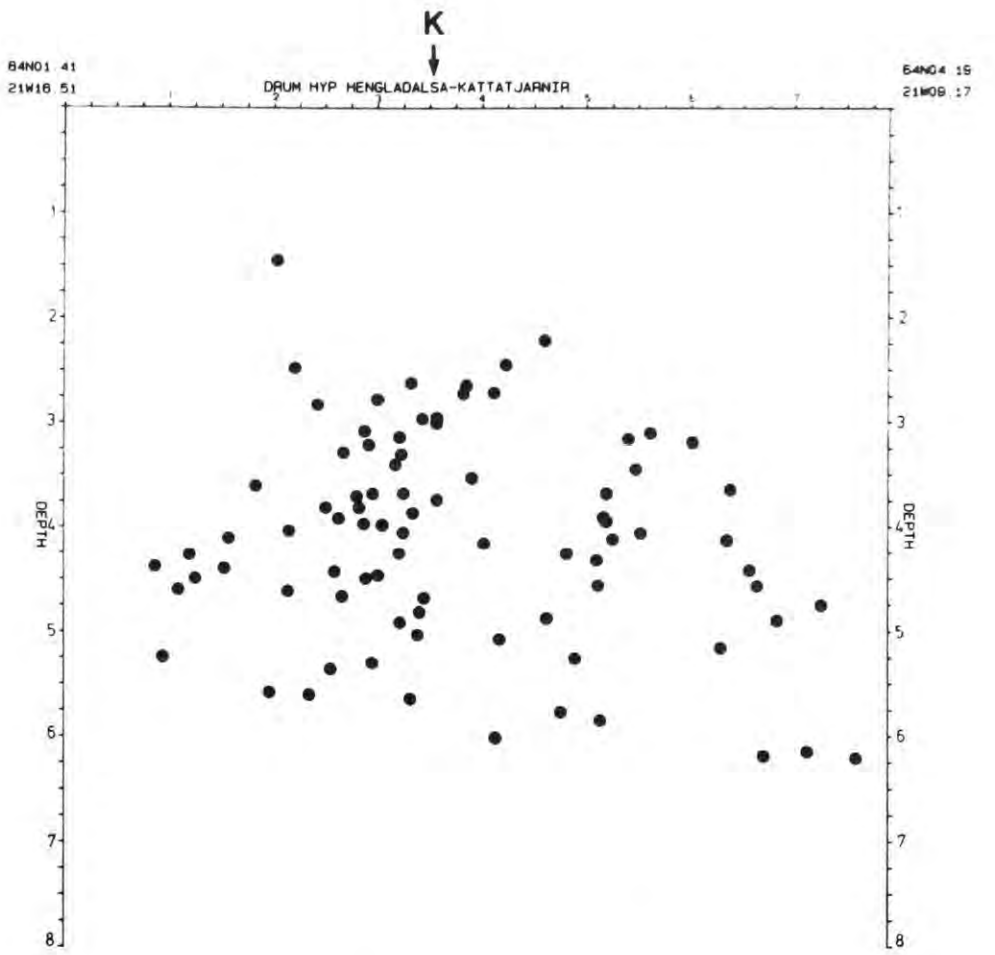

Fig. 4.8 SW-NE cross section Hengladalsa - Kattatjarnir. Drum data. K = Klambragil.

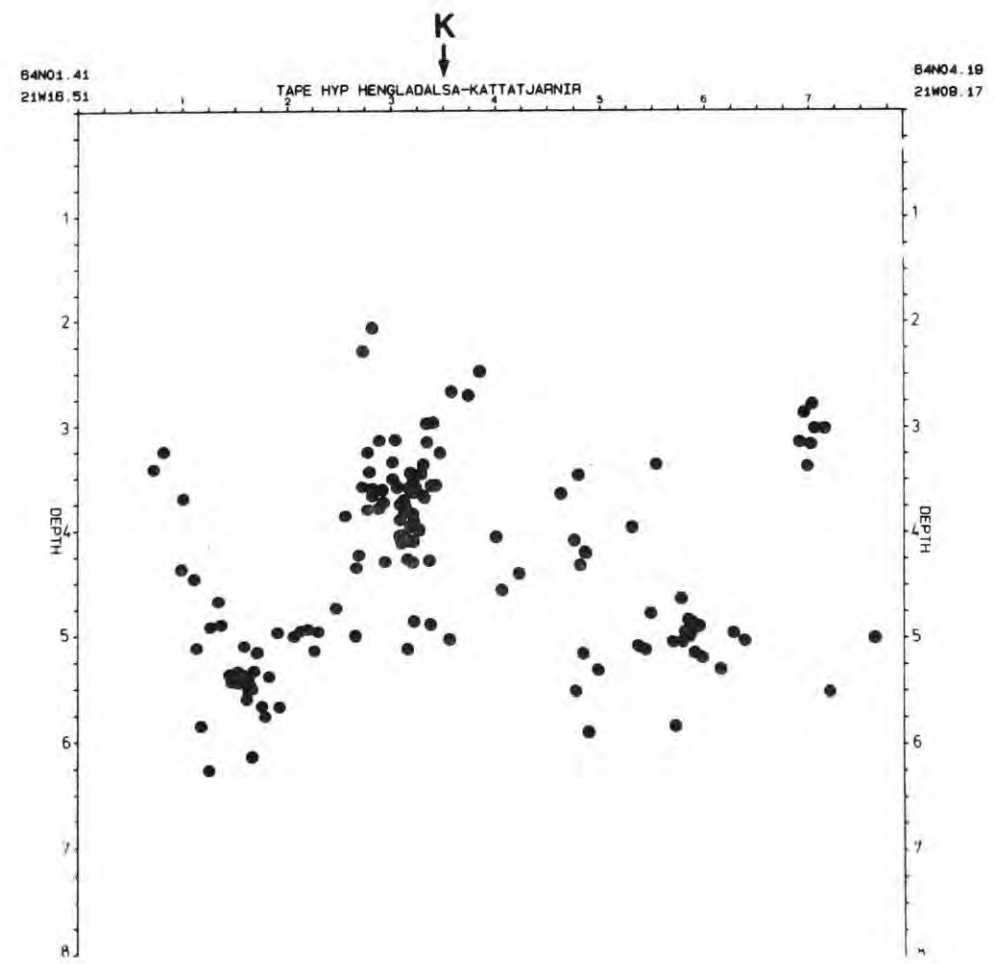

Fig. 4.9 SW-NE cross section Hengladalsa - Kattatjarnir. Tape data. K = Klambragil.

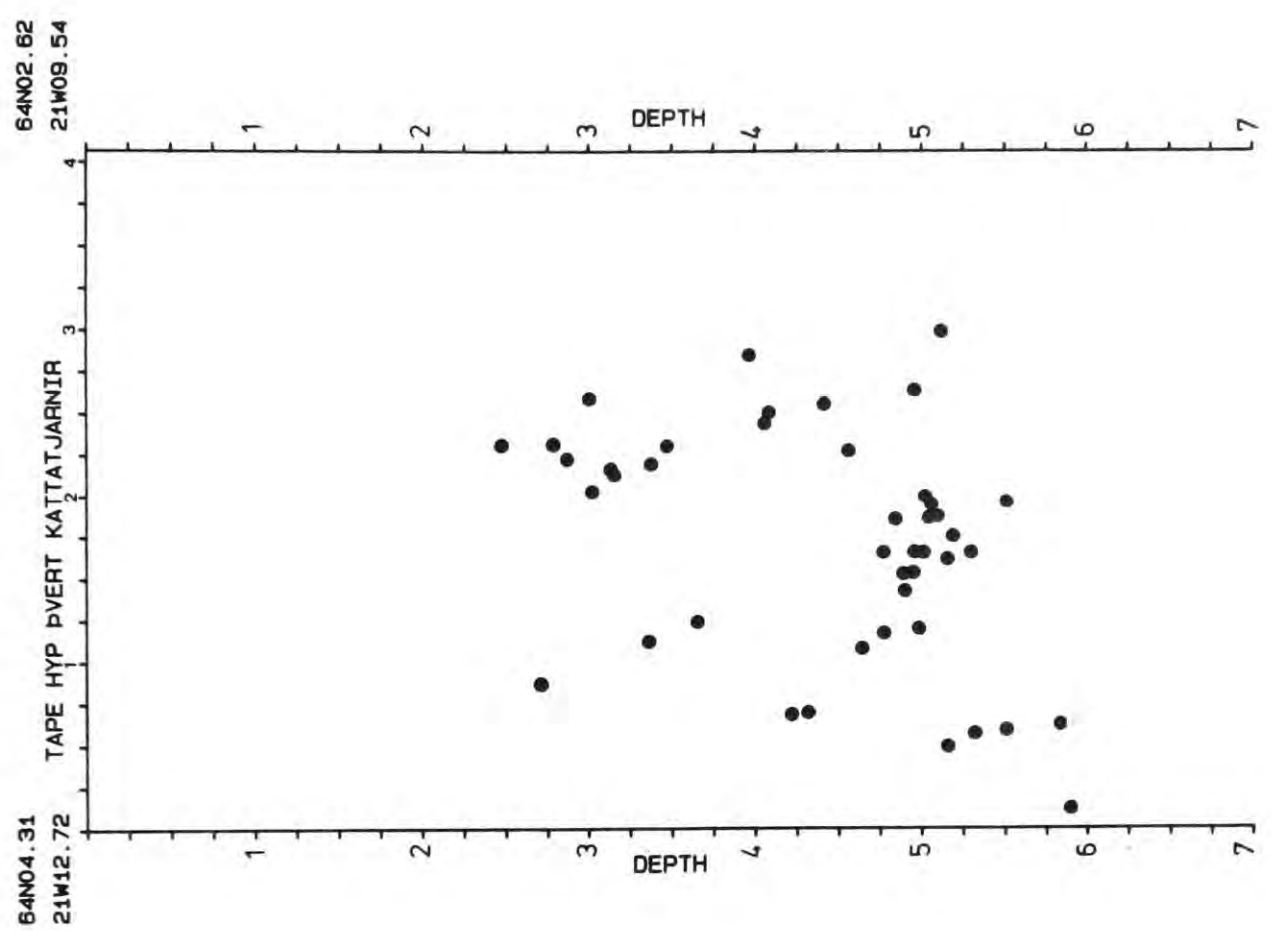

Fig. 4.11 NW-SE cross section across Kattatjarnir. Tape data.

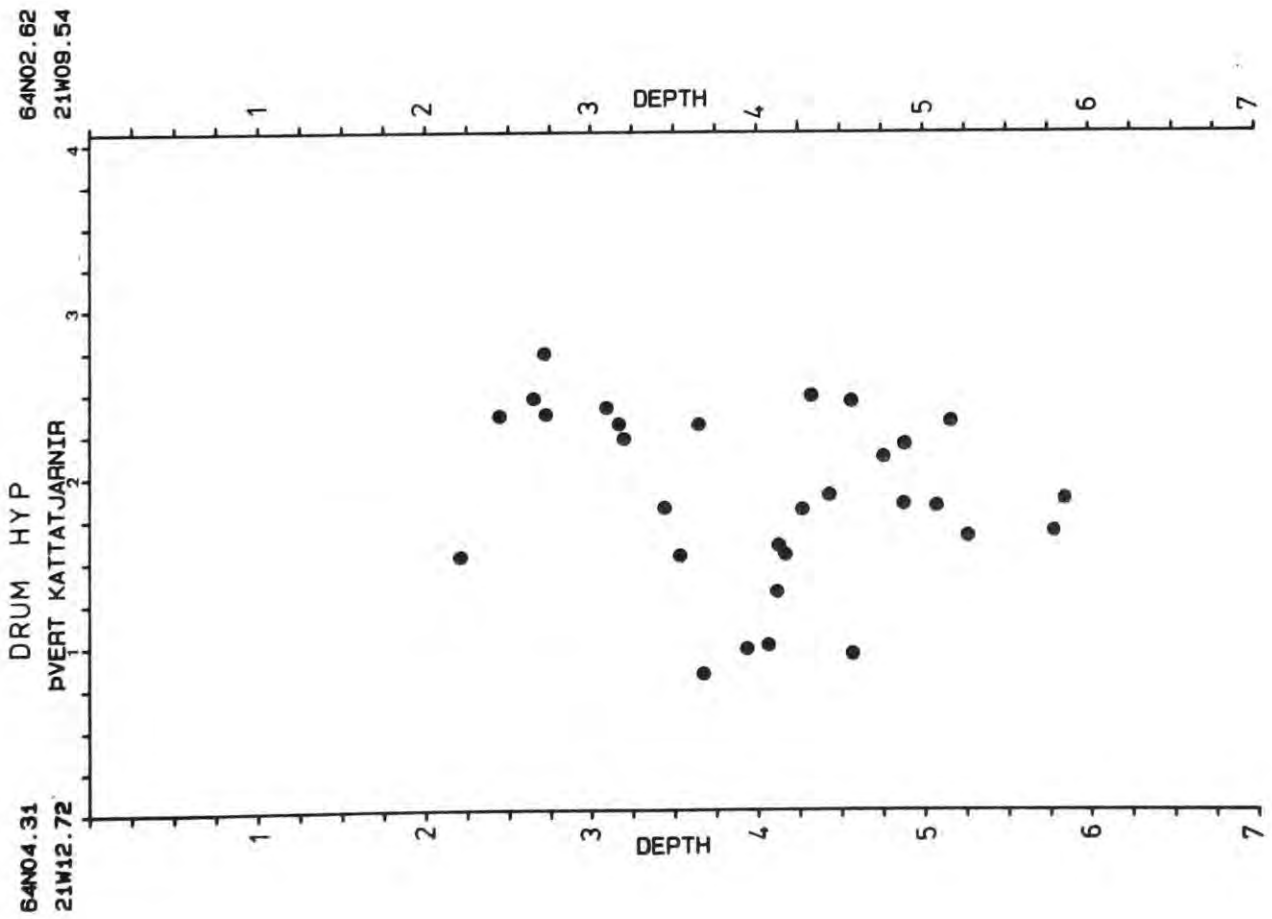

Fig. 4.10 NW-SE cross section across Kattatjarnir. Drum data.

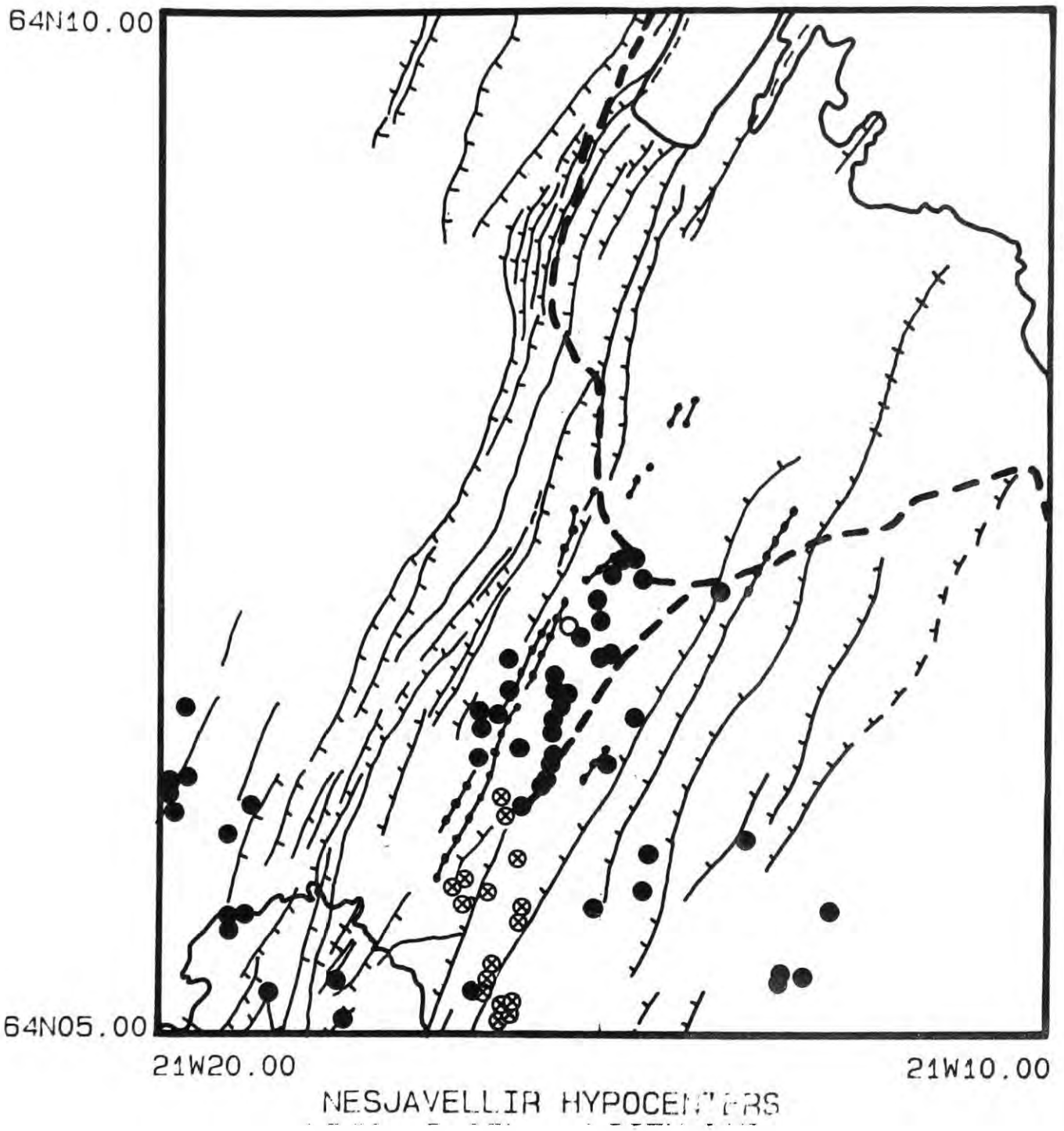

Fig. 4.12 Hypocentres located in the Nesjavellir area N of Hengill. Drum data and tape data. ● earthquake epicentres, ⊗ hot springs and fumaroles, O Nesjavellir drum seismograph.

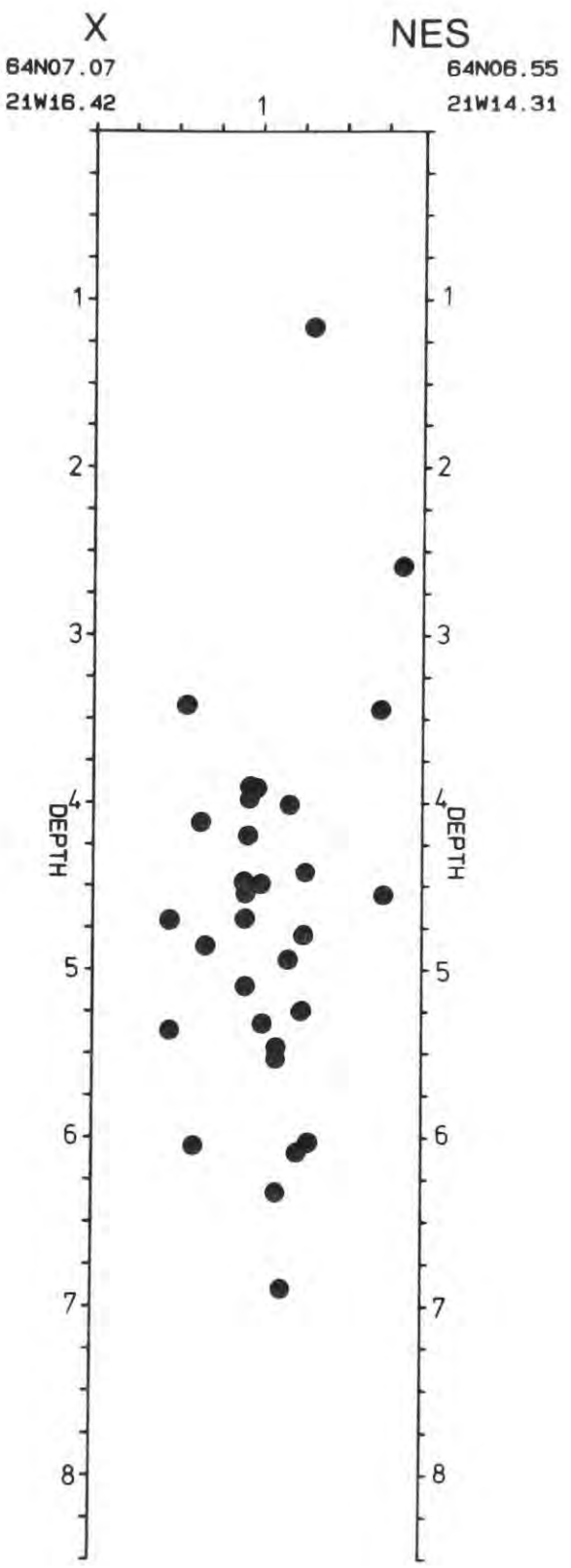

Fig. 4.13 NW-SE cross section across Nesjavellir. Drum and tape data.

- NES, Fig. 4.5). This section shows that the events occupy the depth range 3.5 - 7 km depth, and that the feature is close to vertical.

The data set contains 31 events.

4.3.2.3 Mosfellsheidi

These events form a diffuse cluster due NW of Hengill (Figs. 4.1 and 4.2). The temporal distribution of the tape events indicates that this area was continually active throughout the recording period July - Sept. 1981 (see Section 5.1). Towards the end of the recording period a swarm occurred, and these events clustered between 2 and 4 km depth. The easternmost boundary of the whole group of events is the westernmost fissure of the fissure swarm, i.e. the activity was confined to areas devoid of surface faulting. Examination of the cross sections presented in Figs. 4.6 and 4.7 shows that hypocentral depths in this area (M) lie mostly in the range 3 - 6 km. The occurrence of deep events is indicated in the drum data set (Fig. 4.6) but this is unsubstantiated by the tape data set (Fig. 4.7).

4.3.2.4 The Olfus lowlands

S of 64° N a fairly continuous belt of diffuse activity stretches from W to E at about 63°N57′ (Figs. 4.1 and 4.2). The belt is diffuse, and does not coincide with any visible surface lineament. Concentrations of activity occur in the regions of Hjalli (Hj) and Kirkjuferjuhjaleiga (Ki) (Fig. 4.2). In the

period September 19th-22nd 1981, whilst the radio telemetered network was in operation, a large swarm occurred in the Kirkjuferjuhjaleiga area. 700 events were located in the depth range 1-8 km. This swarm was on the outer edge of the network, so accurate locations were not possible. The largest event (M_{IL} = 2.2) in the tape data set occurred as part of this swarm.

The depth distributions of these events are plotted in Figs. 4.14 and 4.15, which are N - S cross sections of the whole Hengill area for the drum and tape data sets. Hypocentral depths S of 64°N mostly occupy the range 2 - 7 km (Figs. 4.14 and 4.15).

4.3.2.5 64° N

Straddling the 64° line of latitude is an EW trending belt of low seismicity. It is best illustrated by the NS hypocentral cross sections of Figs. 4.14 and 4.15. Very few hypocentres are located in this zone, and earthquake sequences are confined either to the N of 64° N, or to the S - epicentral zones do not cross this "barrier".

4.3.2.6 The fissure swarm

Very few events were located within the most intensely faulted part of the area, the fissure swarm, during the period 1974-1981 (Figs. 4.1 and 4.2). It may hence be stated that for this period the fissure swarm was almost seismically quiescent down to microearthquake levels.

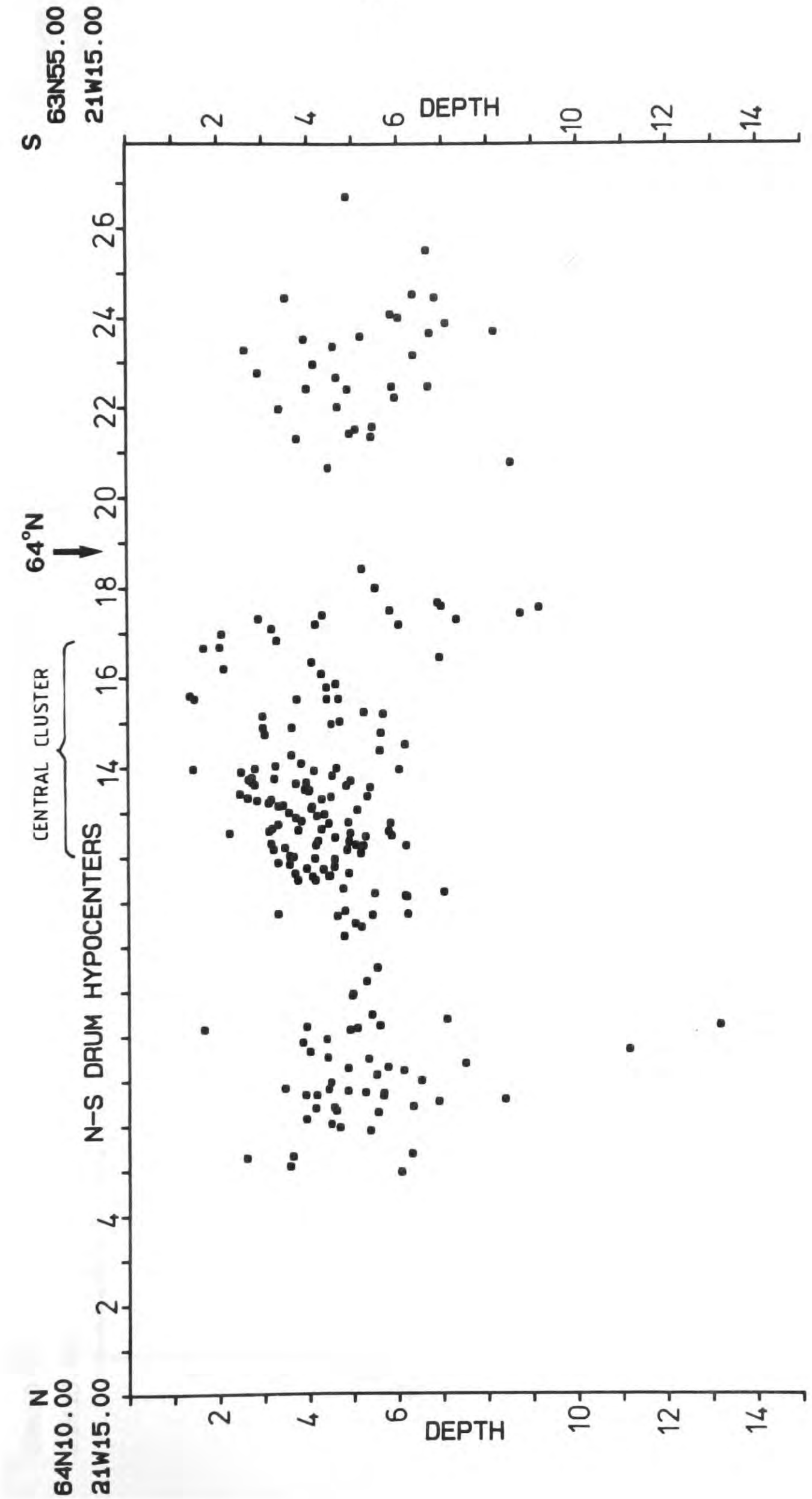

Fig. 4.14 NS cross section of drum data hypocentres.

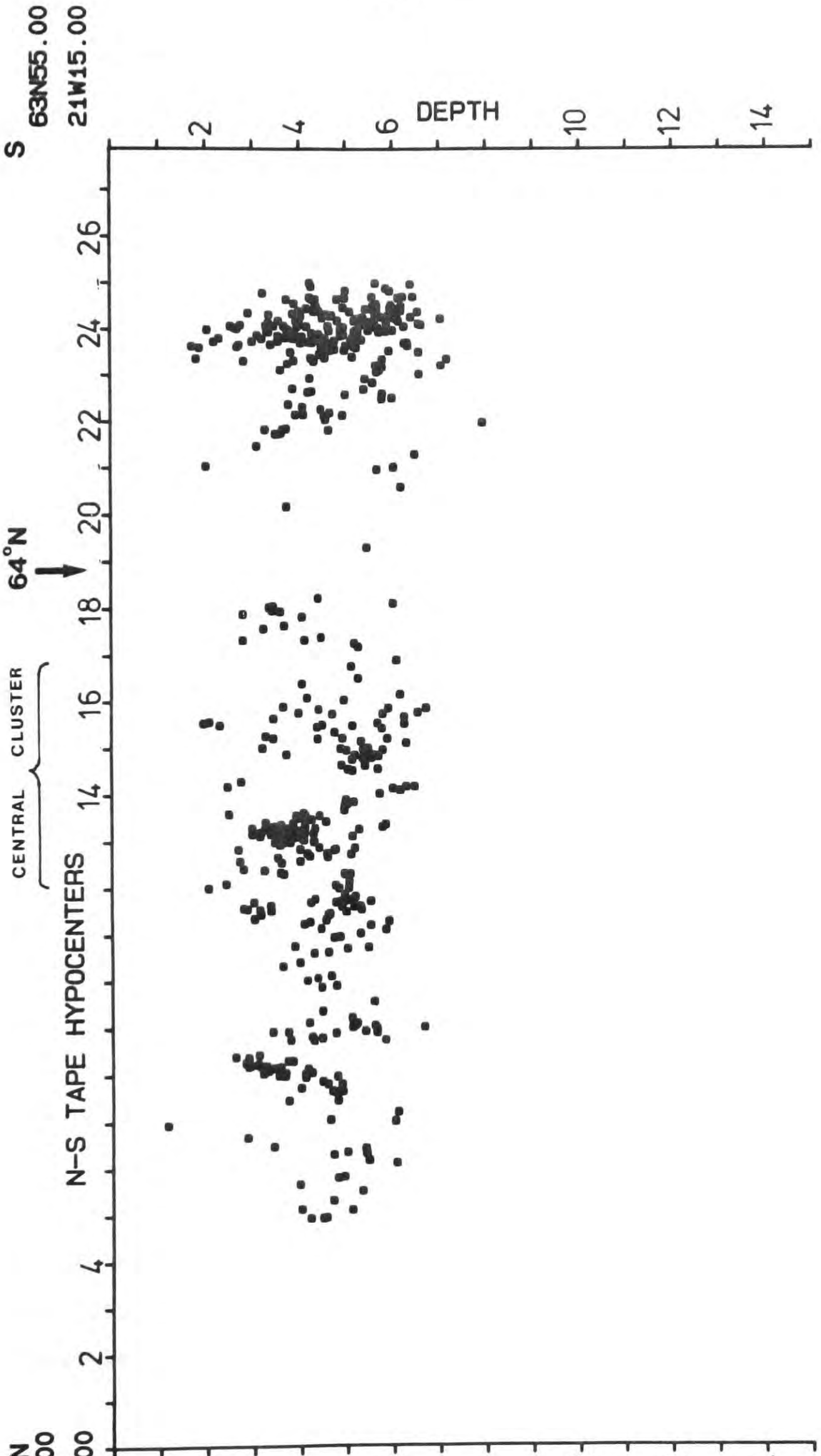

Fig. 4.15 NS cross section of tape data hypocentres.

4.3.2.7 The hypocentral distribution

The hypocentral distribution for the Hengill area in general is illustrated in the N - S cross sections of Figs. 4.14 and 4.15. In the case of the tape data (Fig. 4.15) all the hypocentres lie in the range 1-8 km. In the case of the drum data (Fig. 4.14) the maximum hypocentral depth is 13 km. However, since only 7 events are located deeper than 8 km, this may be the result of poor locations in the drum data set. Most of the events of both data sets lie in the range 2-6 km. Fig. A4.2 (Appendix 4) is a velocity - depth profile for the Hengill - South Iceland crustal model. From this Figure it may be seen that the depth range of the local earthquake activity corresponds to the seismic velocity range approximately 3 - 6.5 km sec^{-1}. Thus the activity is confined to the upper crust, corresponding to oceanic layers 0 - 2 (Flovenz, 1980).

There is a tendency visible in the data sets for a shallowing of the average hypocentral depth in the central cluster (12-17 km along the profiles) relative to more northerly and southerly events (i.e. a doming of the seismic zone beneath the geothermal field), but this also may be a creation of the locator proceedure. Variations detected in the velocity structure within the Hengill area are precisely such as would produce this effect (see Appendix 4). However such distortion is estimated to be less than 5% of the hypocentral depth (see Section 7.2), and so may account for only part of the observed variation.

4.4 Summary of the results

Examination of historic macroseismic data indicates that large magnitude earthquake activity is restricted to the area at or S of 64° N. The fissure swarm may periodically be activated by intense tectonic movements that cause seismicity and fault movements over tens of kilometers, e.g. the 1789 episode.

The monitoring of small magnitude earthquakes over an 8 year period yields a picture of spatial distribution that contrasts with the long term, large magnitude picture. Most events cluster in a small area of approximately 20 km^2 NW of Hveragerdi within which small subclusters of activity may be distinguished, and trends striking NW-SE and SW-NE. Other localised areas of activity occur in Nesjavellir and on Mosfellsheidi. A low background of activity is observed in the fissure swarm and Olfus. A belt of low activity occurs about 64° N. In general the seismicity correlates negatively with surface faulting.

Hypocentral depths mostly occur in the range 2 - 6 km and there is little evidence that seismicity extends to depths greater than 8 km. Activity is thus confined in the main to the upper crust (Flovenz, 1980). There may be a tendency for the average hypocentral depth to shallow beneath the geothermal field.

The general pattern of activity remained constant throughout the whole of the recording period - it was independent of time or magnitude window.

CHAPTER 5

5. LOCAL EARTHQUAKES: TEMPORAL DISTRIBUTION, FREQUENCY-MAGNITUDE RELATIONSHIPS AND b-VALUES

5.1 Temporal distribution

The temporal distribution of the seismicity of the Hengill area is remarkable because of its continuous day to day nature. In this respect it contrasts with all neighbouring seismic areas which are seismically quiescent on a day to day basis. It is dominated by the persistent, 20 km^2 cluster to the NW of Hveragerdi, that comes to the forefront in every data set and time window.

A whole spectrum of sequence types is observed superimposed on a continuous background of single shocks. In addition a few small areas are characterised by continuous low level activity. These features are illustrated in Figs. 5.1 and 5.2 which are plots of distance N of 63°N55 : time for events within the Hengill area for the drum and tape data sets respectively. In Fig. 5.1 the large increase in the rate of event location as a result of the setting up of additional stations in 1979 can be seen clearly. Both Figures demonstrate continuous activity throughout the time period at all latitudes. Particularly prominent in Fig. 5.2 is the consistent belt of activity corresponding to the 15 km point on the vertical axis. Comparison of Figs. 5.2 and 4.2. indicate that this activity corresponds to the Klambragil (K) subcluster. In addition, clusters of events may also be seen where many events occurred within a short space of time, and in a small area, e.g. the

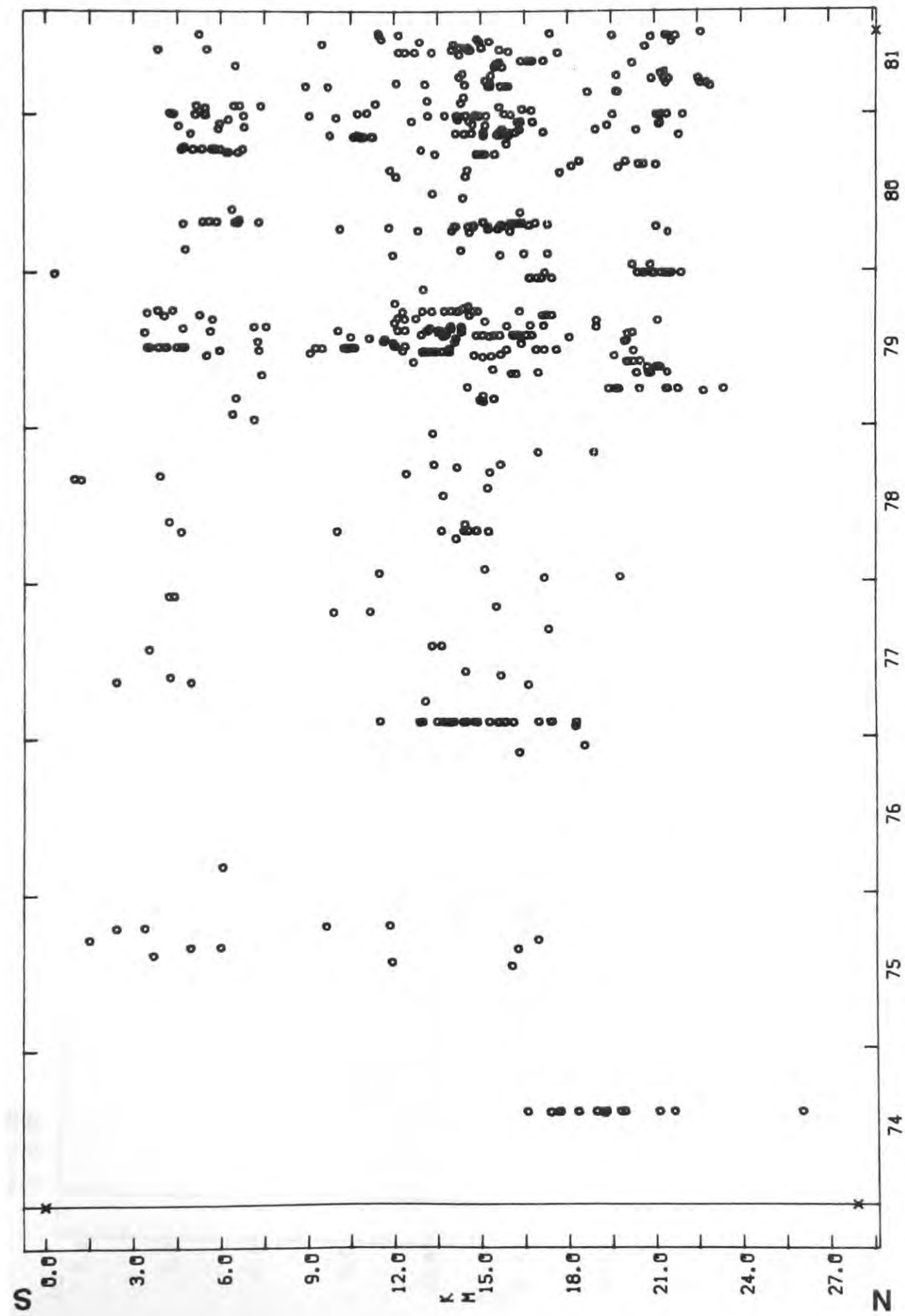

Fig. 5.1 Temporal distribution, drum data, in NS cross section.

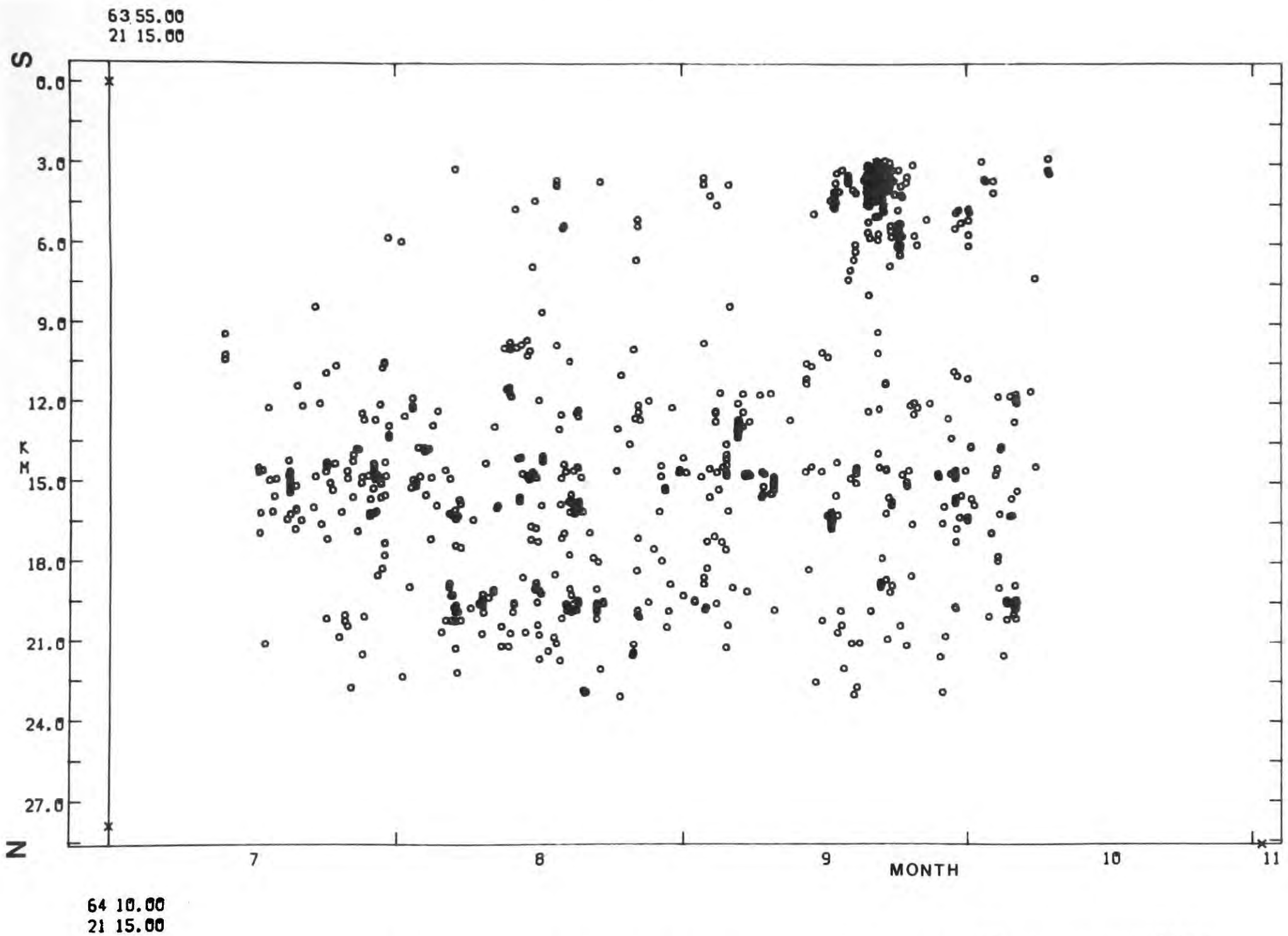

Fig. 5.2 Temporal disribution, tape data, in NS cross section.

swarm that occurred in the Kirkjuferjuhjaleiga (Ki), Olfus area in Sept. 1981 (about 3 km along the vertical axis of Fig. 5.2). This sequence is discussed in more detail in Section 5.2.4.2.

Seismic sequences may be roughly divided into three groups:

1. Mainshock - aftershock sequences
2. Foreshock - mainshock - aftershock sequences
3. Swarm sequences

A sequence is classed as a mainshock sequence if the magnitude of the largest event exceeds that of the second largest by at least 1 magnitude unit (Sykes,1970).

The Hengill area displays great variation in sequence type. All three types of sequence have been observed in the area and some examples are illustrated Fig. 5.3. Sequences over a wide range of magnitudes are also recorded. No spatial pattern in the occurrence of different types of sequence has been observed.

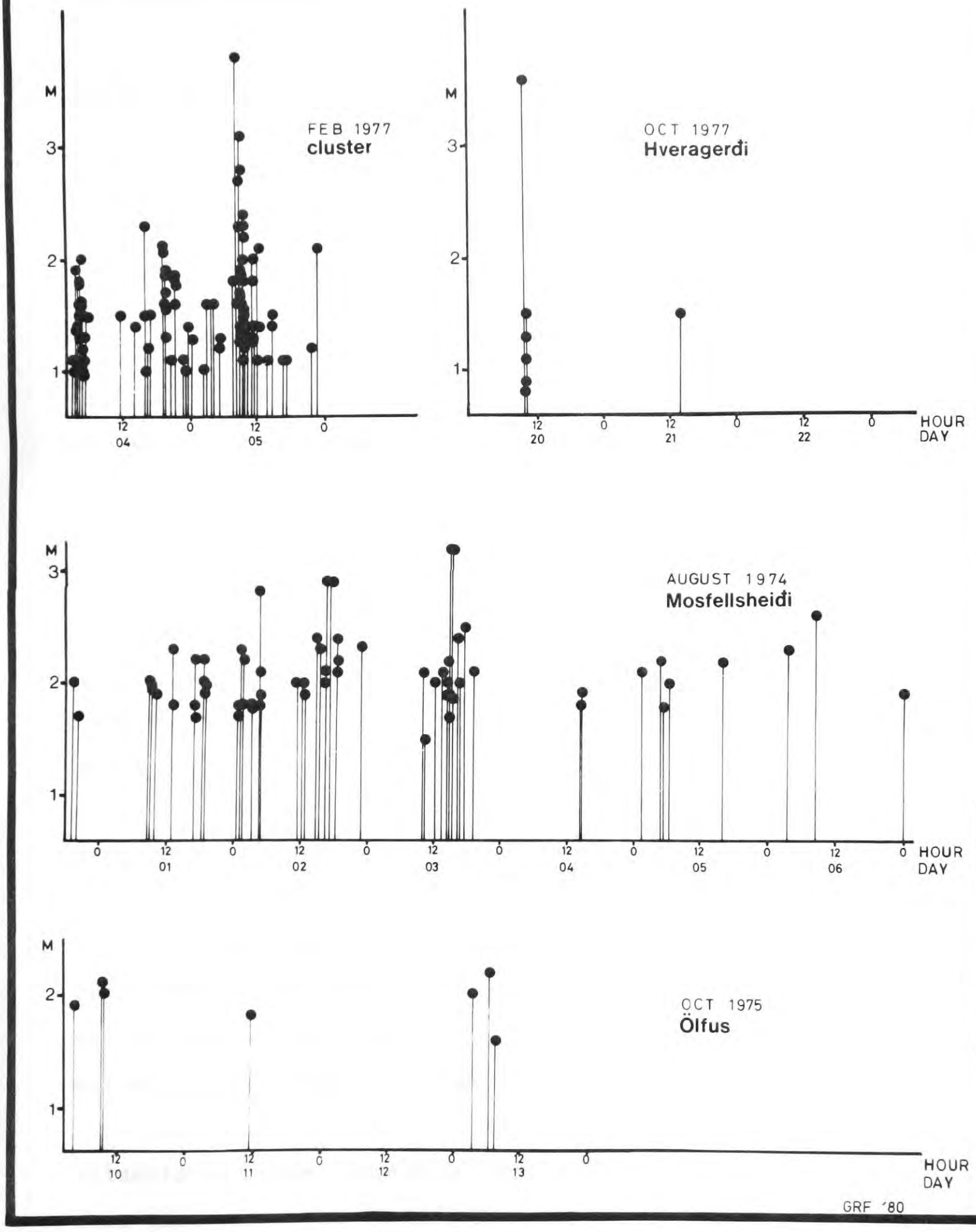

Fig. 5.3 Examples of sequences of various types that have occurred in the Hengill area. Magnitudes are M_{IL}.

5.2 Frequency-magnitude relationships and b-values

5.2.1 Introduction

Richter (1958) found that a plot of log (cumulative number of earthquakes) against magnitude was roughly linear for the world at large and most of the limited areas studied. He expressed this in the equation:

$$\log_{10} N = A - bM$$

where

N = number of shocks of magnitude M or greater per unit time

A, b = constants

The A value is an indication of the seismic rate of the area and time period under investigation. The b value is an indication of the rate of decrease in frequency with increase in magnitude. A b-value of about 1 is typical for most seismic zones (Richter, 1958, p. 359). Variations in the value of b (negative slope) have been investigated both within a single area as a function of magnitude window or time and between different areas. The possibility has been considered that they could be used as a tool for evaluating and detecting variations in properties of the brittle earth's crust, e.g. homogeneity or stress (Mogi, 1963; Scholz, 1968).

Variations in slope with magnitude.

Fig. 5.4 is a hypothetical frequency-magnitude plot that illustrates some commonly observed features. Examination of this plot shows that the slope varies with magnitude. At low magnitudes the negative slope decreases to zero. This is a

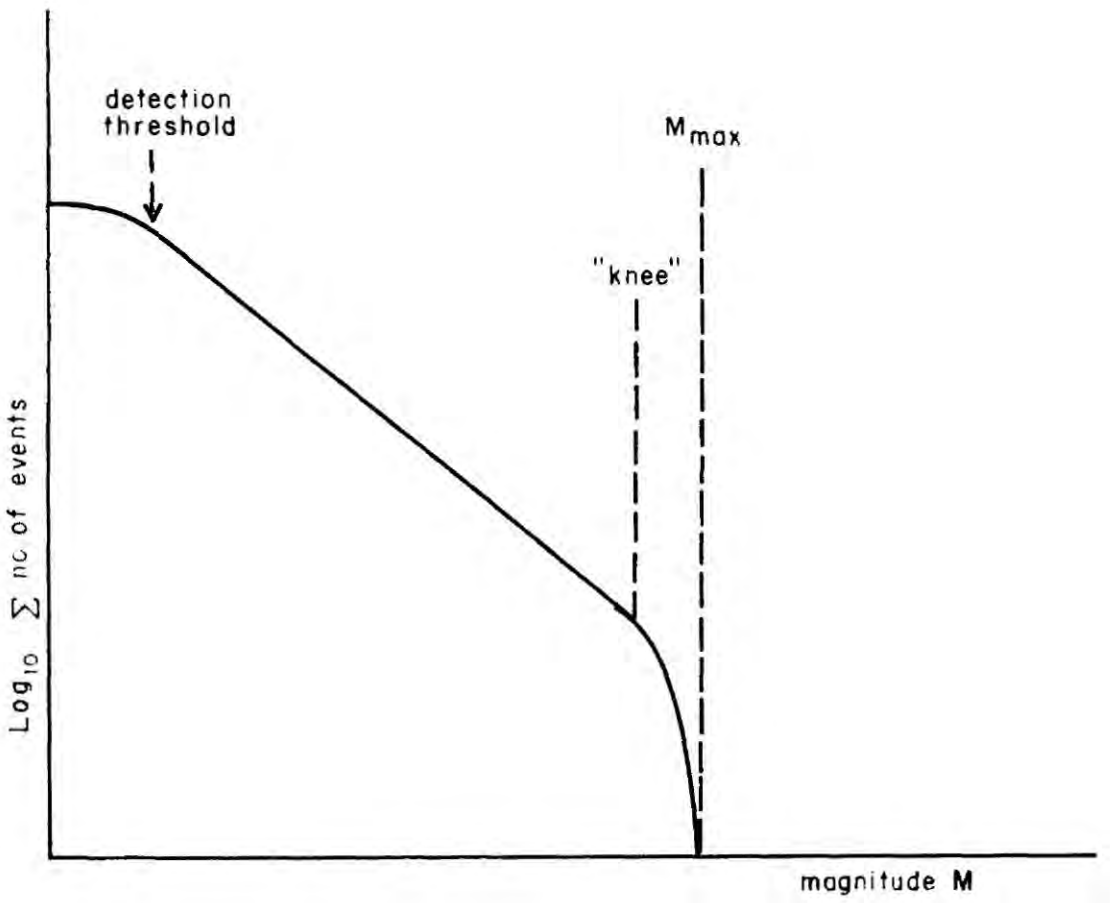

Fig. 5.4 Idealised cumulative frequency - magnitude plot.

general feature of magnitude-frequency plots and is caused by incomplete detection of the smallest events over the whole area. It may be corrected for using the relationship between detection threshold and epicentral distance. The detection threshold is the magnitude at (and above) which detection is complete over the area under investigation.

At high magnitudes the distribution may be asymptotic to a maximum magnitude. Yegulalp and Kuo (1974) observed this behavior in the frequency-magnitude distributions for the entire world and the majority of 46 sub-regions. They calculated statistical predictions for the maximum magnitude earthquakes (M_{MAX}) using Gumbel statistics (Gumbel, 1960) and obtained a

value of M_L = 9.2 for the world. Values for the subregions varied between M_L = 9.1 and 6.5 for 100 year return periods, were highest in the N and W circum-Pacific belt and lowest for the oceans and stable continental masses. Lilwall (1976) calculated a value of m_b = 5.7 for the maximum magnitude earthquake for the British Isles. For data sets taken for the ridge and fracture zone portions of the mid-Atlantic plate boundary, the b-value exhibited by ridge events (b=1.33) is found to be much higher than that exhibited by fracture zone events (b=0.65) in the range $3.2 < M_s < 5.6$ (Francis, 1966; 1968). It is possible that the "roll off" of the frequency-magnitude distribution is affecting the data sample for the ridge zone in this magnitude range, but not the fracture zone. This may be an indication that the maximum magnitude (M_{MAX}) of events for the ridges is lower than for the fracture zones (Einarsson, 1984). This would imply inhomogeneities of the order of 1-10 km in extent for the ridges, but much larger for the fracture zones, a perfectly plausible circumstance. For the Geysers geothermal field, which has an areal extent of about 40 km^2, the asymptotic magnitude is approximately $M_L \sim 4.0$ (Eberhart Phillips and Oppenheimer, 1984).

The magnitude of an earthquake is related, through its seismic moment, to its source dimensions (Wyss and Brune, 1968). Wyss (1979) has shown that the maximum magnitude earthquake is related to the area of the fault and Einarsson (1984) suggests that the upper limit of earthquake magnitude is governed by the size of first order inhomogeneities in the earths crust. The frequencies of small magnitude events relative to each other will not be affected by the upper limits of these physical

parameters and thus the frequency-magnitude distribution is linear at low magnitudes. At larger magnitudes however, it would be expected that this fact would have the effect of decreasing the likelihood of an event occurring. A "roll-off" of the magnitude-frequency plot (i.e. a progressive increase in slope) would then occur in the magnitude range where earthquake source dimensions are of the same order of magnitude as the fault dimensions. This principle appears to be supported by laboratory specimens, where high b values are found to be associated with heterogeneous material (Mogi, 1963), i.e. in the case of such samples we may be observing in the asymptotic region of the distribution.

Variations in b with time

Some examples of b-value variations with time have been documented. The best known of these are cases where a low b-value has been associated with the foreshocks of a large earthquake, and a higher b-value associated with the aftershocks (e.g. Suyehiro et al., 1964; Bufe, 1970; Wyss and Lee, 1973). The reason why a high b value is associated with aftershocks may be that the fault area was made highly inhomogenous by the main rupture, but this does not explain the anomalously low b-value associated with the foreshocks. It has been hypothesised that b is inversely related to stress in the rock volume (Scholz, 1968; Wyss, 1973). This would explain the observations since stress would be expected to be higher at the beginning of a sequence than later on, after it had been partially released.

Variations in b in space

If b is stress related, variations in b from area to area might be exhibited, that would provide a tool for mapping the

stress state of the crust. The possibilities of doing this are somewhat limited, however, because b varies only over a small range, and such variations are usually of the same order of magnitude as the associated uncertainties. The two most serious sources of error are the use of different magnitude scales and small data samples. In order to detect significant variations in b large numbers of earthquakes must be used and their magnitudes determined by a consistent method. This was achieved by Klein et al. (1977) on the Reykjanes Peninsula. They determined b-values of 0.85 ± 0.07, 1.02 ± 0.07 and 0.75 ± 0.11 for 3 portions of their study area. The value 1.02 was shown to be significantly different from the other two. Values comparable to these of 1.09 ± 0.06 and 1.06 ± 0.06 were obtained by Einarsson et al. (1977) for the Borgafjordur area. These values are broadly comparable to each other and to the values obtained for the Hengill area, discussed below, since in all cases the magnitudes used were based on those measured at REY.

In conclusion, the following points may be made:

(a) Frequency-magnitude distributions are in general linear at low magnitudes. The negative slope of this part of the distribution is known as the b-value. b for the world at large is approximately 1 (Richter, 1958). In a number of cases the distributions are asymptotic to maximum magnitudes (M_{MAX}). It may be that this behavior is exhibited in the magnitude range corresponding to earthquakes whose source dimensions are of the same order of magnitude as the fault dimensions.

(b) It has been hypothesised that b is inversely related to stress. This may explain variations in b observed at low

magnitudes e.g. anomalously low b-values associated with foreshocks and low magnitude spatial b-value variations.

(c) Variations in b are difficult to assess since they are commonly small compared with the associated errors. Large uncertainties are especially introduced by the use of different magnitude scales and small data samples.

5.2.2 Composite frequency-magnitude plot

5.2.2.1 The data

In order to investigate the frequency-magnitude distribution of the Hengill area over as large a magnitude range as possible, 4 data sets are combined in the composite plot shown in Fig. 5.5. The b-values and associated errors (95% confidence limits) were calculated using the method of maximum likelihood (Aki, 1965; Page, 1968).

The instrumental magnitudes quoted are local Icelandic magnitudes. They are based on extrapolations of an empirical magnitude scale that was constructed for the REY instrument (Fig. 2.1) for surface waves of about 20 sec period (M_{REY}) by comparison with European seismological stations. (Tryggvason, 1968; 1973). Tryggvason (1973) reports that:

$$M_{REY} = M_S + 0.2$$

Coda length scales were constructed empirically for the station IR (Fig. 3.1) by comparison with REY, and for the stations BMO, KHA and LDJ (Fig. 7.3) by comparison with REY and IR. The IR, BMO, KHA and LDJ scales were extrapolated downwards in order to construct scales for small magnitudes. Where an event was

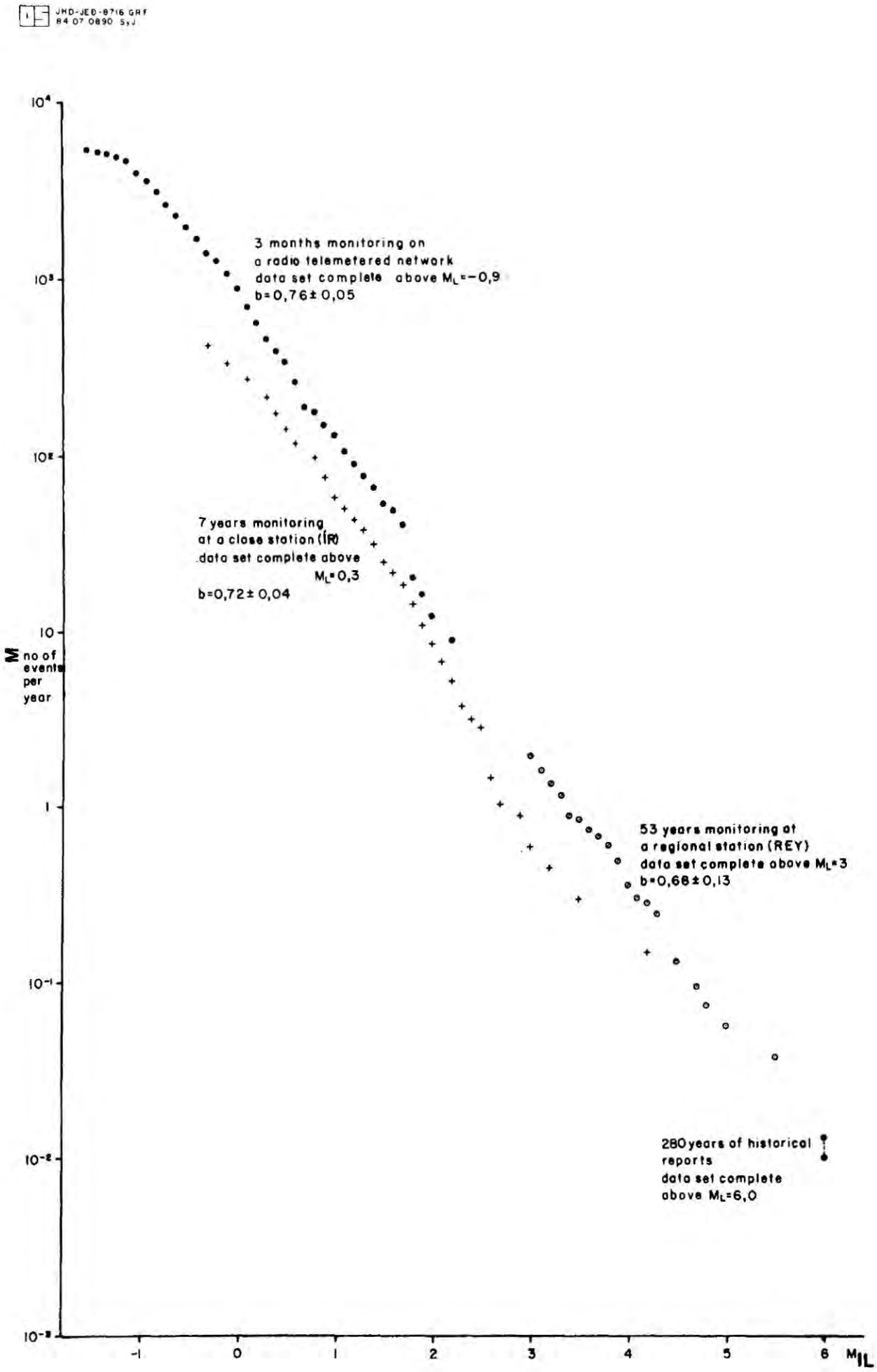

Fig. 5.5 Composite cumulative frequency magnitude plot of events occurring in the Hengill area. The four data sets discussed in the text are plotted on a normalised frequency scale.

recorded at REY the REY magnitude was adopted. Otherwise the magnitudes from all the stations that recorded the event were averaged. This is consistent with Icelandic seismological practice. These magnitudes are herein referred to as M_{IL}.

1. Historic macroseismic data

Three or four events of magnitude 6-6.5 are known to have occurred in the Hengill area since 1700 (see Section 4.1). The magnitudes of the events were estimated from macroseismic data.

The annual rate of events of $M_{REY} \geq 6$ is variable according to the time window taken in the period 1700-1983, and uncertainties are introduced by the arbitrary nature of the end points. Fig. 5.6 is a plot of the periodicity of such events against time. It can be seen that as the data sample becomes progressively larger with time the occurrence rate tends to about 1 event per 100 years (solid line - assuming 3 events), or about 1 event per 75 years (dashed line - assuming 4 events).

These data are plotted at $M_{IL} = 6$ in Fig. 5.5.

2. Data recorded at the regional station REY

Plots of seismicity with time for this data set are presented in Figs A5.1-A5.9 (Appendix 5).

For this data set the frequency-magnitude plot is linear and continuous for $3.0 \leq M_{REY} \leq 4.3$. For $M_{REY} \geq 4.3$ the plot becomes discontinuous. The b-value was calculated to be 0.68 ± 0.13 for $M_{REY} \geq 3$

3. Data recorded on the local seismograph IR

This station is located within the Hengill area and is part of the regional seismograph network. It has been in operation since March 1977. The magnitude scale calculated for this station was:

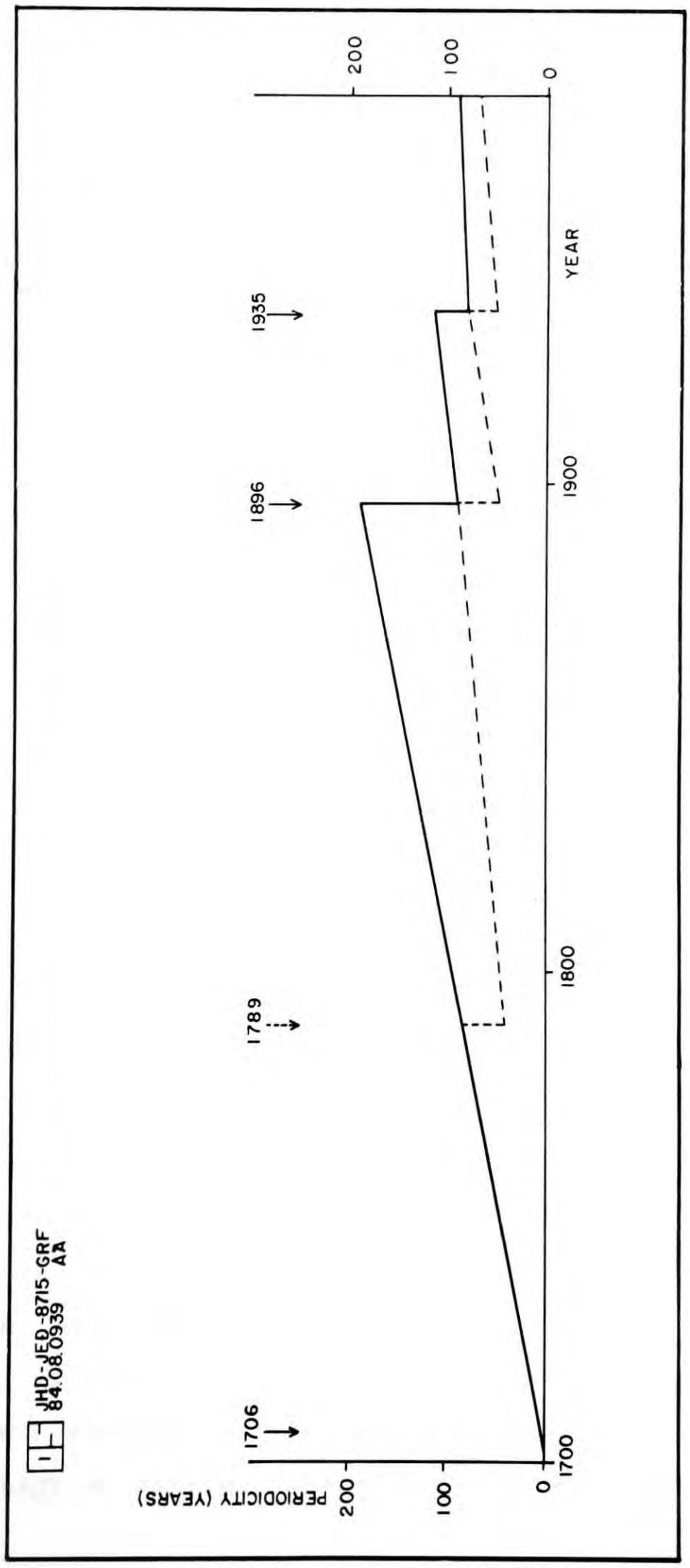

Fig. 5.6 Rate of occurrence of $M_{REY} \geq 6.0$ events vs. time. Solid line discounts the 1789 event, dotted line includes it.

$$M_{IL} = 2.85\log_{10} Ts - 2.32$$

Ts = time in seconds that the recorded peak to peak amplitude of the event was greater than 2 mm at 36dB magnification.

For the 7 year period 1977-1983 an average of 1.9 events per day were recorded at IR from the Hengill area. Plots of seismicity with time for this data set are presented in Figs. A5.10-A5.16 (Appendix 5). The data set contains 1500 events $M_{IL} \geq 0.3$.

The frequency-magnitude plot for IR is linear and continuous for $0.3 \leq M_{IL} \leq 2.3$. The b-value calculated for $M_{IL} \geq 0.3$ is 0.72 ± 0.04.

4. Data recorded on the radio telemetered network

For this network magnitude scales were calculated for 1 station of each tape recorder operated. The relationships obtained were:

station BMO $M_{IL} = 2.51\log_{10} Tmm - 3.37$

" KHA $M_{IL} = 2.26\log_{10} Tmm - 2.69$

" LDJ $M_{IL} = 2.46\log_{10} Tmm - 3.30$

Tmm = coda length in mm of seismogram for which the peak to peak amplitude was $\geq$ 2mm (for amplifier-modulator gain 7 and jet pen gain 0.25. This corresponds to approximate ground velocities of $\leq 3\times10^{-7}$ m sec^{-1} or approximate ground displacements of $\leq 3\times10^{-9}$ m. Tmm = 2.45Ts)

These magnitude scales, and that of IR are illustrated in Fig. 5.7. It may be seen from this figure that the radio telemetered stations (natural frequency 1 Hz) recorded longer codas at high magnitudes than the regional station (natural

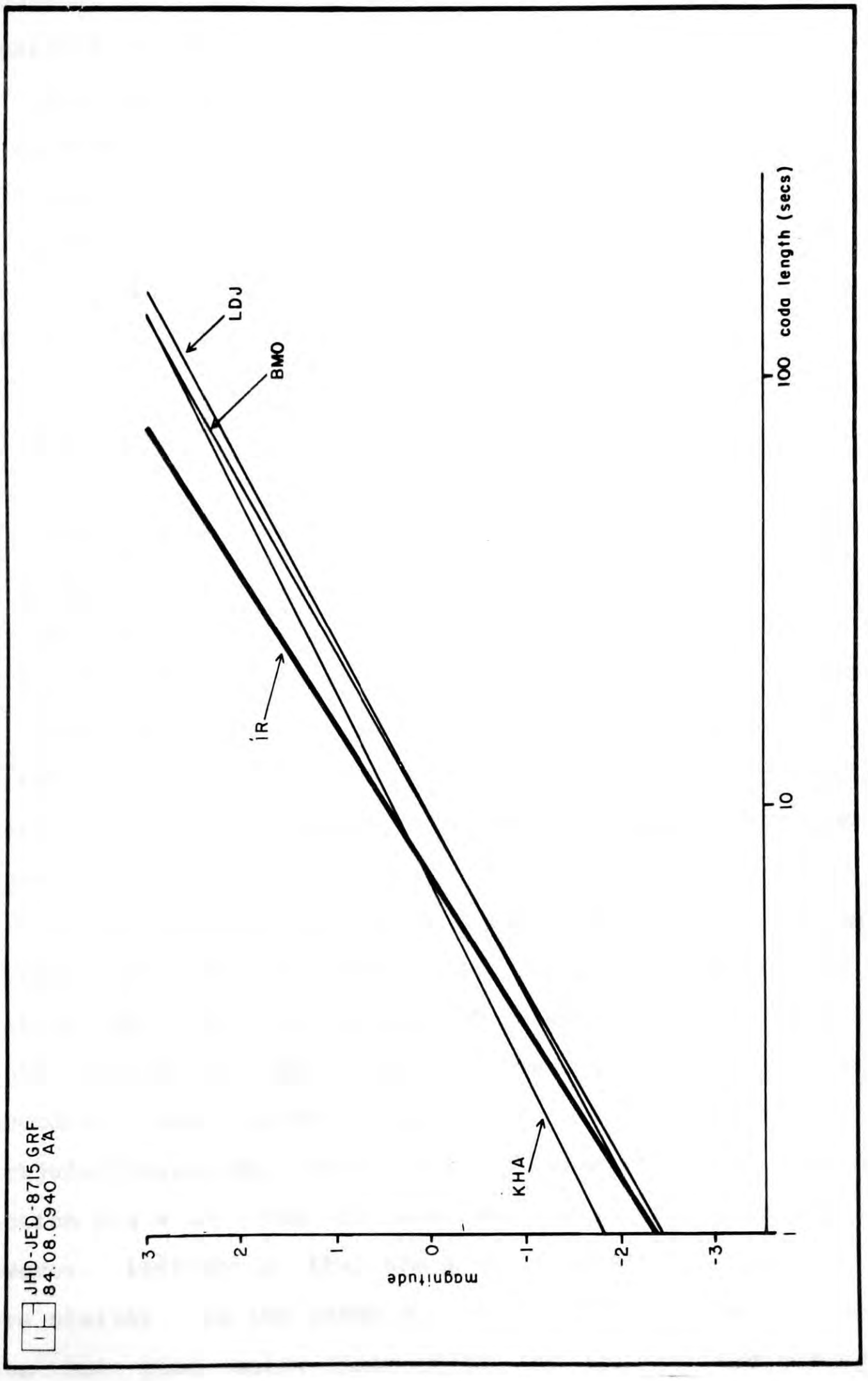

Fig. 5.7 Magnitude scales for stations within the Hengill area.

frequency 2 - 3 Hz) at the gains used, but had similar detection capabilities at lower magnitudes.

For the 90 day period July 12th - Oct 9th 1981 an average of 21 events per day were located on this network. The data set contains 888 events in the range $M_{IL} \geq -0.9$.

The frequency-magnitude plot is linear and continuous for $-0.9 \leq M_{IL} \leq 1.7$. The b-value calculated for $M_{IL} \geq -0.9$, was 0.76 ± 0.05.

5.2.2.2 Discussion

b-values of 0.68 ± 0.13, 0.72 ± 0.04 and 0.76 ± 0.05 were obtained for the 3 instrumental data sets. A value of b of approximately 0.74 for the Hengill area in the range $-0.9 \leq M_{IL} \leq 5.5$ is hence constrained by a large body of data.

The small (statistically insignificant) variations in these 3 values may be in part due to the fact that different instruments with different calibration scales were used for magnitude determination.

It may be noted in Fig. 5.5 that the radio telemetered network data set is vertically offset from that of the local station (IR). This is because the seismicity rate during the 3 month period in 1981 when the radio telemetered network was recording was about twice the average due to the Kirkjuferjuhjaleiga, Olfus swarm of September 19th - 22nd (see Section 5.2.4.2). The IR and REY data sets are colinear, however, indicating that the seismic rates for these data sets were similar. In the range $M_{IL} \geq 2$ the data points of the IR data set plot below those of the REY data set indicating that

activity in this magnitude range was lower in the period 1977-1983 than the average over the last 54 years. This indicates that for $M_{IL} \geq 2$ the statistical sample time was too short for the IR data set.

The average seismic rate of the area over the last 53 years has been approximately one event $M_{IL} = 3.5$ per year or one event $M_{IL} = 0$ per day.

A maximum magnitude earthquake of $M_{IL} = 6\text{-}6.5$ for events in the Hengill area would be in agreement with historical evidence (see Section 5.2.2.1). However the application of Gumbel statistics to the regional station (REY) data set showed that the data obeys the first asymptotic distribution of the largest values, i.e. a straight line on Gumbel probability paper (Gumbel, 1960). It may be deduced from this that there is no statistical evidence in the REY data set for an upper magnitude limit for the Hengill area. The reason for the apparant discrepancy between the REY data set and the historic macroseismic data set may be that the statistical sample time was too short for the REY data set, and the seismic rate at large magnitudes has been higher than average during the last 53 years.

Historical evidence suggests that all these destructive earthquakes are associated with the Olfus area, S of 64^{o} N and that no such large event has occurred in the high temperature geothermal area N of 64^{o} N (Section 4.1). This implies that the Hengill area may be subdivided into two units on the basis of seismicity:

(1) Olfus, and

(2) the high temperature geothermal area.

For each of the 3 instrumental data sets the b-value plot is linear and the value of b approximately the same within the 95% certainty limits. This indicates that no large difference in b-value exists between Olfus and the high temperature geothermal area since the combination of two data sets with different b-values would yield a non-linear curve (Appendix 6). However, historical evidence indicates that the maximum size of event sustainable by the Olfus area is larger than that of the high temperature geothermal area. The two areas are roughly of similar areal extent so this would imply that faulting occurs on a smaller scale in the high temperature geothermal area than in Olfus (Section 5.2.1). Possible forms of the b-value plots for the two areas are shown in Fig. 5.8.

The two areas exhibit frequency-magnitude plots with similar b-values but with "knees" at different magnitudes. Also shown is the form that would result for a composite plot. Two "knees" would be expected, corresponding to the "knees" of Olfus (at higher magnitude) and the high temperature geothermal area (at lower magnitude). The lower magnitude "knee" would give an indication of the maximum magnitude event to be expected within the geothermal area.

There is, however, no statistical evidence in the instrumentally recorded data for the existence of either of these "knees". If there is an upper magnitude limit to events within the high temperature geothermal area then it must occur at $M_{IL} > 4.2$ since an event of this magnitude has been located in the geothermal area (Oct. 1977).

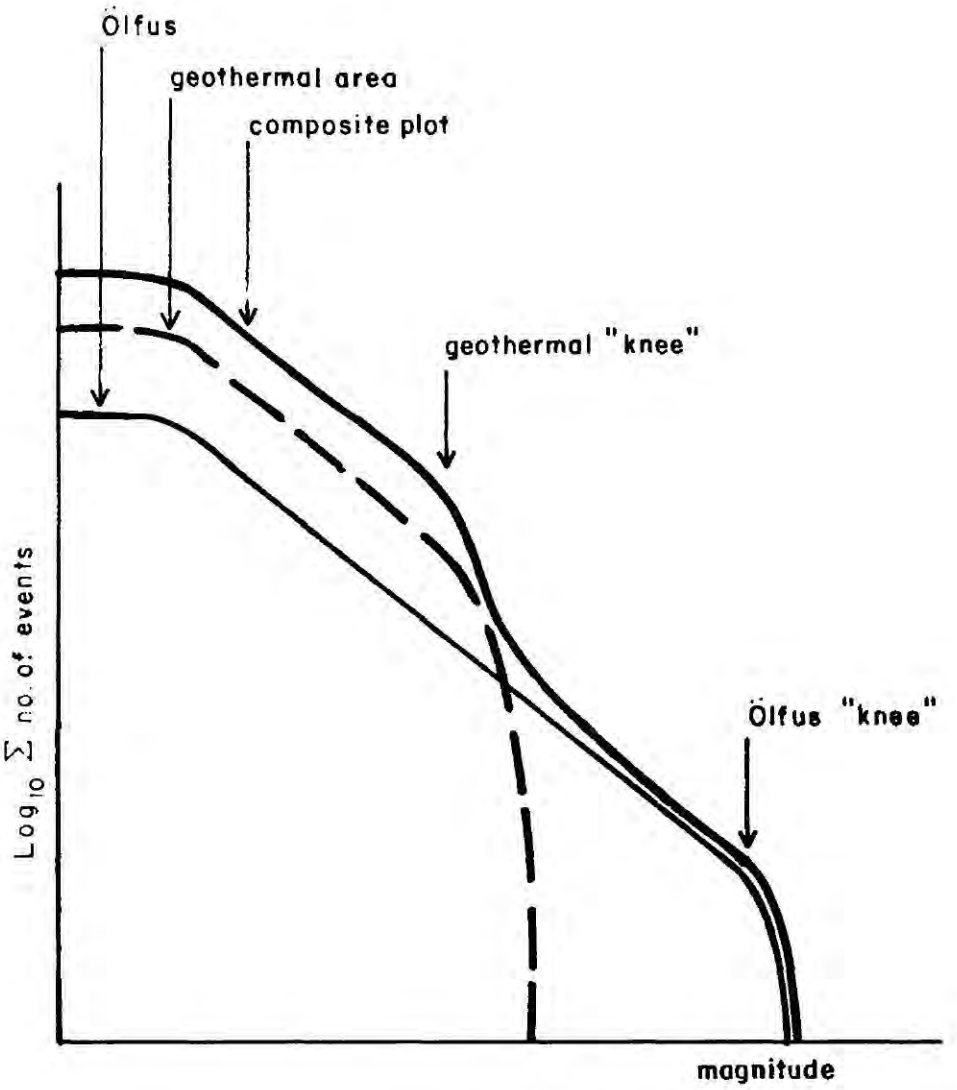

Fig. 5.8 Diagram illustrating the hypothesised forms of the frequency-magnitude plots for the high temperature geothermal area and Olfus and the form of the plot that might be expected from a combination of the two.

5.2.3 Variations in b within the Hengill area

The data collected on the radio telemetered network is a homogeneous data set (see Section 3.2.1) from which were calculated 1918 earthquake locations and corresponding magnitudes in the range $M_{IL} \leq 2.2$. For this low magnitude range a linear frequency-magnitude distribution would be expected. However, there remains the possibility that variations in stress

e.g. due to tectonic or thermal influences, may be reflected in variations in b-value within the area. b-value plots were made for 9 geographical subdivisions of this data set (see Section 4.3.2 and Fig. 4.2 for locations of subdivisions). The results are summarised in Table 5.1 and Fig. 5.9. Individual plots are illustrated in Figs. 5.10 to 5.19.

From Fig. 5.9 it may be deduced that the b-values obtained for many of the geographical subdivisions are not statistically different from one another. The b-values for the areas N of 64° N, S of 64° N, Klambragil, the central cluster, the fissure swarm, the Kirkjuferjuhjaleiga, Olfus swarm and 2.00-3.99 km depth are all within or very close to the 95% confidenoe range for the b-value for the entire area. Examination of Figs. 5.10-5.19 indicate reasonable linearity for these data sets in the magnitude range about $-1.0 \leq M_{IL} \leq 2.0$. If one accepts that the b-value is influenced by the stress state in the source volume then one must conclude that stress in the parts of the Hengill area listed above is similar.

A b-value of 0.86 ± 0.14 was obtained for the 4.00-5.99 km depth range. This is slightly high, and may be an indication of reduction in stress with depth. This might be expected if increase of temperature with depth causes reduction of strength of the rock, as has been hypothesised for SW Iceland in general (Klein et al., 1977).

A b-value of 1.0 ± 0.18 was obtained for the Mosfellsheidi subdivision. This is significantly different from that obtained for the entire area, and higher, which may indicate lower stress than over the rest of the Hengill area. This b-value contrasts with that obtained for the fissure swarm immediately adjacent

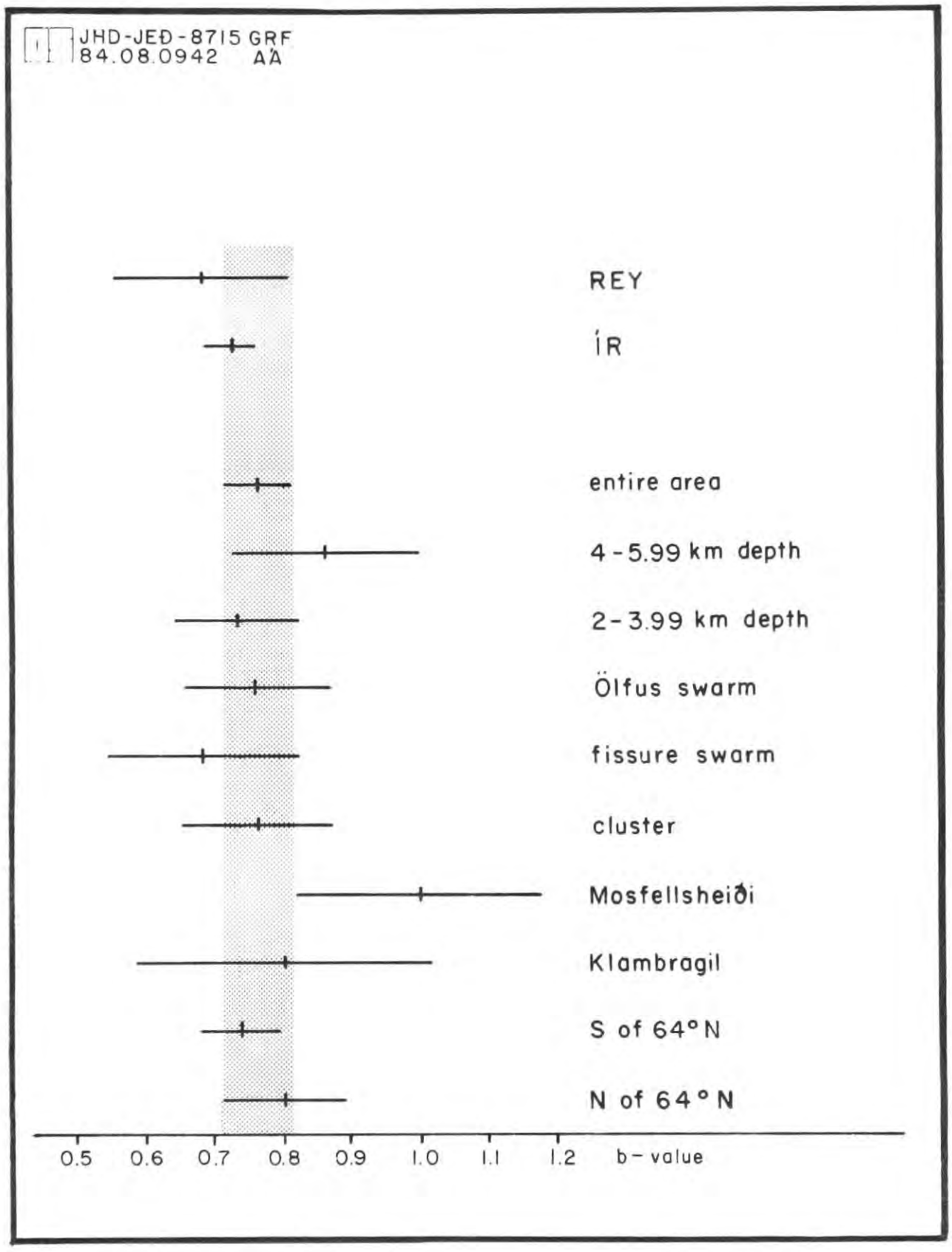

Fig. 5.9 b-values calculated for subdivisions of the Hengill area. Horizontal lines indicate the 95% confidence ranges. Shaded column indicates the 95% confidence range for the entire data set.

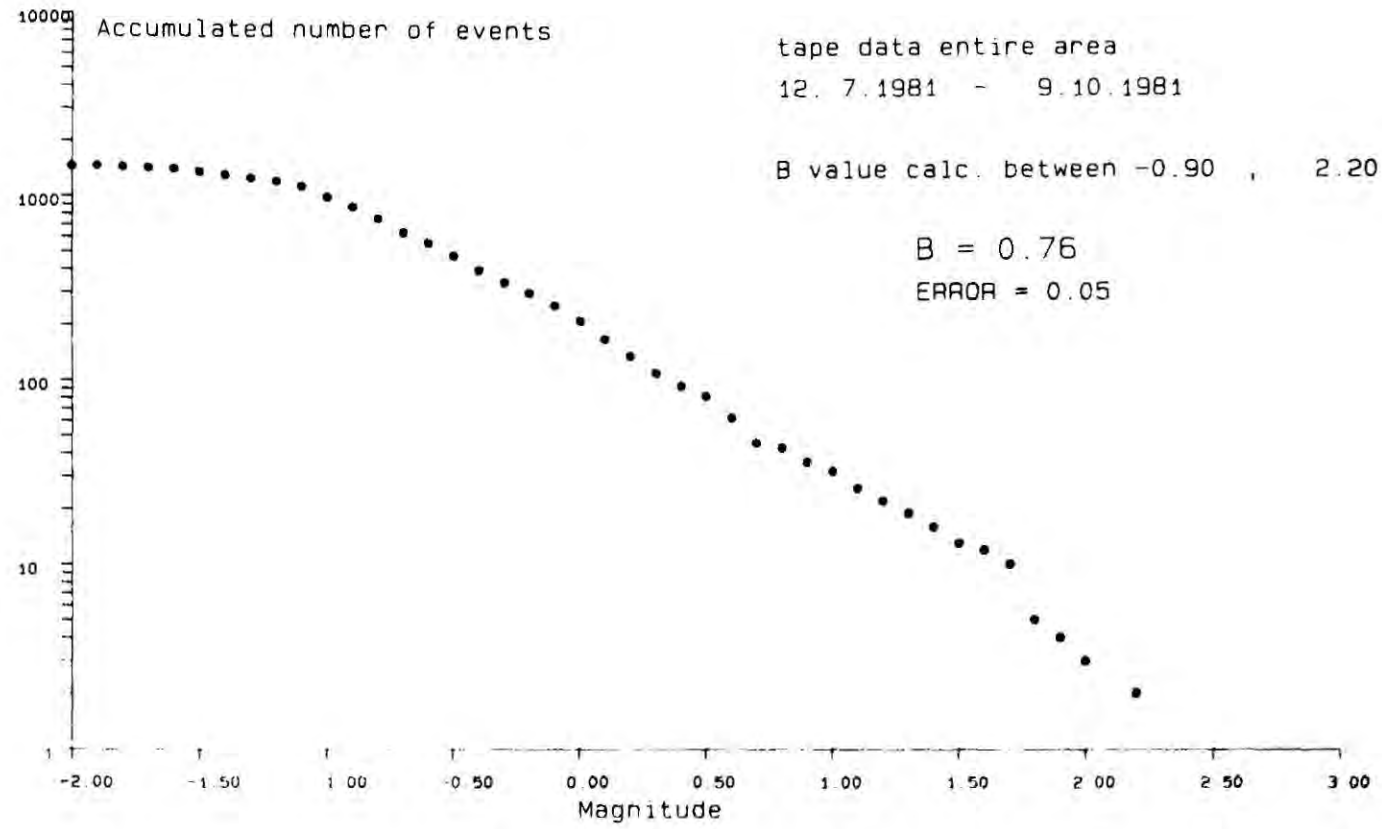

Fig. 5.10 Frequency - magnitude plot - tape data entire area.

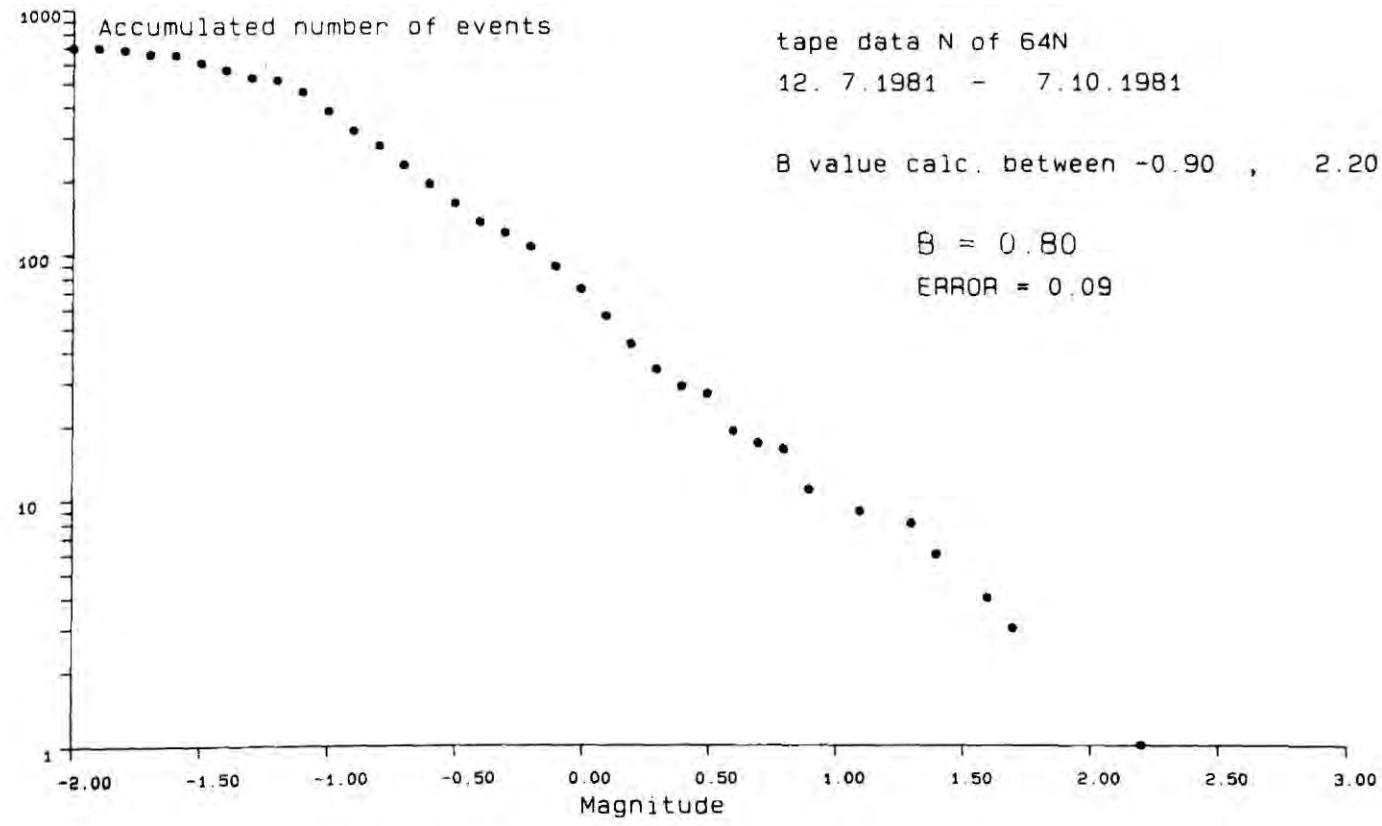

Fig. 5.11 Frequency - magnitude plot - area N of 64° N

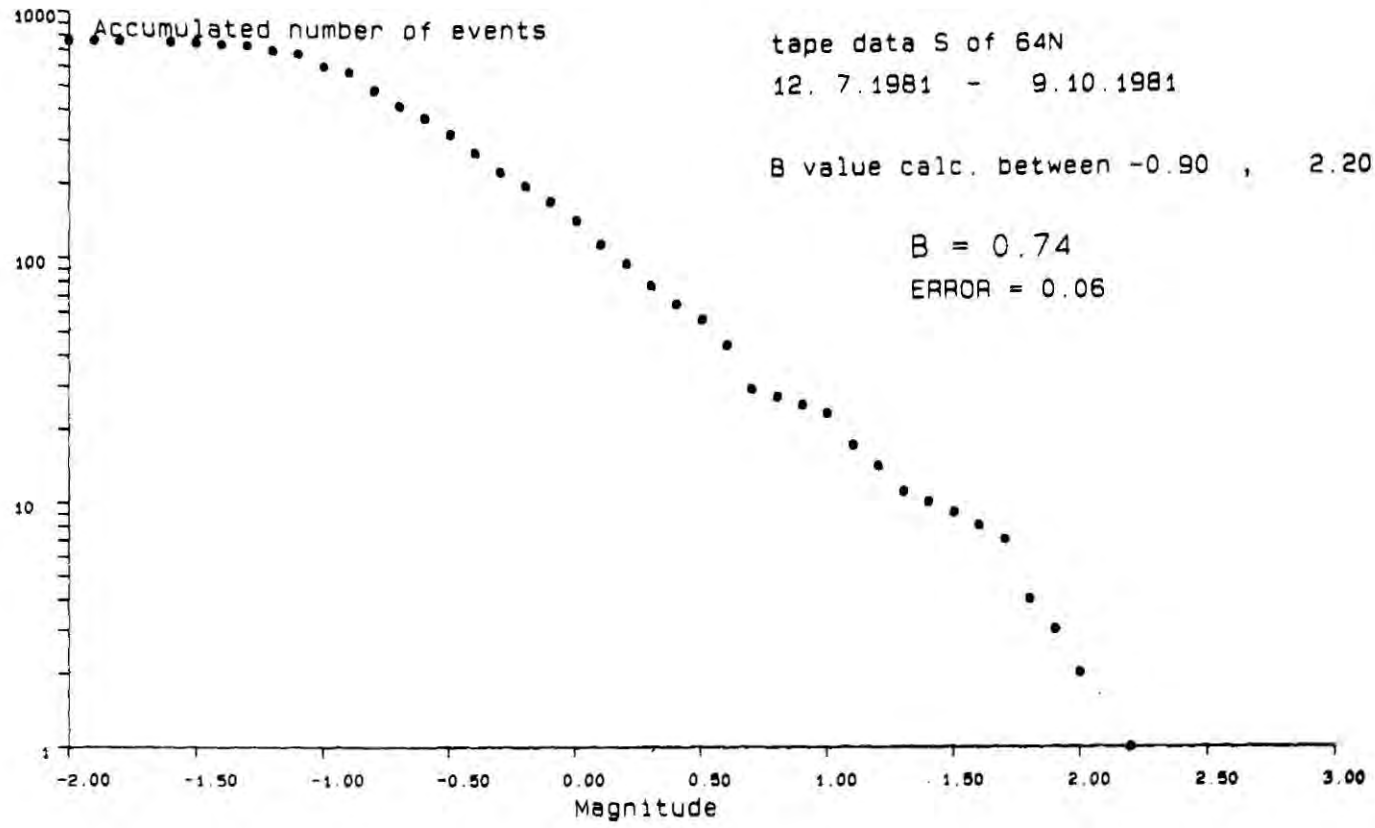

Fig. 5.12 Frequency - magnitude plot - area S of 64°N.

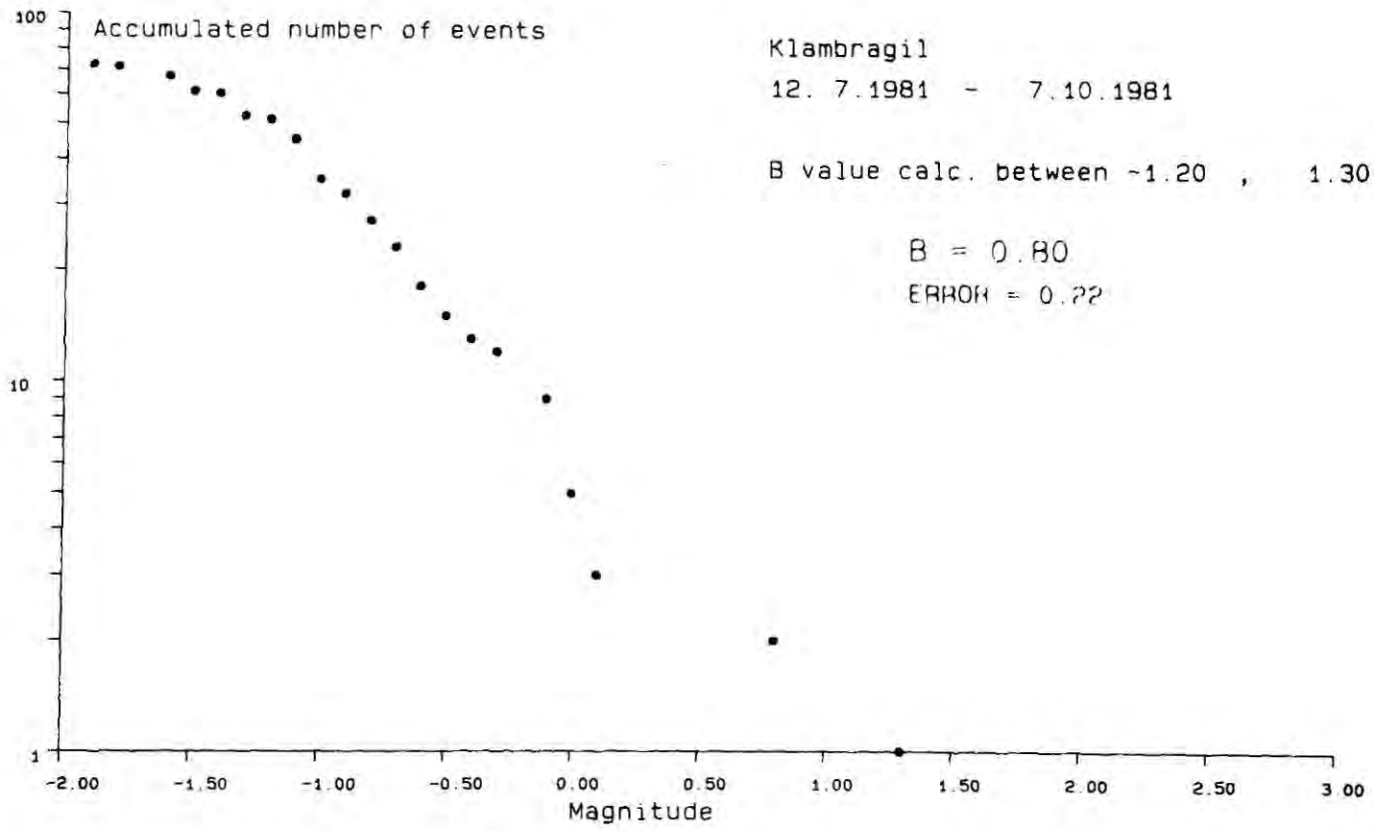

Fig. 5.13 Frequency magnitude plot Klambragil area.

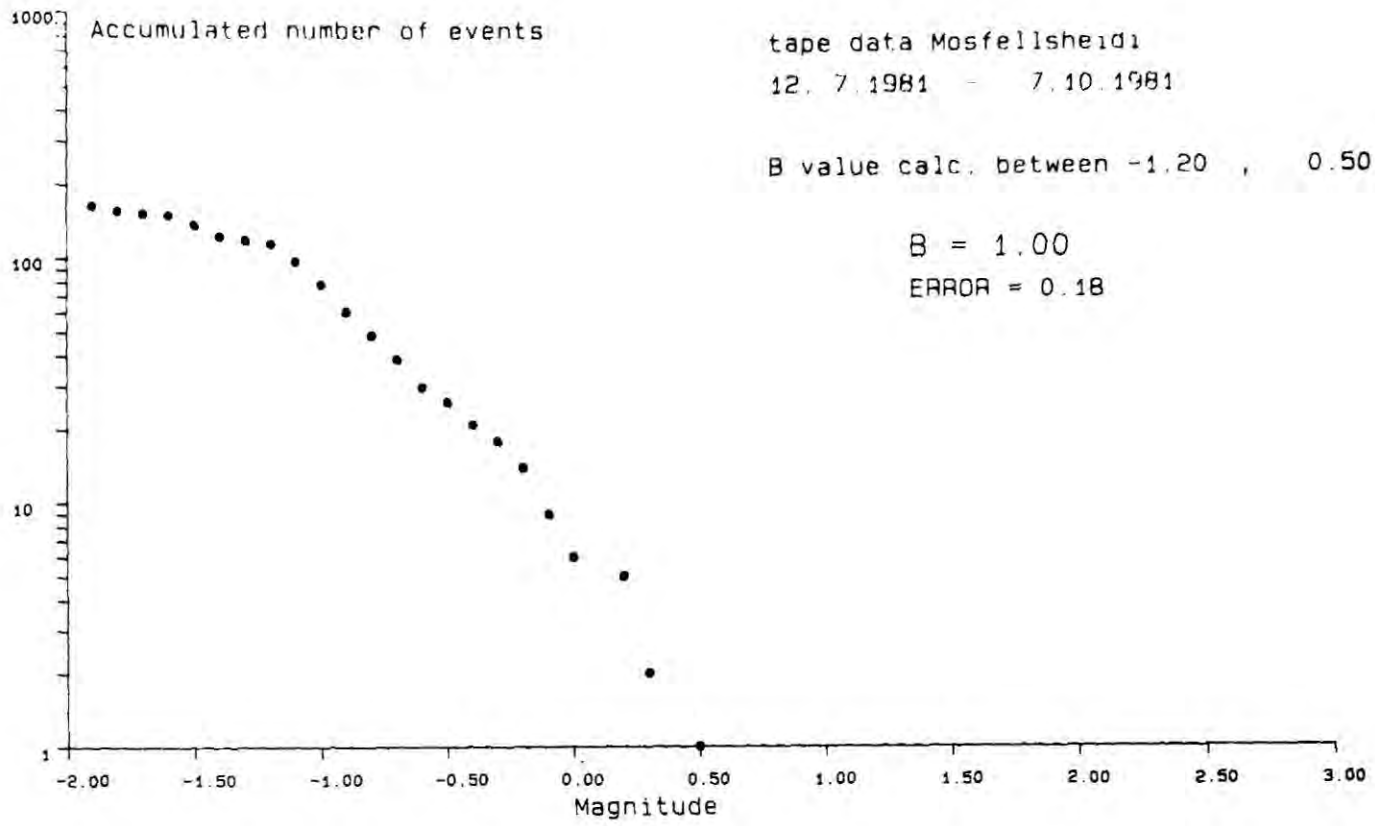

Fig. 5.14 Frequency - magnitude plot - Mosfellsheidi area.

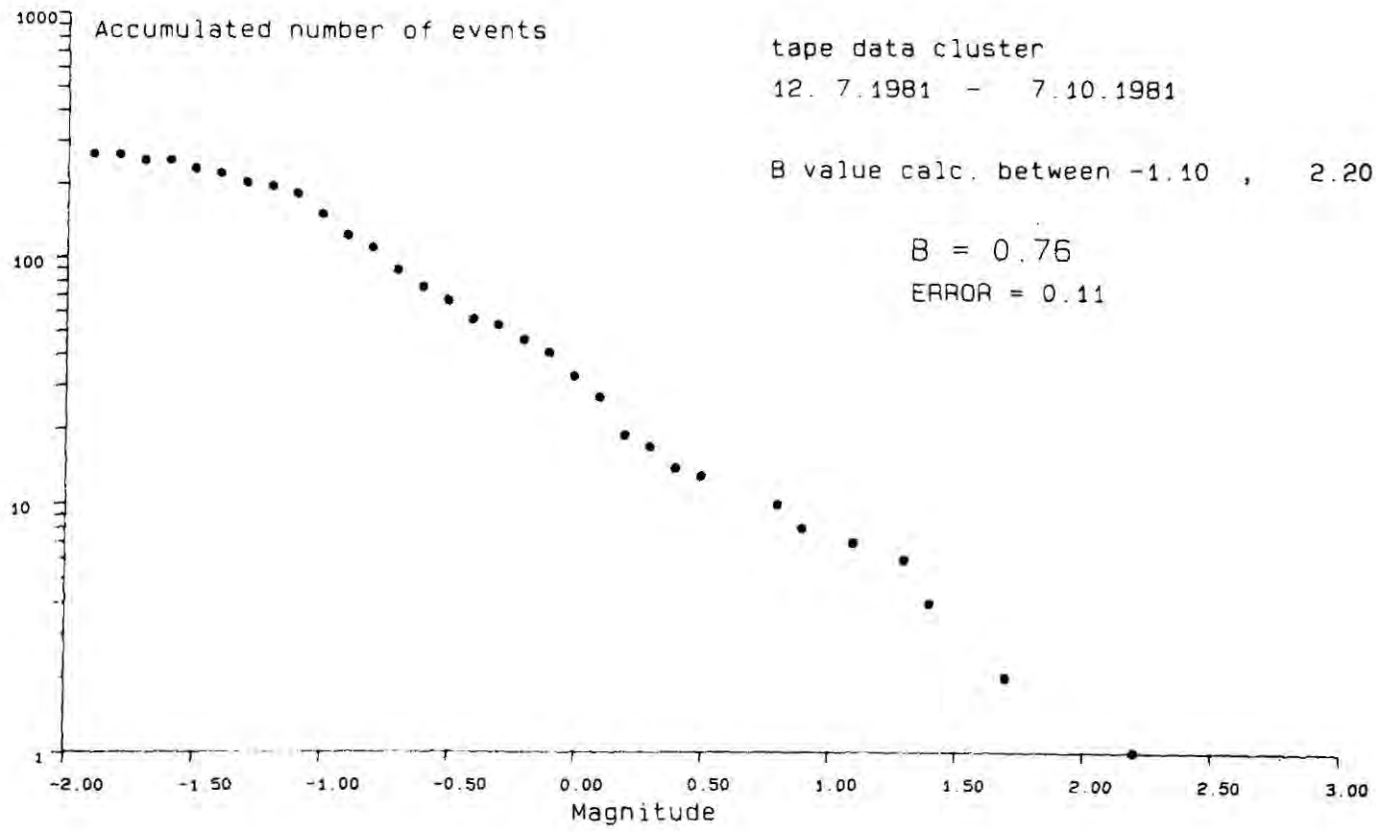

Fig. 5.15 Frequency - magnitude plot - central cluster.

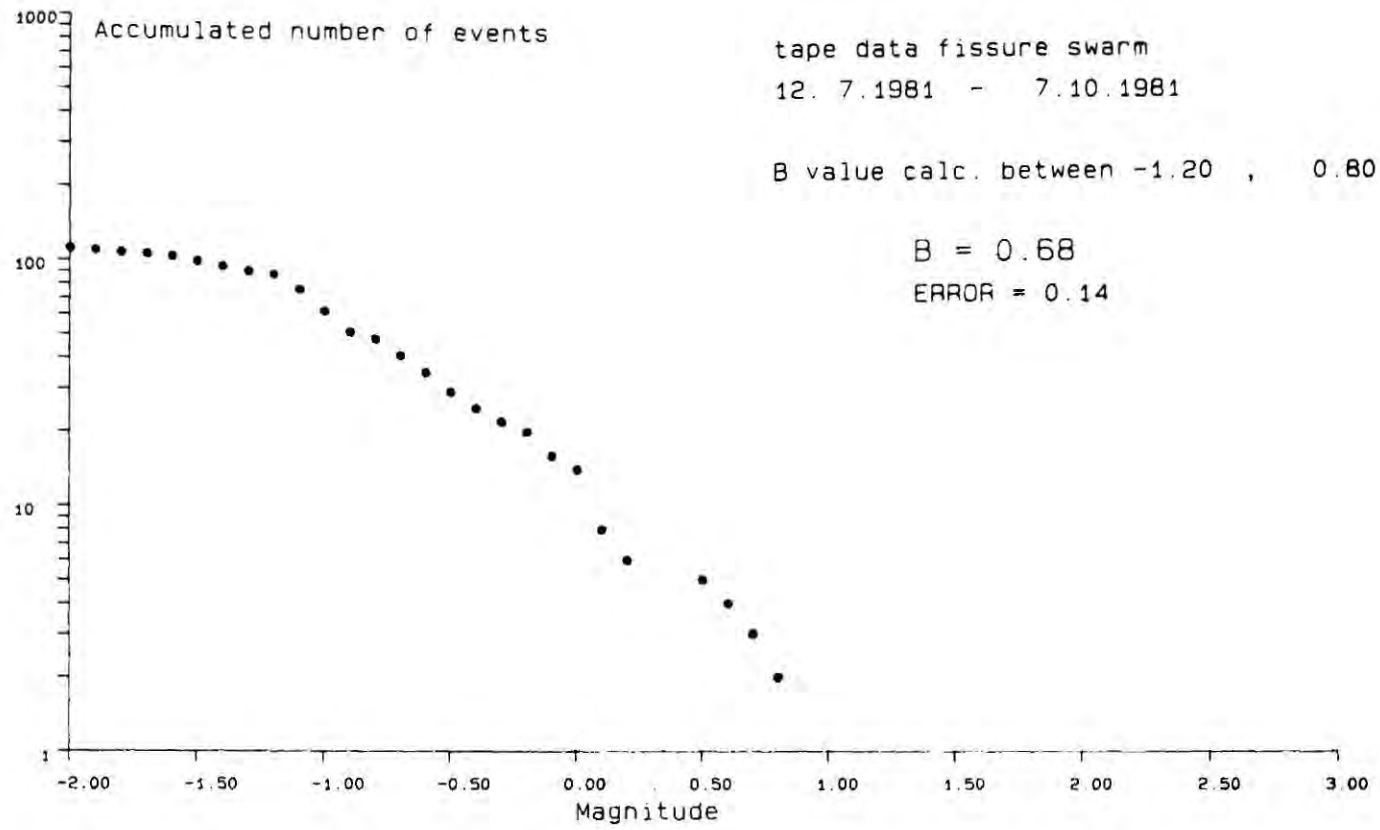

Fig. 5.16 Frequency - magnitude plot - fissure swarm.

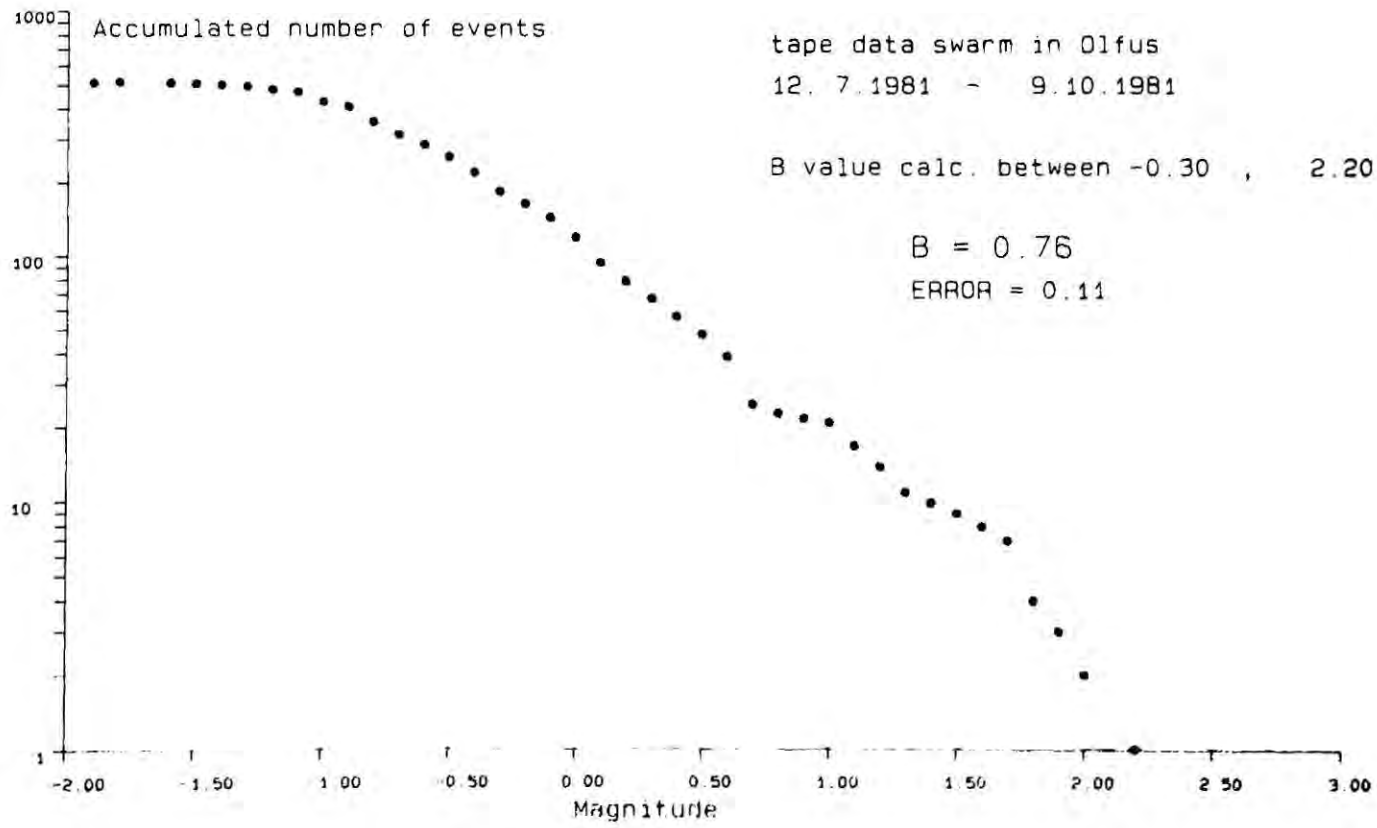

Fig. 5.17 Frequency - magnitude plot - Kirkjuferjuhjaleiga, Olfus swarm.

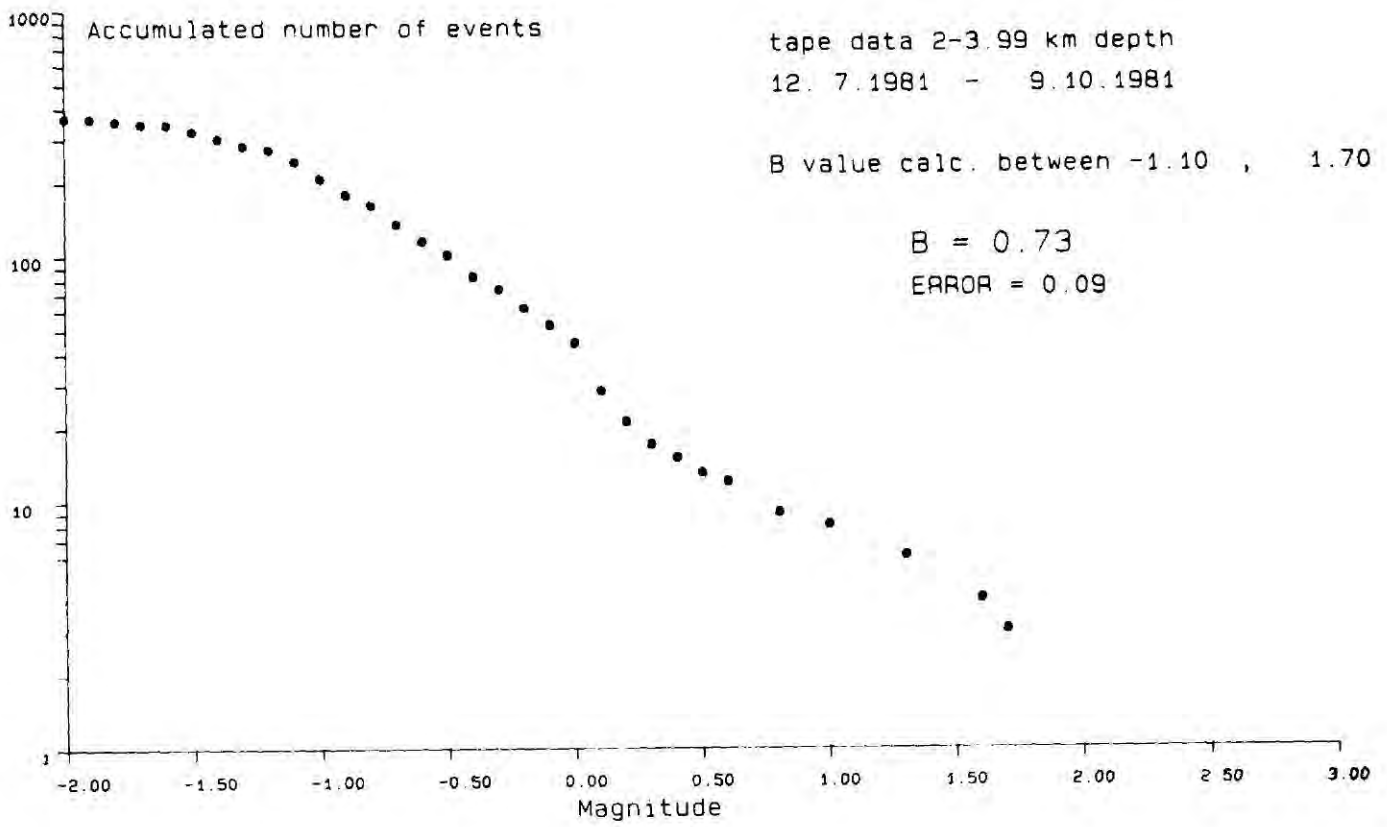

Fig. 5.18 Frequency - magnitude plot - 2.00 - 3.99 km depth.

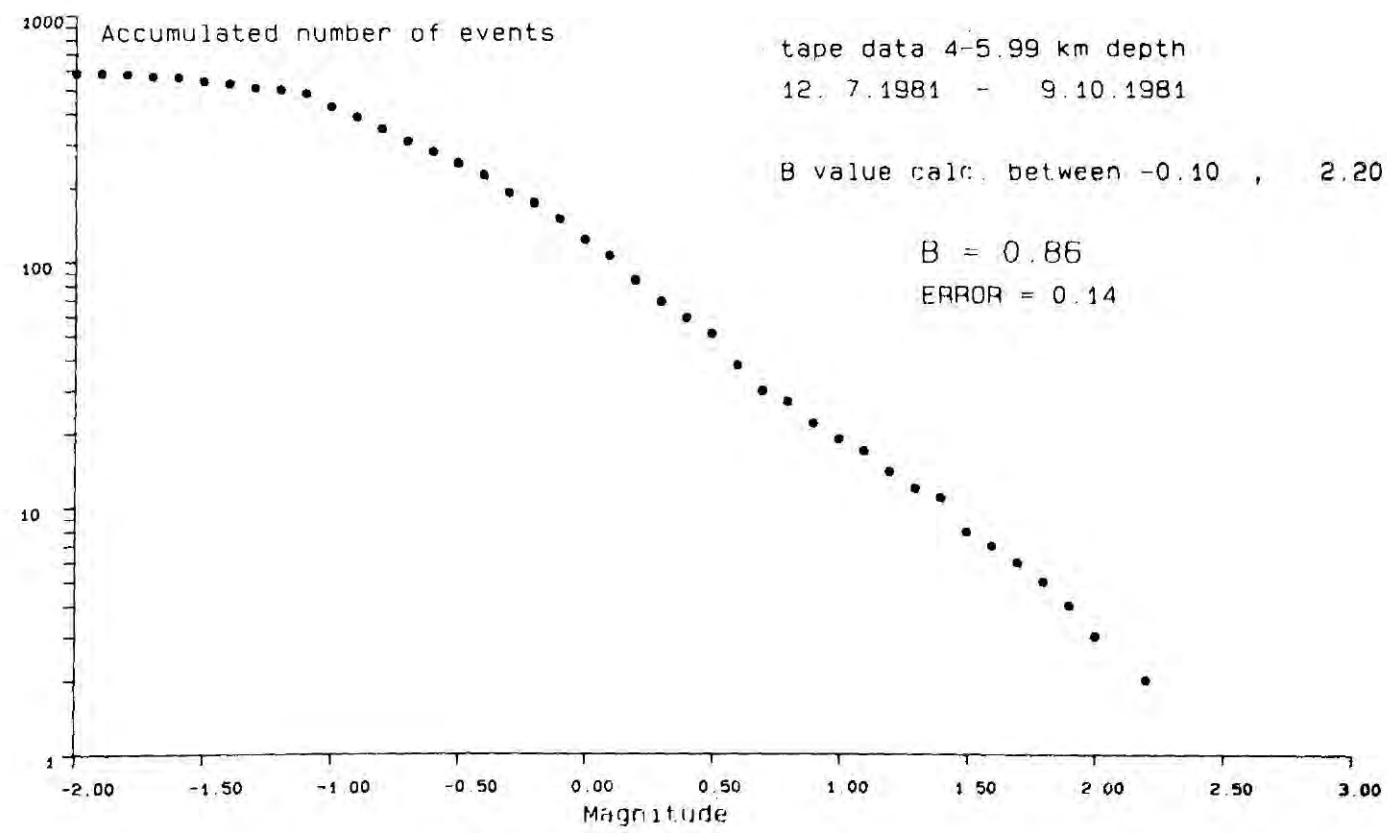

Fig. 5.19 Frequency magnitude plot - 4.00 - 5.99 km depth.

Area	b-value calc. betw. M_{IL}	size of data set for b-val calculation	error (95% conf. limit) ±	b
N of 64° N	-0.9/2.2	318	0.09	0.80
S of 64° N	-0.9/2.2	570	0.06	0.74
Klambragil	-1.2/1.3	51	0.22	0.80
Mosfellsheidi	-1.2/0.5	116	0.18	1.00
cluster	-1.1/2.2	181	0.11	0.76
fissure swarm	-1.2/0.8	87	0.14	0.68
Olfus swarm	-0.3/2.2	184	0.11	0.76
2.00-3.99 km depth	-1.1/1.7	243	0.09	0.73
4.00-5.99 km	-0.1/2.2	149	0.14	0.86
entire area	-0.9/2.2	1424	0.04	0.72

Table 5.1 b values calculated for subdivisions of the Hengill area

(Fig. 4.2), indicating that an abrupt change occurs on the W boundary of the fissure swarm. It may indicate a change from the anomalously low b-values associated with the Hengill area in general to more "normal" intraplate values such as those observed for the Borgafjordur area (Section 5.2.1).

5.2.4 Running b-values

5.2.4.1 Data recorded on the local seismograph IR

Fig. 5.20 is a running b-value plot over the period April 1977-December 1983. The vertical axis is b-value and covers the range 0.5 - 1.0. A sample size of 200 was taken, which results in an uncertainty of ± 0.08 to 0.11 in the data points. The incremental number of earthquakes was 20.

The b-value varies from 0.64 to 0.79, i.e. over a range of 0.15 units. Also shown in Fig. 5.20 are events of $M_{IL} \geq 3.0$ that occurred in the Hengill area during the 7 year period. All of these 4 events occurred in 1977-78 and were accompanied by a decrease in b-value from 0.79-0.65. However, a similar decrease occurred May 1981-June 1982 with no accompanying $M_{IL} \geq 3.0$ seismicity.

The temporal variations in b found in the IR data set are not statistically significant and at the time of writing have not been correlated with any ongoing process in the Hengill area.

5.2.4.2 Data recorded on the radio telemetered network

Fig. 5.21 is a running b-value plot over the period July - Oct. 1981. The vertical axis is b-value and covers the range 0.5 - 2.0. A sample size of 100 was taken which results in an uncertainty of ± 0.12 to 0.22. The incremental number of earthquakes was 10.

The Figure is dominated by a feature around mid September

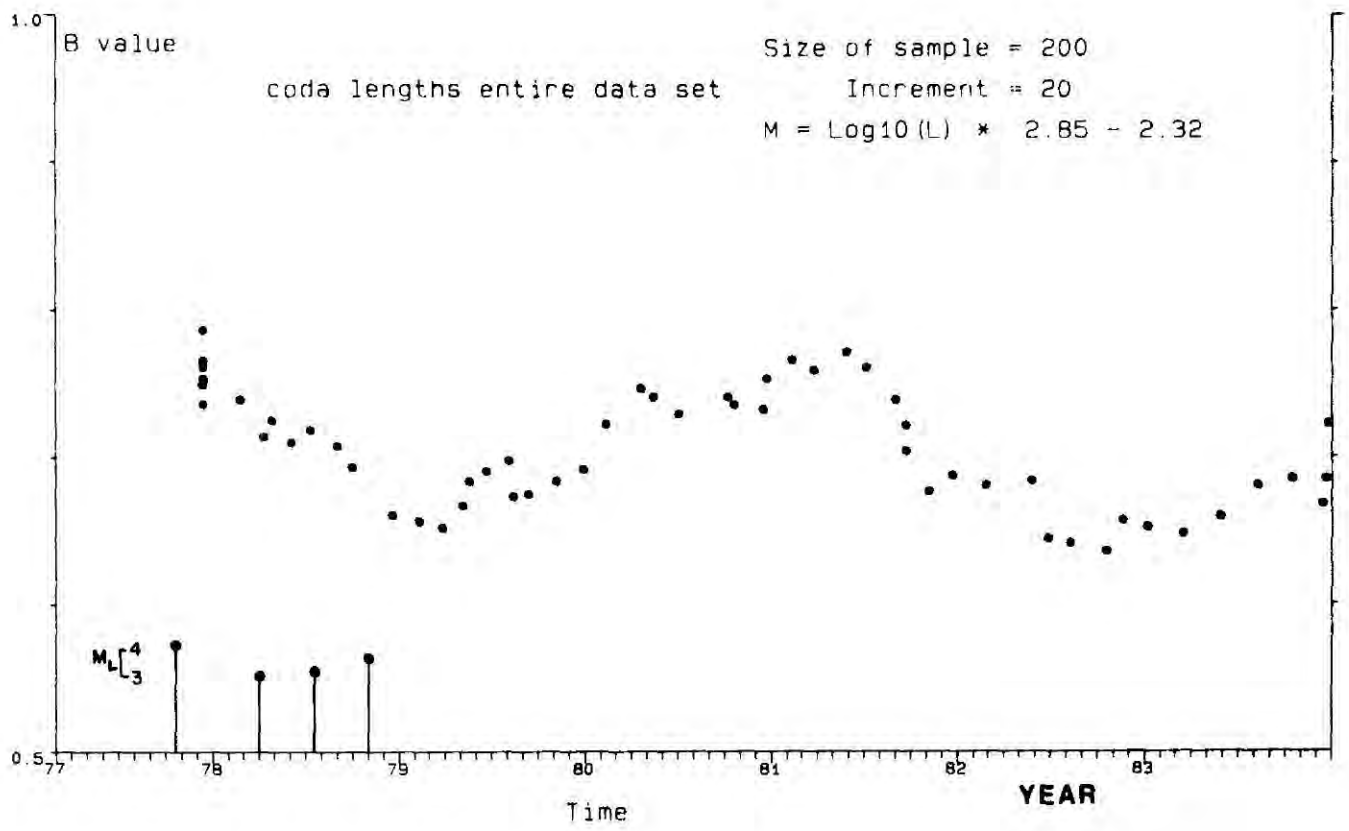

Fig. 5.20 Running b-value plot, 7 year data set from the local station IR.

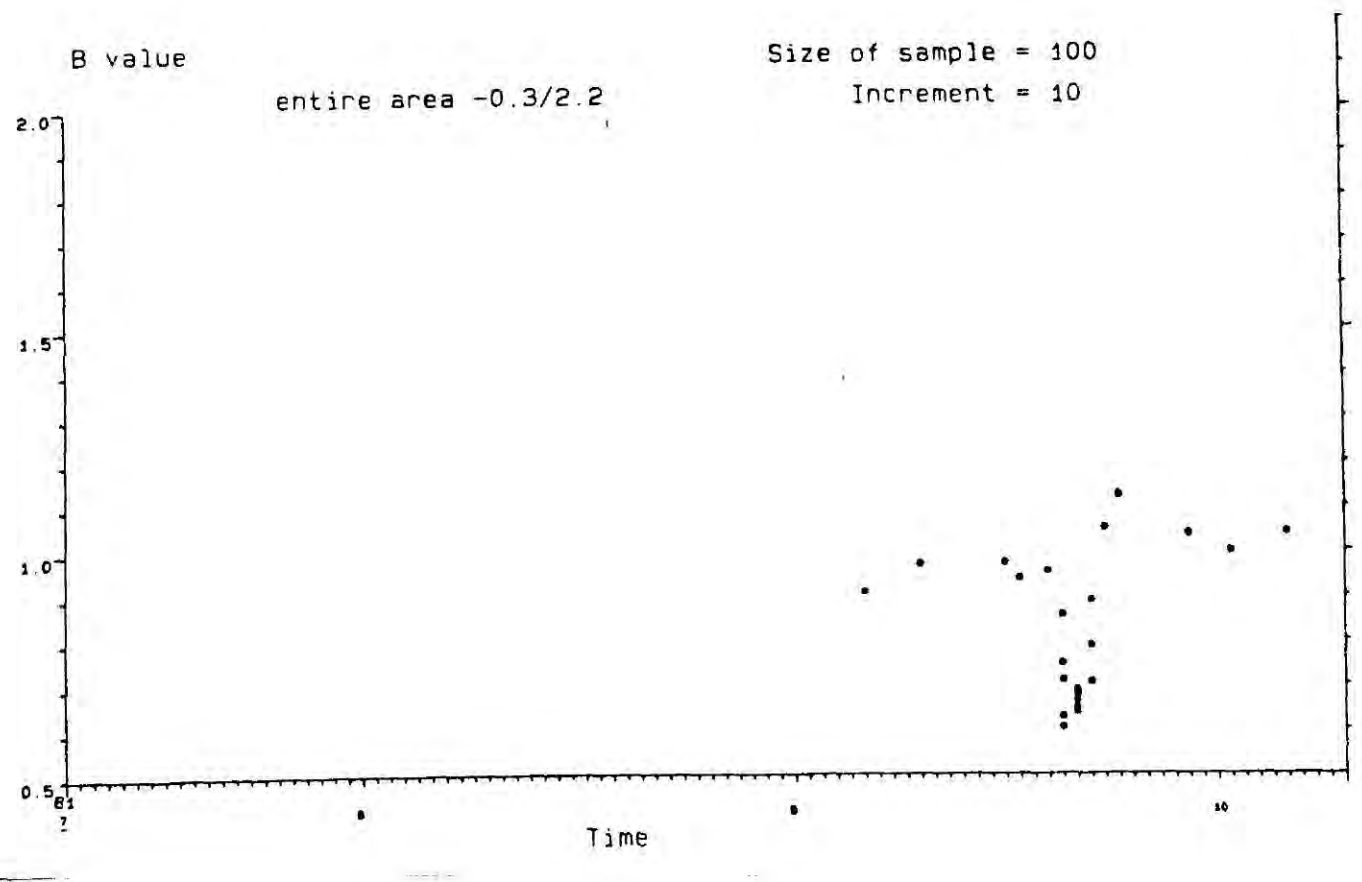

Fig. 5.21 Running b-value plot, 3 month data set from the radio telemetered network.

which corresponds to the swarm near Kirkjuferjuhjaleiga, Olfus. In Fig. 5.22 events S of 64° N only are plotted separately. A sample size of 100 and an increment of 30 was taken since the data set was small (610 events). In Table 5.2 the data points plotted in Fig. 5.22 are listed with their uncertainties. In Fig. 5.23 all the events of $M_{IL} \geq -0.9$ are plotted against time for the period of the swarm alongside the b-value.

The b-value varies from 0.43 to 1.15, i.e. over a range of 0.72 units and the uncertainties vary from 0.08 to 0.22. This is a statistically significant variation. The possibility that they could be due to variations in the location threshold throughout the swarm was ruled out by plotting separate frequency-magnitude diagrams for each day of the swarm. In all cases the distribution was linear for $M_{IL} \geq -0.9$. It can be seen from Fig. 5.23 and Table 5.2 that prior to the swarm the b-value exhibited was relatively high (compared with the rest of the Hengill area) - about 0.85 ± 0.17 but with the onset of the swarm it rapidly decreased to reach its lowest value of 0.43 ± 0.08 towards the end of the 19th September. It rapidly increased on the following day and rose to a high value at the end of the swarm (1.15 ± 0.22). It subsequently decreased to a value of 0.81 ± 0.16, a more "normal" value for the Hengill area in general.

Interpreted in terms of variation in stress within the source region, these results indicate that the onset of the swarm accompanied an increase in stress in the source region. This stress was quickly released during the early part of the swarm during which time most of the largest events occurred ($1.5 \leq M_{IL} \leq 2.2$). The continuation of the swarm resulted in a

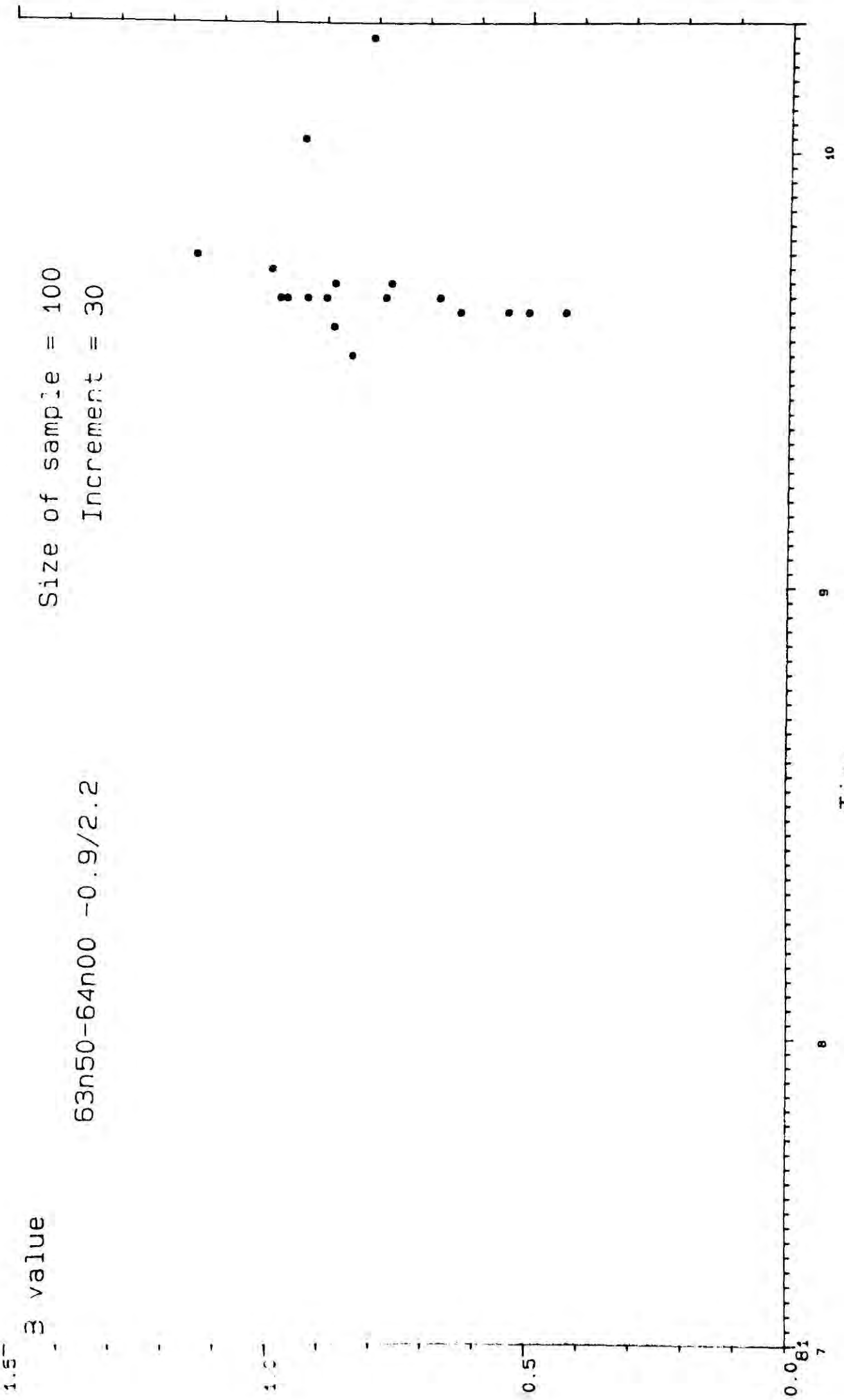

Fig. 5.22 Running b-value plot, events located S of 64°N on the radio telemetered network.

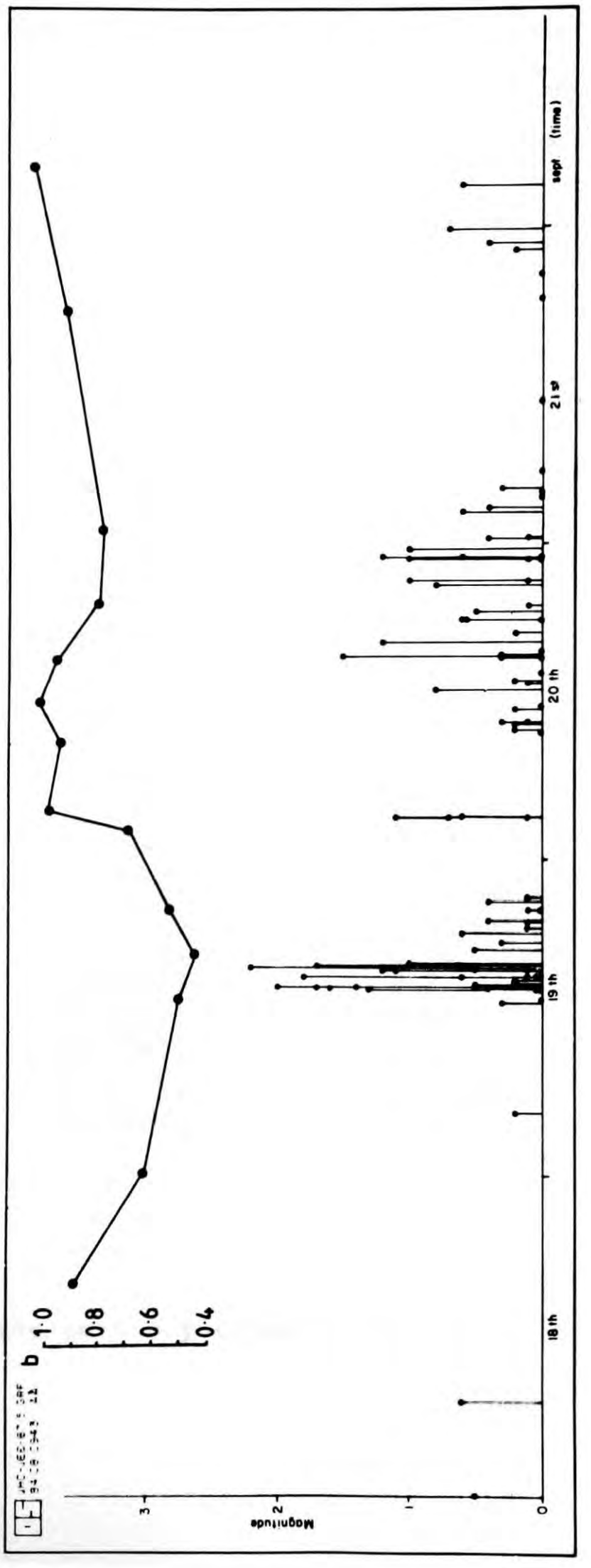

Fig. 5.23 Magnitudes of events of Kirkjuferjuhjaleiga. Olfus swarm and associated b-values. b-values plotted were calculated for the preceeding 100 events in the area S of 64°N

further reduction of stress, and by the end of the swarm stress had again returned to its former level.

These changes in b-value are in a similar style to others reported for earthquake sequences (Rikitake, 1976) and are consistent with those predicted by theory (Section 5.2.1).

Time from - to	B - value	Error
10.07.81 - 16.09.81 -	0.85	0.17
16.09.81 - 18.09.81 -	0.38	0.17
18.09.81 - 19.09.81 -	0.63	0.12
19.09.81 - 19.09.81 -	0.50	0.10
19.09.81 - 19.09.81 -	0.43	0.08
19.09.81 - 19.09.81 -	0.54	0.11
19.09.81 - 20.09.81 -	0.68	0.13
20.09.81 - 20.09.81 -	0.97	0.19
20.09.81 - 20.09.81 -	0.90	0.17
20.09.81 - 20.09.81 -	0.99	0.19
20.09.81 - 20.09.81 -	0.93	0.18
20.09.81 - 20.09.81 -	0.78	0.15
20.09.81 - 21.09.81 -	0.77	0.15
21.09.81 - 21.09.81 -	0.83	0.17
21.09.81 - 22.09.81 -	1.00	0.20
22.09.81 - 23.09.81 -	1.15	0.22
23.09.81 - 01.10.81 -	0.94	0.18
01.10.81 - 08.10.81 -	0.81	0.16

Table 5.2 Data points plotted in Fig. 5.22

5.3 Summary of the results

The temporal nature of the seismicity of the Hengill area is remarkable because of its continuous day to day nature. In this respect it contrasts with all the neighbouring seismic areas. The continuity of the activity is most striking in a 20 km^2 area NW of Hveragerdi, but is also observed for other parts of the area. This fact is the single most important one that facilitated the design of the 1981 radio telemetry monitoring project and guaranteed its success. Sequences of various types are superimposed on continuous background activity.

A b-value of 0.74 ± 0.06 for the Hengill area is constrained by a large body of data. This is low compared to the value 1.0 usually quoted for the global average. Comparable b-value studies on the Reykjanes Peninsula yielded estimates of b of 0.85 ± 0.07, 1.02 ± 0.07 and 0.75 ± 0.11 and in the intraplate Borgafjordur area of 1.09 ± 0.06 and 1.06 ± 0.06. The b-value for the Hengill area is therefore significantly lower than these. These values of b calculated for Iceland are roughly comparable with b-values of 1.33 and 0.65 calculated for the ridge and fracture zone portions of the mid-Atlantic ridge respectively, using M_S.

Evidence has been discussed above that b may be inversely related to stress. If this is the case then the crust of the Hengill area in general may be more highly stressed than that of the Reykjanes Peninsula and the Borgafjordur areas. This enhanced stress level may be due to thermal or tectonic effects.

Historic macroseismic data indicate an upper magnitude

limit of M_{IL} = 6-6.5 for events in Olfus and lower for the high temperature geothermal area N of 64° N. No statistical evidence for either of these limits was found in the instrumentally recorded data, however, possibly because the sample time (53 years) is too short. The historical data thus suggest that the South Iceland Seismic Zone of destructive earthquakes extends into the Hengill area in Olfus, but does not encompass the high temperature geothermal area.

Investigation of local variations of b within the area indicated elevated b-values for the Mosfellsheidi area and the deeper events in general. This may indicate lower stresses in these areas. For all other subdivisions of the area b was statistically constant. If these variations are stress induced then it may be that the strength of the crustal rocks decreases with depth beneath the Hengill area, because of temperature elevation. The high b-value of Mosfellsheidi, relative to the rest of the area, may indicate that the high stress regime associated with the Hengill area terminates abruptly on the W boundary of the fissure swarm. On Mosfellsheidi the stress regime is more characteristic of that observed on the Reykjanes Peninsula and in the intraplate Borgafjordur area.

Calculations of running b-values show that no statistically significant variation was detected over a 7 year period at a local instrument (IR) with detection threshold M_{IL} = 0.3. However, significant variations occurred during a single swarm in the Kirkjuferjuhjaleiga, Olfus area in Sept. 1981. One possible explanation for these variations is that the source volume experienced a stress pulse accompanied by seismic activity.

CHAPTER 6

6. FOCAL MECHANISMS

6.1 Non-double couple focal mechanisms

6.1.1 Introduction

It is generally assumed that all earthquakes occur as a result of shear slip on buried faults (the "double couple" source). Theory predicts that the P-wave radiation pattern generated by such movement would exhibit equal areas of compression and dilation when projected onto the focal sphere. It should be possible to separate these areas of compression and dilation by drawing two orthogonal great circles on the focal sphere, thus dividing it into 4 "quadrants" - two compressional and two dilational. One of the great circles represents the fault plane and the other is named the "auxiliary plane". The widespread acceptance of this theory and its use in the routine interpretation of earthquake radiation patterns is doubtlessly influenced by the fact that the great majority of data are consistent with it.

A number of earthquake radiation patterns have been described that cannot be interpreted simply in terms of a double couple source. The analysis of these events is controversial. Because there are conceptual difficulties with non-double couple sources, and also earthquakes that exhibit such radiation patterns are rare, many authors prefer explanations for them that involve propagation effects. Robson et al. (1968) described some examples of Japanese earthquakes whose

compressional fields project small circles onto the focal sphere. They suggested that such a radiation pattern may be generated by a volumetric source that conserves volume, the "compensated linear vector dipole" (CLVD) source (see Section 6.1.3). They further suggested that such events may be triggered by the upward migration of melts from the upper mantle. Evison (1963) suggested that these events might be generated by rapidly running phase transitions in rock volumes. The CLVD has recently been invoked to account for a sequence of large earthquakes at Mammoth Lakes, CA (Julian, 1983) and it is suggested that they were generated by dyke injection (Julian and Sipkin, 1984; Aki, 1984). Other workers, however, prefer explanations for these events in terms of propagation effects or multiple events (e.g. Given et al., 1982; Wallace, 1984).

Several reports have been made of earthquake radiation patterns from the mid-Atlantic Ridge and its continuation onto the Icelandic landmass that apparantly display non-orthogonal nodal planes (Sykes, 1967; Sykes, 1970; Klein et al., 1977; Einarsson, 1979). These events all display reduced dilational fields and could thus be interpreted as exhibiting an enhanced explosive component. However, because polarity plots from mid-Atlantic Ridge earthquakes are all lower hemisphere, explanations for their observed deviancy from double couple type may be found involving path effects e.g. the focusing of downgoing rays through a sub crestal magma chamber (Solomon and Julian, 1974) or interference between P, pP and sP (Trehu et al., 1981). Lateral inhomogeneities on a very small scale were invoked by Klein et al. (1977) and Einarsson (1979) to account for the non-double couple radiation patterns of small, local

earthquakes on the Reykjanes Peninsula, Iceland.

6.1.2 The Hengill events

A foreknowledge of the spatial distribution of the seismicity of the Hengill area enabled the the deployment of the radio telemetered network in a configuration that provided the optimum net geometry for focal mechanism determinations. Well constrained radiation patterns were determined for 178 events. For 50% of these events the dilational and compressional portions of the focal sphere could not be separated by a pair of orthogonal great circles.

The possibilities were considered that these observations were attributable to instrument malfunction, distortion due to propagation path effects or source complexities. It was possible to rule out the first two influences. A series of refraction shots fired both within the area and at regional distances indicated consistent seismometer response and lateral crustal velocity homogeneity to within 10% in the upper few km (Section 7.2). Such small lateral velocity inhomogeneities are insufficient to account for the extreme deviancy from double couple type observed for the anomalous Hengill events. A suite of teleseisms recorded throughout the monitoring period also indicated consistent seismometer response. In addition, earthquakes exhibiting double couple type radiation patterns were detected interspersed spatially and temporally with the non-double couple events. It was concluded that the "anomalous" radiation patterns were generated by events with source complexities, i.e. that they did not result from shear slip on

fault planes.

The anomalous events are characterised by compressional radiation fields that typically occupy 80% of the focal sphere, and correspondingly severely reduced dilational fields (Fig. 6.1). The dilational arrivals are of normal amplitude. These facts imply that the sources that generate the events exhibit a net explosive component (i.e. a "volume increase"), and are thus not of the CLVD type. The interpretation of them favoured here is that their source mechanisms involve fault planes, but that movement is in the direction normal to the fault plane instead of parallel to it as is the case for a shear dislocation, i.e. that they may be approximated to tensile cracks. The reasons why this model is taken are that the observed anomalous radiation patterns are very similar to that predicted by theory for a tensile crack and also that this model is a reasonable one in an area such as Hengill that contains an accretionary plate boundary and displays features clearly indicative of a tensile stress regime (e.g. open surface fissures, geological offsets).

6.1.3 A general representation of seismic sources

Seismic sources may be described by a general representation that is not based on an assumption of source mechanism, but which is readily interpretable in terms of known source types. This representation is known as the moment tensor representation of the source. The subject is dealt with in depth by Aki and Richards (1980) and a simplified introductory treatment is given by Foulger (1984). This section gives a

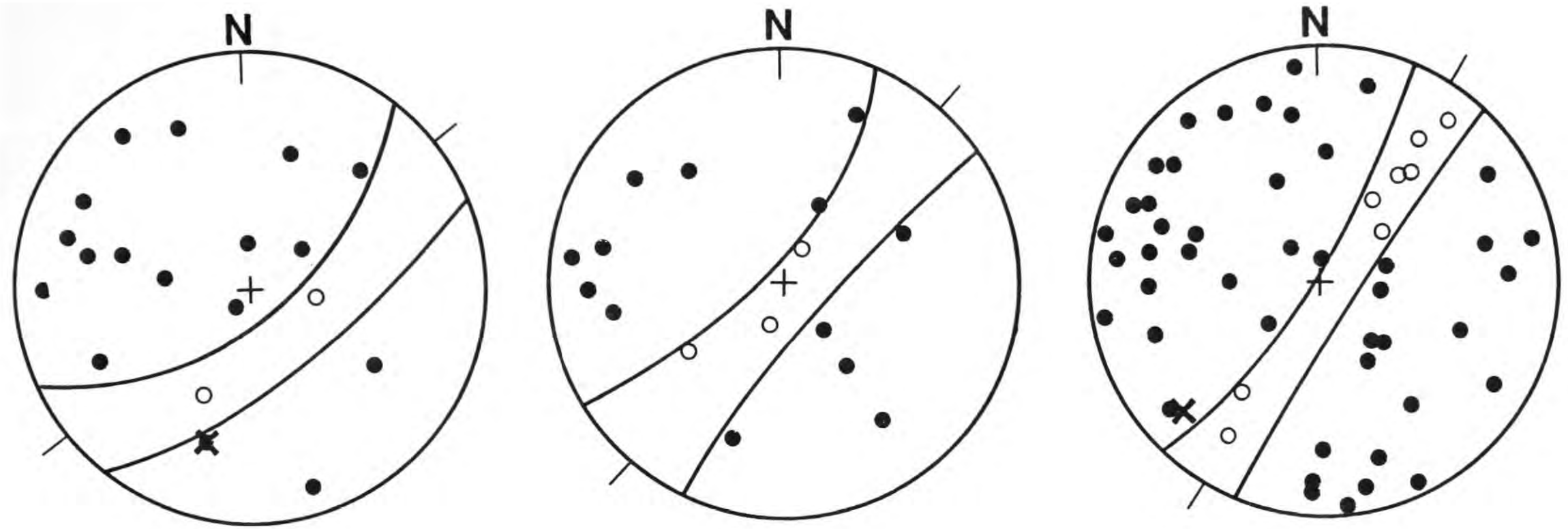

Fig. 6.1 P-wave first motions from two non-double couple events and one composite solution. Upper hemisphere plots in stereographic projection. ● , compressions; O , dilations; X , nodal arrivals; curved lines, small circles of radius θ defining nodal lines of tensile crack solution. a, event 1: depth 4.87 km; M_L=0.1; strike N 53°E; dip=60°, θ =78°. b, Event 2; depth=4.99 km; M_L=0.0; strike=N 42°E; dip=80°; θ =76°. c, composite solution for 3 events; strike normalised; dip=80°; θ =80°.

summary of the main points.

Consider a general seismic source having a body force equivalent given by couples alone. For 3 components of force and 3 possible arm directions, there are 9 generalised couples (Fig. 6.2).

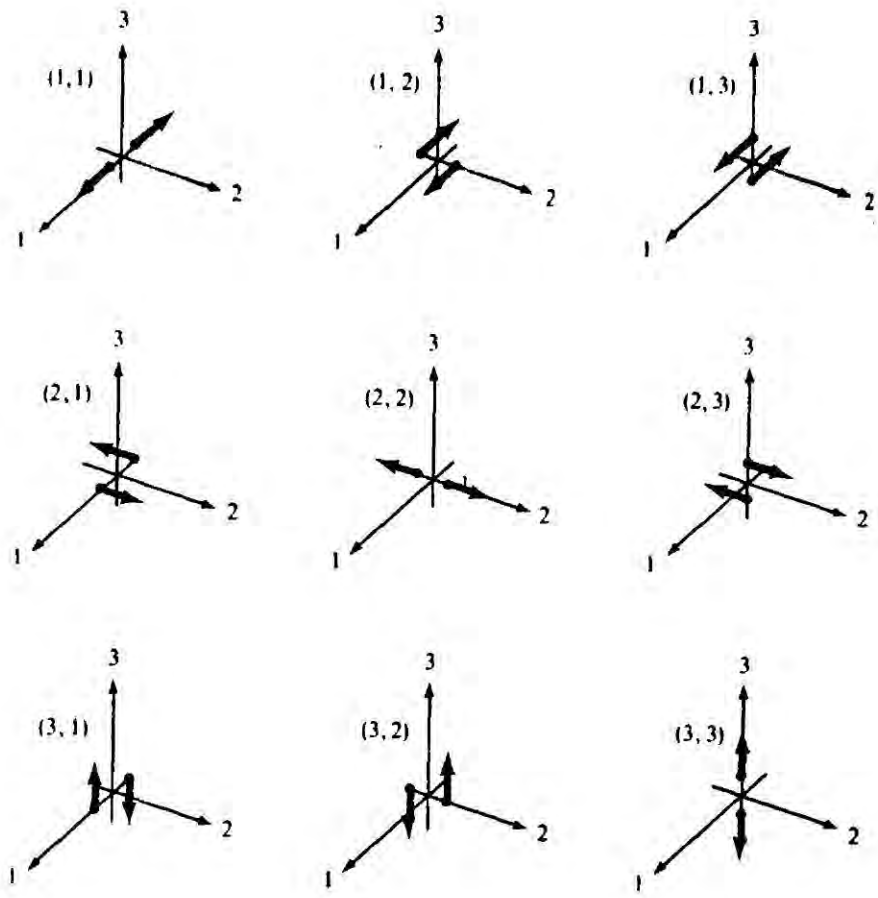

Fig. 6.2 The nine possible couples that are required to obtain equivalent forces for a generally oriented displacement discontinuity in anisotropic media (from Aki and Richards, 1980).

The seismic moment density tensor m has 9 components equal to the strengths of the 9 generalised couples:

$$m = \begin{vmatrix} m_{11} & m_{12} & m_{13} \\ m_{21} & m_{22} & m_{23} \\ m_{31} & m_{32} & m_{33} \end{vmatrix}$$

The components of this tensor are obtainable from the far field radiation pattern (Aki and Richards, 1980):

$$u_n(x,t) = \iint_{\Sigma} m_{pq} * G_{np,q} \, d\Sigma$$

where:

$u_n(x,t)$ = displacement function

m_{pq} = components of the moment density tensor

$G_{np,q}$ = the Green function

Σ = surface area

In order to describe seismic sources in general, only the couples with force and arm in the same direction are needed (cases (1,1), (2,2) and (3,3) of Fig. 6.1). These are known as vector dipoles. For example, in the case of a shear source the the seismic moment density tensor is of the form:

$$m = \text{constant} \times \begin{vmatrix} 1 & 0 & 0 \\ 0 & 0 & 0 \\ 0 & 0 & -1 \end{vmatrix}$$

i.e. the principal moments are in the ratio (1,0,-1).

Because the sum of the principal moments is equal to zero, the shear source has no volumetric component, i.e. it has no net explosive or implosive component. In contrast, a pure

explosion has principal moments in the ratio (1,1,1) and is a source that exhibits a net "volume increase". The tensile crack may be considered to be an elongated explosion, has principal moments in the ratio $(\lambda,\lambda,\lambda+2\mu)$ [λ and μ are the Lame constants] and thus also exhibits a net "volume increase" (Aki and Richards, 1980).

Computational proceedures have been developed that enable least squares solutions for the principal moments to be calculated from the far field radiation pattern (e.g. Randall and Knopoff, 1970; Langston, 1981). In all cases the ratio of the principal moments may be expressed in the form:

$$(a,b,c)$$

A volumetric component (in the case of the source that exhibits a net explosive or implosive mechanism, i.e. $(a+b+c) \neq 0$) may be especially difficult to explain because of the large confining pressures encountered at depth in the earth. Thus some authors avoid the problem by artificially constraining $(a+b+c) = 0$ in their computations (e.g. Julian, in press)

In the case where all three principal moments are non-zero, a three dimensional process is implied. The concept of the seismic moment density tensor is a useful one for considering such sources, since tensor representations of simple sources may be combined linearly to model complex sources.

Where $a+b+c = 0$ and a,b,c are all non-zero, the source may always be decomposed into a "volumetric component" and a pair of orthogonal double couples:

$$(a,b,c) = (d,d,d) + (-\{b-d\},+\{b-d\},0) + (-\{c-d\},0,+\{c-d\})$$

where $d = \frac{1}{3}(a+b+c)$

The orthogonal double couples are sometimes termed the "major"

and "minor" double couples (e.g. Barker and Langston, 1983).

The "compensated linear vector dipole" (CLVD) source has principal moments in the ratio (2,-1,-1). This is thus an example of a three dimensional source that conserves volume.

6.1.4 The moment tensor representation of the non-double couple Hengill events

The preponderance of compressional arrivals indicates a net explosive component and the narrow dilational belt indicates planarity of the source. For these reasons the tensile crack was taken as the basis of a model.

The seismic moment density tensor of a tensile crack is $(\lambda, \lambda, \lambda+2\mu)$, which gives an all-compressive radiation pattern. It differs from a pure explosion only in as much as the amplitude of the radiation is not spherically symmetrical. The superposing of a spherically symmetrical implosion onto this source would result in a source that exhibits a dilational belt:

$$(\lambda, \lambda, \lambda+2\mu) + (-[\lambda+\delta\lambda], -[\lambda+\delta\lambda], -[\lambda+\delta\lambda]) = (-\delta\lambda, -\delta\lambda, [2\mu-\delta\lambda]) \ldots [1]$$

Foulger and Long (1984) (reprint enclosed in pocket at the back of this thesis) and Foulger (1984) suggest that the events are generated by the formation of tensile cracks in the presence of restricted pore fluid flow. Under these conditions there is a pore pressure drop in the volume occupied by the new void. This pore pressure drop generates an omnidirectional implosive pressure pulse that is superimposed on the radiation pattern of the tensile crack and is thus the mechanism that generates the

dilational field. The pressure differential is subsequently equalised by aseismic diffusion of the pore fluid.

A source of this type would exhibit nodal surfaces that trace small circles on the focal sphere (for a shear source the nodal lines are great circles).

Calculation of the seismic moment density tensor for the Hengill non-double couple events

For a general seismic source:

$$u_n(x,t) = \iint_{\Sigma} m_{pq} * G_{np,q} \, d\Sigma$$

In the frequency domain, this reduces to (Julian, in press):

$$\vec{u}(w) = \vec{g}^{T} \vec{m}(w)$$

where $\vec{u}(w)$ is the amplitude or mode of the seismic wave

Referring to Fig. 6.3,

$\vec{g}(w)$ is a column vector whose elements are spectra of Green's function.

$$\vec{g}(w) = [g_{rr}(w) \; g_{r\theta}(w) \; g_{\theta\theta}(w) \; g_{r\phi}(w) \; g_{\theta\phi}(w) \; g_{\phi\phi}(w)]$$

For a homogenous, isotropic medium, as functions of departure angle i (zero=nadir) and departure azimuth $\jmath$, for p waves:

$$g_{rr} = \cos^2 i \qquad g_{r\phi} = -\sin 2i \sin \jmath$$

$$g_{r\theta} = \sin 2i \cos \jmath \qquad g_{\theta\phi} = -\sin^2 i \sin 2\jmath$$

$$g_{\theta\theta} = \sin^2 i \cos^2 \jmath \qquad g_{\phi\phi} = \sin^2 i \sin^2 \jmath$$

$\vec{m}(w)^{T}$ is a column vector of the 6 independent components of the moment tensor for a point source

$$\vec{m}(w) = [m_{rr}(w) \; m_{r\theta}(w) \; m_{\theta\theta}(w) \; m_{r\phi}(w) \; m_{\theta\phi}(w) \; m_{\phi\phi}(w)]$$

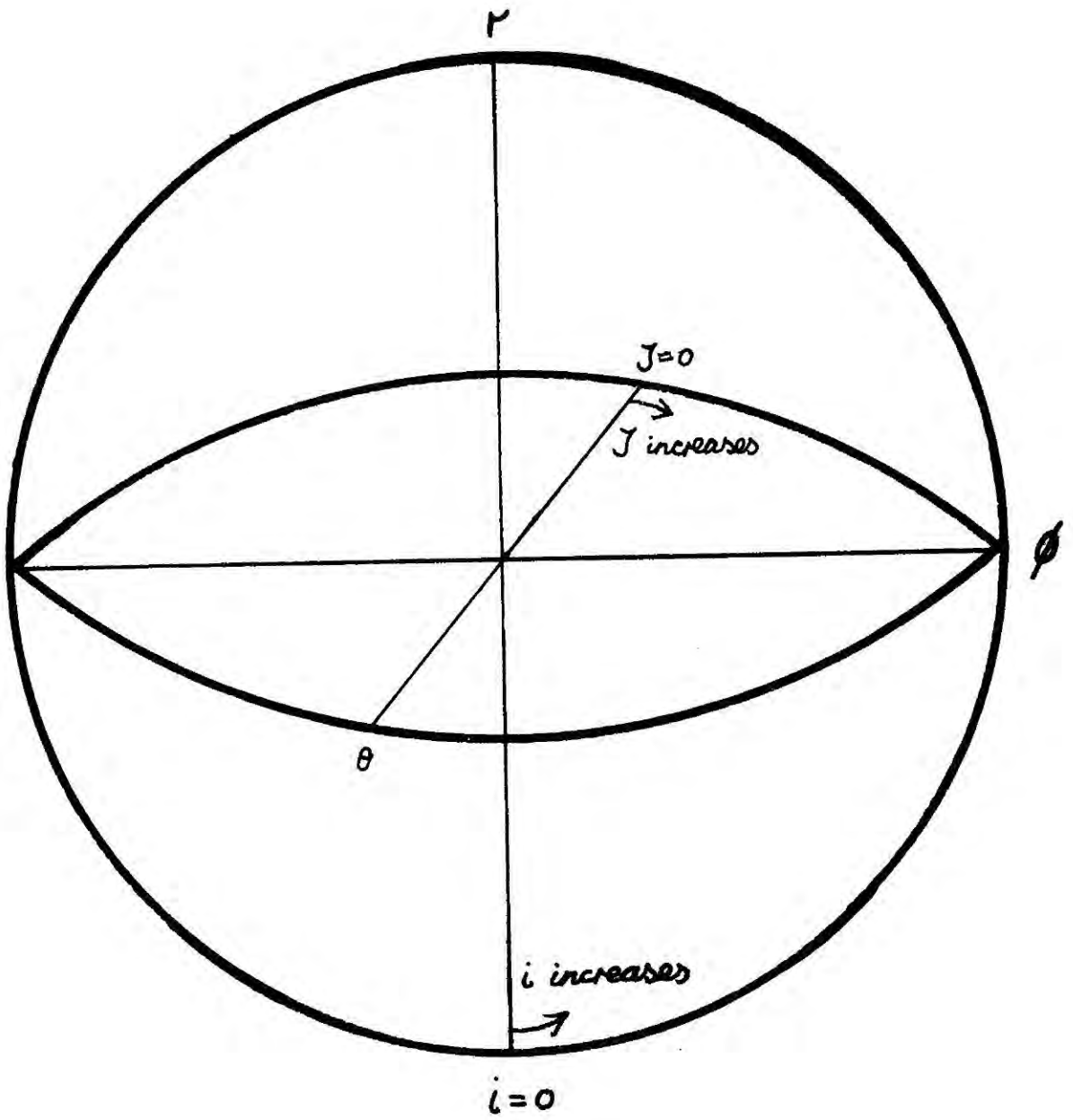

Fig. 6.3 Diagram illustrating the co-ordinate system used in calculating the seismic moment density tensor for the Hengill non-double couple events.

Consider the $\theta\phi$ plane.

$$i = \pi/2 \qquad \sin i = 1 \qquad \sin 2i = 0 \qquad \cos i = 0$$

$$\vec{g}(w) = [0, 0, \cos^2\gamma, 0, -\sin 2\gamma, \sin^2\gamma]$$

Let the dilational components of the seismic moment density tensor be of amplitude x

Then $\vec{u}(w) = [-x, 0, -x, 0, 0, 1]\ [0, 0, \cos^2\gamma, 0, -\sin 2\gamma, \sin^2\gamma]$

$$= 0 + 0 - x\cos^2\gamma + 0 + 0 + \sin^2\gamma$$

at a node, $\vec{u}(w) = 0$

i.e. $x\cos^2\gamma = \sin^2\gamma$

$$\tan\gamma = \sqrt{x}$$

for a typical Hengill event, $\gamma = 10^\circ$

i.e. $x = 0.03$

The moment density tensor for this type of source is therefore:

$$\underline{\vec{m}(w) = [-1, 0, -1, 0, 0, 30]}$$

and approximates to a linear vector dipole source.

Derivation of the volume equation

M_o, the seismic moment, is a fundamental parameter used to measure the strength of an earthquake. For double couple sources:

$$M_o = A\mu u$$

where A = area of the fault plane

μ = rigidity modulus

u = displacement

thus: $M_o = \mu \times$ average slip $\times$ fault area

For a tensile crack:

$$M = V \begin{vmatrix} \lambda+2\mu & 0 & 0 \\ 0 & \lambda & 0 \\ 0 & 0 & \lambda \end{vmatrix}$$

If the Hengill events are approximated to a linear vector dipole (the case where $\delta\lambda \simeq \lambda$, equation [1]), then

$$M = V \begin{vmatrix} 2\mu & 0 & 0 \\ 0 & 0 & 0 \\ 0 & 0 & 0 \end{vmatrix}$$

which reduces to:

$$\underline{M_0 = 2\mu V}$$

<u>The real data</u>

The hypothesis given above for the source mechanism of the Hengill non-double couple events predicts that the nodal surfaces trace small circles on the focal sphere. The radiation patterns of the Hengill events are constrained by a maximum of 23 observations. In the case of the non-double couple events, because of the very small range of the dilational field, only rarely did the number of dilational arrivals exceed 3. The nodal lines are thus not constrained to be small circles by any one event. They are, however, well constrained by composite events (Fig. 6.1) and the great majority of the non-double couple events are consistent with the model. For these reasons the events were interpreted on this basis.

6.2 The mode of strain release in the Hengill area

6.2.1. Presentation of the data

For completeness of documentation, all events for which reasonably good polarity plots were obtained are illustrated in Figs. A7.1 to A7.14 in Appendix 7. The minimum number of data points used to constrain any one solution is 10. Where possible, a shear solution is preferred. In the case of the tensile crack interpretations, small circles were fitted to the data manually using a series of specially constructed graticules. The data have been divided into 12 groups that are suggested by the epicentral distribution (see Section 4.3.2). Each event is labelled by its origin time. The groups are Nesjavellir (N), Mosfellsheidi (M), the fissure swarm (F= all events within the fissure swarm but not included in any other group), Svinahlid (S), Orustuholshraun (O), Astadafjall (A), Klambragil (K), Kyllisfell (KY), Laxardalur (L), the central cluster (C= all events within the cluster NW of Hveragerdi but not included in any other group), Grensdalur (G) and Olfus (O) (Fig. 6.7).

For each group, a summary diagram is also presented in the form of a stereographic projection (see for example, Fig. A7.3). All the events associated with the particular group for which an unambiguous interpretation could be made are represented on these. For the shear solutions the pressure (P) axes and tension (T) axes are represented by open circles and dots respectively. For the tensile crack solutions the planes of the cracks (which, in stereographic projection, bisect the

dilational belts) are represented by great circles. The events for which no solution could be obtained or for which either type of solution would fit equally well are not represented on the summary diagrams. The summary diagrams are displayed together in Fig. 6.4.

6.2.2 The tensile crack events

Examination of Fig. 6.4 indicates that most of the tensile crack events occurred on near vertical planes. The greatest hade measured was 40^{o} . The dominant direction of strike was about N 35^{o}E. This is illustrated in Fig. 6.5 which shows a smoothed plot of the orientation of crack strikes. The width of the dilational belt varied but was never larger than 60^{o}. If the tensile crack interpretation is correct, that the dilational belt is generated by a pressure drop in the pore fluid at the instant of fracturing it would be expected that the width of the belt would be dependent on the magnitude of the pressure drop. The width of the dilational belt might then be governed by such factors as the type and phase of the pore fluid and the porosity of the rock, that would influence the speed of pore fluid flow.

It would be expected that tensile cracks would form normal to the direction of least compressive stress (i.e. greatest tension). Hence the direction of greatest compressive stress would lie in the crack plane. This implies a direction approximately horizontal N 125^{o}E for the least compressive stress (σ_3) in the depth range 2 - 6 km (see Section 6.2.5). The strike and hade of surface extensional features indicates an orientation of horizontal N 115^{o}E for the least compressive

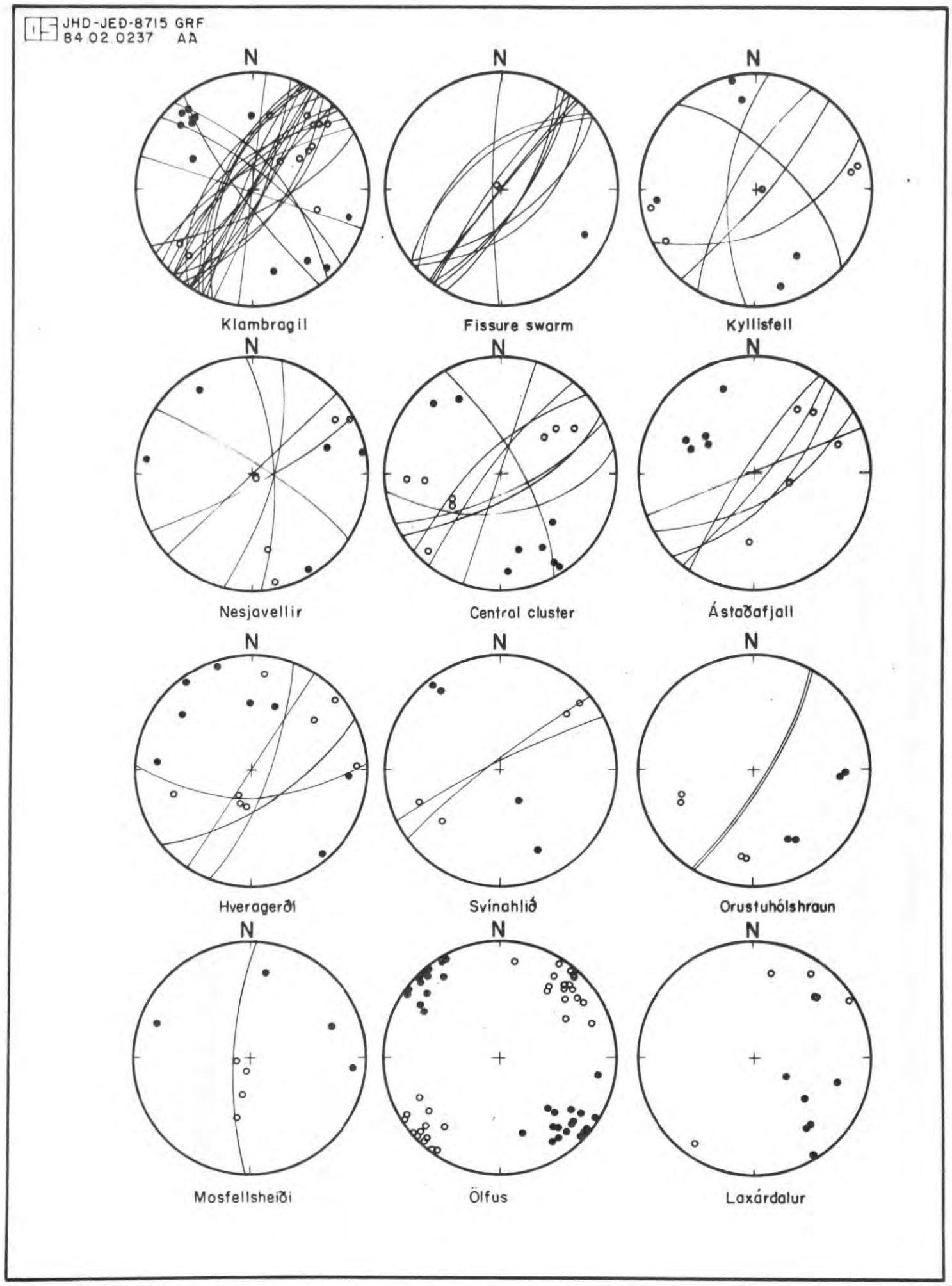

Fig. 6.4 Stereographic summary diagrams for focal mechanism data groups (see Fig. 6.7 for locations). O = P axes, ● = T axes of shear solutions, great circles represent planes of tensile crack solutions.

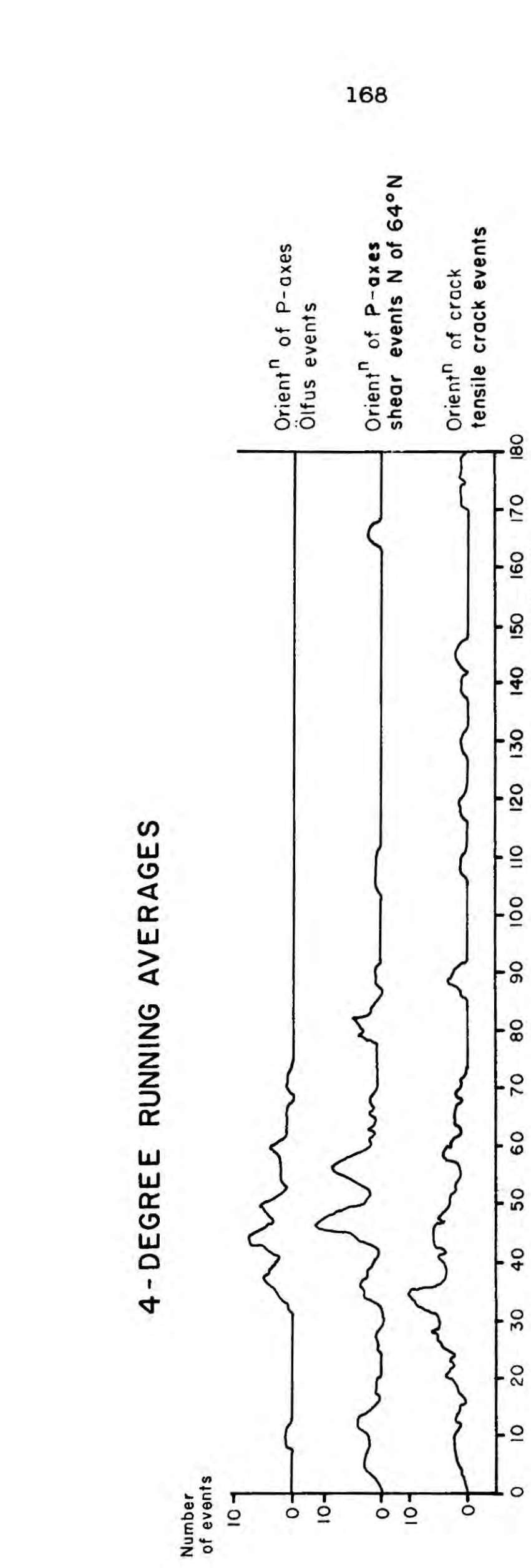

Fig. 6.5 Smoothed plots of orientation of P axes for Olfus shear events, shear events located N of 64°N, and orientation of the crack planes of the tensile crack events.

stress (horizontal and normal to the orientation of the fissure swarm). It is therefore possible that σ_3 rotates dextrally with depth but it is also possible that there is a component of double couple mechanism in some of the tensile crack events. This would have the effect of biasing the apparent orientation of σ_3 dextrally.

The implications of the findings described above are far reaching. It is recognised that fissure opening can occur at the surface and near it since the overburden pressure is zero or small but such fissuring is not generally considered likely to extend very deep since at great depth the confining pressure is very large. That such a process is ongoing in the Hengill area, down to depths of 6 km where confining pressures of about 1.5 kbar would be expected, implies that a very strong tensional stress regime is superimposed onto, and outweighs, the compressional field generated by the overburden. Plate movements are an obvious process that could generate such a tensional stress field.

6.2.3 The shear events

The solutions obtained exhibited faulting which, in general, ranged from strike slip on near vertical NS or EW orientated planes to normal dip slip movement on NE orientated planes. The normal movements indicate subsidence and subsurface faulting on planes with a similar orientation to fault planes observed at the surface. The P axes are orientated preferentially about N 45°E (see Figs. 6.5 and 6.6). They are often close to horizontal but range through to vertical

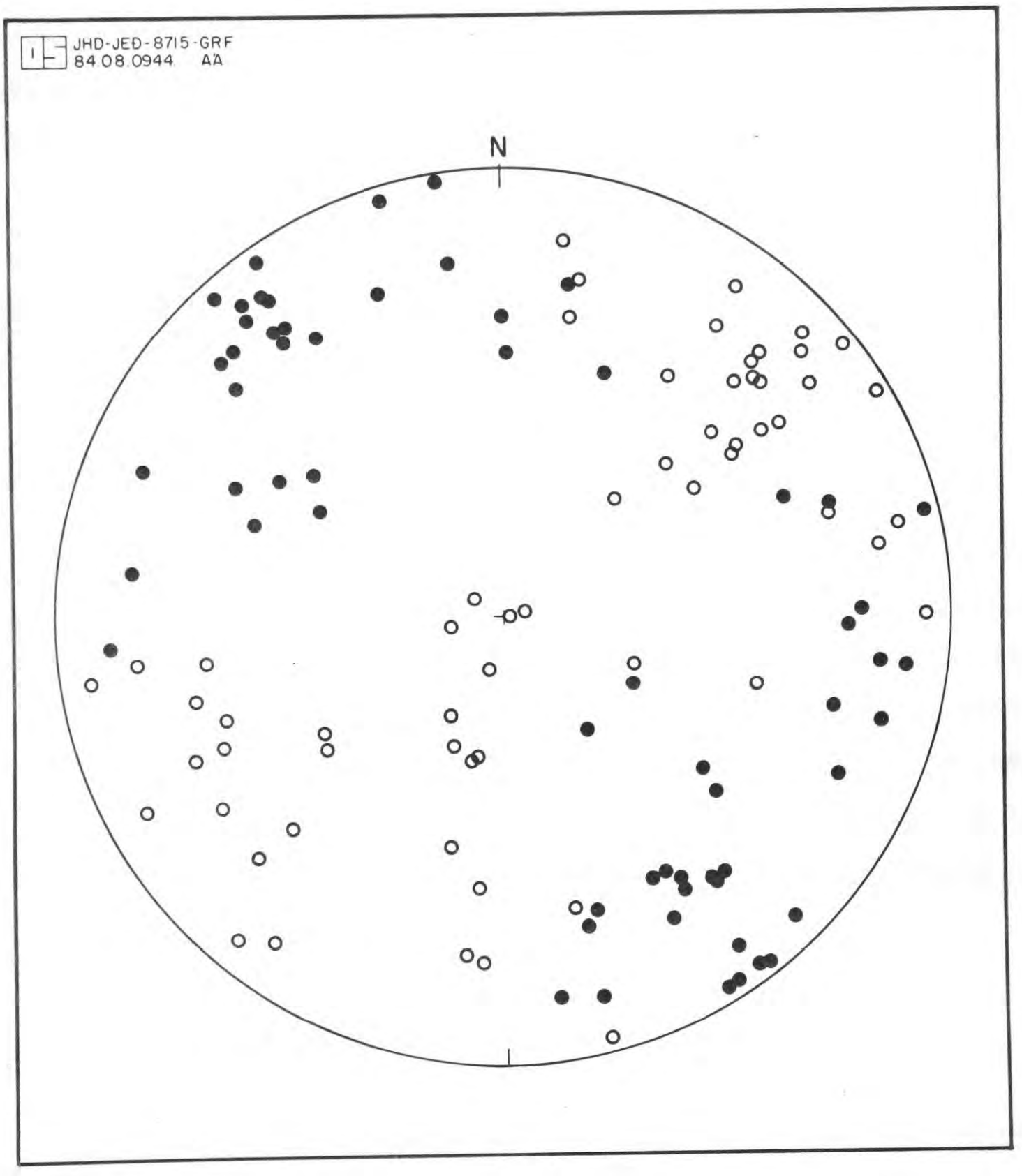

Fig. 6.6 Plot of P - and T - axes of all shear events in stereographic projection. O - P axes, ● - T axes.

(Fig. 6.6). The T axes are normal to the P axes, and usually close to horizontal. Although the P and T axes of the double couple events are not exactly equivalent to the directions of greatest and least compressive stress (see Section 6.2.7), they nevertheless imply an approximately horizontal NW orientation of the direction of least compressive stress, σ_3 , and variation from horizontal, approximately NE, to vertical for the direction of greatest compressive stress σ_1 .

6.2.4 Events for which no solution could be obtained

Approximately 10% of the events did not fit either type of solution. These events all exhibited reduced dilational fields, and may have been due to sources that combined both normal and shear movement. No attempt was made to fit nodal lines to these events. Because the shape of the nodal lines of many of the tensile crack and double couple events are poorly constrained it is possible that some of these events also contain components of both types of movement.

6.2.5 Spatial variations in mechanism

Table 6.1 is a breakdown of events of different type in the data groups depicted in Fig. 6.4. From this table it can be seen that the sizes of the data groups vary from 45 events for Klambragil (K) to only 5 for Mosfellsheidi (M). Also the proportion of double couple to tensile crack solutions is variable. These variations are mapped in Fig. 6.7. A circle is drawn in the location of each data group and the proportion of

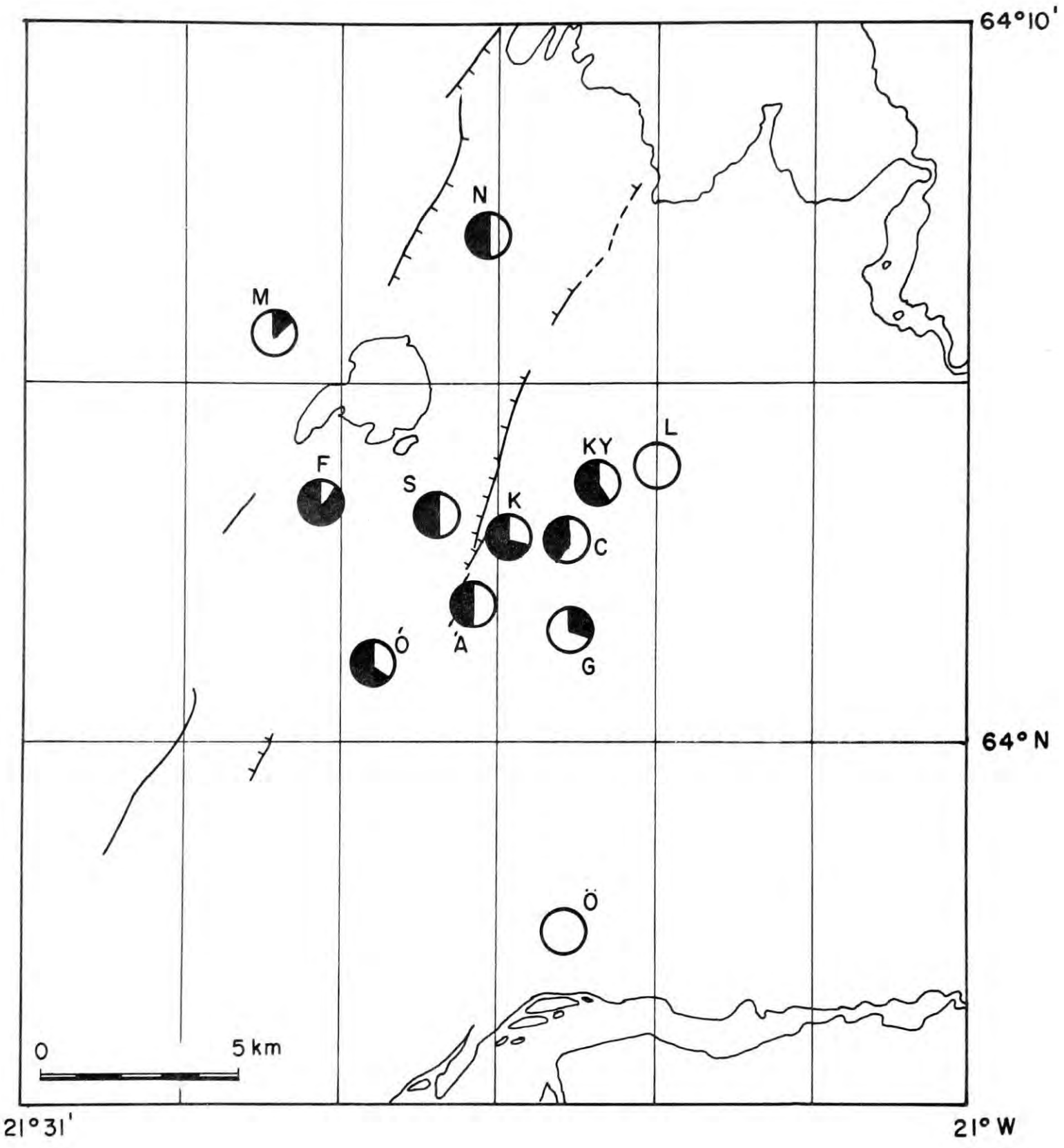

Fig. 6.7 Proportion of tensile crack events represented as proportion of circles filled for the data groups depicted in Fig. 4.4.

events that are unambiguously tensile crack is equal to the proportion of the circle filled.

	number of shear events	number of t.c. event	number with no solution	Total
Klambragil	13	26	6	45
Fissure swarm	1	11	4	16
Kyllisfell	5	5	2	12
Nesjavellir	5	5	-	10
Central cluster	8	8	3	19
Astadafjall	6	5	1	12
Grensdalur	7	3	-	10
Svinahlid	4	2	-	6
Orustuholshraun	4	2	-	6
Mosfellsheidi	4	1	-	5
Olfus	31	-	-	31
Laxardalur	6	-	-	6
totals	94	68	16	178

Table 6.1 Breakdown of events with different focal mechanisms in the spatial data groups.

It can be seen that tensile crack solutions occur preferentially in the cluster NW of Hveragerdi and the fissure swarm, i.e. the high temperature geothermal area. In the Grensdalur (G), Mosfellsheidi (M), Laxardalur (L) and Olfus (O)

areas, which are peripheral to or outside the high temperature area tensile crack type events are subsidiary or absent. The transition from tensile crack type to shear type strain release is abrupt on the W boundary of the fissure swarm. There is thus a clear indication that the tensile crack type events are associated with some deep process associated with the high temperature geothermal area.

In the case of the shear events, the data group for Olfus (O) exhibits primarily strike slip movement whereas events that exhibit a large normal component of faulting are confined to the area N of 64°N (Figs. A7.1 to A7.14)

Fig. 6.8a illustrates depth distribution for the tensile crack and the double couple data groups. For the depth distribution the data are divided into 3 sets representing different parts of the area. The depth distribution for Klambragil shows similar ranges for both types of event except that the tensile crack events extend to greater depths. The seismicity in this small area is also shallower than that of the rest of the high temperature area. The depth distribution for all areas except Klambragil and Olfus shows a definite tendency for the tensile crack events to occur at greater depths than the double couple events. It is possible that the tensional stress field that enables tensile crack formation is strongest in the deeper part of the seismic zone and that strain is preferentially released by shear movements at shallower depth. The distribution of double couple . events in Olfus shows the greater depth range of events in this part of the area, in agreement with the observations described in Section 4.3.2.7.

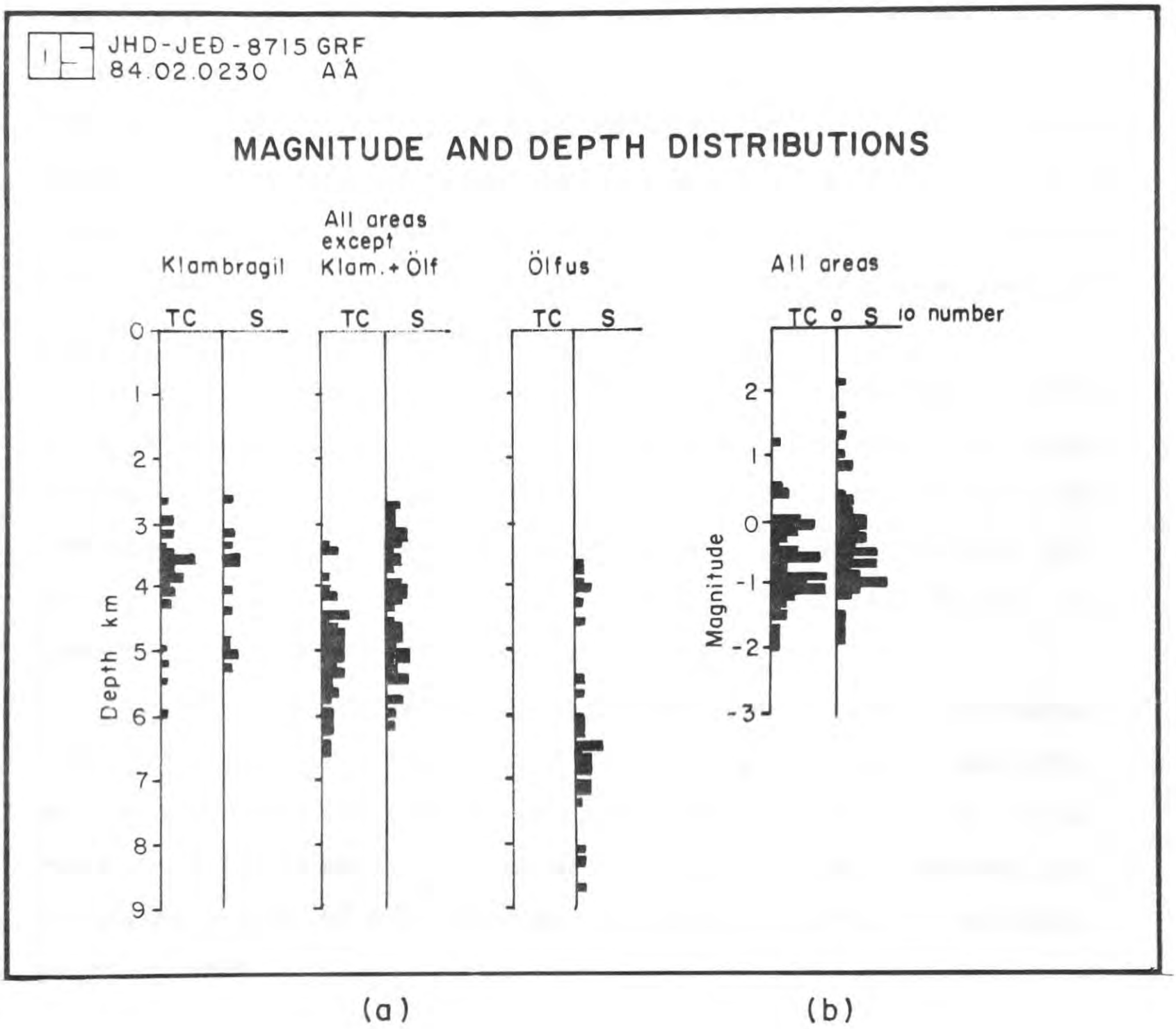

Fig. 6.8 (a) Depth distributions of tensile crack and shear events for the Klambragil and Olfus data groups and all other areas. (b) Magnitude (M_{IL}) distributions of tensile crack and shear events, entire data set.

6.2.6 Magnitude variations in mechanism

The plot of magnitude distribution (Fig. 6.8b) shows that the shear events occupy the range $-2.0 < M_{IL} < 2.2$ and the tensile crack events $-2.0 < M_{IL} < 1.4$. Thus for the set of events for which solutions were obtained (representing 3 months recording) the largest shear event was 0.8 magnitude units larger than the largest tensile crack event. For this data set 95% of the seismic stress release was therefore by shear failure and 5% by tensile crack failure.

The swarm that occurred in the Kirkjuferjuhjaleiga, Olfus area 19th-22nd Sept. 1981 is not included in the data set since it was located too far outside the tape network for the radiation patterns to be well constrained. Because of this, the data presented in Fig. 6.8 are a typical 3-month sample as regards number of events (Section 5.2.2.2).

These observations are in agreement with the hypothesis that tensile crack type events are limited to small magnitudes and thus account for only a very small percentage of the total seismic strain energy release of the Hengill area. However the recording period of 3 months was too short to provide definite proof of this.

6.2.7 Implications for fault plane determination for the shear events.

That the shear and tensile crack events are interspersed in the same volume of rock, is demonstrated by the depth distribution. Also both types of event may occur in a single

sequence (e.g. the 810905 sequence in the Astadafjall area, Fig. A7.14). This may be explained by the process illustrated in Fig. 6.9.

The opening of tensile cracks close together results in the build up of stress in the intermediate rock volume which is then released by shear failure on a plane connecting the cracks (Hill, 1977). For tensile cracks forming at the same depth (i.e. with horizontal separations only) strike slip earthquakes would be generated. For tensile cracks forming at different depths (i.e. with vertical separations) earthquakes with a normal component of shear movement would be generated. Strike slip shear faulting preferentially occurs on either NS or EW orientated planes (Section 6.2.3). These two alternatives are illustrated in Fig. 6.9. It can be seen that the release of shear stress on EW orientated vertical planes implies a left lateral tensile crack configuration, and movement on NS orientated vertical planes implies a right lateral tensile crack configuration.

According to McKenzie (1969), for a fresh break in homogeneous rock the direction of greatest compressive stress (σ_1) lies between the P-axis of the shear focal mechanism solution and the fault plane (see Fig. 6.10). In the case of the Hengill events the P axes of the shear events are preferentially orientated about N 45° E whereas the orientation of the tensile crack events indicates an average horizontal direction of about N 35° E for the greatest compressive stress in the depth range of the events (Sections 6.2.2 and 6.2.3 and Fig. 6.5). With this information, and from inspection of Fig. 6.10 it may be deduced that in the case of the strike slip

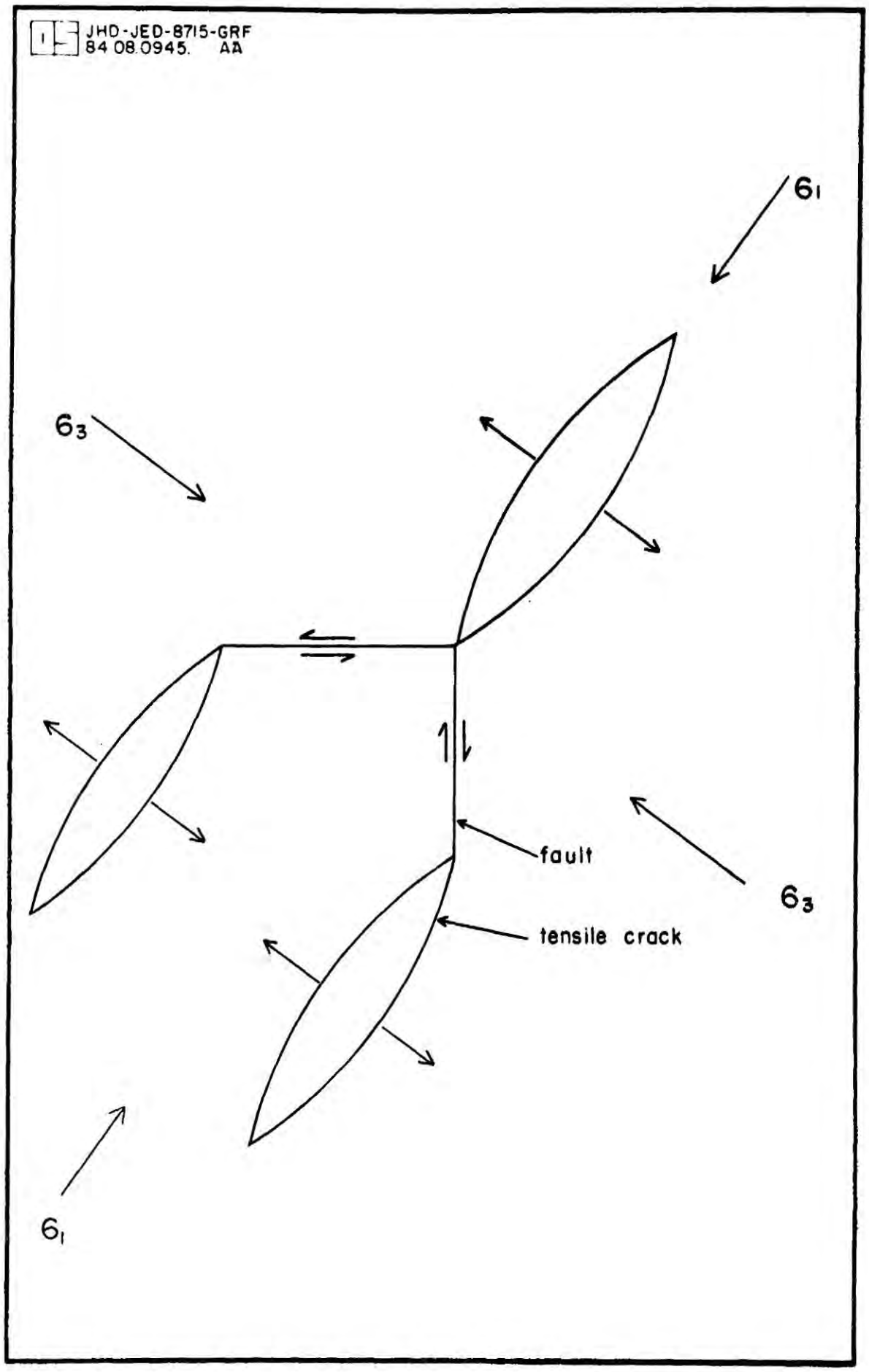

Fig. 6.9 Schematic diagram of tensile crack opening and accompanying shear seismicity on planes connecting the cracks. σ_1 and σ_3 signify the greatest and least compressive stresses respectively.

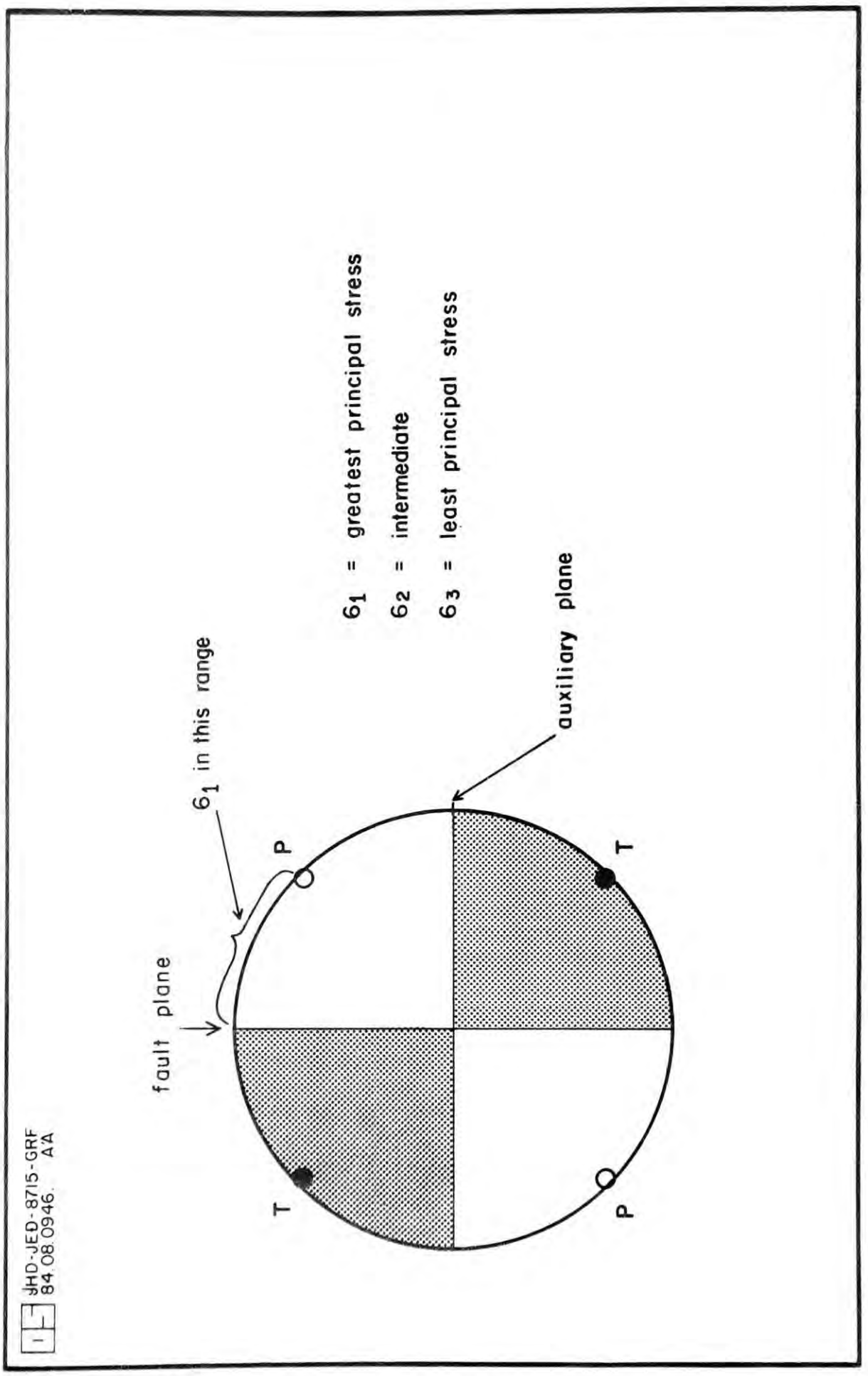

Fig. 6.10 Diagram showing relationship between P- and T-axes, the fault and auxilliary planes of a shear earthquake focal mechanism, and the range of possible directions

shear events, the plane of fracture will be the more northerly striking plane, and a right lateral tensile crack configuration is implied. The strike slip shear seismicity associated with the high temperature geothermal area therefore indicates that right lateral movement on northerly striking planes is the most common mode of faulting.

It can be seen from Fig. 6.9 that if fracturing of this nature occurred in a zone, then the orientation of the entire activated zone would be intermediate between that of the tensile cracks and the shear fault planes. As has been described above this situation is observed at the surface in the Hengill area. The trend of surface faulting is N 25° E, intermediate between the NS striking fault plane typical of the double couple focal mechanism solutions and the N 35° E strike typically exhibited by the tensile crack events. This is a strong indication that the deduction of fault plane made above is correct. The P and T axes of the double couple events and the orientation of the tensile cracks and surface features are thus all consistent with the same stress field.

If it is assumed that the mode of faulting observed for the high temperature geothermal field extends S into the Olfus area then this implies that faulting there is right lateral strike slip on NS orientated planes. This is consistent with the mode of faulting observed for large destructive earthquakes in the South Iceland Seismic Zone, of which Olfus forms the westernmost part (Einarsson et al., 1981; Einarsson and Eiriksson, 1982).

6.3 Summary of the results

Good constraint was obtained for the radiation patterns of 178 small earthquakes located within the Hengill area. Of these, 50% were interpretable as demonstrating shear movement on fault planes, 40% as movements normal to the fault plane (tensile cracks) and 10% did not fit either interpretation, and may have been intermediate events.

Preferential orientation of the dilational fields of the tensile crack events indicates a direction of horizontal N 125° E for the least compressive stress (σ_3) in the seismic volume. That these events occur at depth in the earths crust indicates that σ_3 must be negative and large enough to outweigh the overburden pressure of several kilometers of rock. The shear events observed indicate strike slip and normal movements and an orientation of the axes of principal stress consistent with that demonstrated by the tensile crack events.

The tensile crack events were confined to the high temperature geothermal area. The ratio of tensile crack type events to shear events was greatest in the interior of the high temperature area where the heat loss is highest, and was lower in peripheral areas. Outside the high temperature area faulting was almost entirely shear. The tensile crack events indicate a strong tensional stress regime, but their occurrence also appears to be dependent on some high temperature geothermal process. Normal shear faulting was almost absent in Olfus. The events for which focal mechanism solutions were obtained occupied the depth range 2 - 6 km. There was a tendency for the tensile crack type events to occur at greater depth than the

shear events beneath the high temperature geothermal area. This may indicate that the conditions under which tensile crack type events form occur preferentially at greater depth within the seismic volume. The Klambragil data group exhibits activity at anomalously shallow depth and a very high proportion of tensile crack type events. The strike slip shear events of Olfus occur to greater depths than earthquakes occurring N of 64°N.

During the 3 month recording period tensile crack type events were confined to small magnitudes and accounted for only 5% of the seismic stress release. This is consistent with the hypothesis, but not proof that such events are confined to small magnitudes.

The tensile crack events were interspersed with shear events in space, and also the two types were seen together in sequences. It was concluded that the shear events represented movements on fault planes connecting the tensile cracks, a process originally hypothesised by Hill (1977). The deduction of the direction of least compressive stress from the orientation of the tensile cracks, allowed the fault plane of the strike slip shear events to be identified as primarily the NS striking one. In the case of the mixed earthquake sequences this implies that activity occurs on right laterally arranged en echelon tensile cracks connected by NS orientated shear fault planes. The combined trend of the whole activated zone would then be expected to be more northerly than that of the tensile cracks. This is consistent with observations of the trend of surface tectonic features.

Extrapolation of these deductions to the Olfus area indicates that the type of faulting there may be right lateral

strike slip on NS orientated planes. This is consistent with the mode of faulting of the South Iceland Seismic Zone.

CHAPTER 7

7. TELESEISMS AND EXPLOSIONS

7.1 Teleseisms

7.1.1 Introduction

Teleseismic arrivals approach recorders at steep angles, and hence sample the crust beneath a network at much greater depths than local or regional sources. Their relative arrival times may be interpreted in terms of lateral and vertical velocity variations. This is known as the method of relative delays (Long and Mitchell, 1970). The structures of a number of large regions have been studied using this method e.g. East Africa (Savage, 1979) and Iceland (Tryggvason, K. et al., 1984). It has also been applied on a smaller scale to a number of volcanic areas containing geothermal prospects (see Foulger, 1982, for review). However, teleseismic waves typically have wavelengths of several km, which limits the scale of structures that they can resolve. The collecting and processing of this type of data has now become routine proceedure (Stauber and Iyer, 1983).

Where the data are of sufficient quality an "Aki inversion" may be performed (Aki et al., 1977). The volume of interest is divided up into blocks and the observed teleseismic delays modelled by varying the velocity in each block. This has been achieved for several areas including Yellowstone (Iyer, 1979) and the Coso Hot Springs, California (Reasenberg et al., 1980). A number of other studies have been perfomed and simple

interpretations presented, often involving zones of partial melt or magma chambers. For Long Valley, California, Steeples and Iyer (1975) modelled a magma chamber 14 km in diameter, with velocity contrast of 15% on the basis of relative delays of up to 0.3 sec. In the Geysers-Clear Lake area, California, delays of about 1 sec were considered to indicate a magma chamber with a core of severely molten rock extending down to a depth of 20 km (Iyer et al., 1979).

During the 90 day period of recording on the Hengill radio telemetered seismometer network in 1981, 21 well recorded teleseisms were monitored yielding a data set containing 328 arrival times. Because the time available for modelling these data was limited, work did not proceed further than reducing and correcting the raw data and producing a simple qualitative interpretation.

7.1.2 Delay measurement

Paper playouts of the teleseismic records were made on a scale of 5 cm:1 sec. In order to measure the relative onsets of the first P arrival as accurately as possible, a "typical" P waveform was selected for each event. This was traced onto transparent paper and the first arrival marked. The tracing was then superimposed onto the waveforms recorded at all the other stations for that event and the picking of the rest of the first arrivals aided by comparison of the total waveform. The absolute arrival times of the first P-wave onsets at the stations were thus measured. This picking method is reported by Corbishley (1969) and Savage (1979) to give the best accuracy.

The theoretical arrival times of the events at the stations were calculated using programme MANETA (Savage, 1979) (see Section 3.3.2). Source locations were taken from the Preliminary Determination of Epicenter (PDE) listings of the U.S. Coast and Geodetic Survey (USCGS). In order to correct for the stations height above datum the average velocity of the crust above sea level was required. A velocity of 3.0 km sec^{-1} was used since this was the value obtained by Palmason (1971) for the surface layer in the area S of L. Thingvallavatn (Profile 42) and was shown to be a reasonable average by refraction shots fired in 1981 (see Section 7.2 and Appendix 4. The "raw delay times" were then obtained by subtracting the calculated theoretical arrival times from the observed.

According to Long and Mitchell (1970), each raw delay time may be expressed as the sum of six terms:

$$T = S + T_o + T_e + T_t + T_i + e$$

where

T is the raw delay time

S is the delay due to material with anomalous velocity beneath the station.

T_o arises from errors in the earthquake focal data,

T_e is the delay due to material with anomalous velocity beneath the source,

T_t is the error due to inaccuracies in the travel time tables and calculations,

T_i is the instrumental delay for which correction may be made, and

e is the error due to misreading and poor timing of the

seismogram.

This may be expressed as:

$$T = S + E$$

where

E is a composite error term ($= T_o + T_e + T_t + T_i + e$)

For a single event, the value E will be approximately the same at all stations, because for a very distant event the source to station path is virtually the same except for directly beneath the station network. S will vary from station to station due to velocity anomalies directly beneath the station array. Each event will be associated with a different E value. The S-value profile across the station network will also vary for the different events because the events approach the stations from different azimuths and angles and hence sample different portions of the volume beneath the station array.

In order to calculate S-values, i.e. the delays associated with anomalous material directly beneath the stations, the programme SEPD (Savage, 1979) was used (see Section 3.3.2). This programme calculates least-squares values for the error terms E and the station delays S. An arbitrary zero was declared for the station delay at KDN (Fig. 7.3). In order to examine azimuthal variation in the station delays, the events were grouped according to geographical location and separate calculations made for each group.

7.1.3 Discussion of the results

Fig. 7.1 is a stereographic plot of the world coastlines

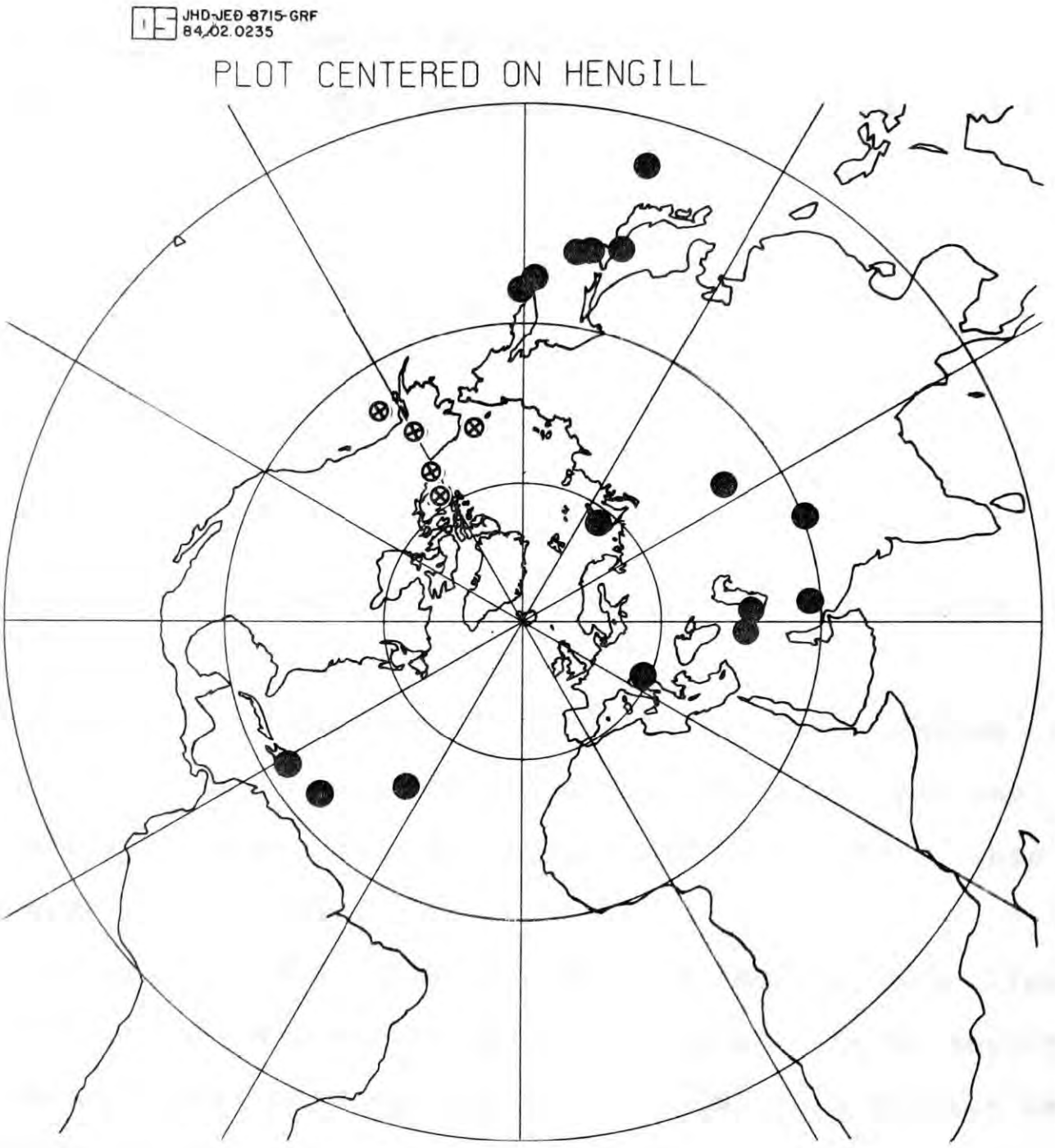

Fig. 7.1 Plot of world coastlines and teleseism locations in stereographic projection centred on the Hengill area. ● represents upper hemisphere epicentre, ⊗ represents lower hemisphere epicentre.

centred on Hengill, and drawn out to 90°. The locations of all the teleseisms used in this study are plotted. Lower hemisphere epicentres are indicated by crosses. These events are all in the Tonga-Fiji area. The epicentres fall roughly into four groups :-

- Europe and W Asia
- Japan - Kuriles
- West Indies - Atlantic
- Tonga - Fiji

In the case of the latter two groups, P-wave onsets were poor.

The angles of incidence of the incoming rays varied from 32° to 10° with increase in epicentral distance, but was, for the majority of rays, in the region 27° to 15°. This is illustrated in Fig. 7.2.

In Table 7.1 the relative station delays are listed, calculated using all events equally weighted. As is mentioned above, an arbitrary zero was assigned to KDN, this station being peripheral to the main area of interest. Because of this arbitrary zero, the error associated with each station delay does not indicate significance (or insignificance) in that delay in an absolute sense, but only relative to the other stations.

Fig. 7.3 is a contoured plot of the delays listed in Table 7.1. The features displayed by this Figure reflect some kind of average structure for the volume beneath the station array down to indeterminate depth, since the different rays used to calculate each relative station delay sampled slightly different

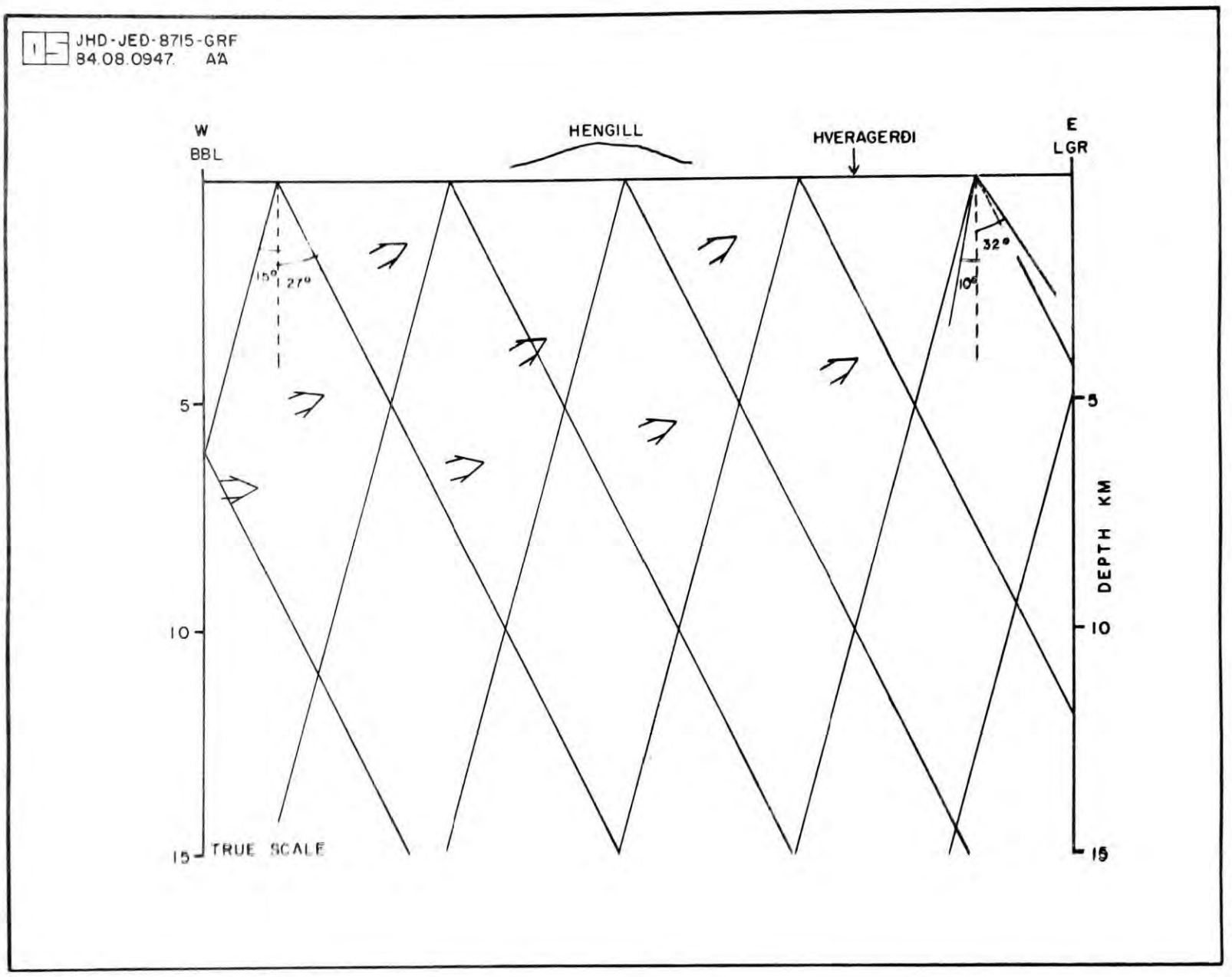

Fig. 7.2 WE cross section of the Hengill area showing the range of angles of incidence of the teleseismic (lines) and regional explosion (arrows) rays.

Station Name	Delay time (sec)	no. of events	error (sec) ±
BBL	0.01	9	0.03
BHU	-0.12	15	0.02
BSL	-0.04	12	0.02
BVA	-0.06	13	0.02
BLA	-0.05	10	0.02
BEN	-0.03	14	0.02
BMO	-0.04	17	0.05
KST	0.07	13	0.03
KDN	0.00	21	0.02
KKL	-0.04	18	0.02
KDL	-0.04	14	0.02
KDA	-0.05	19	0.02
KMI	0.09	15	0.01
KHE	-0.04	14	0.02
KHA	0.03	16	0.02
KKA	-0.02	14	0.03
KSA	-0.08	10	0.02
LBO	0.07	9	0.02
LDY	-0.02	17	0.02
LLA	0.02	15	0.01
LGR	-0.04	11	0.02
LDJ	-0.04	17	0.02
LKA	-0.09	15	0.02

Table 7.1 Relative teleseismic delays calculated using all 21 events

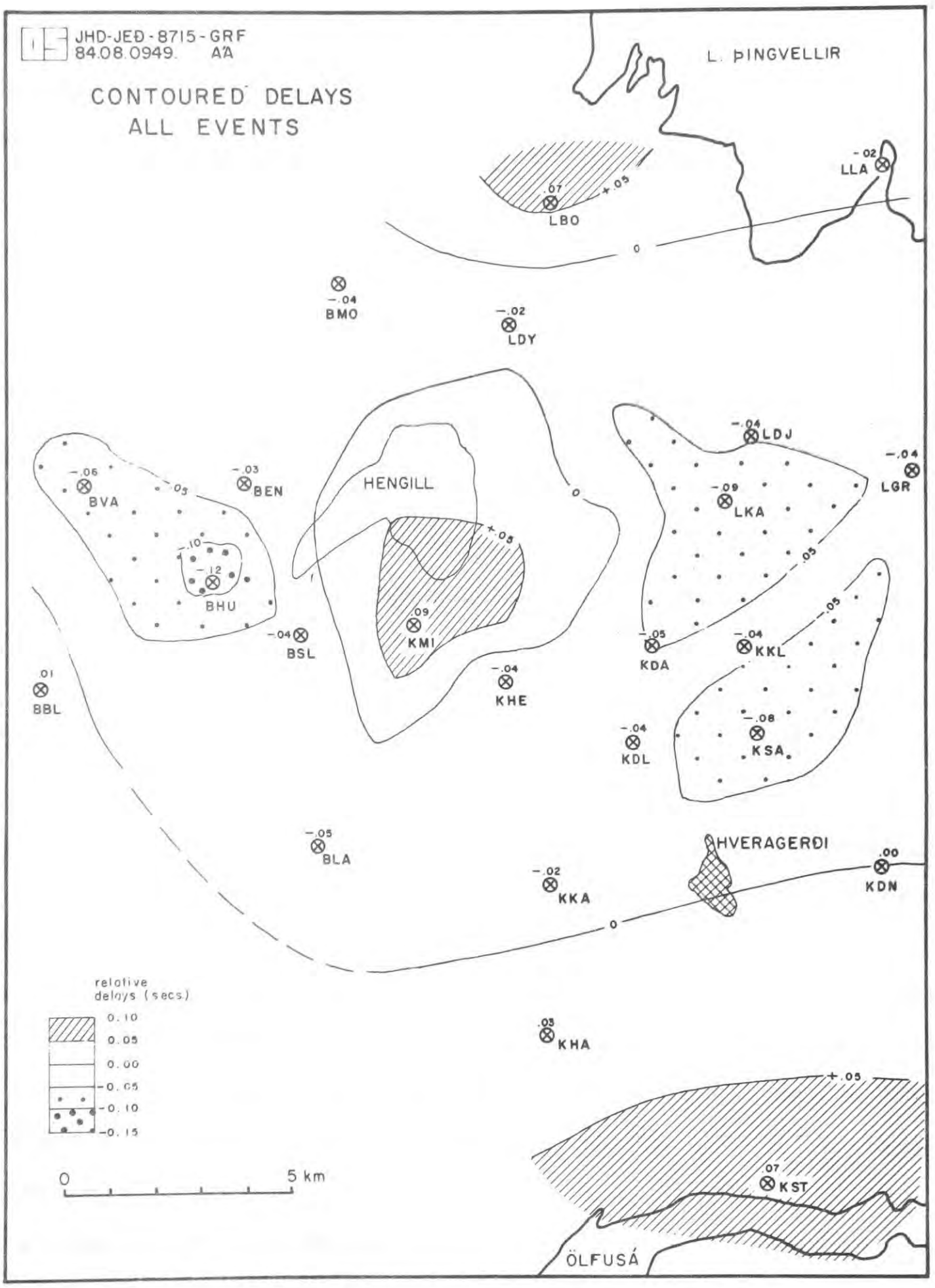

Fig. 7.3 Contoured plot of teleseismic delays. Stations are labelled with their mnemonic codes (see Appendix 3). Delay contours are at intervals of 0.05 sec.

portions of the volume (Fig. 7.2). It should also be borne in mind that the scale of resolvable structures is limited by the wavelength of the incoming rays, which is about 6 km in this case.

The broad picture that emerges from Fig. 7.3 is that positive delays (= low velocity (Vp)) are associated with Nesjavellir, Hengill and Olfus relative to Husmuli (see Fig. 2.3) and the area N of Hveragerdi (respectively W and E of Hengill). The maximum relative delay is associated with KMI, directly S of Hengill, which is about 0.2 ± 0.03 sec slow compared with BHU to the W and LKA to the E. The gradient of the delay contours is steeper to the W than to the E. The shape of the positive delay anomaly associated with KMI is not well constrained to the N because no stations were deployed on or to the N and E of Hengill, but it does not extend as far N as the station LDY. Passing further N to station LBO, N of Nesjavellir, the delay is seen to increase again. It is possible that a low velocity anomaly is associated with Hengill that is cut off from a more northerly anomaly of unknown extent in the fissure swarm that extends little farther S than L. Thingvallavatn. That the positive anomaly associated with KMI does not extend very far S is fairly well constrained by the stations BLA and KHE. The areas of relatively early arrivals to the W and E of Hengill are constrained by 2 and 3 stations respectively.

It was found that this picture remained constant if the data set was narrowed down to the best arrivals only, or subdivided into azimuthal groups. Thus it very likely shows real relative arrival time variations over the Hengill area that

are of the scale of the resolving limit of the seismic waves (6 km diameter).

In Fig. 7.4 the relative delays associated with different azimuths have been plotted for each station. Positive delays (low Vp) relative to the arbitrary zero are plotted as (thick) solid lines and negative delays (high Vp) as (thick) dashed lines. The lengths of these "delay lines" are proportional to the size of the relative delays and represent a velocity contrast of approximately ± 10%. The lengths of the ray paths drawn (thin lines) are the projection onto the surface of the ray paths down to approximately 10 km.

In order to constrain the depth of the structures causing the relative delays, azimuthally separated delays must be examined where ray paths cross, and attempts made to maximise consistency in the data by varying the depth of the delay lines. In Fig. 7.4 the mid points of the delay lines are projected at 5 km depth. Projection at greater depths would result in the mid points of the delay lines migrating outwards from the station along the ray paths.

It can be seen by inspection of Fig. 7.4 that fairly good consistency of the data is displayed. In the region of the KMI positive anomaly, rays approaching BSL and BEN from the E exhibit positive delays relative to those from the N and SW. Rays approaching stations LDJ and LKA from the SW, and KDA and KKL from the N exhibit positive delays whereas those from other azimuths exhibit negative delays. This may be an indication that the negative anomaly in the area N of Hveragerdi does not extend much farther W than the stations LDJ and LKA.

It can also be seen from Fig. 7.4 that a progressive

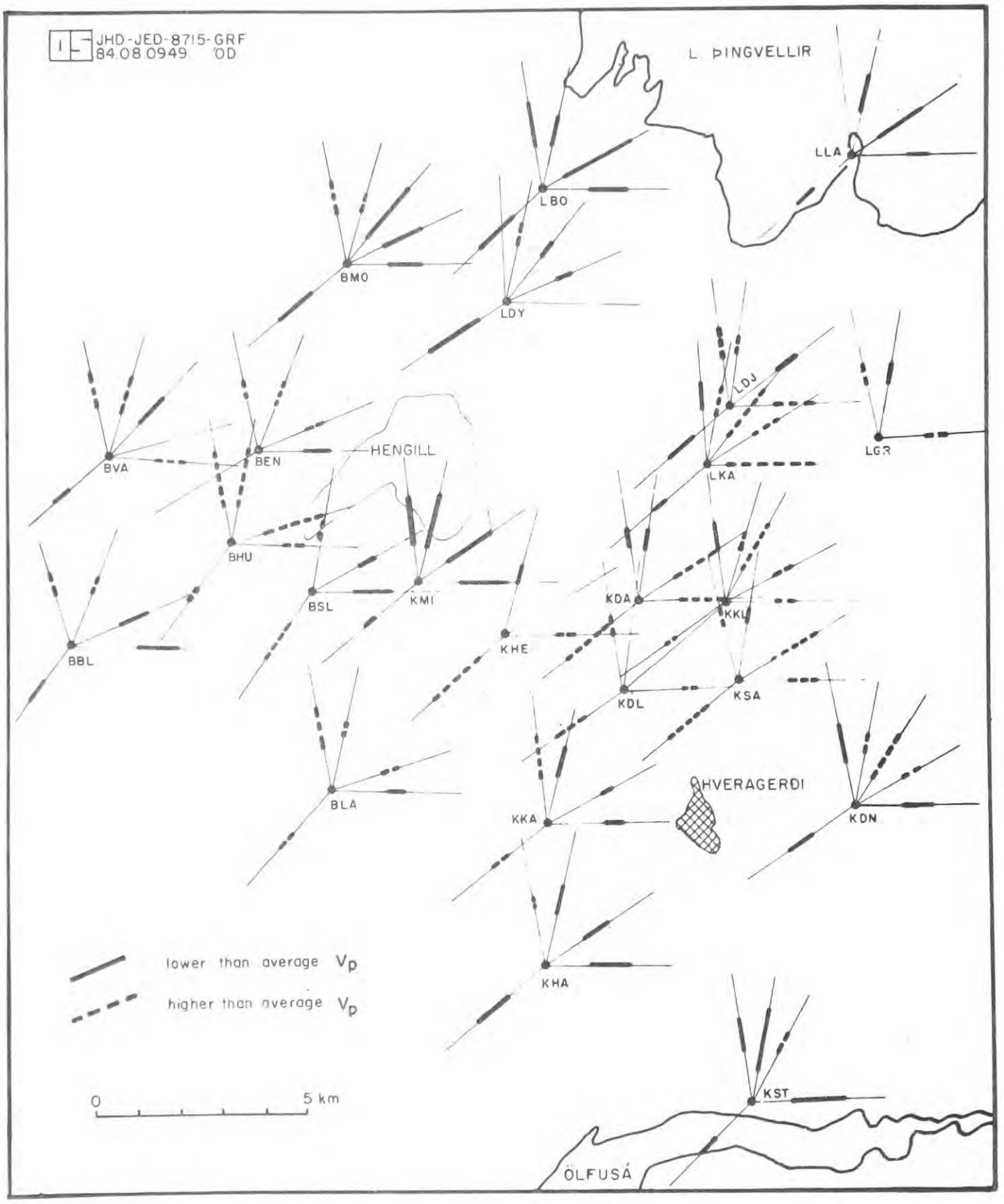

Fig. 7.4 Azimuthal plot of teleseimic delays. Thin lines are the surface projection of ray paths down to 10 km depth. Thick lines represent relative teleseismic delays, and are the surface projection of the ray paths that would give rise to the observed delays assuming a 10% velocity anomaly.

increase of the projection depth of the delay lines would not significantly change the consistency of the data until about 15 km depth, when deterioration would begin. This is most easily seen in the area of the KMI positive anomaly because of its limited areal extent.

There is also the possibility that the anomalies apparent in the data result from structures at different depths. If variation in the relative depths of the anomalous structures is also allowed then it becomes practically impossible to place any depth constraint on them. However, if it is assumed that the anomalous structures are all at approximately the same depth, then it may be concluded that they are likely to be shallower than 15 km.

7.2 Explosions

7.2.1 Introduction

Refraction studies have not been widely applied in the field of geothermal prospecting since large velocity contrasts do not result from temperature variations of a few hundred degrees at low temperatures. However during the period of deployment of the radio telemetered network a number of explosions were made in order to investigate possible lateral variations in velocity structure within the Hengill area. These shots were also intended to provide sources of known origin time and location that might be used to test the accuracy of the locator proceedure.

Five explosions were made. Three of these were located within the Hengill area, and two at more distant sites. They were, respectively, the Olfus, Djaknapollur, Thingvallavatn, Graenavatn and Reykjavik explosions. Their coordinates are given in Table 7.2 (refer to Figs. 2.1 and 3.1).

7.2.2 Delay measurement

The crustal model used to locate the local earthquakes, referred to here as the Hengill-South Iceland crustal model, is an average model that fits the observational data of a number of refraction profiles made in the Hengill area and South Iceland by Palmason (1971). It contains four layers with linear velocity gradients over a constant velocity halfspace, and is documented in detail in Appendix 4.

In order to test the locator procedure for accuracy the 3 local explosions were located using the Hengill-South Iceland model and HYPOINVERSE. The errors in the calculated epicentres were 400 m, 320 m and zero. These results give some idea of the accuracy of the earthquake locations discussed in Section 4.3.2. However, if it is assumed that the majority of the error in the earthquake locations is due to the departure of the real crustal structure from the model, then the relative locations of events in a small area will not be significantly affected, only the absolute location of the group.

All five explosions were located a second time, using the true location as a trial hypocenter and the true origin time. The first iteration of the programme was printed out (see Appendix 4) which listed calculated travel times to all the stations from the true locations, and the differences between these and the observed travel times. These delays give information about the departure of the Hengill-South Iceland crustal model from the true Hengill crustal structure. HYPOINVERSE does not take account of stations height above sea level, thus the travel time residuals were corrected using the equation:

$$T = \frac{h \cos i}{V}$$

where T (secs) is the correction factor

h (km) is the stations height above sea level

i (deg) is the emergence angle

V (km sec^{-1}) is the velocity of the surface layer

For the three local explosions, 59 travel times were measured.

explosion	co-ordinates	HYPOINVERSE location	error in location	shot-reciever dist.(km)
Olfus	63N56.27′	63N56.39′	400m to NE	0.3-22.8
	21W09.50′	21W09.18′		
Djaknapollur	64N05.17′	64N05.02′	320m to SE	0.2-16.1
	21W10.10′	21W09.92′		
Thingvallavatn	64N09.07′	64N09.07′	none	3.7-20.5
	21W11.40′	21W11.40′		
Graenavatn	63N53.05′		-	32.9-54.5
	22W03.40′			
Reykjavik	64N11.07′		-	22.1-43.6
	21W51.12′			

Table 7.2 Co-ordinates of explosions, location errors and epicentral distances.

In order to examine lateral variations in crustal structure within the area, a ray diagram is presented in Fig. 7.5. In this Figure the ray paths are projected onto the surface as thin lines. Positive delays, (i.e. late arrivals, indicating Vp lower than defined in the Hengill-South Iceland crustal model) are indicated by thick lines placed at the mid point of the ray path, with length proportional to the size of the delay. Negative delays (i.e. early arrivals, indicating Vp higher than

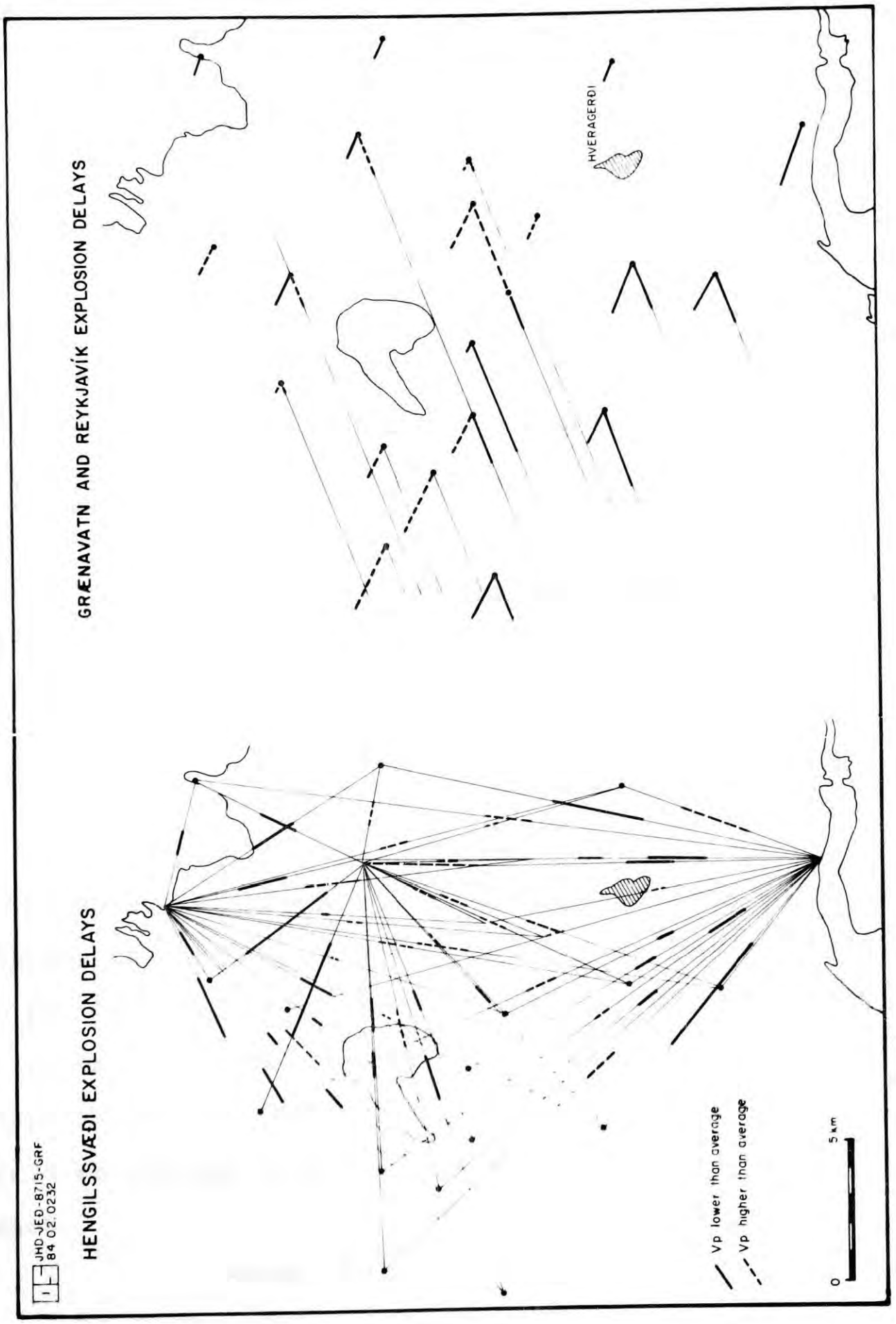

Fig. 7.5 Ray diagram of explosion data (a) the local explosions, (b) the regional explosions (Graenavatn explosion approaches from the SW. Reykjavik from the NW). Thin lines are the surface projection of ray paths, thick lines represent travel time residuals.

defined in the Hengill- South Iceland crustal model) are indicated by thick dashed lines. Fig. 7.5a shows the delays measured for the 3 local explosions.

In the case of the two regional explosions, the velocity structure of the crust between the shots and the Hengill area is known to be different from that defined in the Hengill-South Iceland model. For the Graenavatn explosion, this resulted in systematic early arrival of the waves by about 0.30 sec at the stations of the network. In order to correct for this a 0.30 sec delay was added to all delays calculated, which gave an average delay of zero for the stations that recorded the shot. In the case of the Reykjavik explosion, waves recorded arrived at the stations progressively earlier with increasing distance from the shot point. Hence a correction was made to the arrivals that was proportional to distance. The relationship used was:

correction (sec) = 1.52 - 0.0243 x epicentral distance (km)

This relationship is a least squares linear fit to the observational data, and yielded a correlation coefficient of 0.84 (see Fig. 7.6). The 1.52 sec threshold is arbitrary since the shot instant was not recorded for this explosion. Application of correction factors calculated by this formula gave an average delay of zero for the stations that recorded the shot.

The corrected delays are plotted in Fig. 7.5b. In examining Fig. 7.5, it should be borne in mind that the delays from the 3 local shots, the Graenavatn shot and the Reykjavik

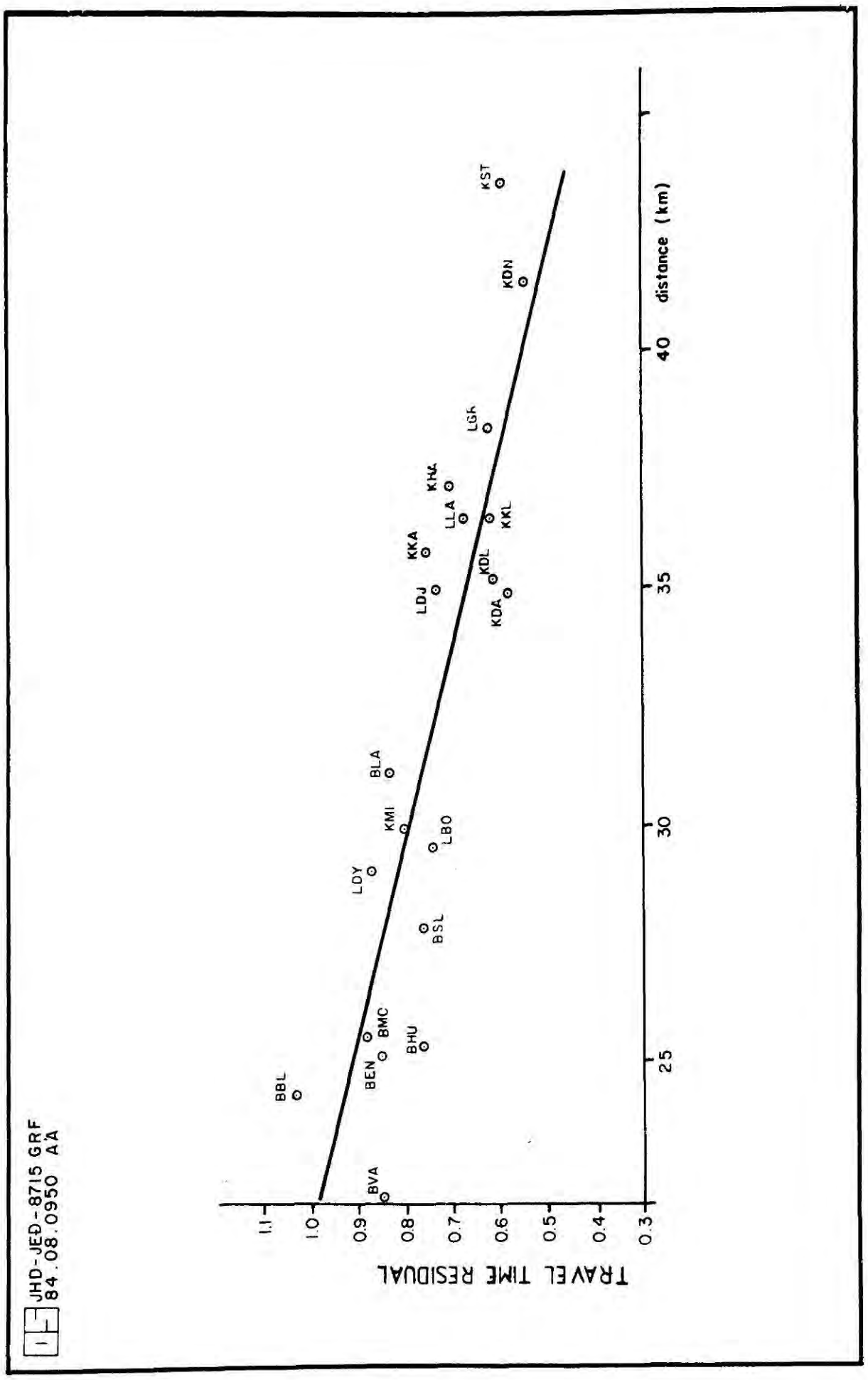

Fig. 7.6 Correction relationship applied to the arrival times of the Reykjavik explosion data.

shot are relative to 3 different crustal models and their magnitudes are thus not directly comparable. However, the variation in the delays over the area within each of the 3 data groups are comparable.

7.2.3 Discussion of the results

The Hengill-South Iceland crustal model prediots that the depth of penetration of seismio rays inoreases with inoreasing ray path length in the manner shown in Fig. 7.7. This Figure shows the maximum depth of penetration against source-reciever distance. This penetration depth would be achieved beneath the mid point of the ray path. The majority of the ray path will pass through the crust at shallower depths than the maximum. At shot-receiver distances greater than 4.5 km the rays will penetrate deeper than 1 km and in the range 9-25 km the depth of penetration will be 2.5 - 3.5 km with a considerable portion of the ray path falling in this depth range. The regional shots, that were 22-55 km distant from the receivers penetrated up to 9 km depth, though not beneath the Hengill area. Approximate path trajectories for the explosions are shown as arrows in the vertical cross section of Fig. 7.2.

It can be seen in Fig. 7.5a that for the local shots the negative delays (Vp higher than average) mostly cluster in the area to the N of Hveragerdi, whereas positive delays, sometimes relatively large, are restricted to Olfus, the fissure swarm and the area to the N and NE of Hengill. This strongly indicates the presenoe of a body N of Hveragerdi that exhibits higher seismio velocities than those of the surrounding areas. Becouse

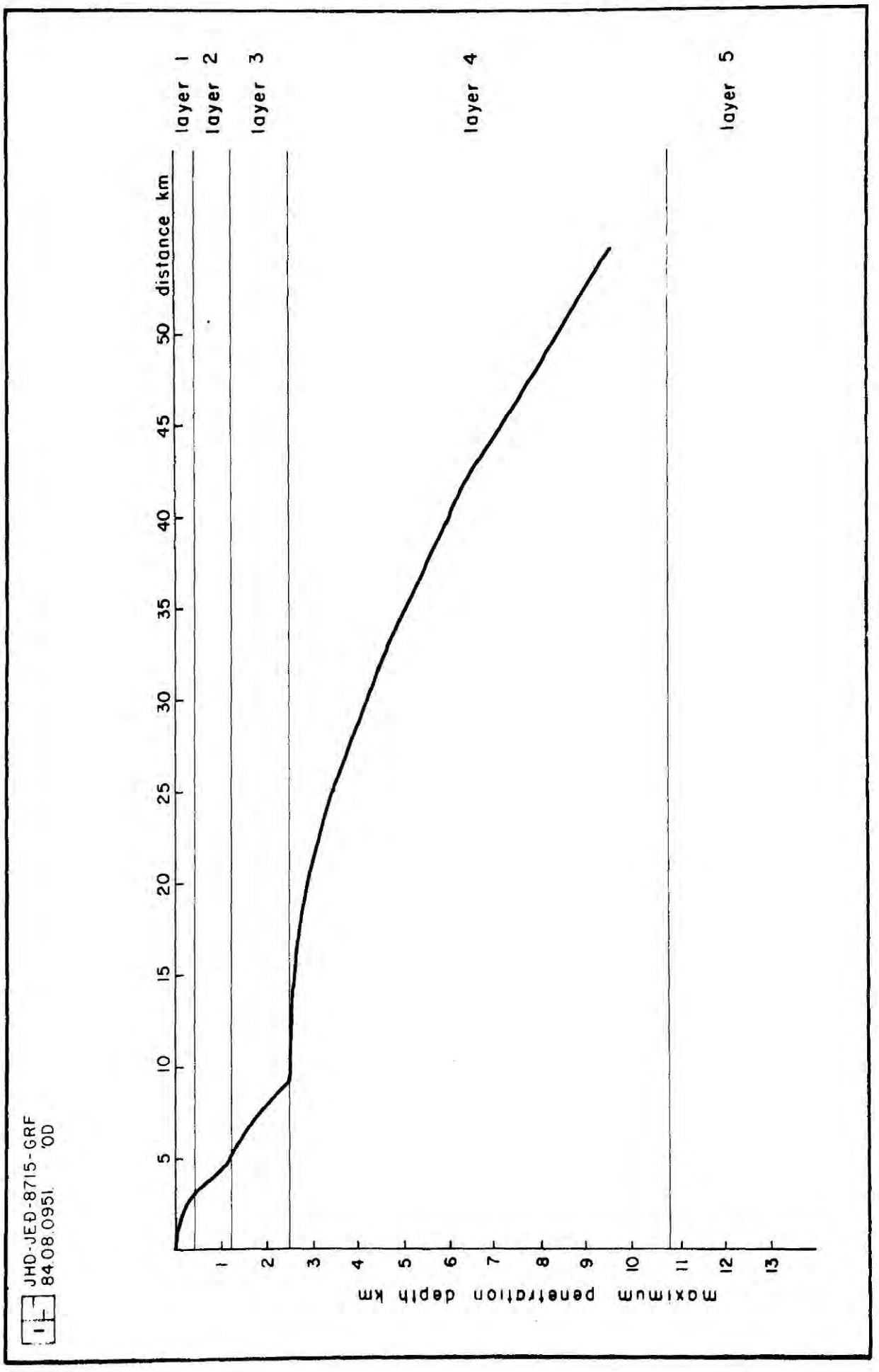

Fig. 7.7 Plot of source - receiver distance : maximum penetration depth for a surface source and the Hengill South Iceland crustal model.

of the great variation in the shot-receiver path lengths, firm depth constraint cannot be placed on this body by the simplistic treatment of the data presented here. However, it can be said that the majority of the rays penetrated the crust in the range 1-3.5 km, and the fact that great consistency is displayed despite the variation in penetration depth strongly indicates that the anomaly encompasses this depth range.

In the case of the regional event delays illustrated in Fig. 7.5b a similar pattern is observed. Rays recorded at the stations immediately N of Hveragerdi appear to have an enhanced apparent velocity relative to those recorded at stations in Olfus, the fissure swarm and the areas to the N and NE of Hengill. In addition, a high apparent velocity is displayed by rays recorded by the stations W of the fissure swarm, especially those in the Husmuli area. The data are again highly consistent.

7.3 Synthesis

A superficial perusal of relative P-wave arrival time data from teleseismic sources and local and regional explosions indicates a consistent pattern of delays over the Hengill area. Seismic velocities in the area to the N of Hveragerdi and the Husmuli area are high relative to the rest of the area and exceptionally low velocities are associated with bodies of rock beneath N Nesjavellir, Hengill and Olfus. That this general pattern is exhibited by all the data sets suggests that the bodies associated with these velocity contrasts may extend from near surface to several kilometers depth.

The local and regional explosion data indicate that velocities vary from the average by ± 5% in the upper few kilometers. In the case of the teleseismic data higher velocity contrasts are required at depth if the whole anomaly is to be accommodated in the upper 10 km or so of crust. Velocity variations of ± 10% from the average at depth were taken in the model presented here.

A suggested interpretation of these data is shown in Figs. 7.8 and 7.9 which are, respectively, a WNW cross section S of Hengill and a SSW cross section longitudinal along the fissure swarm (see Fig. 7.3). The velocity in the depth range 0-2 km is allowed to vary by ± 5% and that in the range 2-10 km by ± 10%. Velocity gradations doubtless occur, but are not shown in these simplistic cross sections. The main features exhibited are:

(a) A 'chimney' of low velocity material beneath Hengill, flanked to the W and E by high velocity bodies. The low

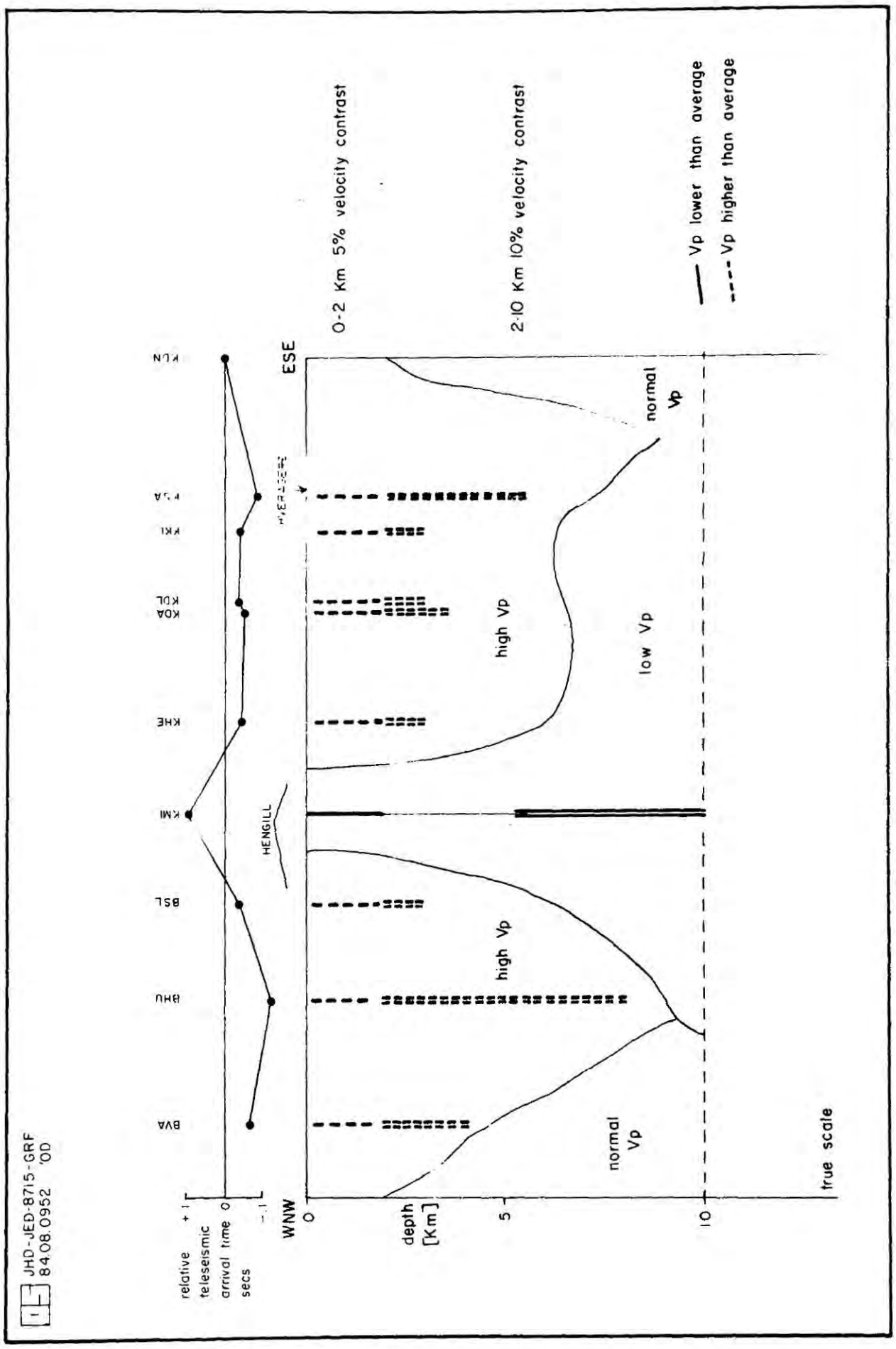

Fig. 7.8 WNW - ESE cross section of the Hengill area S of Hengill illustrating a possible interpretation of the teleseismic and explosion delay data. The teleseismic

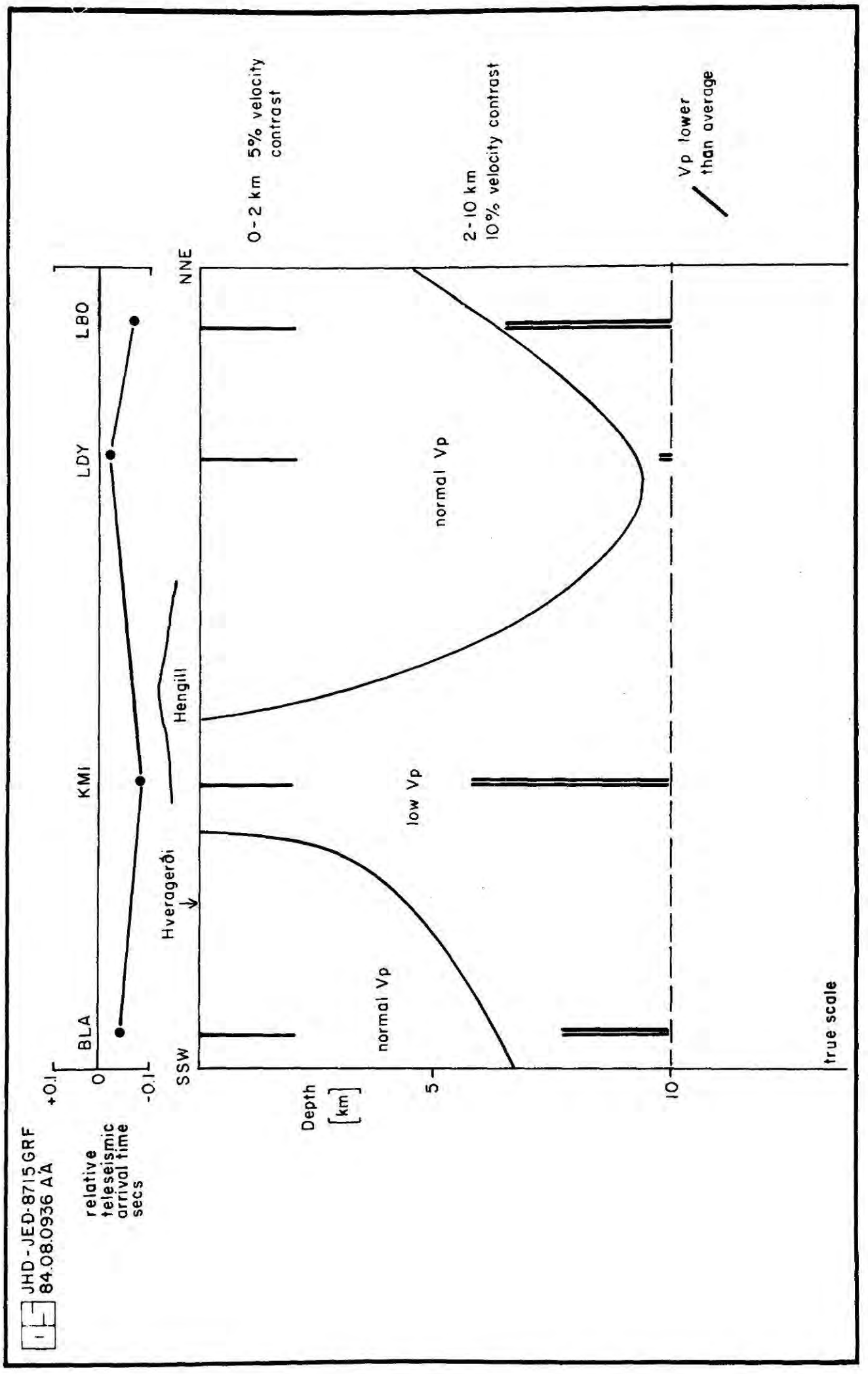

Fig. 7.9 SSW - NNE cross section of the Hengill area along the fissure swarm illustrating a possible interpretation of the teleseismic and explosion delay data. The

velocity chimney may widen with increasing depth, and underlie the area to the E (i.e the area N of Hveragerdi).

(b) The low velocity body associated with Hengill is not continuous along the fissure swarm but disappears in the area between Hengill and L. Thingvallavatn.

Because the sizes of the bodies exhibiting anomalous velocities could not be resolved, neither could the absolute velocity contrasts. The model presented above is one possible model that could account for the observations. Smaller bodies (not less than 6 km in diameter at depth) and larger velocity contrasts would also produce the same delay data.

CHAPTER 8

8. SYNTHESIS

8.1 A structural model for the Hengill area

8.1.1 Broad structure as indicated by previous work

The Hengill area contains an accretionary plate boundary whose surface expression is a swarm of open fissures and faults that crosses the area with a trend of N 25°E. Contained within it is the 803 m high Hengill central volcano. The broad picture that emerges from the application of many research methods to the Hengill area involves an extinct volcanic centre (the Grensdalur volcanic centre) located in the area N of Hveragerdi, and an active one beneath Hengill (the Hengill volcanic centre). Volcanic activity is thought to have been transferred from the Grensdalur centre to the Hengill centre early in the Bruhnes geomagnetic epoch, about 700,000 yrs ago.

On the N, E and S slopes of Hengill an area of hot springs and fumaroles is observed, which extends to the SE encompassing the whole area between Hengill and Hveragerdi. Geochemical, hydrological and borehole studies indicate that the geothermal area is hottest in the vicinity of Hengill and cooler to the SE. The area is not symmetrical about the fissure swarm as might be expected in a spreading environment : the Mosfellsheidi area to the W is topographically distinct from the area to the E, and is also devoid of geothermal manifestations. To the E of the fissure swarm the low, flat Olfus lowlands S of 64°N contrast with the rugged topography of the area N of 64°N.

8.1.2 The transverse structure

A transverse structure that runs from Mosfellsheidi in the W, SE to Ingolfsfjall has long been recognised. It is orientated approximately normal to the fissure swarm, transects Hengill and passes through the Grensdalur area. From NW to SE it is delineated by hyaloclastite ridges, fissures, erosional features (Kyrgil and Klambragil), a topographical high (Olkelduhals) and changes in surface fault trends. It is proposed here that the Grensdalur system originally occupied the fissure swarm, but was transported off axis by the migrating E plate. The transverse structure marks the trajectory of migration of the Grensdalur volcanic centre and is thus broadly analagous to the Greenland-Scotland Ridge whose structure is thought to be influenced by the migration of the Iceland hotspot.

The presence of a volcanic centre on an accretionary plate boundary affects the development of the area locally in two ways. Firstly the linear stress field of the spreading plate boundary will be modified by the radial field associated with the volcanic centre (Ode, 1957; Muller and Pollard, 1977). Secondly volcanic production both intrusive and extrusive may be enhanced in the immediate vicinity of the centre, resulting in the formation of a topographic high.

A radial stress field associated with a central volcano may be modelled by a pressurised, circular orifice (Ode, 1957). In the case of the Hengill area, this is superimposed onto a homogenous, linear, regional stress field associated with the plate boundary. The maximum principal stress trajectories

resulting from this combination, and along which tensional features will preferentially develop, are illustrated schematically in Fig. 8.1. From this Figure it may be seen that such a model predicts that tensional features orientated normal to the plate boundary would develop in the neighbourhood of the central volcano.

Whilst still active the site of the volcanic centre will be marked by a topographic high. After extinction its erosion will contrast with that of the surrounding areas because of its contrasting structure. Initially it will erode down faster than the surrounding areas because of its greater elevation. In later stages a fast erosion rate may be maintained by its elevated temperature, which speeds up chemical decomposition and enables the process of progressive fracturing by the action of groundwater (Section 8.1.3). This may result in the old volcanic centre being represented by a topographic depression in its final stages. Erosional features associated with faults, fissures and dykes will mirror their trends, and hence may exhibit a component parallel to the old spreading direction as well as normal to it.

It is proposed here that in the Hengill area, NW-SE orientated tectonic features have formed in response to the modified stress regimes in the neighbourhood of the volcanic centres. In the NW these are recent tectonic features associated with the presently active Hengill volcanic centre, and in the SE they are erosional features associated with the extinct Grensdalur volcanic centre. A high volcanic production rate in the neighbourhood of the presently active Hengill centre has resulted in the build up of a topographic high whereas in

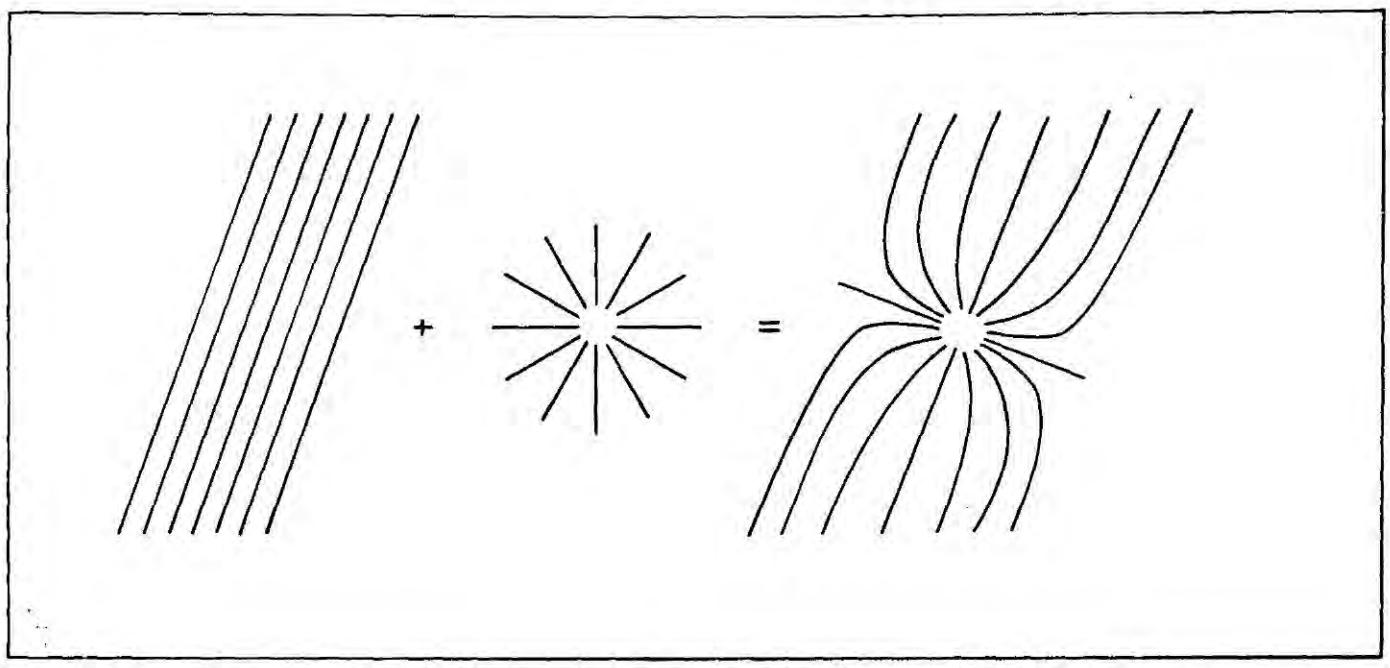

Fig. 8.1 Pattern of maximum principal stress trajectories caused by the addition of a radial and a linear stress system (after Ode, 1957).

the case of the extinct Grensdalur volcanic centre erosion has been speeded up by geothermal processes and the centre is marked by a topographic depression. Because the Grensdalur system is a remnant volcanic centre that drifted off axis with the E plate, and was replaced in the same location by the Hengill centre, its trajectory is parallel to the spreading direction and colinear with the transverse tectonic features of both volcanic centres described above. For this reason the transverse structures associated with the two volcanic centres are colinear and form a single, long, well developed structure.

In Fig. 8.2 a position for the axis of this structure is proposed based on the locations of surface tectonic features. Its strike is N 125°E. This is parallel to the direction

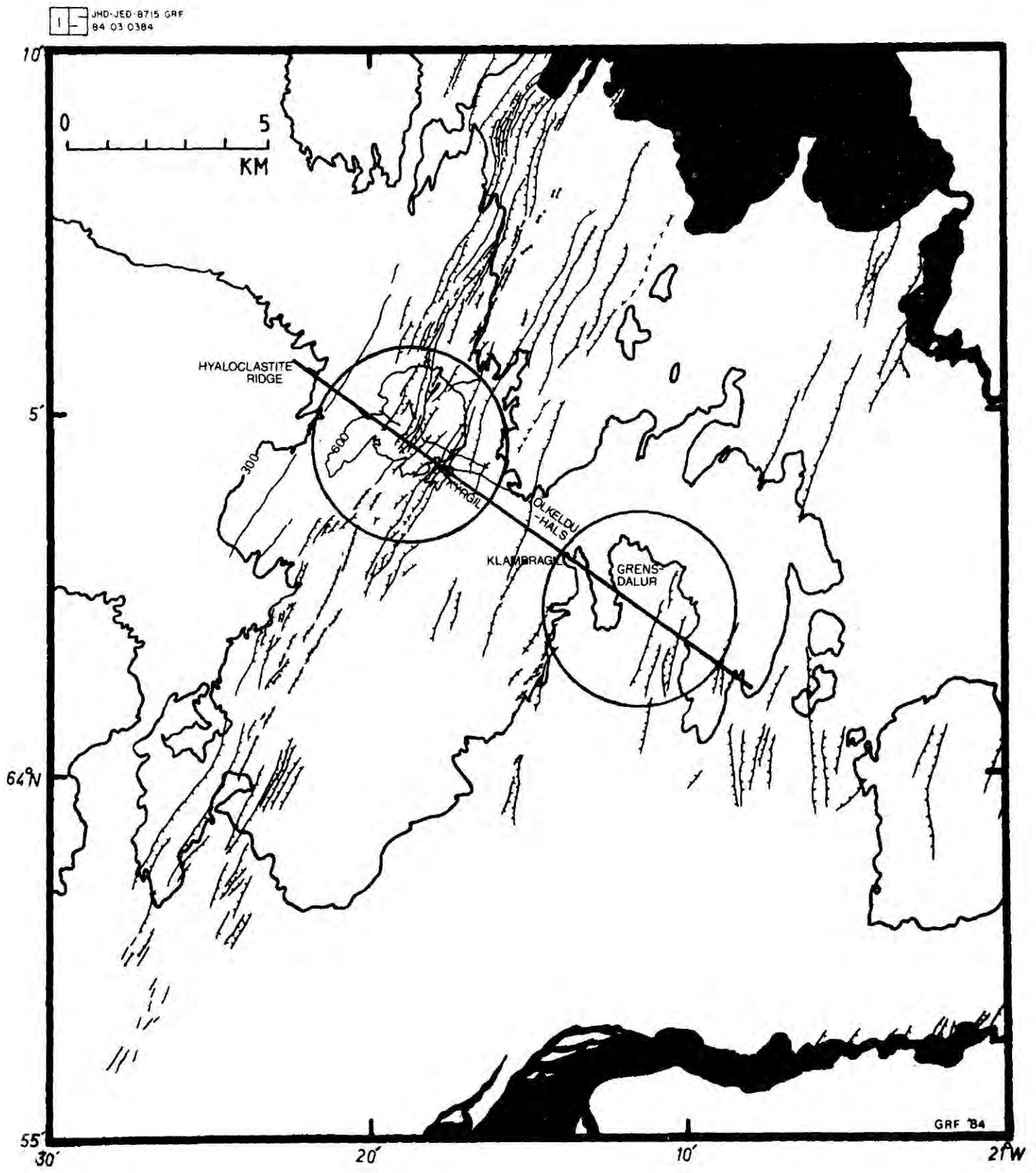

Fig. 8.2 Map of the Hengill area showing the proposed locations of the double volcanic system and the transverse structure.

of σ_3 inferred by the tensile crack type earthquakes observed in this area (Section 6.2.2). A position for the extinct Grensdalur volcanic centre is also suggested, based on the geological and geophysical evidence available. This is represented by the SE circle in Fig. 8.2, and encloses the Grensdalur topographic low. The circle indicating the presently active volcanic centre encloses the topographic high of Hengill. The volcanic centres are given diameters of 5 km, based on the extent of their surface features. The axis of the transverse structure connects their centres. As would be expected, volcanic activity associated with the Grensdalur centre continued longest on its NW margin, i.e. on Tjarnahnukur, near Klambragil (see Section 2.2.1 and Fig. 2.3).

8.1.3 Cooling rock

It has been proposed that the penetration of water into hot rock boundaries is the mechanism by which heat is removed from hot rock intrusions at depth (Lister, 1974; 1976; 1977; 1980). Circulating groundwater causes rapid cooling, and small cracks form, continuously expanding the system of circulation channels and maintaining close contact between the groundwater and a retreating hot rock boundary. This process can account for the very large heat losses observed over geothermal areas such as Yellowstone and Grimsvotn, Iceland, which cannot be explained by thermal conduction alone. Also direct observations of the Heimey, Iceland lava flow indicate that this process is probably occurring there (Bjornsson et al., 1980). That background small magnitude seismicity is commonly observed in geothermal areas is

in agreement with the hypothesis that the process may occur seismically (Ward et al., 1969; Ward and Bjornsson, 1971). Where focal mechanism studies have been conducted, strain release is generally observed to conform with regional tectonics (Combs and Hadley, 1977; Majer and McEvilly, 1979; Walter and Weaver, 1980).

The seismicity of the Hengill area at low magnitudes is consistent with this picture. It is unusual because of its persistant day to day nature and correlates positively with surface heat loss. The area sits astride an accretionary plate boundary where strong extensional tectonics are displayed and over the high temperature geothermal area the majority of events exhibit tensile crack type failure. Observations are consistent with the theory that these events are confined to small magnitudes. In that case the larger magnitude events known to occur within the Hengill high temperature geothermal area may be shear type events associated with tectonic movements. The seismicity of the Hengill area at low magnitudes thus exhibits characteristics that are consistent with its being generated by the process of cooling contraction cracking due to the action of circulating groundwaters on hot rock at depth. It is thus concluded that this process is occurring seismically in the Hengill area.

The volume calculation

The total thermal contraction of the hot rock volume beneath the Hengill area can be estimated. The natural heat loss of the Hengill area is estimated to be 350 MW (Bodvarsson, 1951). If attributed to cooling rock the rate of volume

contraction can be calculated using the equation:

$$\Delta V = \frac{H \gamma}{C_p \rho}$$

where ΔV is the contraction rate, H is the rate of heat loss, γ is the coefficient of thermal expansion ($\simeq 16.2 \times 10^{-6}\ K^{-1}$), ρ is the density($\simeq 3 \times 10^{3}$ kg m^{-3}) and C_p is the specific heat of basalt at constant pressure ($\simeq 1.3 \times 10^{3}\ J\ kg^{-1}\ K^{-1}$). Application of this equation to the Hengill area gives a contraction rate of:

$$\Delta V = 4.5 \times 10^{4}\ m^{3}\ y^{-1}$$

The approximate volume of the tensile cracks formed seismically can be calculated from their local magnitudes using the relations:

$$\log M_0 = 15.1 + 1.7 M_L \quad \text{(Wyss and Brune, 1968)}$$

$$M_0 = 2\mu V \quad \text{(Section 6.1.4)}$$

where M_0 is the seismic moment, M_L is local magnitude, μ is the rigidity modulus and V is the volume of the crack formed. Fig. 8.3 illustrates the relationship between magnitude and volume diagrammatically (line A). Also plotted in this Figure is the relationship corrected for the b-value of the Hengill area (line B). This shows the volume created per year against magnitude. The result is further corrected by assuming that only 5% of the stress was released in tensile crack formation

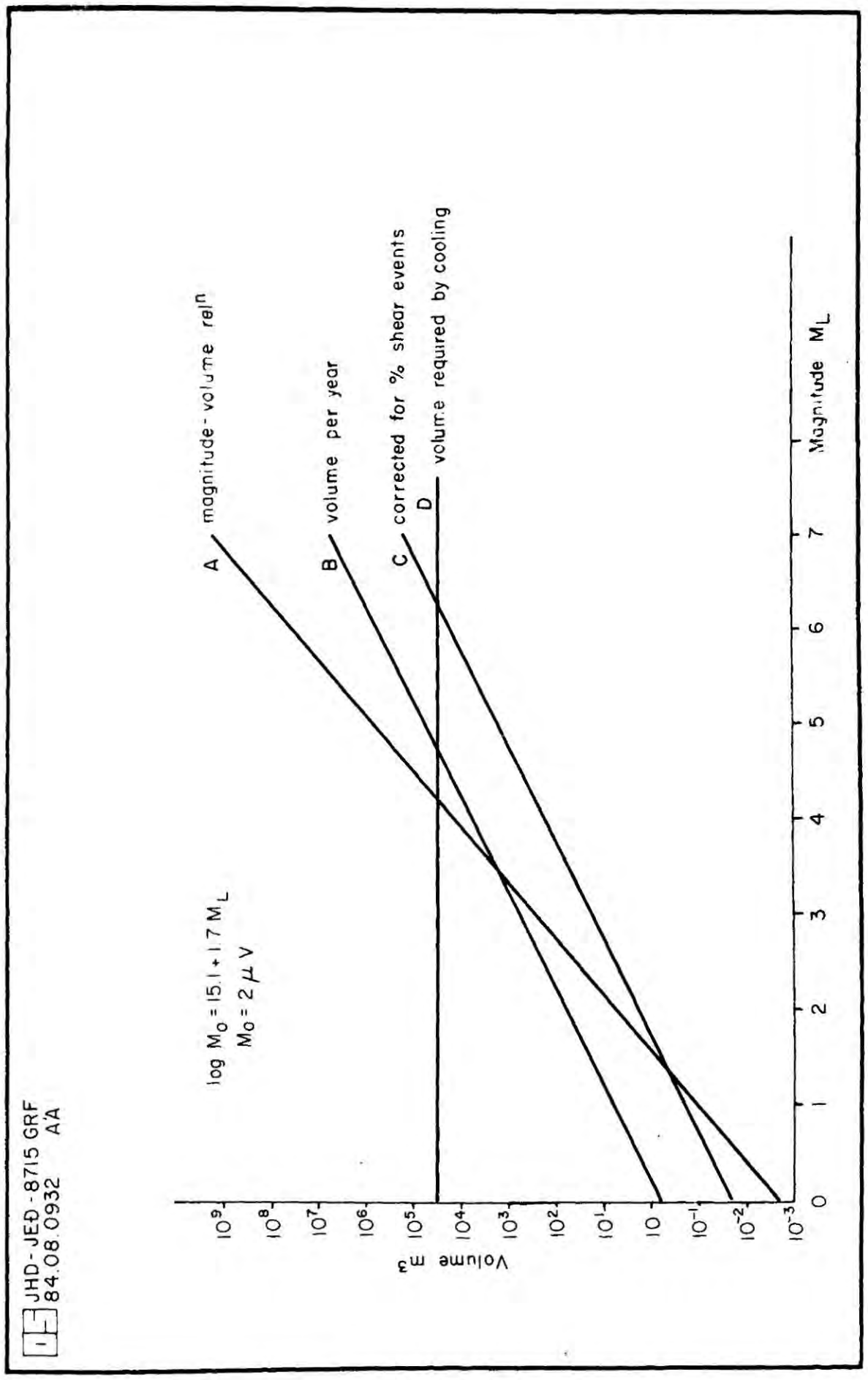

Fig. 8.3 Magnitude - volume relationships for tensile crack type fracturing. See text for explanation.

(line C) (Section 6.2.6). Because the relationship is logarithmic, the total volume produced by events up to a given magnitude is of the order of that of the largest event.

The contraction required to produce the natural heat loss is plotted as a horizontal line at $V = 4.5 \times 10^4 \ m^3 \ y^{-1}$ in Fig. 8.3 (line D). It can be seen that line D intersects line C at magnitude $M_L = 6.3$. This implies that events of up to about magnitude 6 must occur within the geothermal area in order for the contraction predicted by the surface heat loss to be accommodated seismically.

It has been argued in Section 5.2.2.2 that all the large earthquakes occurring in the Hengill area are located outside the geothermal area. Seismicity within the geothermal area is probably confined to relatively low magnitudes. Also the largest event observed with a tensile crack mechanism during the 3 month recording period had a magnitude of $M_{IL} = 1.2$, and there is thus no evidence that tensile crack events occur with magnitudes greater than this. The seismic rate of the geothermal area is therefore insufficient to account for the required contraction rate. This suggests that only a very minor part of the volume change resulting from the heat loss occurs seismically.

The implication of these facts is that if only a part of the contraction can be accounted for seismically then some, possibly most, must proceed aseismically. A possible explanation for this is as follows: as heat is removed by circulating fluids, the rock contracts and tensile stress builds up. When this reaches the breaking strength of the rock it fractures, forming a tensile crack which provides a new path for

the fluids and enables cooling to proceed more quickly. Contraction due to this subsequent cooling will be accommodated by aseismic widening of the initial crack and seismic crack propagation. This process is illustrated schematically in Fig. 8.4. In some cases crack formation may trigger a seismic sequence, and some regional stress release occur also. In these cases mixed sequences may occur (Section 6.2.7, Fig. 6.9).

8.1.4 Implications for the high temperature geothermal reservoir.

The spatial distribution of the tensile crack type events may be looked upon as a map of rapidly cooling volumes of rock that feed surface heat loss. In Fig. 8.5 the tectonic structure proposed for the Hengill area (Fig. 8.2) is plotted on a map of epicentres located during the 1981 radio telemetry project (c.f. Fig. 4.2). Most of the earthquake epicentres associated with the geothermal area lie within the Grensdalur volcanic centre or on its proposed perimeter. From this it may be concluded that the greatest heat loss occurs from beneath the Grensdalur volcanic centre. It is proposed here that two major heat sources feed the geothermal area. One heat source is relatively hot and young and is associated with the presently active Hengill volcanic centre. The other is cooler and older and is associated with the extinct Grensdalur volcanic centre. In Fig. 8.6 a structure for the geothermal area is suggested. The extents of the cores of the heat sources feeding the geothermal reservoir are outlined and are based on the tectonic map of Fig. 8.2. The few hot springs and fumaroles that do not

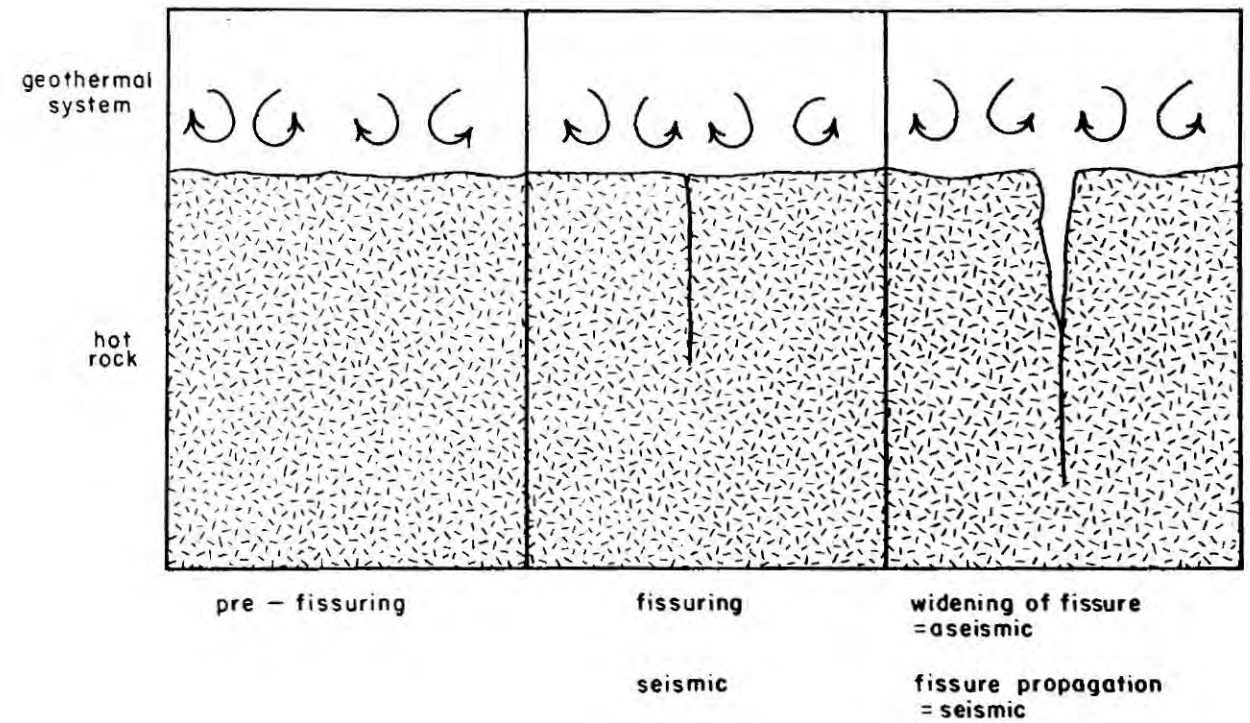

Fig. 8.4 Schematic illustration of the process of fracture formation, propagation and aseismic widening in a fluid cooled, hot rock environment.

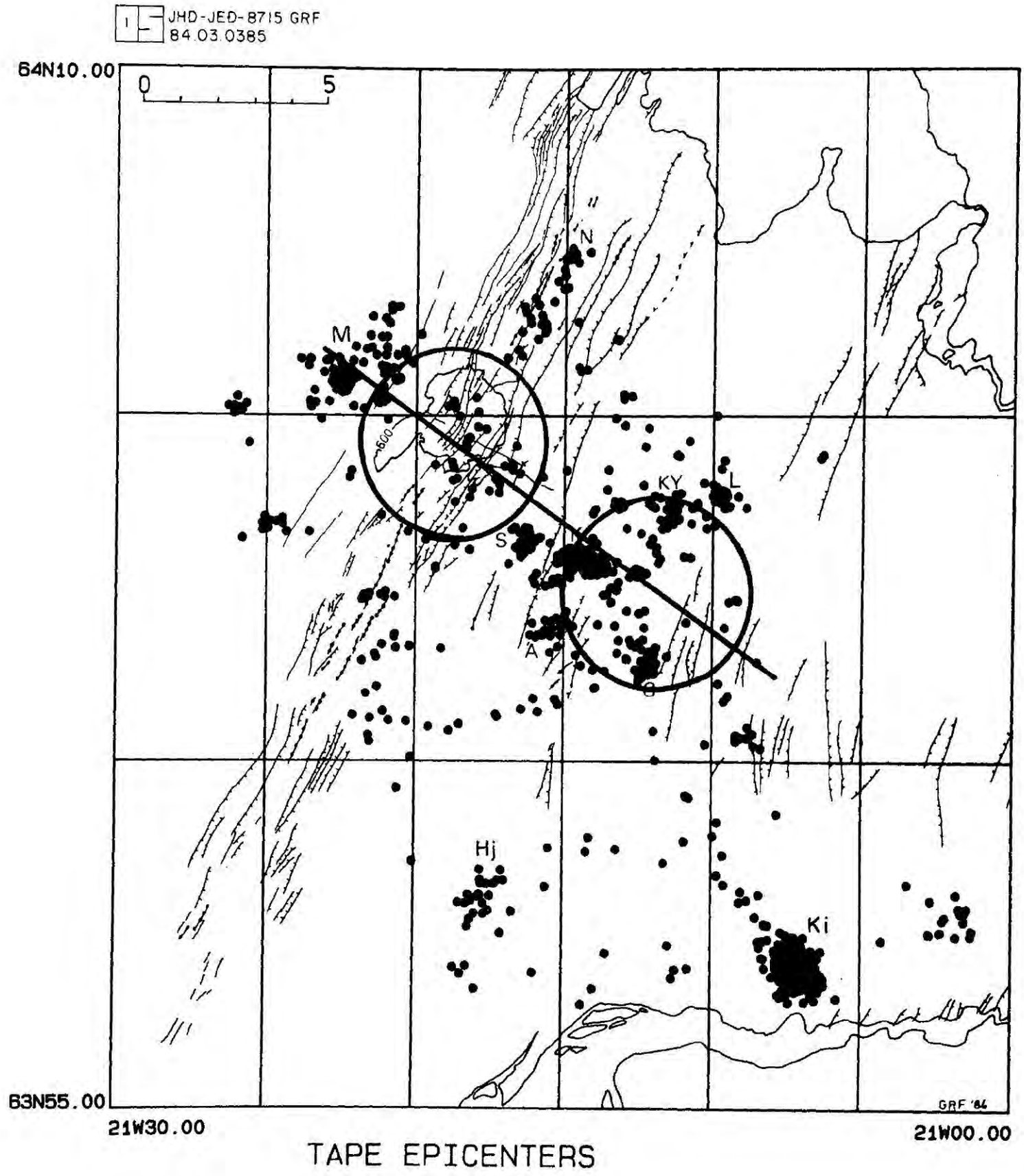

Fig. 8.5 The double volcanic system and connecting transverse structure plotted on a map of tape data epicentres (see Fig. 2.2).

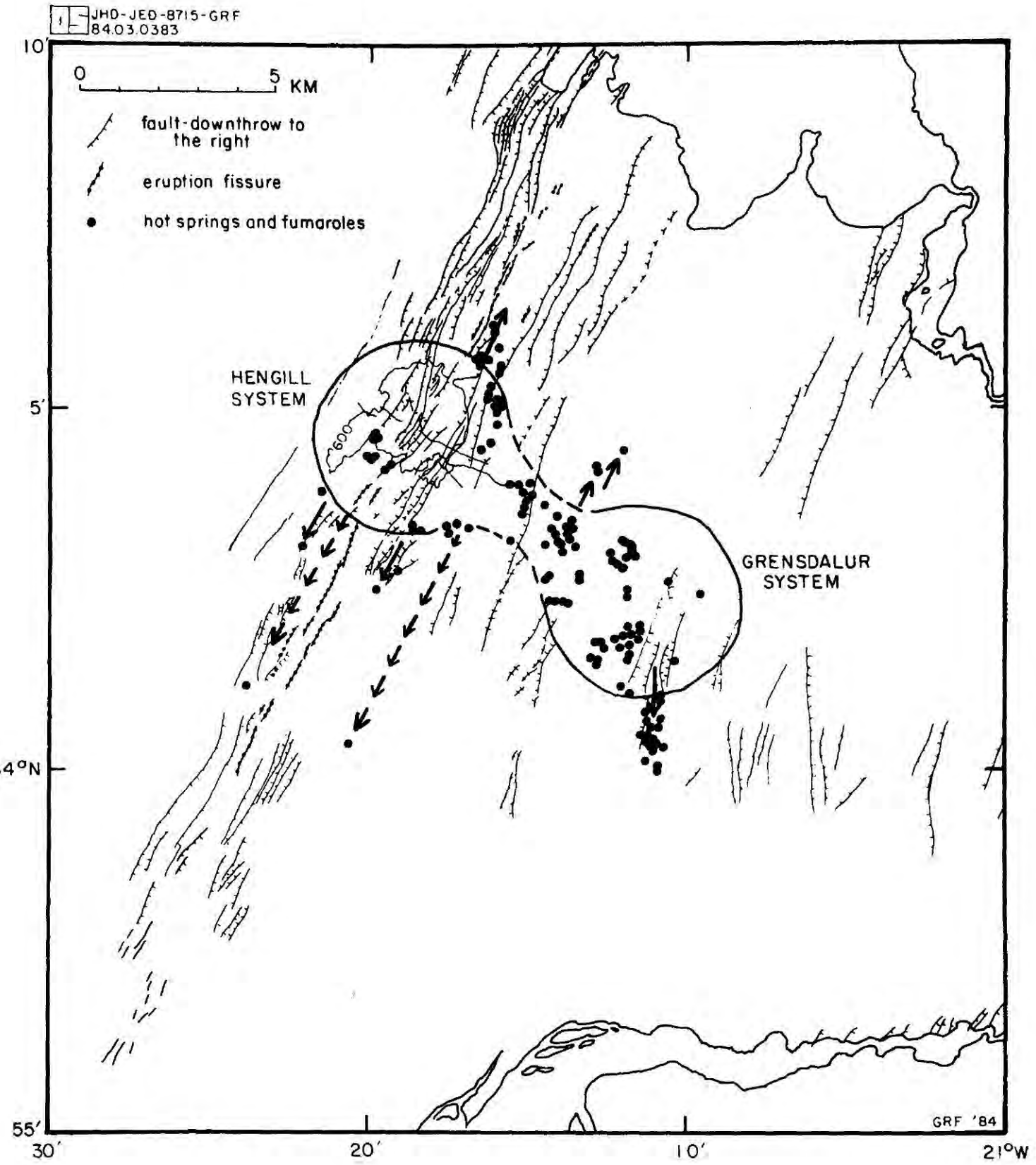

Fig. 8.6 Proposed structure of the high temperature area. The extents of the cores of the heat sources feeding the geothermal fields are outlined and lateral subsurface flow is indicated by arrows.

lie directly above these heat sources may be explained by lateral subsurface flow along faults or fissures or they may be fuelled by additional, minor heat sources unconnected to the two main ones at shallow depth. In general hypocentral depths lie in the range 2 - 6 km and this may be an indication of the vertical extent of the cooling contraction heat extraction process.

In Table 8.1 is a suggested comparison of the two major geothermal systems. The two systems are distinct and different in many respects and it is to be expected that the properties of the two geothermal reservoirs and their geothermal fluids are also distinct and different.

In addition to this broad structural picture, the detailed seismicity throws light on smaller scale features within the area. The small volumes demarcated by subclusters within the central cluster may be connected to particularly good aquifers that allow efficient heat removal and thus encourage high seismicity. The NW-SE trend of earthquake epicentres observed in the central cluster (see Figs. 4.1 and 4.3) is mirrored by a similar trend in the hot spring distribution displaced approximately 1 km to the N (see Fig. 2.4). The heat that fuels this NW-SE trend of hot springs is thus probably being mined from the volume demarcated by the NW-SE trend of hypocentres. This indicates that geothermal fluids may flow to the surface along an aquifer with a SW dip. This is illustrated in Fig. 8.7 which is a transverse cross section of this trend (cf Fig. 4.9). The feature exhibits a hade of 15^{o}. It contains the Klambragil (K) subcluster, a seismic zone of particular interest because of its high seismic rate, persistance, unusually shallow depth

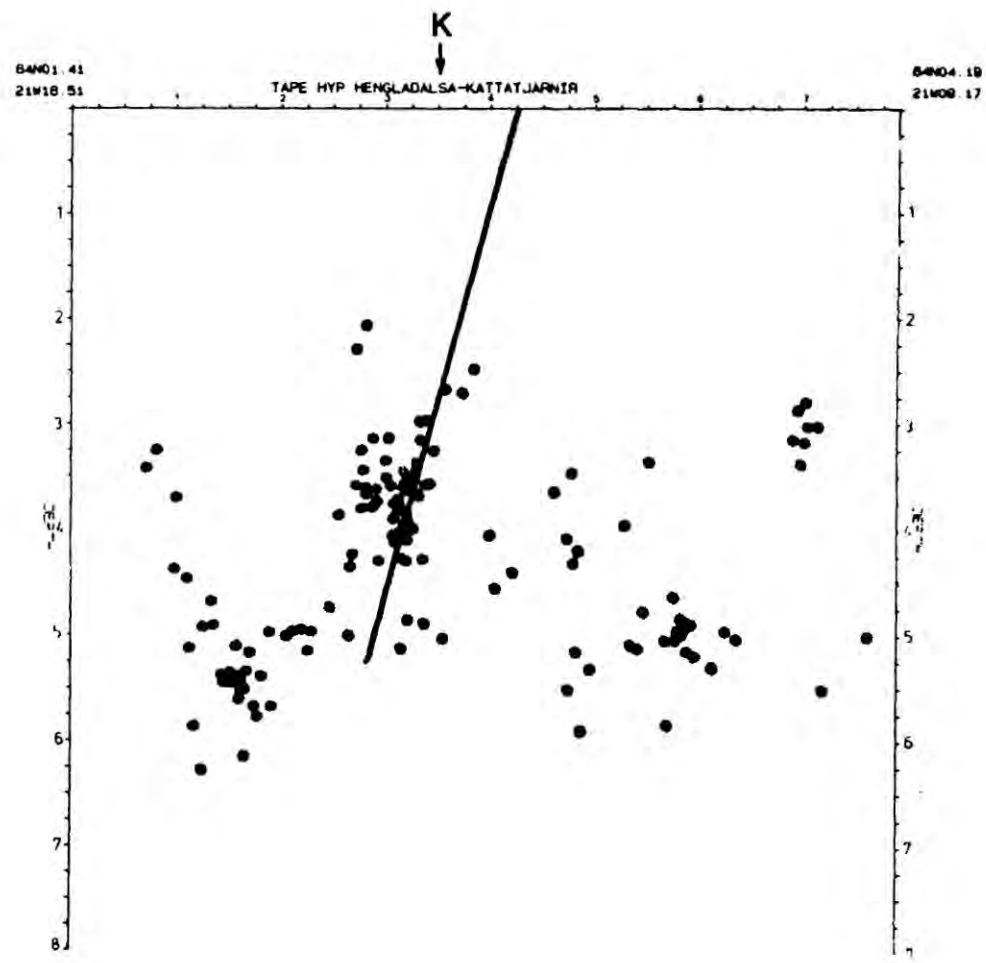

Fig. 8.7 SW-NE cross section of the transverse structure illustrating hypocentres located on the 1981 radio telemetry network. The position of a proposed fault or fault zone dipping SW with hade 15° is indicated.

	Hengill system		Grensdalur system
1.	Hot, partially molten source	1.	Hot, solidified source
2.	Periodic magma injections	2.	No periodic magma injections
3.	Reservoir hot	3.	Reservoir cool
4.	Good reservoir "cap"	4.	Poor, fissured reservoir "cap"
5.	Thick pile of rock over reservoir	5.	Reservoir deeply eroded
6.	Small surface heat loss relative to heat content of source	6.	Large surface heat loss relative to heat content of source
7.	Periodic rifting episodes forming fissures	7.	No periodic rifting episodes
8.	Heat exchange maintained mainly from below by magmatic activity	8.	Heat exchange maintained mainly from above by groundwater activity
9.	Geothermal swarms and microearthquake activity continuous but infrequent	9.	Geothermal swarms and microearthquake activity continuous and frequent

Table 8.1 Comparison of the Hengill and Grensdalur geothermal systems

(3.25-4.25 km) and high proportion of tensile crack type events. It is possible that this subcluster demarcates a volume that is delivering a particularly large amount of heat and that feeds the intense geothermal displays of Klambragil and Olkelduhals. This is consistent with geochemical and geological evidence suggesting the presence of a third, minor heat source in this area (Fig. 2.12). Since mislocation of the earthquake epicentres may be up to 400 m (Table 7.2) the estimated hade of the aquifer may be in error by up to 6°.

The proposed aquifer is colinear with the transverse structure (Section 8.1.2). It is thus possible that the transverse structure is a weak zone in the crust which is exploited by the circulating groundwaters. The structure is observed to continue to the NW of Hengill in the Mosfellsheidi area, an area that is also seismically active. Although no hot springs or fumaroles are observed in the Mosfellsheidi area, and resistivity soundings indicate that in general the geothermal reservoir terminates abruptly on the W boundary of the fissure swarm (Fig. 2.5) there may thus be an indication in the seismic data that locally the reservoir extends 2 or 3 km to the NW of Hengill along the transverse structure. The fact that tensile crack type events are very subsidiary on Mosfellsheidi may be an indication that no heat source underlies that area and that if the reservoir extends beneath it then it must be fed by lateral flow from Hengill.

Other examples may be noted of imperfect correlation between seismicity and surface heat loss. No hot springs or fumaroles are observed in the area of the NE-SW trend in the central cluster (Figs. 4.1 and 4.3). Also no hot springs are

observed above the earthquake hypocentral zone in Nesjavellir. Hot springs and fumaroles are, however observed S of the latter where no earthquakes were located. It may be that these seismic volumes do represent heat sources, but that they are not overlain by fracture zones that enable vertical flow of the geothermal fluids. In that case hot fluids may flow short distances laterally before emerging at the surface. It is also possible that the two volumes mentioned above may be heat sources of low output. In Nesjavellir the events were few and only 50% were of tensile crack type. In the NE-SW trend of the central cluster the mode of faulting changes from predominately tensile crack type at its SW end (the Kyllisfell (KY) subcluster) to solely shear type at its NE end (the Laxardalur (L) subcluster). This may indicate the termination of the heat source to the NE.

It may be that continuous small magnitude seismicity is only exhibited by geothermal systems during a certain stage of their lifetimes when the conditions of permeability, temperature and availibility of groundwater are right. The reason why little activity is associated with Hengill may be that the reservoir is much hotter than that associated with the Grensdalur system, the cap rock relatively impermeable and surface heat loss relatively small. The onset of seismic activity in the N part of Nesjavellir may mark the point at which the temperature of the heat source falls below a certain critical value. The lack of seismicity associated with the hot springs immediately N of Hveragerdi may indicate that these springs are fed by lateral flow from the Grensdalur system, which would also be consistent with the results of borehole

measurements (Section 2.2.2).

8.1.5 The Olfus lowlands

E of the fissure swarm the aseismic belt about 64° N marks the boundary between the high temperature geothermal area and the Olfus lowlands. A low background of activity occurs S in Olfus. It may be that these events occur in response to a general weakening of the crust by the low temperature geothermal area in Olfus (Section 2.2.2). Focal mechanisms are interpreted as indicating right lateral strike slip movements on NS striking faults. In that case the area may be dissected by faults with NS trend and not by a single large EW trending fault as might be predicted by simplistic plate tectonic considerations. In particular the areas Kirkjuferjuhjaleiga (Ki) in the E and Hjalli (Hj) in the W exhibit relatively high seismicity (Figs. 4.1 and 4.2) which may indicate particular faults. This interpretation would suggest that the area would exhibit NS uniformity and EW non-uniformity, in agreement with the structural picture that emerges from resistivity investigations of the low temperature geothermal area.

8.1.6 Deep structure

The results of the teleseismic and explosion data in general support the hypothesis presented above. The Hengill and Grensdalur volcanic centres are structurally distinct in the depth range 0 - 10 km, the former being associated with relatively low velocities and the latter with high velocities.

The low velocities may be due to young eruptives at shallow depth possibly underlain by partial melt, and the high velocities denser, intrusive, solidified, relatively cool material. An abrupt structural change occurs on the W boundary of the fissure swarm - the low velocity anomaly associated with the Hengill central volcano does not extend beneath Mosfellsheidi. A structural change is indicated about 64° N and relatively low velocities are associated with Olfus.

b-value variations within the area also indicate that the Mosfellsheidi area is tectonically distinct from the fissure swarm and the areas E of it. Similar b-values were, however, calculated for the tectonically dissimilar Grensdalur and Olfus areas. It may be that the similarly high stress levels associated with each of these areas are due to different causes. Within the high temperature geothermal field high stress may be thermally induced and in the Olfus area it may be tectonic stress due to the presence of the W end of the South Iceland zone of destructive earthquakes.

8.1.7 Implications for crustal accretion.

The model presented above implies that the Grensdalur volcanic centre has migrated 7.5 km off axis in a N 125°E direction. This indicates a more southerly spreading direction than the N 100°E direction inferred by Bjornsson (1983) from the orientation of the Charlie-Gibbs fracture zone. If an approximate age of 700,000 yrs is assigned to the Grensdalur system (Bjornsson et al., 1974) an average migration rate of about 1 cm yr^{-1} is indicated. This may be taken as a very rough

estimate of the half spreading rate of the Western Volcanic zone at this point on the accretionary plate boundary in Iceland.

The spreading rate of the Reykjanes Ridge has been estimated to be about 1 cm yr^{-1} (Talwani and Eldholm, 1977). Since the accretionary plate boundary in the south of Iceland is double (see Fig. 1.2) a spreading rate of approximately 1/2 cm yr^{-1} might be a more realistic estimate for the Western Volcanic Zone. The discrepancy between this and the geological estimate may arise because the Grensdalur volcanic centre continued to be active until it had migrated several km away from the boundary. The geological estimate is, however, of the same order as the kinematic estimate. This confirms that the Grensdalur volcanic centre was probably transported off boundary by plate movements and not that the accretionary plate boundary jumped west. This conclusion would be in keeping with the gross tectonic history of Iceland, which involves solely eastward ridge jumps. It may thus be estimated that the Grensdalur volcanic centre lay on the accretionary plate boundary approximately 1.4 Ma ago.

8.2 Wider implications

8.2.1 Icelandic geothermal areas

It has been suggested here (Section 8.1.3) that the continuous small magnitude background seismicity of the Hengill area is associated with rock volumes at depth that are cooling and contracting rapidly under the action of circulating ground water and steam. Because the area sits astride an accretionary plate boundary it is subject to a large tensional stress regime. Fracturing in this environment results in tensile crack formation.

The association of continuous background small magnitude earthquake activity and Icelandic geothermal systems has long been recognised (Ward and Bjornsson, 1971). It has been argued here that the anomalously high level of seismicity in the Hengill area has much to do with the presence of a double (and therefore unusually large) high temperature geothermal area. The background level of activity of the presently active Hengill central volcano-fissure swarm-geothermal system alone is not anomalous when compared with other Icelandic systems. The implication of this is that the background seismicity of Icelandic geothermal areas in general may mark the subsurface areas where heat is being removed from hot rock by circulating groundwater fluids. Imperfect correlation with surface heat loss may indicate that some lateral flow of the geothermal fluids occurs before they reach the surface. Such lateral flow probably does not occur over long distances, however, because of the very strong buoyancy forces associated with high temperature

fluids. (The specific gravity of water at pressures corresponding to a few km depth above the critical temperature, for instance, is about 0.3). The absence of seismicity need not necessarily imply that the rocks in that volume are not hot, but simply that they are not rapidly cooling down (e.g. beneath Hengill).

The question is also raised as to whether tensile crack type seismicity does not occur in other central volcano-fissure swarm-geothermal systems. It is interesting to note that a large proportion of the solutions obtained for events within the Hengill fissure swarm were tensile crack type (Fig. 6.4). To date, the only other earthquake study that has been done in sufficient detail in such an environment is the work done at Reykjanes by Klein et al., (1977). That study also revealed earthquake radiation patterns of a similar type to the Hengill tensile crack events. The fact that so many high temperature areas occur along the accretionary plate boundary in Iceland may well be due to the fact that the strong tensional stress regime associated with the boundary causes the stresses due to thermal contraction to be relieved by the formation of tensile cracks, which are optimum for aquifer formation.

Since Icelandic fissure swarm/geothermal systems also lie on or close to the accretionary plate boundary, it would be expected that periodic, tectonic episodes should also occur, with accompanying seismicity. Where such episodes have been observed, the earthquake source mechanisms exhibit predominately shear movements. This seismicity would be superimposed on the continuous, "geothermal" seismicity, but would display a contrasting temporal distribution. Sequences such as the Sept. 1972 swarm on Reykjanes, (Klein et al., 1977) and the

Sept. 1981 Kirkjuferjuhjaleiga, Olfus swarm (Section 5.2.4.2) were sequences of this type. It is appropriate to note that in the case of the background activity that could prove useful as a geothermal prospecting tool a continuous temporal distribution of activity would be anticipated that would ensure the successful aquisition of a data set by a relativly short monitoring project.

8.2.2 Dyke injection on accretionary plate boundaries

The observation of tensile crack formation at several kilometers depth in the earth's crust near to an accretionary plate boundary has wider implications for the crustal accretion process.

The accretion of the shallow crust by dyke injection is indicated by offshore research, and the mechanism by which this is achieved has been observed at Krafla in N Iceland (Section 1.2.3). Such a process must necessarily involve large movements of crustal blocks in the direction normal to a fault plane that is itself orientated normal to the direction of least compressive stress. To date, however, neither the formation of such fractures nor movements normal to them have been observed seismically. Although some large teleseismic focal mechanisms with enhanced explosive components have been reported from the Mid Atlantic Ridge, accretionary plate boundaries generally exhibit normal dip-slip shear faulting (Section 6.1.1). Dyke injection events in the Krafla area are generally accompanied by relatively minor seismicity and much of the crustal widening is a result of the widening of pre-existing fissures. For example

during the July 1978 event 30 km of the plate boundary was rifted and the crust widened by up to 1 m. The largest earthquake recorded during the swarm that accompanied this event was of magnitude M_{IL} = 4.1 (Bjornsson et al., 1979; Einarsson and Brandsdottir, 1980).

It is proposed here that the formation of long fractures parallel to the accretionary plate boundary is achieved by cumulative small magnitude cooling contraction fracture during inter episodic periods of volcanic quiesence. This process may be short lived where narrow dykes are injected, which cool quickly. These form sheet complexes where the individual dykes are separated by fracture planes that are their cooled margins. This is consistent with the observation that small magnitude background seismicity is absent in the fissure swarms away from central volcanoes (P. Einarsson, pers. comm.). At central volcanoes, however, where there is a greater supply of magma, large heat losses may be maintained over long periods, and the cooling-contraction process be continuous.

During dyke injection events magma intrusion proceeds along the fracture planes that are the cooled edges separating the old dykes. These fracture planes are connected by shear movements on planes joining them and are widened aseismically to accomodate the dyke volume. The maintainance of a highly fractured and porous state by cooling contraction fracturing in the volume of a central volcano facilitates the upward migration and accumulation of magma and this process may thus be a contributary factor in the mechanism that perpetuates central volcanoes.

This concept may be summarised:

A feature of central volcanoes and their associated fissure swarm systems is fracture complexes that are zones of weakness in the brittle crust. Hot mantle material preferentially emplaces along those fracture complexes and engineers their perpetuation by thermal stresses.

8.3 Conclusions

Seismological studies were conducted in the Hengill area in the 7 year period 1978-1984. Local earthquake, teleseismic and explosion data were collected and processed. The results are consistent with a structure involving an extinct volcanic centre in the Grensdalur area and an active one now underlying Hengill. A transverse structure connects the two and represents the migration trajectory of the Grensdalur volcanic centre.

The action of cool circulating groundwater fluids on hot rock at depth results in the formation of cooling contraction cracks and accounts for the ongoing small magnitude seismicity observed over the geothermal area. In the tensile stress regime of the accretionary plate boundary the type of fracture formed is tensile crack. Volume calculations indicate that aseismic fracture opening occurs subsequent to formation.

The spatial distribution of local earthquake activity indicates that the two volcanic centres are the sites of separate heat sources feeding distinct geothermal fields. It would be expected that the two fields exhibit contrasting reservoir characteristics. The transverse structure may represent a fault zone in the crust that is an aquifer for geothermal fluids. High level persistant small magnitude earthquake activity such as that associated with the Grensdalur system is possibly only exhibited by geothermal systems at a certain stage in their lifetime. The low level background seismicity of the structurally distinct Olfus lowlands occurs on NS trending faults, possibly in response to the low temperature geothermal area.

The results of teleseismic and explosion relative velocity studies show that the two volcanic systems exhibit velocity anomalies that extend to approximately 10 km depth. High stress levels over the whole area may be due to both thermal and tectonic influences.

The ongoing small magnitude seismicity that is a feature of Icelandic high temperature geothermal areas thus demarcates volumes of rock that are rapidly cooling down and feeding the geothermal system. It may therefore provide a geothermal prospecting tool. The formation of cooling contraction tensile cracks on accretionary plate boundaries offers an explanation for the mechanism of dyke injection.

ACKNOWLEDGEMENTS

I would like to thank Profs. J.F.Dewey and M.H.P. Bott for the privilege of working at the Dept. of Geological Sciences, University of Durham. I am also grateful to the Geophysics Division, University of Iceland, for permission to submit this material for a Ph.D. degree. I extend special thanks to my supervisors Drs. Pall Einarsson and R.E.Long for their guidence and generous personal support throughout my study course. I am also especially indebted to Dr. Axel Bjornsson and Prof. Sveinbjorn Bjornsson for unstinting practical, scientific and personal help.

I am grateful to Gudbjorg Gudsteinsdottir and family, Nesjavellir, Sigrun Thorsteinsdottir and family, Stori-Hals, Hjalti Thordason and family, Bjarnastadir, Birgir Palsson and family, Gufudalur, and Egill Gudmundsson and family, Krokur, who made the Hengill seismological research programme both logistically possible and also a highly enjoyable and entertaining experience.

During the 1981 monitoring project Thorsteinn Egilson was a first class field assistant and Robert Jones provided technical assistance and worked extremely long hours to maintain the network.

In addition to those mentioned above, many individuals contributed to the work. I especially acknowledge the efforts of Gudbjorg Aradottir, Dave Asberry, Bryndis Brandsdottir, Arni Gunnarsson, Wojcieck Gulgowski, Keith Gymer, Henry Johansen, Hrefna Kristmannsdottir, Eggert Larusson, Marteinn Sverisson, Sigurdur Emil Palsson, Kristjan Saemundsson, Thorunn

Skaftadottir, Ragnar Stefansson, Jon Sveinsson, the staff of Computing Services, University of Iceland (Reiknistofnun Haskolans) and the staff of the University of Durham Computer Centre.

Some of the seismographs of the regional network were built with the support of the Nato Research Grants Programme (Grant No. 715). Geostore equipment was loaned for the 1981 tape monitoring project by the Natural Environmental Research Council, U.K. The United Nations University Geothermal Training Programme, Iceland, contributed to the 1979 pilot monitoring project.

The project was jointly funded by the Reykjavik Municipal District Heating Service (Hitaveita Reykjavikur), the National Energy Authority, Iceland (Orkustofnun) and the Science Institute, University of Iceland (Raunvisindastofnun Haskolans), and in this context I would like to thank Johannes Zoega (HR) and Dr. Gudmundur Palmason (OS).

REFERENCES

Aki, K. 1984. Evidence for magma intrusion during the Mammoth Lakes earthquakes of May 1980 and implications of the absence of volcanic (harmonic) tremor. J. Geophys. Res., 89, 7689-7696.

Aki, K. 1965. Maximum liklihood estimate of b in the formula log N = a - bM and its confidence limits. Bull. Earthquake Res. Inst., Tokyo University, 43, 237-239.

Aki, K. and Richards, P.G. 1980. Quantitative Seismology, Vol. 1, (Freeman, San Franoisoo), 557 pp.

Aki, K., Christoffersson, A. and Husebye, E.S. 1977. Determination of the 3-dimensional seismic structure of the lithosphere. J. Geophys. Res., 82, 277-296.

Angenheister, G., Bjornsson, S., Einarsson, P., Gebrande, H., Goldflam, P., Jacoby, W.R., Litvinenko, I.V., Loncarevic, B., Miller, H., Palmason, G., Pavlenkova, N.I., Richard, S., Solomon, S.C., Weigel, W. and Zverev, S.M. 1980. Reykjanes Ridge Seismic Experiment (RRISP 77). J. Geophys., 47, 228-238.

Arnason, B. 1976. Groundwater systems in Iceland traced by deuterium. Soc. Sci. Islandica, Rit. 42, 236 pp.

Arnason, B., Theodorsson, P. Bjornsson, S., and Saemundsson, K. 1969. Hengill, a high temperature thermal area in Iceland. Bull. Volcanol., 33, 245-260.

Arnorsson, S. and Gunnlaugsson, E. 1984. . New gas geothermometers for geothermal exploration-calibration and application. Submitted to Geochim. Cosmochim. Acta.

Barker, J.S. and Langston, C.A. 1983. A teleseismic body-wave analysis of the May 1980 Mammoth Lakes, California, earthquakes. Bull. Seismol. Soc. Am., 73, 419-434.

Bath, M. 1960. Crustal structure of Iceland. J. Geophys. Res., 65, 1793-1807.

Beblo, M., Bjornsson, A., Arnason, K., Stein, B. and Wolfgram, P. 1983. Electrical conductivity beneath Iceland - constraints imposed by magnetotelluric results on temperature, partial melt, crust- and mantle structure. J. Geophys., 53, 16-23.

Beblo, M. and Bjornsson, A. 1980. A model of electrical resistivity beneath NE-Iceland: correlation with temperature. J. Geophys., 47, 184-190.

Beblo, M. and Bjornsson, A. 1978. Magnetotelluric investigation of the lower crust and upper mantle beneath Iceland. J. Geophys., 45, 1-16.

Beloussov, V.V. and Milanovsky, Y.Y. 1977. On tectonics and tectonic position of Iceland. Tectonophysics, 37, 25-40.

Bjornsson, A. 1984. Dynamics of crustal rifting in NE-Iceland. J. Geophys. Res., in press.

Bjornsson, A. 1976. Hengilssvaedi-flugsegulkort (Aeromagnetic map of the Hengill area). National Energy Authority, Iceland map Fnr. 14320.

Bjornsson, A. and Hersir, G.P. 1981. Geophysical reconnaissance study of the Hengill high-temperature area, SW-Iceland. Geothermal Resources Council, Trans., 5, 55-58.

Bjornsson, A., Johnsen, G., Sigurdsson, S., Thorbergsson, G., and Tryggvason, E. 1979. Rifting of the plate boundary in North Iceland 1975-1978. J. Geophys. Res., 84, 3029-3038.

Bjornsson, A., Saemundsson, K., Einarsson, P., Tryggvason, E. and Gronvold, K. 1977. Current rifting episode in North Iceland. Nature, 266, 318-323.

Bjornsson, A., Tomasson, J. and Saemundsson, K. 1974. Hengilssvaedid. Stada jardhitarannsokna vorid 1974. (The Hengill area, the state of geothermal research in spring 1974). National Energy Authority, Iceland Report OS JHD 74 15, 11pp.

Bjornsson, H., Bjornsson, Sv. and Sigurgeirsson, Th. 1980. Penetration of water into hot rock boundaries of magma at Grimsvotn. Nature, 295, 580-581.

Bjornsson, S. 1983. Crust and upper mantle beneath Iceland. in: Structure and Development of the Greenland-Sootland Ridge, ed. M.H.P. Bott et al., Plenum Press, New York and London, 31-62.

Bjornsson, S. 1975. Jardskjalftar a Islandi. (Earthquakes in Iceland.) Natturufraedingurinn, 45, 110-133.

Bodvarsson, G. 1951. Skyrsla um rannsoknir a jarhita i Hengli, Hveragerdi og nagrenni, arin 1947 - 1949 (Report on geothermal research in Hengill, Hveragerdi and vicinity, 1947 - 1949.) Tim. V.F.I., 36, 1-48.

Bott, M.H.P. 1984. Plate tectonic evolution of the Icelandic transverse ridge and adjacent regions. J. Geophys. Res., in press.

Bott, M.H.P., 1983a. Deep structure and geodynamics of the Greenland-Scotland Ridge; an introductory review. in: Structure and Development of the Greenland-Scotland Ridge, ed. M.H.P. Bott et al., Plenum Press, New York and London, 3-10.

Bott, M.H.P. 1983b. The crust beneath the Iceland-Faeroe Ridge. in: Structure and Development of the Greenland-Scotland Ridge, ed. M.H.P. Bott et al., Plenum Press, New York and London, 63-76.

Bott, M.H.P. 1974. Deep structure, evolution and origin of the Icelandic transverse ridge. in: Geodynamics of Iceland and the North Atlantic Area, ed. L. Kristjansson, D. Reidel Pub. Co., Dordrecht, 33-47.

Bott, M.H.P. 1973. The Structure of the Iceland-Faeroe Ridge. J. Geol. Soc., 129, 321.

Bott, M.H.P. and Gunnarsson, K. 1980. Crustal structure of the Iceland-Faeroe Ridge. J. Geophys., 47, 221-227

Brandsdottir, B. and Einarsson, P. 1979. Seismic activity associated with the September 1977 deflation of the Krafla central volcano in North-Eastern Iceland. J. Volcanol. Geothermal Res., 6, 197-212.

Bufe, C.G. 1970. Frequency-magnitude variations during the 1970 Danville earthquake swarm. Earthquake Notes, 41, 3-7.

Christensen, N.I. and Wilkens, R.H. 1982. Seismic properties, density, and composition of the Icelandic crust near Reydarfjordur. J. Geophys. Res., 87, 6389-6395.

Combs, J. and Hadley, D. 1977. Microearthquake investigation of the Mesa geothermal anomaly, Imperial Valley, California. Geophysics, 42, 17-33.

Corbishley, D.J. 1969. Measurements of the derivative of the P-wave travel time curve by means of an array network. Ph.D. thesis, University of Durham, 99 pp.

Eberhart-Phillips, D. and Oppenheimer, D.H. 1984. Induced seismicity in the Geysers geothermal area, California. J. Geophys. Res., 89, 1191-1207.

Einarsson, P. 1984. Seismicity along the eastern margin of the North American plate. Geol. Soc. Am., in prep.

Einarsson, P. 1979. Seismicity and earthquake focal mechanisms along the mid-Atlantic plate boundary between Iceland and the Azores. Tectonophysics, 55, 127-153.

Einarsson, P. 1978. S-wave shadows in the Krafla caldera in NE Iceland, evidence for a magma chamber in the crust. Bull. Volcanol., 41, 1-9.

Einarsson, P. and Eiriksson, J. 1982. Earthquake fractures in the districts Land and Rangarvellir in the South Iceland Seismic Zone. Jokull, 32, 113-120.

Einarsson, P., Bjornsson, S., Foulger, G., Stefansson, R. and Skaftadottir, T. 1981. Seismicity pattern in the South Iceland seismic zone. In: Earthquake Prediction - An International Review, Maurice Ewing Series 4, Am. Geophys. Union, 141-151.

Einarsson, P. and Brandsdottir, B. 1980. Seismological evidence for lateral magma intrusion during the July 1978 deflation of the Krafla volcano in NE Iceland. J. Geophys., 47, 160-165.

Einarsson, P. and Bjornsson, S. 1979. Earthquakes in Iceland. Jokull, 29, 37-43.

Einarsson, P., Klein, F. and Bjornsson, S. 1977. The Borgarfjordur earthquakes of 1974 in west Iceland. Bull. Seismol. Soc. Am., 67, 187-208.

Einarsson, T. 1954. A Survey of Gravity in Iceland. Soc. Sci. Islandica, Rit 30, 22 pp.

Eiriksson, J. 1973. Jardlagaskipun ytra Midsudurlands. (Stratigraphy of mid-South Iceland). B.S. thesis, University of Iceland, 98 pp

Evans, J.R. and Sacks, I.S. 1980. Lithospheric structure in the North Atlantic from observations of Love and Raleigh waves. J. Geophys. Res., 85, 7175-7182.

Evans, J.R. and Sacks, I.S. 1979. Deep structure of the Iceland plateau. J. Geophys. Res., 84, 6859-6866.

Evison, F.F. 1963. Earthquakes and faults. Bull. Seismol. Soc. Am., 50, 117-134.

Featherstone, P.S., Bott, M.H.P. and Peacock, J.H. 1977. Structure of the continental margin of south-eastern Greenland. Geophys. J.R. astr. Soc., 48, 15-27.

Flovenz, O.G. 1980. Seismic structure of the Icelandic crust above layer three and the relation between body wave velocity and the alteration of the basaltic crust. J. Geophys. 47, 211-220.

Foulger, G.R. 1984. The Hengill geothermal area : seismological studies 1978-1984. Science Institute, University of Iceland Report RH-07-84, National Energy Authority, Iceland Report OS-84073/JHD-12, 196 pp.

Foulger, G. 1982. Geothermal exploration and reservoir monitoring using earthquakes and the passive seismic method. Geothermics, 11, 259 268.

Foulger, G. 1981. The seismological field project of June-October 1981 in the Hengill area. Science Institute, University of Iceland Report RH-81-18, 50 pp.

Foulger, G. and Long, R.E. 1984. Anomalous focal mechanisms: evidence for tensile crack formation on an accreting plate boundary. Nature, 310, 43-45.

Foulger, G. and Einarsson, P. 1980. Recent earthquakes in the Hengill-Hellisheidi area in SW Iceland. J. Geophys., 47, 171-175.

Foulger, G. and Olafsson, M. 1980a. Earthquake hypocenter locator and plot systems. 1. Maintenance manual. Science Institute, University of Iceland Report RH-80-01, 29pp.

Foulger, G. and Olafsson, M. 1980b. Earthquake hypocenter locator and plot systems. 2. User manual. Science Institute, University of Iceland Report RH-80-02, 24pp.

Francis, T.J.G. 1968. The detailed seismicity of mid-ocean ridges. Earth Planet Sci. Lett., 4, 39-46.

Francis, T.J.G. 1968. Seismicity of mid-ocean ridges and its relation to properties of the upper mantle and crust. Nature, 220, 899-901.

Gebrande, H., Miller, H. and Einarsson, P. 1980. Seismic structure of Iceland along RRISP - profile 1. J. Geophys., 47, 239-249.

Gibson, I.L., Iceland Research Drilling Project. 1979. Crust of oceanic affinity in Iceland. Nature, 281, 347-351.

Given, J.W., Wallace, T.C. and Kanamori, H. 1982. Teleseismic analysis of the 1980 Mammoth Lakes earthquake sequence. Bull. Seismol. Soc. Am., 72, 1093-1110.

Gumbel, E.J. 1960. Statistics of extremes. Columbia University Press, 375 pp.

Hermance, J.F. 1981. Crustal genesis in Iceland: geophysical constraints on crustal thickening with age. Geophys. Res. Lett., 8, 203-206.

Herrin, E. 1968. Introduction to 1968 seismological tables for P-phases. Bull. Seismol. Soc. Am., 58, 1193-1241.

Hersir, G.P. 1980. Electrical and electromagnetic measurements across the Mid-Atlantic Ridge in SW Iceland, with special reference to the high temperature area of Hengill. unpublished Specialearbejde Report, Laboratoriet for Geofysik, Aarhus Universitet, Denmark, 165 pp.

Hersir, G.P., Bjornsson, A. and Pedersen, L.B. 1984. Magnetotelluric survey across the active spreading zone in south west Iceland. J. Volcanol. Geothermal Res., 20, 253-265.

Hill, D.P. 1977. A model for earthquake swarms. J. Geophys. Res., 82, 1347-1352.

Iyer, H.M. 1979. Deep structure under Yellowstone National Park, U.S.A. : a continental "hotspot". Tectonophysics, 56, 165-197.

Iyer, H.M., Oppenheimer, D.H. and Hitchcock, T. 1979. Abnormal P-wave delays in the Geysers-Clear Lake geothermal area, California. Science, 204, 495-497.

Jakobsson, S.P. 1972. Chemistry and distribution pattern of recent basaltic rocks in Iceland. Lithos, 5, 365-386.

Johnsen, G.V., Bjornsson, A. and Sigurdsson, S. 1980. Gravity and elevation changes caused by magma movement beneath the Krafla caldera, north east Iceland. J. Geophys., 47, 132-140.

Jonsson, J. 1983. Eldgos a sogulegum tima a Reykjanesskaga. (Historic eruptions on the Reykjanes Peninsula). Natturufraedingurinn, 52, 127-139.

Julian, B.R. Analyzing seismic-source mechanisms by linear programming. Geophys. J. R. astr. Soc., in press.

Julian, B.R. 1983. Evidence for dyke intrusion earthquake mechanisms near Long Valley Caldera, California. Nature, 303, 323-325.

Julian, B.R. and Sipkin, S.A. 1984. Earthquake processes in the Long Valley Caldera area, California. unpublished manuscript.

Keen, C.E., Fricker, A., Keen, M.J. and Blinn, L. 1980. Reykjanes Ridge crest studied by surface waves with an earthquake pair technique. J. Geophys., 47, 265-270.

Klein, F.W. 1978. Hypocenter location program HYPOINVERSE. U.S. Geol. Surv. Open-File Report, 78-694.

Klein, F.W., Einarsson, P. and Wyss, M. 1977. The Reykjanes Peninsula, Iceland, earthquake swarm of September 1972 and its tectonic significance. J. Geophys. Res., 82, 865-888.

Langston, C.A. 1981. Source inversion of seismic waveforms: the Koyna, India, earthquakes of 13 September 1967. Bull Seismol. Soc. Am., 71, 1-24.

Lilwall, R.C. 1976. Seismicity and seismic hazard in Britain. Natural Environmental Research Council, Inst. Geol. Sci., Seismol. Bull. no. 4, 9 pp.

Lister, C.R.B. 1980. Heat flow and hydrothermal circulation. Ann. Rev. Earth Planet. Sci., 8, 95-117.

Lister, C.R.B. 1977. Qualitative models of spreading center processes, including hydrothermal penetration. Tectonophysics, 37, 203-218.

Lister, C.R.B. 1976. Qualitative theory on the deep end of geothermal systems. Proc. 2nd U.N. Symp. Dev. and Use of Geothermal Resources, 459-463.

Lister, C.R.B. 1974. On the penetration of water into hot rock. Geophys. J. R. astr. Soc., 39, 465-509.

Long, R.E. and Mitchell, M.G. 1970. Teleseismic P-wave delay time in Iceland. Geophys. J.R. astr. Soc., 20, 41-48.

Majer, E. and McEvilly, T.V. 1979. Seismological investigations at the Geysers geothermal field. Geophysics, 44, 246-269.

McKenzie, D.P. 1969. Earthquakes and the directions of principal stresses. Bull. Seismol. Soc. Am., 59, 591-601.

Mogi, K. 1963. The fracture of a semi-infinite body caused by an inner stress origin and its relation to earthquake phenomena (second paper). Bull. Earthquake Res. Inst., University of Tokyo, 41, 595-614.

Moller, D. and Ritter, B. 1980. Geodetic measurements and horizontal crustal movements in the rift zone of NE Iceland. J. Geophys., 47, 110-119.

Moorbath, S., Sigurdsson, H. and Goodwin, R. 1968. K-Ar ages of the oldest exposed rocks in Iceland. Earth Planet. Sci. Lett., 4, 197-205.

Muller, O.H. and Pollard, D.D. 1977. The stress state near Spanish Peaks, Colorado determined from a dike pattern. Pageoph., 115, 69-86.

Nakamura, K. 1970. En echelon features of Icelandic fissures. Acta Natur. Island., 2, 3-15.

Nunns, A.G. 1983. Plate tectonic evolution of the Greenland-Scotland Ridge and surrounding regions. in: Structure and Development of the Greenland-Scotland Ridge, ed. M.H.P. Bott, et al., Plenum Press, New York and London, 11-30.

Ode, H. 1957. Mechanical analysis of the dyke pattern of the Spanish Peaks area, Colorado. Bull. Geol. Soc. Am., 68, 567-576.

Page, R. 1968. Aftershocks and microaftershocks of the great Alaska earthquake of 1964. Bull. Seismol. Soc. Am., 58, 1131-1168.

Palmason, G. 1981. Crustal rifting and related thermo-mechanical processes in the lithosphere beneath Iceland. Geologische Rundschau, 70, 244-260.

Palmason, G. 1980. A continuum model of crustal generation in Iceland; kinematic aspect. J. Geophys., 47, 7-18.

Palmason, G. 1974. Heat flow and hydrothermal activity in Iceland. in: Geodynamics of Iceland and the North Atlantic Area, ed. L. Kristjansson, D. Reidel Publ. Co., Dordrecht, 297 306.

Palmason, G. 1973. Kinematics and heat flow in a volcanic rift zone with application to Iceland. Geophys. J.R. astr. Soc., 33, 451-481.

Palmason, G. 1971. Crustal structure of Iceland from explosion seismology. Soc. Sci. Islandica, Rit. 40, 187 pp.

Palmason, G. 1963. Seismic refraction investigation of basalt lavas in N and E Iceland. Jokull, 13, 40-60.

Ragnars, K., Armannsson, H. and Steingrimsson, B. 1979. Olfusdalur, maelingar i borholum G3, G6 og G7 (Well logs of boreholes G3, G6 and G7, Olfusdalur). National Energy Authority, Iceland, Report OS79053/JHD25, 51 pp.

Randall, M.J. and Knopoff, L, 1970. The mechanism at the focus of deep earthquakes. J. Geophys. Res., 75, 4965-4976.

Reasenberg, P., Ellsworth, W. and Walter, A. 1980. Teleseismic evidence for a low-velocity body under the Coso geothermal area. J. Geophys. Res., 85, 2471-2483.

Richter, C.F. 1958. Elementary Seismology. W.H. Freeman and Company, San Francisco and London, 768 pp.

Rikitake, T. 1976. Earthquake Prediction. Elsevier, New York, 357 pp.

Robson, G.R., Barr, K.G. and Luna, L.C. 1968. Extension failure: an earthquake mechanism. Nature, 218, 28-32.

Saemundsson, K. 1979. Outline of the geology of Iceland. Jokull, 29, 7-28.

Saemundsson, K. 1978. Fissure swarms and central volcanoes of the neovolcanic zones of Iceland. Geol. J. Spec. Issue, 10, 415-432.

Saemundsson, K. 1974. Evolution of the axial rifting zone in Northern Iceland and the Tjornes fracture zone. Geol. Soc. Am. Bull., 85, 495-504.

Saemundsson, K. 1967. Vulkanismus und Tektonik des Hengill - Gebietes in Sudwest-Island. (Volcanology and tectonics of the Hengill area in SW Iceland). Acta Natur. Island., 2 (7), 109 pp.

Saemundsson, K. and Bjornsson, S. 1970. Umsogn um hahitasvaedi i Hengli og Krisuvik med tilliti til virkjunar fyrir hitaveitu hofudborgarsvaedisins. (Evaluation of the high temperature areas of Hengill and Krisuvik, with regard to exploitation for hot water for the Reykjavik area). National Energy Authority, Iceland, Report OSJHD 202, 16 pp.

Sanford, A.R. and Einarsson, P. 1982. Magma chambers in rifts. in: Continental and Oceanic Rifts, Amer. Geophys. Un., Geodynamics Series, 8, 147-168.

Savage, J.E.G. 1979. A seismic investigation of the lithosphere of the Gregory Rift. Ph.D. thesis, University of Durham, 382 pp.

Scholz, C. 1968. The frequency-magnitude relation of microfracturing in rock and its relation to earthquakes. Bull. Seismol. Soc. Am., 58, 399-415.

Sigurdsson, H. and Sparks, R.S.J. 1978a. Rifting episode in N. Iceland in 1874-1875 and the eruptions of Askja and Sveinagja. Bull. Volcanol., 41, 149-167.

Sigurdsson, H. and Sparks, S.R.J. 1978b. Lateral magma flow within rifted Icelandic crust. Nature, 274, 126-130.

Sigurdsson, O. 1980. Surface deformation of the Krafla fissure swarm in two rifting events. J. Geophys., 47, 154-159.

Sigvaldason, G.E., Steinthorsson, S., Oskarsson, N. and Imsland, P. 1974. Compositional variation in recent Icelandic tholeiites and the Kverkfjoll hot spot. Nature, 251, 579-582.

Solomon, S.C. and Julian, B.R. 1974. Seismic constraints on ocean-ridge mantle structure: anomalous fault-plane solutions from first motions. Geophys. J. R. astr. Soc., 38, 265-285.

Spickernagel, H. 1980. Results of height measurements in northern Iceland 1965/1977. J. Geophys., 47, 120-124.

Stauber, D.A. and Iyer, H.M. 1983. Inversion for seismic velocity structure using teleseismic traveltimes to arrays of stations. IUGG XVIII General Assembly, IASPEI, Abstract.

Steeples, D.W. and Iyer, H.M. 1975. Teleseismic P-wave delays in geothermal exploration. Proc. 2nd U.N. Symp. Dev. and Use of Geothermal Resources, 1199-1206.

Stefansson, V. 1973. Rafleidnimaelingar i Olfusi og Floa 1973 (Conductivity measurements in Olfus and Floi 1973.) National Energy Authority, Iceland, Report OS-JHD.

Stefansson, V. 1975. Rafleidnimaelingar vid Thorlakshofn (Conductivity measurements near Thorlakshofn.) National Energy Authority, Iceland Report, OS-JHD-7519.

Stefansson, V., Tomasson, J., Gunnlaugsson, E., Sigvaldason, H. Franzson, H. and Sigurdsson, O. 1983. Nesjavellir - hola NG-6, borun, rannsoknir og vinnslueiginleikar. (Nesjavellir well NG-6, drilling, research and production characteristics.) National Energy Authority, Iceland Report OS83023/JHD04.

Steingrimsson, B. and Stefansson, V. 1979. Nesjavellir, hitastig og thrystingur i jardhitasvaedinu. (Nesjavellir, temperature and pressure in the geothermal area.) National Energy Authority, Iceland, Report OS79032/JHD15, 31 pp.

Suyehiro, S., Asada, T., and Ohtake, M. 1964. Foreshocks and aftershocks accompanying a perceptible earthquake in central Japan. Papers Meteorol. Geophys., 15, 71-88.

Sykes, L.R. 1970. Earthquake swarms and sea floor spreading. J. Geophys. Res., 75, 6598-6611.

Sykes, L.R. 1967. Mechanism of earthquakes and nature of faulting on the mid-oceanic ridges. J. Geophys. Res., 72, 2131-2153.

Talwani, M. and Eldholm, O. 1977. Evolution of the Norwegian-Greenland sea. Bull. Geol. Soc. Am., 88, 969-999.

Thorbergsson, G., Magnusson, I.T., Gunnarsson, A., Johnsen, G.V. and Bjornsson, A. 1984. Landmaelingar og thingdamaelingar a Hengilssvaedi 1982 og 1983. (Distance and gravity measurements in the Hengill area 1982 and 1983.) National Energy Authourity, Iceland, Report OS-84003/VOD-03 B, 58 pp.

Thoroddsen, T. 1899. Jardskjalftar a Sudurlandi (Earthquakes of Southern Iceland.) Hid Islenzka Bokmenntafelag, Kaupmannahofn, 199 pp.

Torfason, H., Hersir, G.P., Saemundsson, K., Johnsen, G.V. and Gunnlaugsson, E. 1983. Vestur-Hengill. Yfirbordsrannsokn jardhitasvaedisins. (West Hengill. Surface research of the geothermal area.) National Energy Authority, Iceland, Report OS-83119/JHD-22, 113 pp.

Torge, W. and Kanngieser, E. 1980. Gravity and height variations during the present rifting episode in northern Iceland. J. Geophys., 47, 125-131.

Trehu, A.M., Nabelek, J.L. and Solomon, S.C. 1981. Source characterisation of two Reykjanes Ridge earthquakes: surface waves and moment tensors; P waveforms and nonorthogonal nodal planes. J. Geophys. Res., 86, 1701-1724.

Tryggvason, E. 1980. Subsidence events in the Krafla area. J. Geophys., 47, 141-153.

Tryggvason, E. 1979. Jardskjalftar a Islandi 1950-1959 (Earthquakes in Iceland 1950-1959.) Science Institute, University of Iceland, Report RH-79-06, 90 pp.

Tryggvason, E. 1978a. Jardskjalftar a Islandi 1930-1939 (Earthquakes in Iceland 1930-1939.) Science Institute, University of Iceland, Report RH-78-21, 92 pp.

Tryggvason, E. 1978b. Jardskjalftar a Islandi 1940-1949 (Earthquakes in Iceland 1940-1949.) Science Institute, University of Iceland, Report RH-78-22, 51 pp.

Tryggvason, E. 1974. Vertical crustal movements in Iceland. In: Geodynamics of Iceland and the North Atlantic Area, ed.

L. Kristjansson, Reidel Pub. Co., Dordrecht, 241-262.

Tryggvason, E. 1973. Seismicity, earthquake swarms and plate boundaries in the Iceland region. Bull. Seismol. Soc. Am., 63, 1327-1348.

Tryggvason, E. 1968. Measurement of surface deformation in Iceland by precision levelling. J. Geophys. Res., 73, 7039-7050.

Tryggvason, E. 1964. Arrival times of P-waves and upper mantle structure. Bull. Seismol. Soc. Am., 54, 727-736.

Tryggvason, E. and Bath, M. 1961. Upper crustal structure of Iceland. J. Geophys. Res., 66, 1913-1925.

Tryggvason, K., Husebye, E.S. and Stefansson, R. 1984. Seismic image of the hypothesised Icelandic hotspot. Tectonophysics, 100, 97-119.

Vogt, P.R. 1983. The Iceland mantle plume: status of the hypothesis after a decade of new work. in: Structure and Development of the Greenland-Scotland Ridge, ed. M.H.P. Bott et al., Plenum Press, New York and London, 191-216.

Walker, G.P.L. 1974. The structure of eastern Iceland. in: Geodynamics of Iceland and the North Atlantic Area, ed. L. Kristjansson, D. Reidel Pub. Co., Dordrecht, 177-188.

Wallace, T. 1984. A re-examination of the moment tensor solutions of the 1980 Mammoth Lakes earthquakes. unpublished manuscript.

Walter, A.W. and Weaver, C.S. 1980. Seismicity of the Coso range, California. J. Geophys. Res., 85, 2441-2458.

Ward, P.L. and Bjornsson, S. 1971. Microearthquakes, swarms and the geothermal areas of Iceland. J. Geophys. Res., 76, 3953-3982.

Ward, P.L., Palmason, G. and Drake, C.C. 1969. Microearthquakes and the mid-Atlantic Ridge in Iceland. J. Geophys. Res., 74, 665-684.

Wyss, M. 1979. Estimating maximum expectable magnitude of earthquakes from fault dimensions. Geology, 7, 336-340.

Wyss, M. 1973. Towards a physical understanding of the earthquake frequency distribution. Geophys. J. R. astr. Soc., 31, 341-359.

Wyss, M. and Lee, W.H.K. 1973. Time variations of the average earthquake magnitude in central California. In: R.L. Kovach and A. Nur ed., Proceedings of the Conference on Tectonic Problems on the San Andreas Fault system. Stanford Univ. Publ. Geol. Sci., 13, 24-42.

Wyss, M. and Brune, J.N. 1968. Seismic moment, stress and source dimensions for earthquakes in the California-Nevada region. J. Geophys. Res., 73, 4681-4694.

Xi-Xiang, Z. 1980. Interpretation of subsurface temperature measurements in the Mosfellssveit and Olfusdalur geothermal areas, SW-Iceland. UNU geothermal training programme, Iceland. Report 1980-7.

Yegulalp, T.M. and Kuo, J.T. 1974. Statistical prediction of the occurrence of maximum magnitude earthquakes. Bull. Seismol. Soc. Am., 64, 393-414.

Zverev, S.M., Litvinenko, I.V., Palmason, G., Yaroshevskaya, G.A., Osokin, N.N. and Akhmetjev, M.A. 1980a. A seismic study of the rift zone in Northern Iceland. J. Geophys., 47, 191-201.

Zverev, S.M., Litvinenko, I.V., Palmason, G., Yaroshevskaya, G.A. and Osokin, N.N. 1980b. A seismic crustal study of the axial rift zone in southwest Iceland. J. Geophys., 47, 202-210.

APPENDIX 1

THE 1981 RADIO TELEMETRY PROJECT - FIELD LOGISTICS

Out stations

In all cases the out station equipment was checked before setting off into the field.

A hole up to 1 m deep and 1/2 m diameter was dug at each site, with bedrock base. This was lined with a 20 l paint drum with 1/2 of its base cut out. The drums used were made of steel, which was undesirable since metal objects can affect the functioning of the seismometer. Unfortunately this fact did not come to our notice until after all the out stations had been set up. The seismometer was placed on the bedrock, and adjusted to the vertical. Where necessary the bedrock was levelled with a hammer and chisel. The amplifier-modulator was stood in the paint drum on the half-base. The drum was sealed with its lid, and covered with a sheet of polythene.

A 2 m length of metal water pipe was used as a mast and was held upright by 3 steel wire guys. These were attached to the top of the mast by means of metal hooks, and to the ground to boulders or rock outcrops. The guy wires were fixed with cable clamps, and tightened with cable tensioners. In order to prevent the mast from rotating in the wind, a 30 cm length of angle iron was screwed to its base by an exhaust pipe clip, and boulders piled onto this "foot".

The transmitting aerial was then clamped to the top of the mast. The transmitter, which was about the same size as a beer can (but sometimes less functional) was placed in a plastic bag and taped to the mast just below the aerial with the plugs

pointing downwards. This was to prevent rain water leaking into the transmitter via the plug seals. The equipment was then connected up. The aerial was plugged into the transmitter, and the excess cable taped to the mast. The seismometer was plugged into the amplifier-modulator. The amplifier-modulator was then connected to the transmitter by running the cable along the ground to the base of the mast, up the inside of the mast, out of the top, and down to the transmitter. A branch cable connected a 12 volt lead acid battery to the transmitter. All cables on the ground were buried to camouflage them from sheep. Hence no visible cables were within chewing reach.

Batteries used were 60-70 amp hr lead acid batteries. A type with a carrying handle was used, which proved very useful when transporting them in the field. The batteries were placed in plastic bags and buried, to protect them from the weather and theft.

When all the equipment was installed, the test box was plugged into the amplifier-modulator and the gain adjusted. It was adjusted so that the low frequency background noise (1-2 sec. period) could be heard, but not high frequency wind and cultural noise. The gains were set variously at 4, 5, 6, 7 or 8. After recording commenced, however, it was found that the audio response of the test boxes was not the same as the response of the recording system as a whole. Several out stations had to be revisited and the gains increased by up to 3 settings (Table A1.1).

gain setting	no. of stations at beginning of recording	no. of stations at end of recording
4	2	-
5	2	-
6	5	3
7	13	20
8	1	

Table A1.1 Gain settings of amplifier-modulators

It was concluded from this experience that it would have been better to have set all the stations on gain 7 to start with, and to have adjusted them after the first paper playouts were examined.

Where time and circumstance allowed, the recording station was then visited, the receiving aerial and receiver set up, and the station tested for transmission integrity by plugging the test box into the receiver.

Recording stations

2 m high masts accommodated the receiving aerials at the recording stations. Up to 6 aerials were placed on each mast, which was probably a little too crowded. However, no problems with cross talk were encountered as a result of this practice. The receivers were taped to the mast. Cables connecting the receivers to the tape recorders were shielded from sheep teeth by passing them through a length of plastic water pipe. The

tape recorders were housed in waterproof aluminium boxes and stood on wooden frames to facilitate levelling. Cables passed into the boxes through a small hole cut in the underside. A seismometer was installed at each recording site, and connected directly to the tape recorder. Power was supplied by 12 volt lead acid batteries - a 60-70 amp hr battery for the seismometer, and a 110 amp hr battery for the tape recorder.

Installing the equipment

Accessibility was difficult in the area. Out of 23 sites, it was possible to drive up to 11 in the Land Rover, 9 sites were established and maintained by foot, and a pack horse was used for 3. For the recording sites it was imperative to select locations that could be driven right up to, because of the weight of the equipment and the great difficulty in making repairs and adjustments in the open.

When the radio transmitting stations were established by foot, the equipment necessary was transported in rucksacks, (a total weight of about 30 kg per station). The work of establishing the station fell naturally into two parts - placing and levelling the seismometer, and erecting the mast. Hence, it was found convenient to have two people. The addition of an extra person slowed the work and made it more difficult, and when there were four people it was impossible to get anything at all done.

Theim mun verr gefast heimskra manna rad
er fleiri koma saman.

A pack saddle and saddle bags were hired for use with the horse. It was possible to pack equipment for two stations at a time.

During recording, when station maintenance was largely a matter of changing batteries, two wooden boxes with hooks were made, into which the batteries fitted. These could either be hung onto a rucksack frame or onto the pack saddle. This solved the problem of the batteries slipping about inside the packs and spilling acid.

Operating the equipment

Whilst recording was in progress the work naturally divided itself into two parts :

a) changing out-station batteries. This represented about 30 hours work per week.

b) changing tapes and playing them back on the replay equipment. This also represented about 30 hours work per week.

Time spent on maintenance and administration varied greatly, but averaged of the order of 100 hours per week.

Batteries at out stations were changed at intervals of 20 to 40 days, and recording station batteries more frequently. It should be noted for future projects using this equipment that there was a possibility of adjusting the power consumption of the transmitters, so it would have been possible to have lower power transmitters for the close stations. The reported range of the transmitters is .200 kms. For the short distances involved in this project, signals were relatively so powerful that orientation of the transmitting and receiving aerials was almost irrelevant to reception. In one case vandals turned the

receiving mast (at Blakollur) through 90° but for none of the stations was reception affected. In one or two cases masts fell down, but the signal was never lost.

Explosions

Detonations were made in Olfus, Djaknapollur, Thingvallavatn, Graenavatn in Krisuvik and outside Reykjavik harbour. 25 kg of dynamite were used for the local explosions and 50 kg in Graenavatn. It was found on playing back that 50 kg was too little at such a distance, so 100 kg was used in Reykjavik harbour.

Monitoring of the data collected on tape

During the recording period, all tapes were played back at speed of 7 1/2" sec^{-1} (i.e. 80 x recording speed). Malfunctions could thus be detected as quickly as possible. It was found necessary to play back the whole tape since some malfunctions, e.g. transmitters drifting off frequency, occurred only part of the time, and these stations often sounded good when they were checked out at tape changes. By playing the whole tape back as soon as it was changed, it was possible to keep as up to date an overview of the functioning of the equipment as possible. At this speed it took about 1 hour to obtain a paper record of seven of the channels.

Malfunctions

Data loss is calculated as follows as percentage lost recording time during the period 12th July to 9th October.

It should be noted that tape recorder breakdowns were much

more damaging than radio link and other failures, since up to 10 stations were lost at a time in such cases.

	% data loss
tape recorder breakdowns	4.9
radio link breakdown and drifting	5.7
other	3.2
total	13.8

Total recording time = 90 x 3 = 270 tape days.
thus, the total data loss was equivalent to = 37.3 tape days

"Other" malfunctions included batteries running out, mechanical damage to tapes, amplifier - modulator failure, breakdown of insulation between receiving aerial and mast, vandalism, and cross talk.

No equipment was stolen or damaged. There were 3 instances of vandalism: a battery was disconnected, a receiving mast rotated through 90 ^{o} and a mast was collapsed.

Data loss was very severe when recording first started, so some of the worst tapes were wiped and reused at the end of the project.

Cost

The whole field project cost about $50,000. This figure includes all expenses associated with the 4 month field project, and one year's salary for one scientist.

APPENDIX 2

HYPOCENTER LOCATOR AND PLOT SYSTEM (HLPS)

HLPS is a user system that permits the input, processing and archiving of earthquake data to be done by the giving of simple mnemonic commands. It was necessary and desirable to design such a system for the following reasons :

(1) It enabled systemmatic processing to be performed safely by persons trained or untrained in computing after a very small amount of instruction.

(2) It speeded processing up.

(3) Improvements in computing facilities and utilities could be exploited as these became available simply by incorporating them into the system, thus avoiding the need to retrain users.

HLPS presently contains 20 VAX/VMS command files, each of which performs a particular data processing function by means of passing commands to the system and running Fortran programmes that are stored on a common directory :

INPUT and INPUTH facilitate the input and formatting of arrival time data. LOCATE runs the hypocentre locator programme HYPOINVERSE and prints and stores output data. ADJUST permits the selection of unsatisfactory events for location and their deletion from the archive data files. DELETE permits the deletion of events from the final archive data files. COMPRESS deletes unused disc space. LIST accesses the data files and produces listings according to specification. RANGE displays the range of events on disc. MICROMAG and MACROMAG facilitate

the addition of magnitude data to the archive files. NEWTAPE initialises new archive tapes. SAVE copies archive data from computer disc to tape, and RESTORE performs the inverse process. EMAP (earthmap), DMAP (depthmap) and TMAP (timemap) are epicentre/hypocentre plotting utilities. BVALUE calculates and plots single and running b-values. TTGEN generates traveltime tables for use with HYPOINVERSE. GETMAR selects events from archive on the basis of marsden numbers. MAGSCALE calculates least squares straight lines for magnitude data.

HLPS is availible in PDP/RT-11 (Foulger and Olafsson, 1980a, b) and VAX/VMS from the Geophysics Division, University of Iceland.

APPENDIX 3

SEISMOMETER STATION LOCATIONS

A list of station locations is presented in Tables A3.1 and A3.2. Stations with two letter code names are (or were) of the drum recorder type, and part of the Icelandic regional network, with the exception of HK (Krokur), see Section 3.2.4. Stations with 3 letter code names were stations of the radio telemetered network deployed in 1981.

I	NAME	---LAT----	----LON----	PDLY1	SDLY1	HT
1	KL	63. 55.52	22. 0.01	0.00	0.00	175
2	MV	64. 1.23	22. 13.76	0.00	0.00	
3	FJ	64. 2.77	20. 34.57	0.00	0.00	
4	DJ	64. 5.98	20. 47.69	0.00	0.00	
5	KI	64. 0.26	20. 46.89	0.00	0.00	
6	BJ	64. 3.95	20. 56.50	0.00	0.00	
7	LS	64. 7.46	20. 20.30	0.00	0.00	
8	RK	64. 8.30	21. 54.30	0.00	0.00	51
9	RN	63. 50.39	22. 39.17	0.00	0.00	30
10	MV	64. 1.23	22. 13.76	0.00	0.00	19
11	RH	64. 8.40	21. 37.40	0.00	0.00	10
12	GU	64. 3.24	22. 37.31	-0.20	-0.36	
13	HS	66. 6.70	20. 7.30	0.25	0.44	20
14	AK	65. 41.20	18. 6.40	-0.05	-0.09	24
15	TN	63. 51.92	22. 26.62	0.00	0.00	
16	VA	64. 1.09	21. 50.35	0.00	0.00	137
17	IR	64. 2.51	21. 22.54	0.00	0.00	300
18	SL	63. 56.63	21. 0.09	0.00	0.00	000
19	RE	64. 7.61	21. 54.70	0.00	0.00	
20	LV	64. 12.93	20. 45.18	0.00	0.00	100
21	AR	63. 47.58	20. 6.90	0.10	0.18	090
22	SE	63. 32.94	19. 36.56	0.00	0.00	180
23	SK	63. 27.21	19. 5.88	0.60	1.07	050
24	SM	64. 48.60	21. 22.80	0.00	0.00	070
25	HV	64. 52.10	19. 34.10	0.10	0.18	640
26	LA	64. 10.90	19. 13.40	0.00	0.00	430
27	SF	63. 30.00	19. 50.00	0.00	0.00	120
28	SH	63. 23.85	20. 17.60	0.00	0.00	120
29	BV	64. 5.87	19. 9.48	0.00	0.00	560
30	VF	64. 12.07	18. 59.02	0.00	0.00	620
31	SB	63. 43.25	18. 37.30	0.46	0.82	200
32	KK	63. 47.10	18. 3.50	0.00	0.00	026
33	KV	63. 58.68	16. 36.30	0.00	0.00	030
34	SA	64. 3.09	20. 25.04	0.00	0.00	
35	SG	64. 10.76	19. 7.19	0.00	0.00	580
36	HL	64. 0.44	20. 9.60	0.00	0.00	100
37	ST	64. 12.63	21. 29.10	-0.12	-0.21	210
38	HG	64. 1.03	21. 11.31	0.00	0.00	80
39	HN	64. 6.93	21. 15.44	0.00	0.00	180
40	HH	64. 2.08	21. 3.46	0.00	0.00	100
41	HB	63. 56.59	21. 19.16	0.00	0.00	40
42	HK	64. 5.94	21. 7.01	0.00	0.00	120

Table A3.1 Station locations. NAME=name of station, LAT=latitude, LON=longitude, PDLY1=P-wave station delay, SDLY1=S-wave station delay, WT=station weight, HT=station height above s.l.

	NAME	LAT.	LON.	PDLY1	SDLY1	HT
43	HF	63. 30.05	19. 44.20	0.00	0.00	110
44	HE	64. 0.34	19. 40.90	0.00	0.00	940
45	HI	64. 23.90	19. 20.70	0.00	0.00	060
46	BSL	64. 3.03	21. 22.12	0.00	0.00	320
47	BHU	64. 3.69	21. 24.96	0.00	0.00	260
48	BBL	64. 2.26	21. 29.01	0.00	0.00	310
49	BVA	64. 4.62	21. 28.19	0.00	0.00	230
50	BLA	64. 0.36	21. 21.61	0.00	0.00	410
51	BEN	64. 4.80	21. 25.68	0.00	0.00	260
52	BNO	64. 6.78	21. 21.17	0.00	0.00	320
53	KST	63. 56.33	21. 9.19	0.00	0.00	5
54	KDN	64. 0.15	21. 6.34	0.00	0.00	185
55	KKL	64. 2.81	21. 10.17	0.00	0.00	280
56	KDL	64. 1.72	21. 13.30	0.00	0.00	200
57	KDA	64. 2.65	21. 12.54	0.00	0.00	350
58	KMI	64. 2.97	21. 19.19	0.00	0.00	460
59	KHE	64. 2.34	21. 16.59	0.00	0.00	370
60	KHA	63. 58.22	21. 15.86	0.00	0.00	150
61	KKA	63. 59.90	21. 15.17	0.00	0.00	310
62	KSA	64. 1.85	21. 9.68	0.00	0.00	390
63	LBO	64. 8.12	21. 15.32	0.00	0.00	250
64	LDY	64. 6.48	21. 16.39	0.00	0.00	380
65	LLA	64. 8.52	21. 6.34	0.00	0.00	130
66	LGR	64. 4.93	21. 5.36	0.00	0.00	240
67	LDJ	64. 5.28	21. 9.94	0.00	0.00	230
68	LKA	64. 4.48	21. 11.08	0.00	0.00	360

Table A3.2 Station locations. Column headings as for Table Table A3.1

APPENDIX 4

THE HENGILL - SOUTH ICELAND CRUSTAL MODEL

The crustal model parameters are given in Table A4.1. The depth column gives the depth to the top of each layer, and the velocity column gives the velocity at the top of that layer. The velocity within each layer increases linearly to that given for the top of the layer beneath. Layer 5 is a constant velocity halfspace.

LAYER	VEL	DEPTH
1	3.000	0.000
2	3.300	0.400
3	4.500	1.200
4	5.800	2.500
5	7.000	10.600

Table A4.1 Hengill - South Iceland crustal model parameters.

This crustal model was derived by making a composite travel time plot of all first arrivals for explosion profiles 35 - 42 and L3, shot by Palmason (Palmason, 1971). These profiles cover the Hengill area and South Iceland. The program TTGEN (Klein, 1978) was then used to model this data to find a crustal structure that fitted the observational data (Fig. A4.1). A halfspace velocity of 7.0 km sec^{-1} was used, based on the results of Angenheister et al. (1980).

A diagram of the velocity-depth profile for this crustal model is presented in Fig. A4.2.

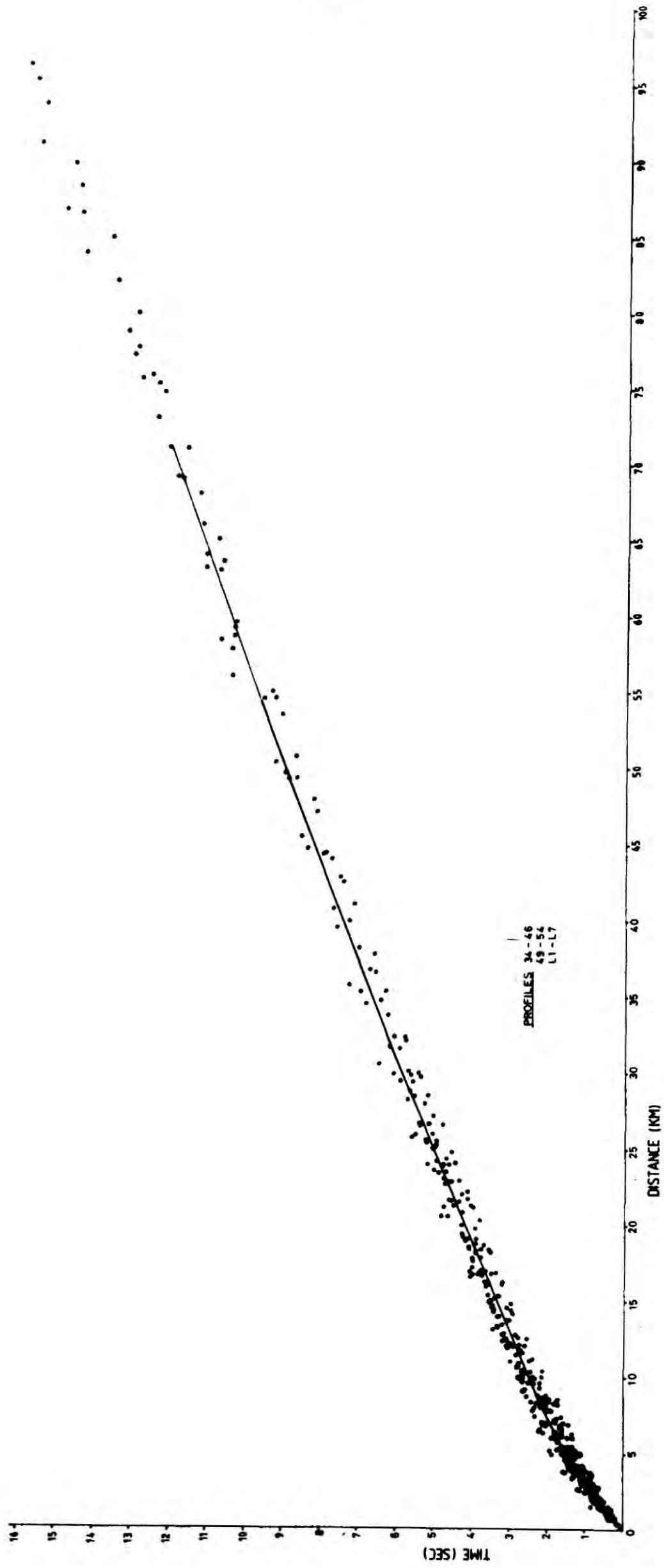

Fig. A4.1 Composite travel time plot of all first arrivals for explosion profiles 35 - 42 and L3 shot by Palmason (1971) (black dots). Line is a travel time plot for the Hengill-South Iceland crustal model.

Lateral variations in the crustal structure within the area and their effect on the hypocentral locations

Examination of explosion data taken from Palmason (1971) indicated variations in the velocity structure within the Hengill area. Profile 42 was taken as indicative of the velocity structure N of 64°N. Profiles L3, L4 and L5 were taken as representitive of the area S of 64°N. Profiles L3, L4 and L5 consistently indicated lower velocities than profile 42. The indication of these data is hence that the velocities S of 64°N may be lower than those of the Hengill-South Iceland crustal model, and those N of 64°N higher.

The explosion data described in Section 7.2 and listed in Tables A4.2 - A4.6 indicate an area of relatively high velocities to the N of Hveragerdi, surrounded by areas that exhibit relatively low velocities. These results are hence consistent with those of Palmason (1971).

Variations such as these, that may be up to 5% in magnitude are unlikely to have a large affect on the epicentral determinations where station coverage is good. However the calculated hypocentral depth of an event is heavily dependent on the arrival times measured at close stations. Hence velocity variations in the immediate vicinity of the event may not be cancelled out and significantly distort the focal depth. Underestimation of the velocity in the hypocentral volume will result in the calculation of erroneously small hypocentral depths. Conversely, if the real velocities are lower than those defined in the crustal model, hypocentral depths calculated will be too deep. In the case of the Hengill area the local velocity variations described above have the effect that hypocentres in

the central cluster are artificially shallowed and those in the surrounding areas, including the fissure swarm and Olfus are artificially deepened by up to 5%.

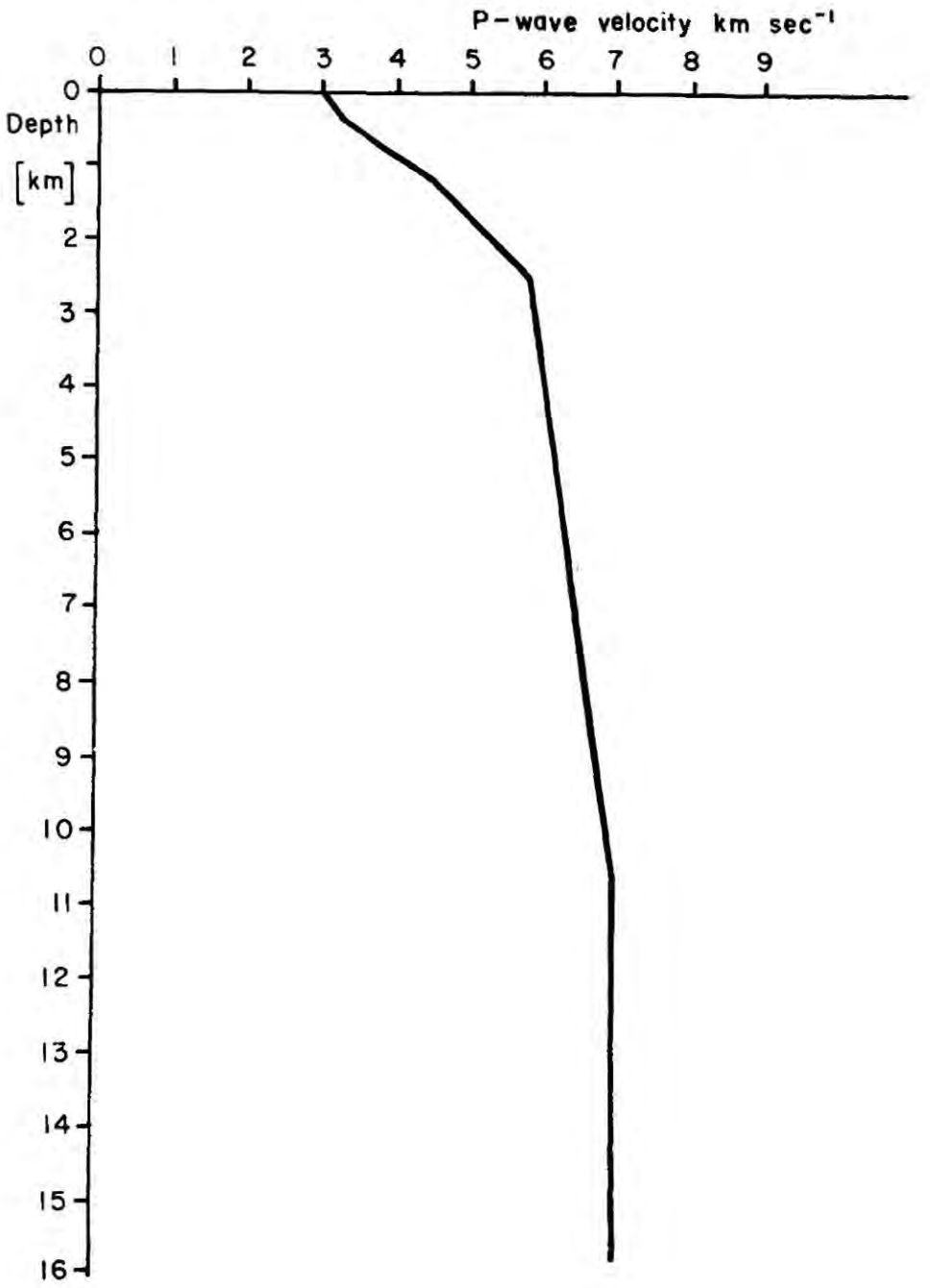

Fig. A4.2 Velocity-depth profile for the Hengill-South Iceland crustal model.

YR	MO	DA	ORIGIN	LAT N	LON W	DEPTH	RMS	ERH	ERZ	GAP
31-	8	12	1621 16.27	63 56.27	21 9.50	0.01	0.09	0.82	31.61	206

STA	DIST	AZM	AN	P/S	W	SEC	+CCOR	(TOBS	-TCAL	-DLY	=RES)	WT
KST	0.3	69	97	P		16.33	0.00	0.06	0.08	0.00	-0.02	1.00
KST	0.3	69	97	P		16.33	0.00	0.06	0.08	0.00	-0.02	1.00
KHA	6.3	305	39	P		18.04	0.00	1.77	1.77	0.00	0.00	1.00
HB	7.1	275	37	P		18.20	0.00	1.93	1.93	0.00	0.00	1.00
KDN	7.6	19	35	P		18.17	0.00	1.90	2.03	0.00	-0.13	1.00
KKA	8.2	326	34	P		18.44	0.00	2.17	2.13	0.00	0.04	1.00
HG	8.9	351	32	P		18.50	0.00	2.23	2.28	0.00	-0.05	1.00
KSA	10.3	0	31	P		18.88	0.00	2.61	2.51	0.00	0.10	1.00
HH	11.9	24	30	P		19.00	0.00	2.73	2.78	0.00	-0.05	1.00
KDA	12.1	349	30	P		19.03	0.00	2.76	2.81	0.00	-0.05	1.00
KKL	12.1	358	30	P		19.17	0.00	2.90	2.82	0.00	0.08	1.00
BLA	12.4	308	30	P		19.37	0.00	3.10	2.87	0.00	0.23	1.00
KHE	12.7	333	30	P		19.21	0.00	2.94	2.91	0.00	0.03	1.00
IR	15.7	318	30	P		19.90	0.00	3.63	3.43	0.00	0.20	1.00
BSL	16.2	321	30	P		19.83	0.00	3.56	3.52	0.00	0.04	1.00
LGR	16.3	10	30	P		19.97	0.00	3.70	3.54	0.00	0.16	1.00
LDJ	16.6	359	30	P		19.83	0.00	3.56	3.60	0.00	-0.04	1.00
BHU	18.6	318	30	P		20.19	0.00	3.92	3.92	0.00	0.00	1.00
BEN	19.6	324	30	P		20.35	0.00	4.08	4.09	0.00	-0.01	1.00
LDY	19.9	343	30	P		20.39	0.00	4.12	4.15	0.00	-0.03	1.00
BMO	21.6	335	30	P		20.68	0.00	4.41	4.45	0.00	-0.04	1.00
BVA	21.7	316	30	P		20.67	0.00	4.40	4.46	0.00	-0.06	1.00
LLA	22.8	6	30	P		20.84	0.00	4.57	4.65	0.00	-0.08	1.00
SL	35.5	48	29	P		18.00	0.00	1.73	6.76	0.00	-5.03	0.00

Table A4.2 Observed and calculated travel times for Olfus explosion. (YR, MO, DA, ORIGIN)=date and time of explosion, (LAT N, LON W, DEPTH)=co-ordinates and depth of explosion, (STA, DIST, AZM, AN)=station, distance from shot, azimuth and emergence angle, SEC=arrival time, TOBS=observed travel time, TCAL=calculated travel time, DLY=station delay, RES=travel time residual, WT=station weight.

YR	MO	DA	ORIGIN	LAT N	LON W	DEPTH	RMS	ERH	ERZ	GAP
81-	8-	13	1645 15.80	64 5.17	21 10.10	0.01	0.09	0.23	31.61	63

STA	DIST	AZM	AN	P/S	W	SEC+CCOR	(TOBS	-TCAL	-DLY	=RES)	WT
LDJ	0.2	37	96	P		15.92 0.00	0.12	0.06	0.00	0.06	1.00
LKA	1.5	213	79	P		16.41 0.00	0.61	0.49	0.00	0.12	1.00
LGR	3.5	97	57	P		16.86 0.00	1.06	1.10	0.00	-0.04	1.00
KKL	4.4	181	45	P		16.93 0.00	1.13	1.35	0.00	-0.22	1.00
KDA	5.1	203	42	P		17.26 0.00	1.46	1.51	0.00	-0.05	1.00
HN	5.4	307	41	P		17.40 0.00	1.60	1.57	0.00	0.03	1.00
KSA	6.2	176	39	P		17.51 0.00	1.71	1.74	0.00	-0.03	1.00
LLA	6.8	26	37	P		17.76 0.00	1.96	1.88	0.00	0.08	1.00
LBO	6.9	323	37	P		17.87 0.00	2.07	1.89	0.00	0.18	1.00
KDL	7.0	202	37	P		17.65 0.00	1.85	1.90	0.00	-0.05	1.00
KHE	7.5	226	36	P		17.77 0.00	1.97	2.00	0.00	-0.03	1.00
HG	7.8	138	35	P		17.80 0.00	2.00	2.06	0.00	-0.06	1.00
HH	7.8	136	35	P		17.90 0.00	2.10	2.08	0.00	0.02	1.00
KMI	8.4	241	33	P		18.03 0.00	2.23	2.19	0.00	0.04	1.00
BMO	9.4	289	31	P		18.35 0.00	2.55	2.37	0.00	0.18	1.00
KDN	9.8	161	31	P		18.20 0.00	2.40	2.42	0.00	-0.02	1.00
BSL	10.6	243	30	P		18.38 0.00	2.58	2.55	0.00	0.03	1.00
KKA	10.7	203	30	P		18.32 0.00	2.52	2.57	0.00	-0.05	1.00
BEN	11.0	267	30	P		18.48 0.00	2.68	2.63	0.00	0.05	1.00
IR	11.3	244	30	P		18.50 0.00	2.70	2.67	0.00	0.03	1.00
BHU	12.3	257	30	P		18.57 0.00	2.77	2.84	0.00	-0.07	1.00
BLA	12.9	227	30	P		18.79 0.00	2.99	2.96	0.00	0.03	1.00
KHA	13.8	200	30	P		18.84 0.00	3.04	3.10	0.00	-0.06	1.00
BVA	14.7	267	30	P		19.09 0.00	3.29	3.26	0.00	0.03	1.00
BBL	16.1	251	30	P		19.38 0.00	3.58	3.50	0.00	0.08	1.00
SL	23.0	75	29	P		19.50 0.00	3.70	5.52	0.00	-1.82	0.00
VA	33.5	257	29	P		22.00 0.00	6.20	6.43	0.00	-0.23	1.00

Table A4.3 Observed and calculated travel times for Djaknapollur explosion. Column abbreviations as for Table A4.2.

YR	MO	DA	ORIGIN	LAT N	LON W	DEPTH	RMS	ERH	ERZ	GAP
81-	8-	13	21 1 15.49	64 9.07	21 11.40	0.01	0.07	0.46	31.61	186

STA	DIST	AZM	AN	P/S	W	SEC+CCOR	(TOBS	-TCAL	-DLY	=RES)	WT
LBO	3.7	241	54	P		16.70	0.00	1.21	1.16	0.00	0.05	1.00
LLA	4.2	104	48	P		16.83	0.00	1.34	1.30	0.00	0.04	1.00
HN	5.2	220	42	P		16.90	0.00	1.41	1.52	0.00	-0.11	1.00
LDJ	7.2	170	36	P		17.51	0.00	2.02	1.94	0.00	0.08	1.00
LGR	8.9	149	32	P		17.84	0.00	2.35	2.27	0.00	0.08	1.00
BMO	9.0	242	32	P		17.89	0.00	2.40	2.29	0.00	0.11	1.00
KKL	11.7	175	30	P		18.17	0.00	2.68	2.74	0.00	-0.06	1.00
KDA	11.9	135	30	P		18.30	0.00	2.81	2.79	0.00	0.02	1.00
BEN	12.7	232	30	P		18.43	0.00	2.94	2.92	0.00	0.02	1.00
KMI	12.9	210	30	P		18.51	0.00	3.02	2.96	0.00	0.06	1.00
KHE	13.2	199	30	P		18.48	0.00	2.99	3.00	0.00	-0.01	1.00
KSA	13.4	174	30	P		18.57	0.00	3.08	3.05	0.00	0.03	1.00
KDL	13.8	137	30	P		18.57	0.00	3.08	3.10	0.00	-0.02	1.00
BSL	14.2	218	30	P		18.69	0.00	3.20	3.18	0.00	0.02	1.00
HH	14.4	153	30	P		18.70	0.00	3.21	3.22	0.00	-0.01	1.00
BHU	14.3	223	30	P		18.69	0.00	3.20	3.28	0.00	-0.08	1.00
HG	14.9	179	30	P		18.70	0.00	3.21	3.30	0.00	-0.09	1.00
IR	15.2	217	30	P		18.90	0.00	3.41	3.34	0.00	0.07	1.00
BVA	15.9	239	30	P		19.03	0.00	3.54	3.47	0.00	0.07	1.00
KDN	17.1	166	30	P		19.11	0.00	3.62	3.67	0.00	-0.05	1.00
KKA	17.3	191	30	P		19.14	0.00	3.65	3.71	0.00	-0.06	1.00
BLA	18.1	208	30	P		19.33	0.00	3.84	3.85	0.00	-0.01	1.00
BBL	18.9	229	30	P		19.51	0.00	4.02	3.98	0.00	0.04	1.00
KHA	20.5	191	30	P		19.65	0.00	4.16	4.25	0.00	-0.09	1.00
LV	22.3	71	30	P		20.00	0.00	4.51	4.56	0.00	-0.05	1.00
VA	34.9	245	20	P		22.00	0.00	6.51	6.65	0.00	-0.14	1.00

Table A4.4 Observed and calculated travel times for Thingvallavatn explosion. Column abbreviations as for Table A4.2.

YR	MO	DA	ORIGIN	LAT N	LON W	DEPTH	RMS	ERH	ERZ	GAP
81-	8-	12	1915 16.52	63 53.05	22 3.40	0.01	0.26	15.45	31.61	316

STA	DIST	AZM	AN	P/S	W	SEC+CCOR	(TOBS	-TCAL	-DLY	=RES)	WT
VA	13.3	35	30	P		20.50 0.00	3.98	3.88	0.00	0.10	1.00
BBL	32.9	58	29	P		22.91 0.00	6.39	6.33	0.00	0.06	1.00
BVA	35.8	53	29	P		23.01 0.00	6.49	6.80	0.00	-0.31	1.00
BLA	36.6	68	28	P		23.33 0.00	6.81	6.93	0.00	-0.12	1.00
BHU	37.0	57	28	P		23.21 0.00	6.69	7.00	0.00	-0.31	1.00
HB	37.5	79	28	P		23.40 0.00	6.88	7.07	0.00	-0.19	1.00
IR	37.5	62	28	P		23.60 0.00	7.08	7.09	0.00	-0.01	1.00
BSL	38.3	61	28	P		23.51 0.00	6.99	7.21	0.00	-0.22	1.00
BEN	39.0	56	28	P		23.53 0.00	7.01	7.31	0.00	-0.30	1.00
KHA	39.9	76	28	P		23.77 0.00	7.25	7.45	0.00	-0.20	1.00
KMI	40.4	62	28	P		23.96 0.00	7.44	7.53	0.00	-0.09	1.00
KKA	41.3	72	28	P		23.98 0.00	7.46	7.67	0.00	-0.21	1.00
KHE	41.8	65	28	P		24.04 0.00	7.52	7.76	0.00	-0.24	1.00
BMO	42.7	53	28	P		24.11 0.00	7.59	7.90	0.00	-0.31	1.00
HG	44.9	70	27	P		24.40 0.00	7.88	8.24	0.00	-0.36	1.00
KDA	45.0	66	27	P		24.34 0.00	7.82	8.27	0.00	-0.45	0.92
LDY	45.3	56	27	P		24.48 0.00	7.96	8.30	0.00	-0.34	1.00
KKL	46.9	67	27	P		24.77 0.00	8.25	8.55	0.00	-0.30	1.00
LDJ	49.0	62	26	P		25.01 0.00	8.49	8.87	0.00	-0.38	1.00
LLA	54.5	58	26	P		25.90 0.00	9.38	9.68	0.00	-0.30	1.00

Table A4.5 Observed and calculated travel times for Graenavatn explosion. Column abbreviations as for Table A4.2.

YR	MO	DA	ORIGIN	LAT N	LON W	DEPTH	RMS	ERH	ERZ	GAP
81-	9-	18	1713 55.20	64 11.07	21 51.12	0.02	0.98	21.91	31.61	277

STA	DIST	AZM	AN	P/S	W	SEC+CCOR	(TOBS	-TCAL	-DLY	=RES)	WT
RK	5.8	207	40	P		57.80	0.00	2.60	1.65	0.00	0.95	1.13
				S	2	59.90	0.00	4.70	2.94	0.00	1.76	0.48
VA	18.5	178	31	P		60.20	0.00	5.00	3.91	0.00	1.09	1.13
BVA	22.1	122	31	P	4	0.00	0.00	-55.20	4.52	0.00	-59.72	0.00
BBL	24.3	132	30	P	4	0.00	0.00	-55.20	4.90	0.00	-60.10	0.00
BEN	25.1	117	30	P	4	0.00	0.00	-55.20	5.03	0.00	-60.23	0.00
BHU	25.3	122	30	P	4	0.00	0.00	-55.20	5.06	0.00	-60.26	0.00
BMO	25.5	108	30	P	4	0.00	0.00	-55.20	5.10	0.00	-60.30	0.00
BSL	27.8	122	29	P	4	0.00	0.00	-55.20	5.48	0.00	-60.68	0.00
IR	28.1	124	30	P		61.60	0.00	6.40	5.52	0.00	0.88	1.13
LDY	29.0	107	30	P	4	0.00	0.00	-55.20	5.67	0.00	-60.87	0.00
LBO	29.5	100	30	P	4	0.00	0.00	-55.20	5.76	0.00	-60.96	0.00
KMI	29.9	120	30	P	4	0.00	0.00	-55.20	5.83	0.00	-61.03	0.00
BLA	31.1	129	29	P	4	0.00	0.00	-55.20	6.03	0.00	-61.23	0.00
KHE	32.3	120	29	P	4	0.00	0.00	-55.20	6.23	0.00	-61.43	0.00
LKA	34.6	110	29	P	4	0.00	0.00	-55.20	6.61	0.00	-61.81	0.00
KDA	34.9	116	29	P	4	0.00	0.00	-55.20	6.66	0.00	-61.86	0.00
LDJ	35.0	107	29	P	4	0.00	0.00	-55.20	6.67	0.00	-61.87	0.00
KDL	35.2	119	29	P	4	0.00	0.00	-55.20	6.70	0.00	-61.90	0.00
KKA	35.8	125	29	P	4	0.00	0.00	-55.20	6.79	0.00	-61.99	0.00
LLA	36.5	97	29	P	4	0.00	0.00	-55.20	6.91	0.00	-62.11	0.00
KKL	36.5	114	29	P	4	0.00	0.00	-55.20	6.91	0.00	-62.11	0.00
KHA	37.2	129	28	P	4	0.00	0.00	-55.20	7.03	0.00	-62.23	0.00
KSA	37.7	117	28	P	4	0.00	0.00	-55.20	7.10	0.00	-62.30	0.00
HB	37.9	135	28	P		63.10	0.00	7.90	7.13	0.00	0.77	1.13
LGR	38.4	107	28	P	4	0.00	0.00	-55.20	7.21	0.00	-62.41	0.00
KDN	41.5	119	28	P	4	0.00	0.00	-55.20	7.71	0.00	-62.91	0.00
KST	43.6	128	28	P	4	0.00	0.00	-55.20	8.04	0.00	-63.24	0.00

Table A4.6 Observed and calculated travel times for Reykjavik explosion. Column abbreviations as for Table A4.2.

APPENDIX 5

SEISMICITY CHARTS FOR THE PERIOD 1980-1983, TAKEN FROM THE REGIONAL STATION REY AND THE LOCAL STATION IR.

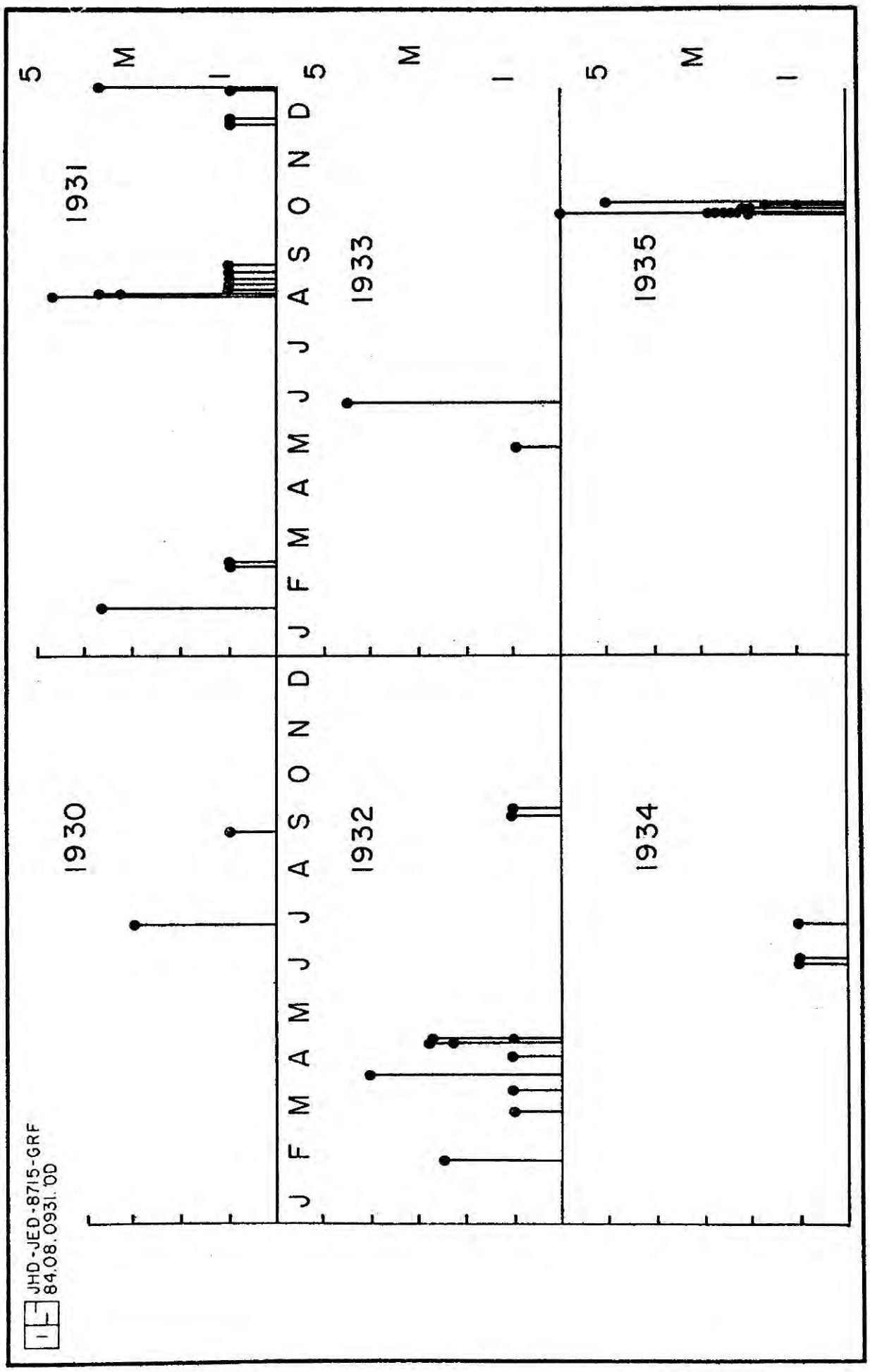

Fig. A5.1 1930 - 1935

Figs. A5.1 - A5.9 Seismicity charts based on the station REY. Events reported as felt but not recorded are indicated as magnitude 1 events.

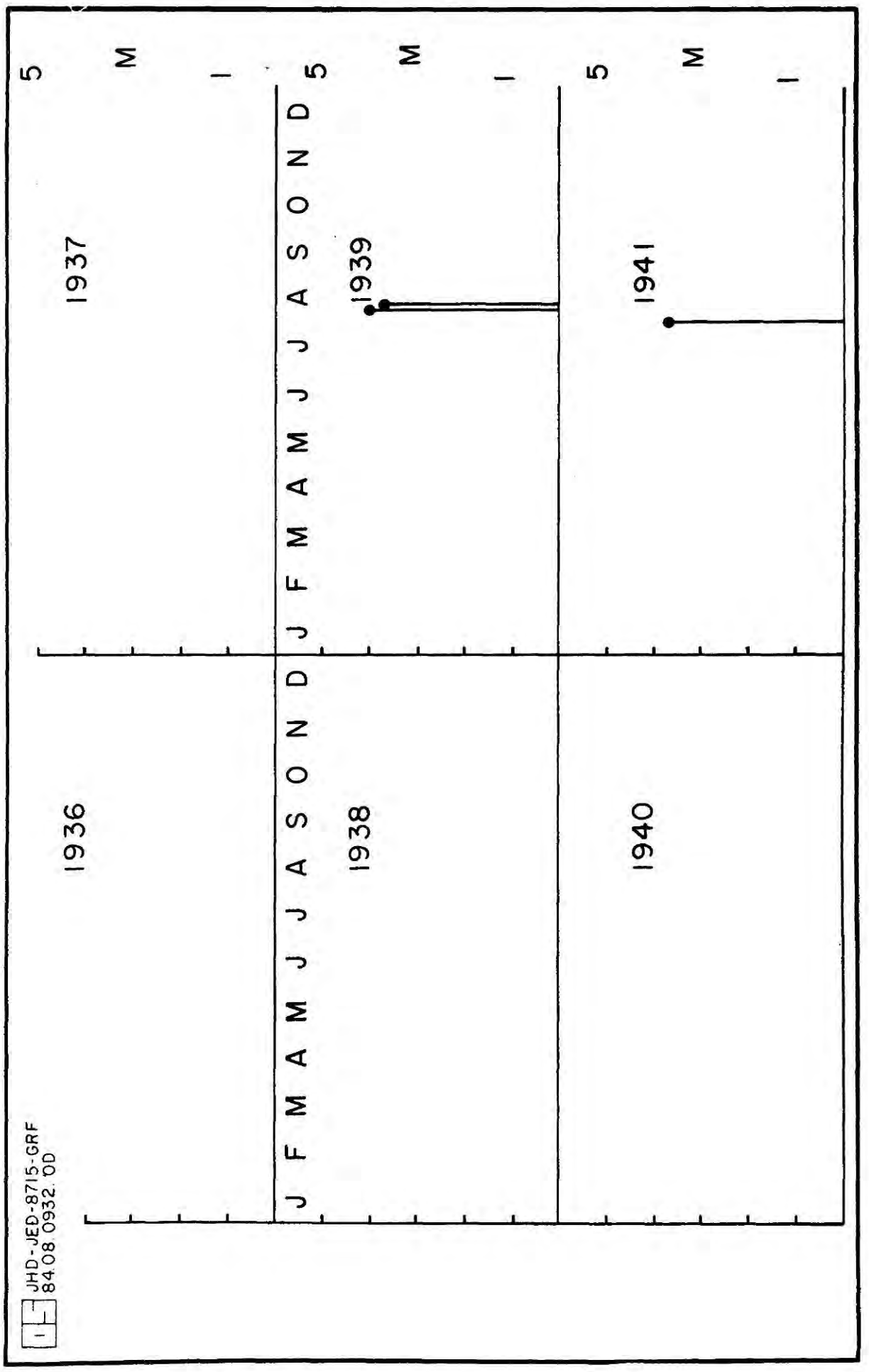

Fig. A5.2 1936 - 1941

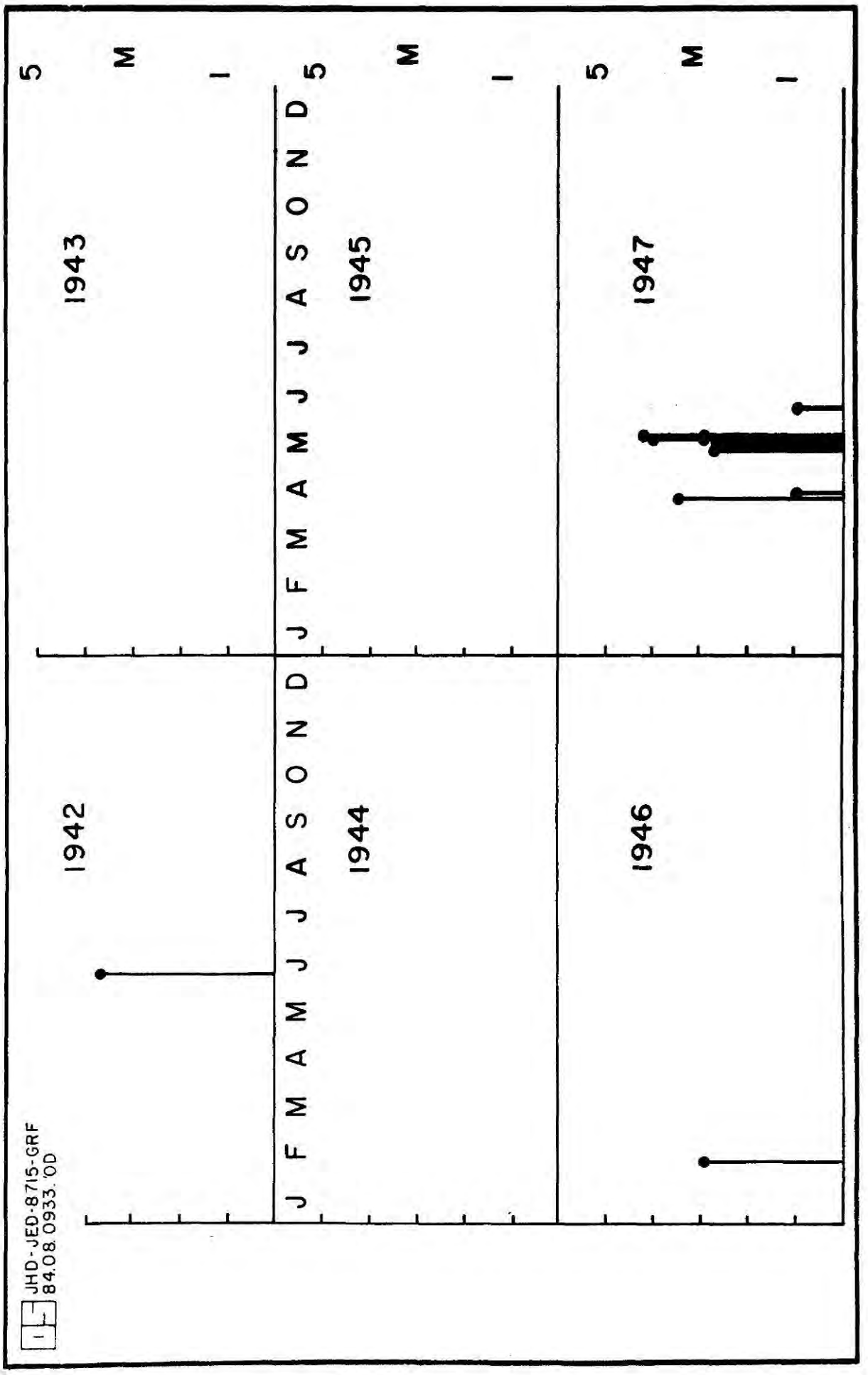

Fig. A5.3 1942 - 1947

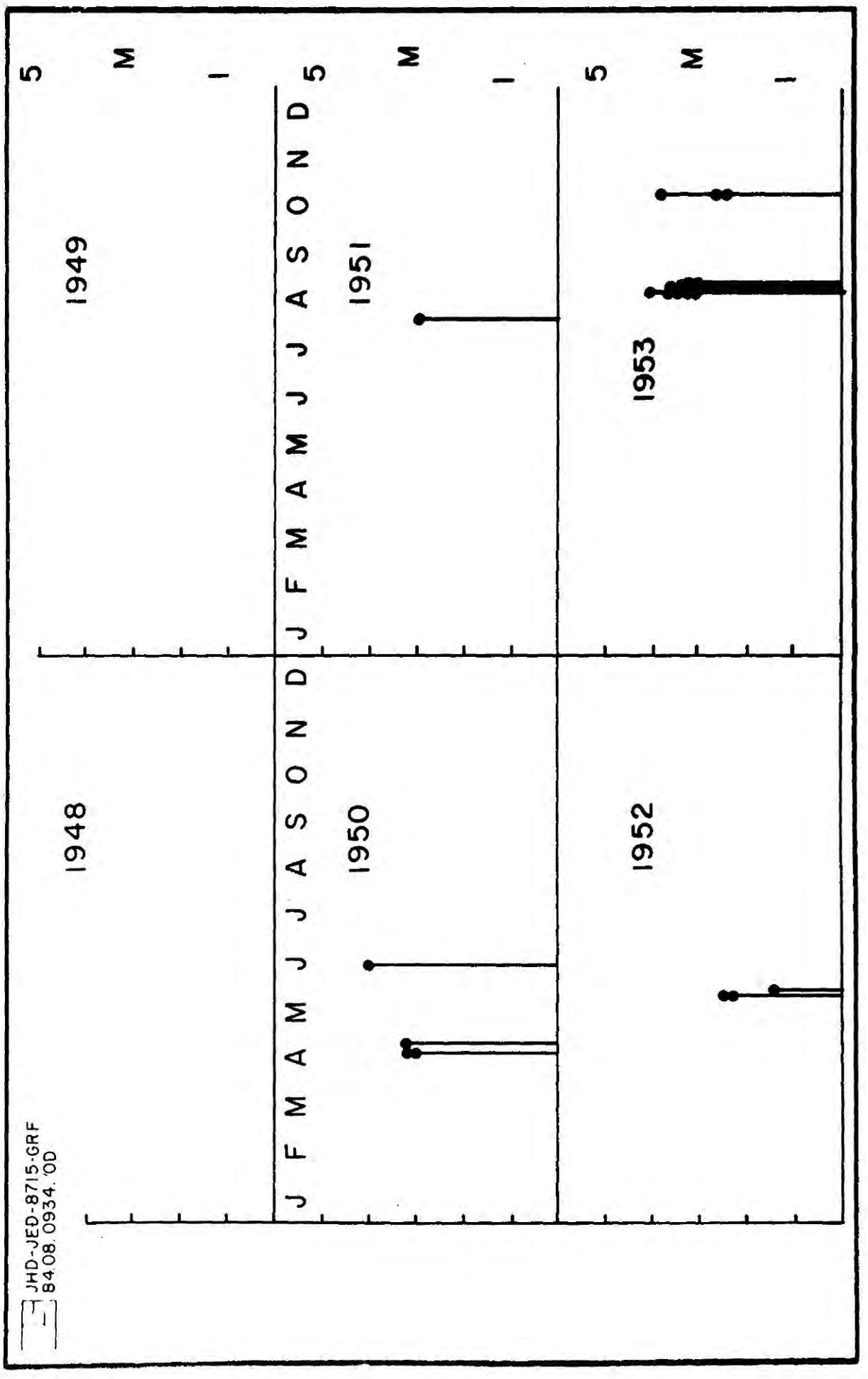

Fig. A5.4 1948 - 1953

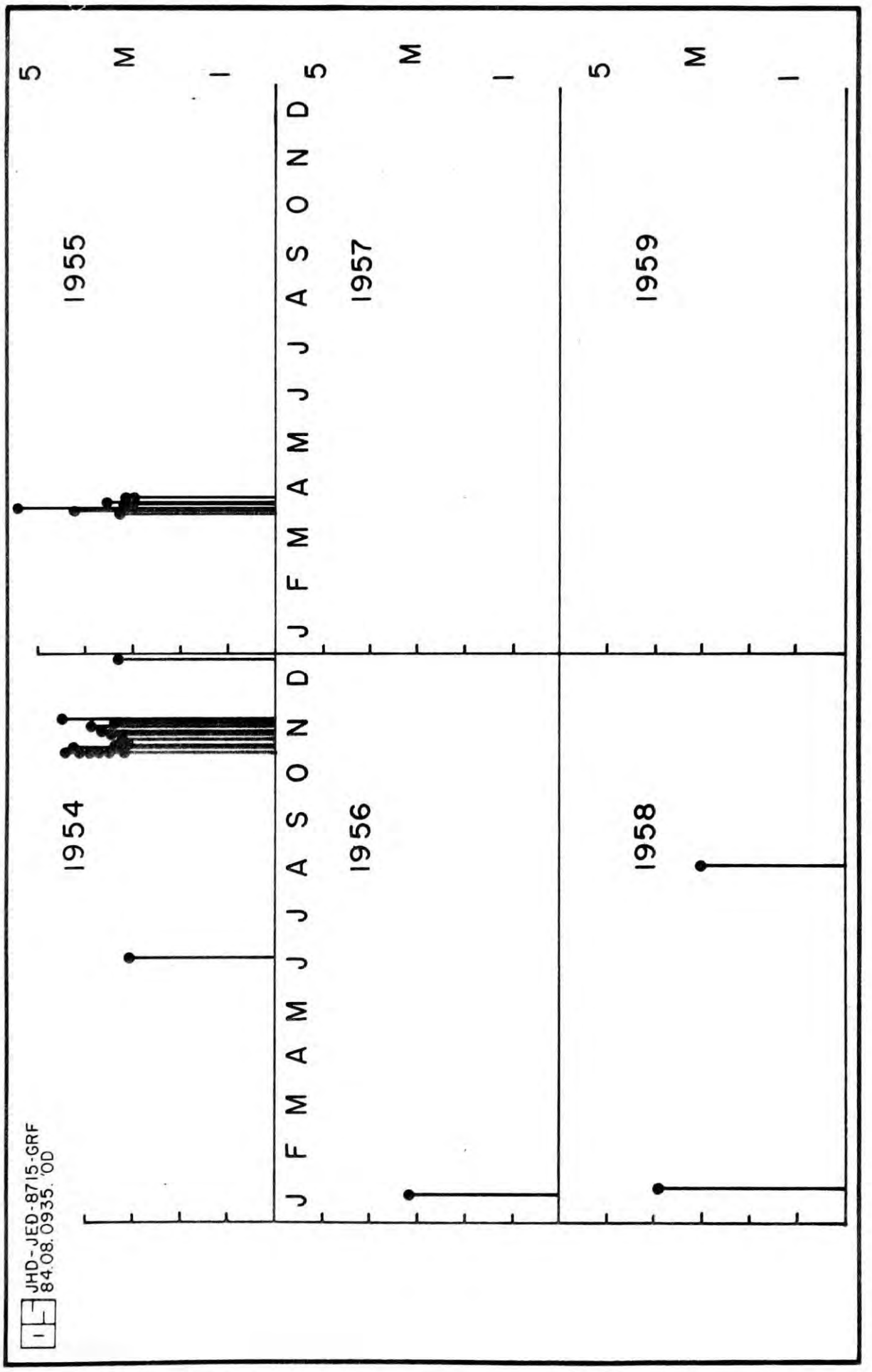

Fig. A5.5 1954 - 1959

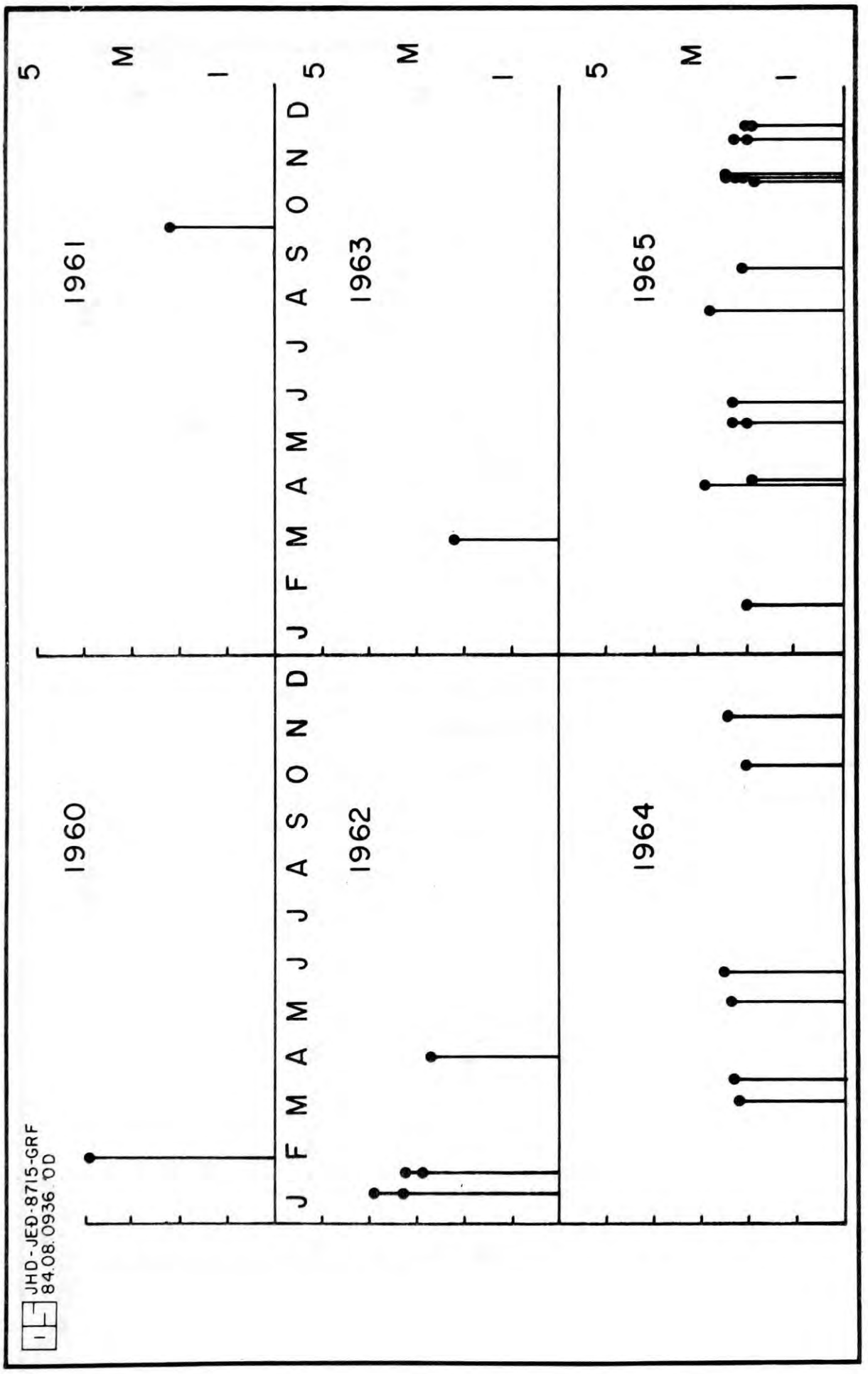

Fig. A5.6 1960 - 1965

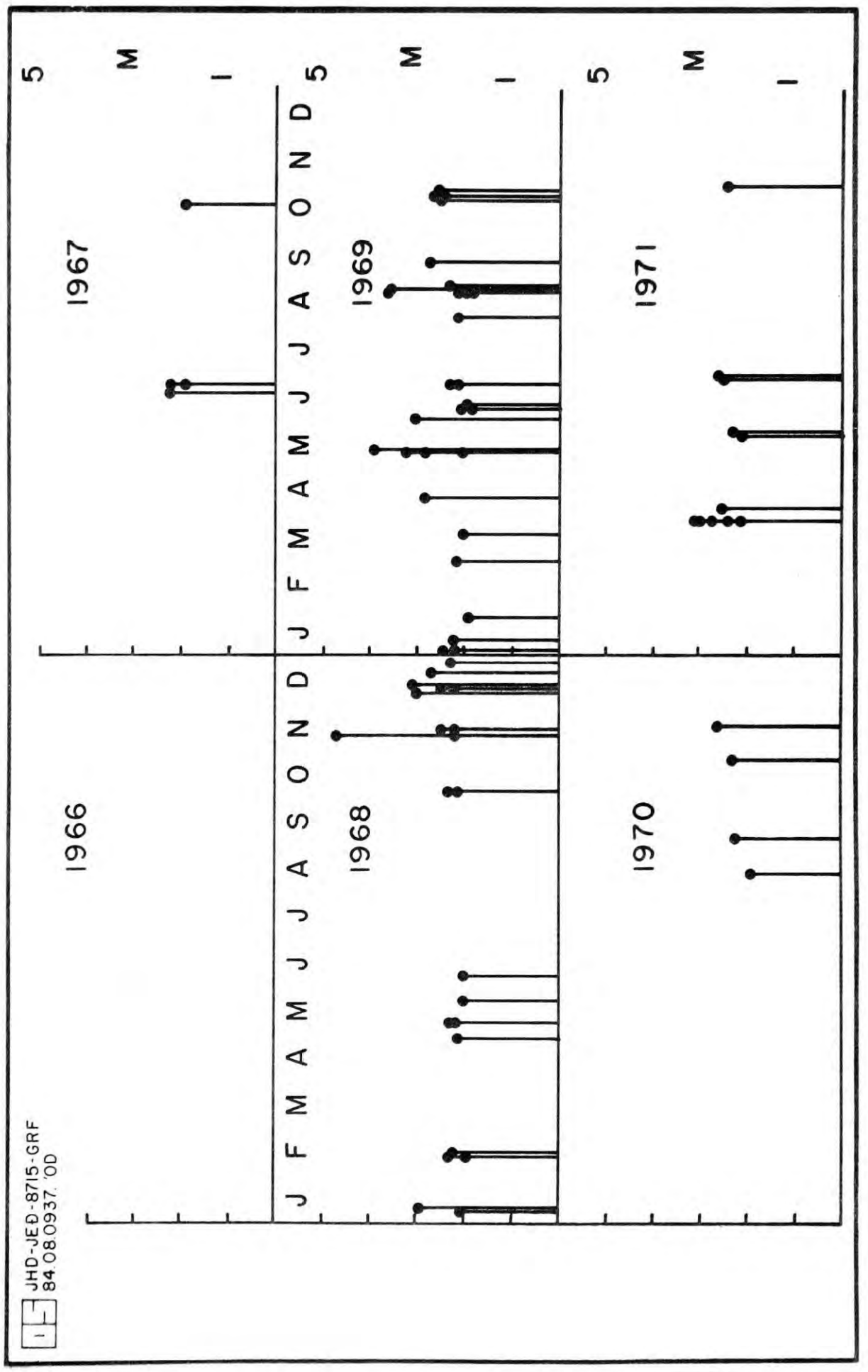

Fig. A5.7 1966 - 1971

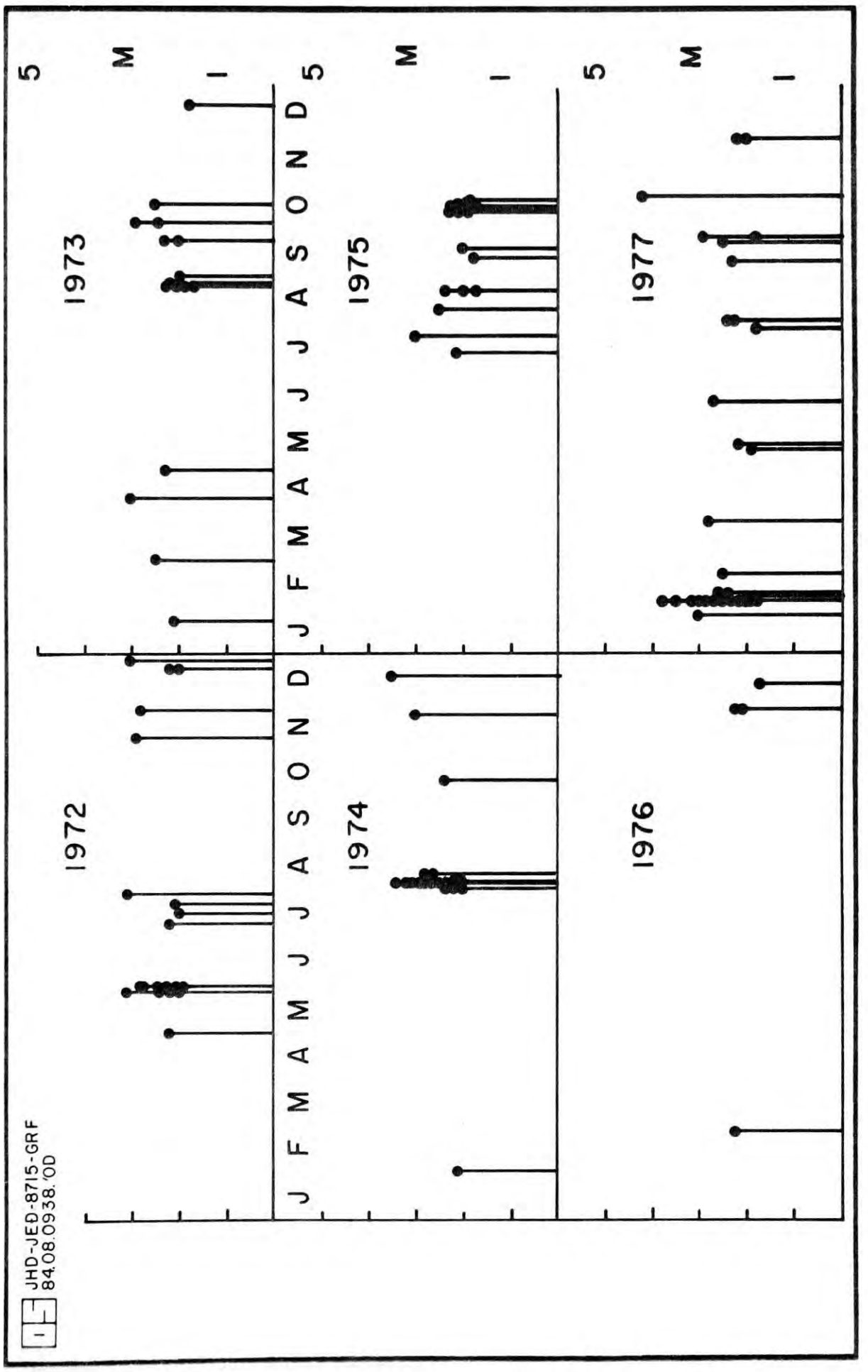

Fig. A5.8 1972 - 1977

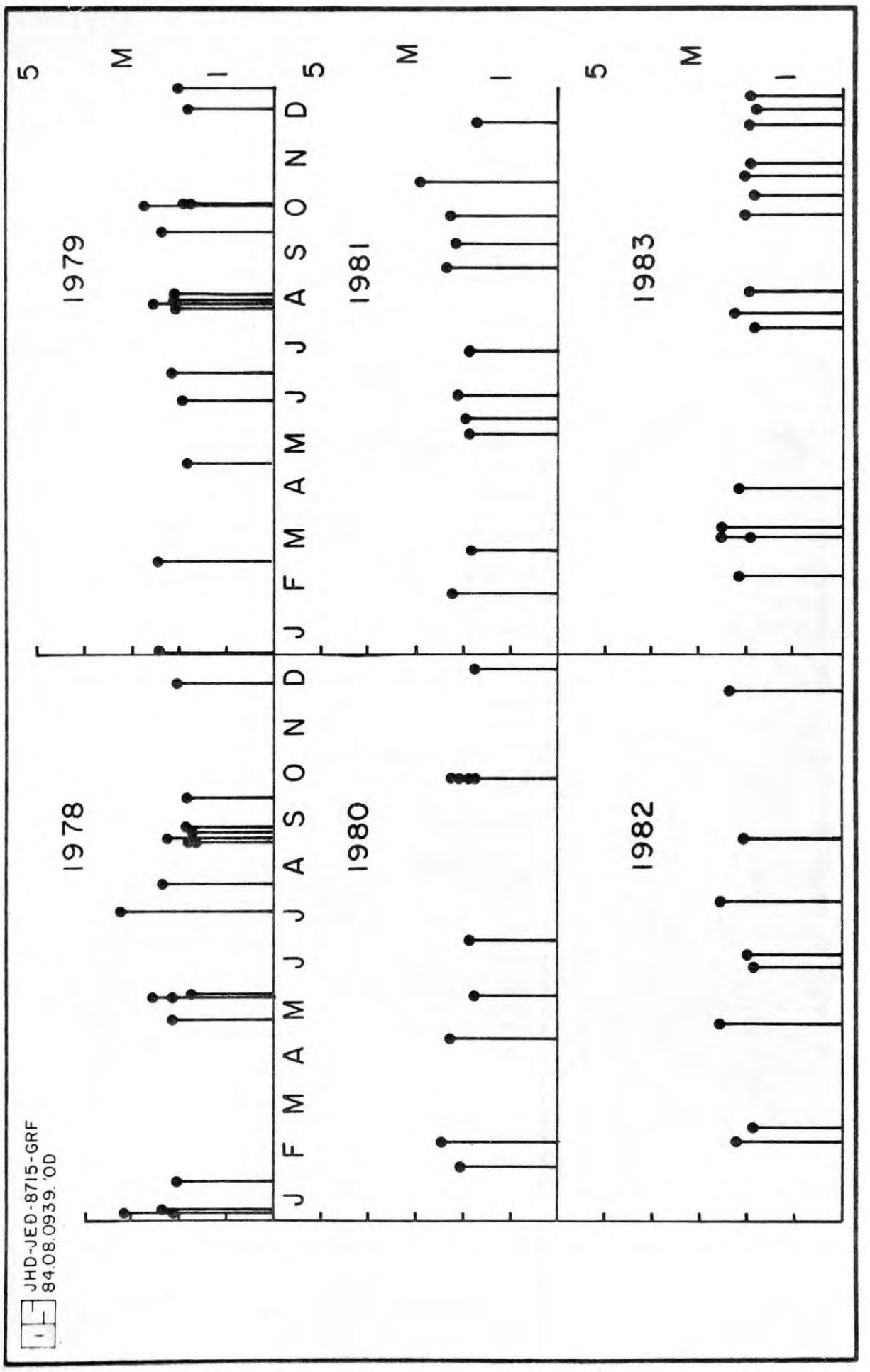

Fig. A5.9 1978 - 1983

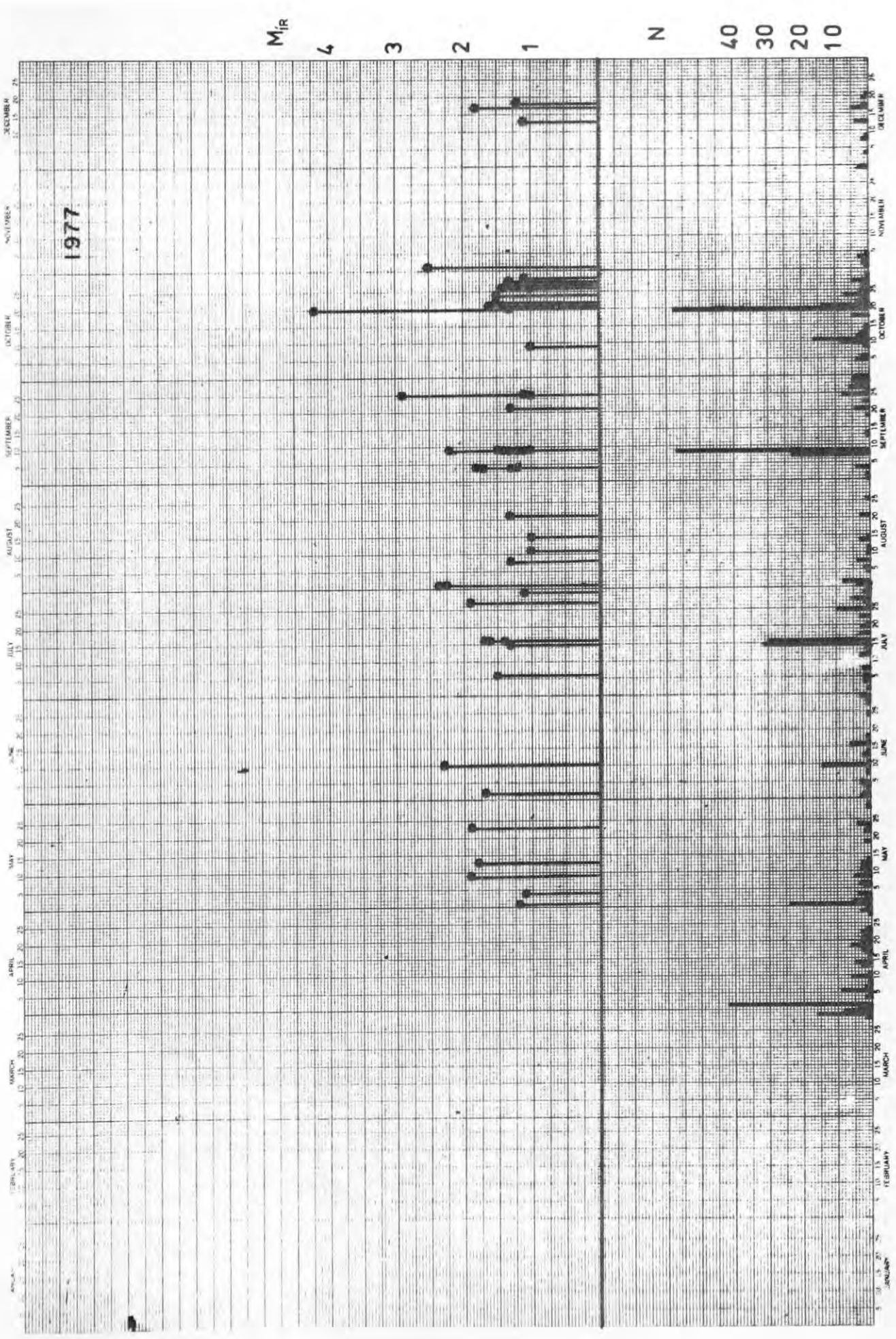

Fig. A5.10 1977

Figs A5.10 - A5.16 Seismicity charts based on the station IR. M is coda length magnitude computed for IR, N is number of events.

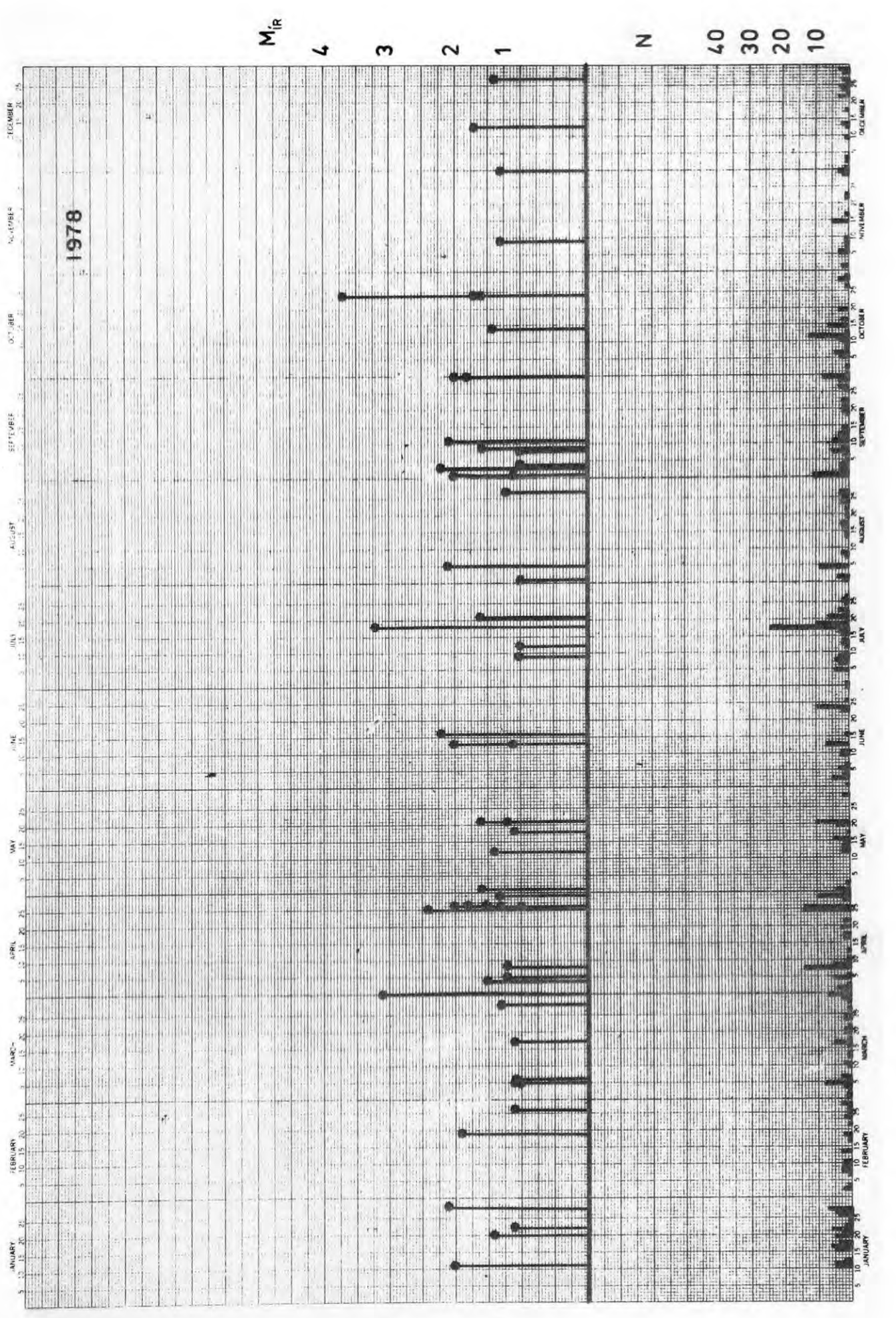

Fig. A5.11 1978

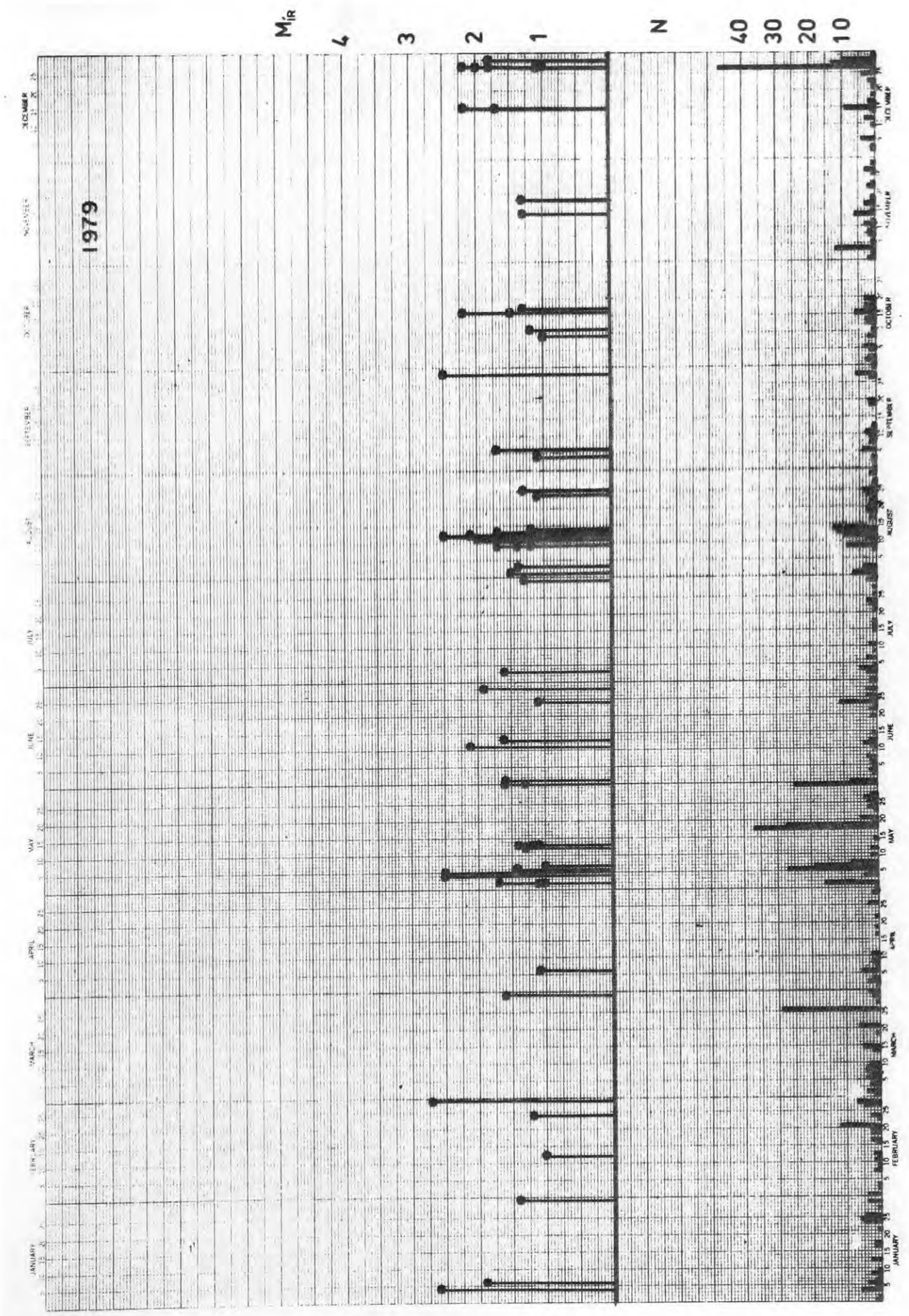

Fig. A5.12 1979

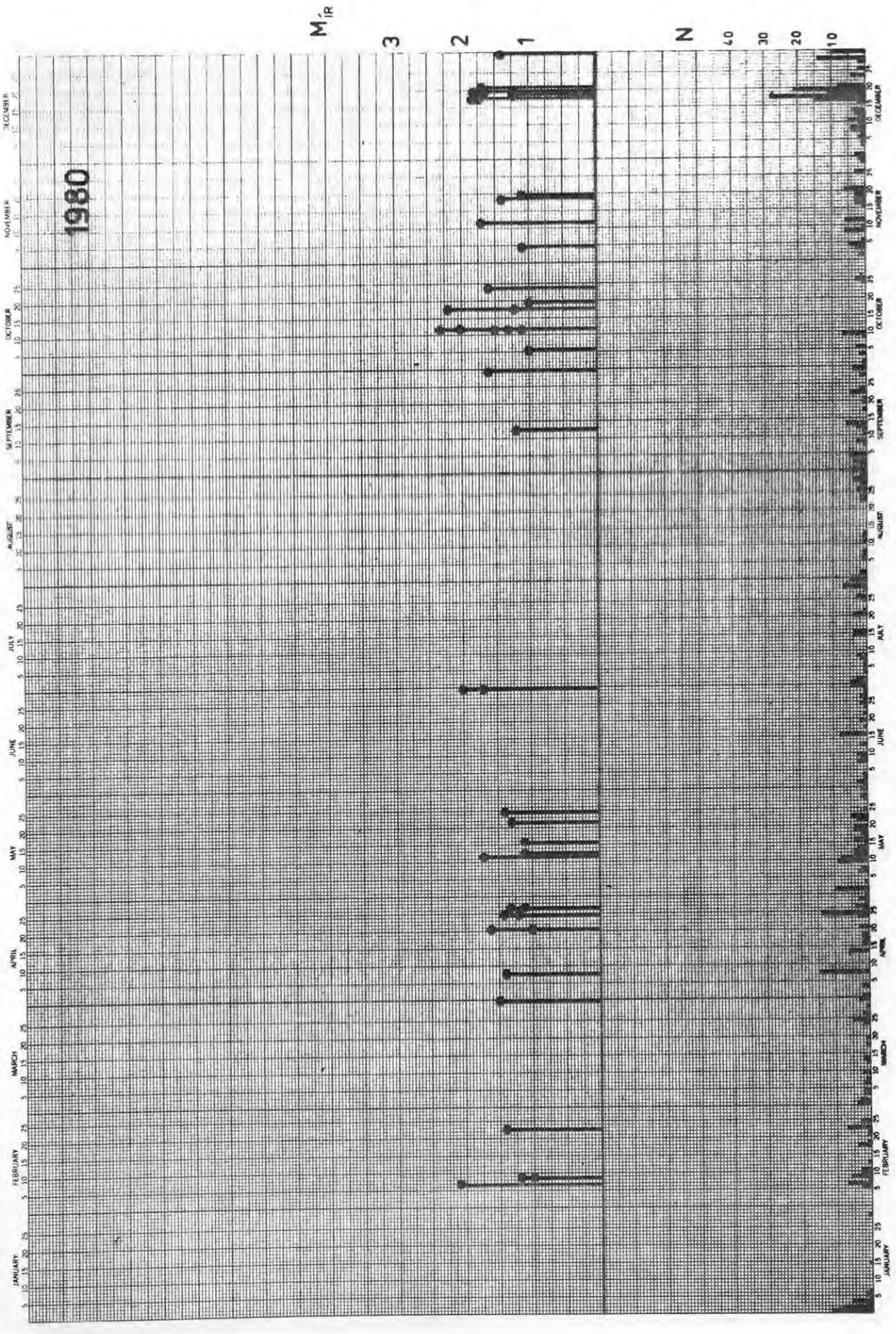

Fig. A5.13 1980

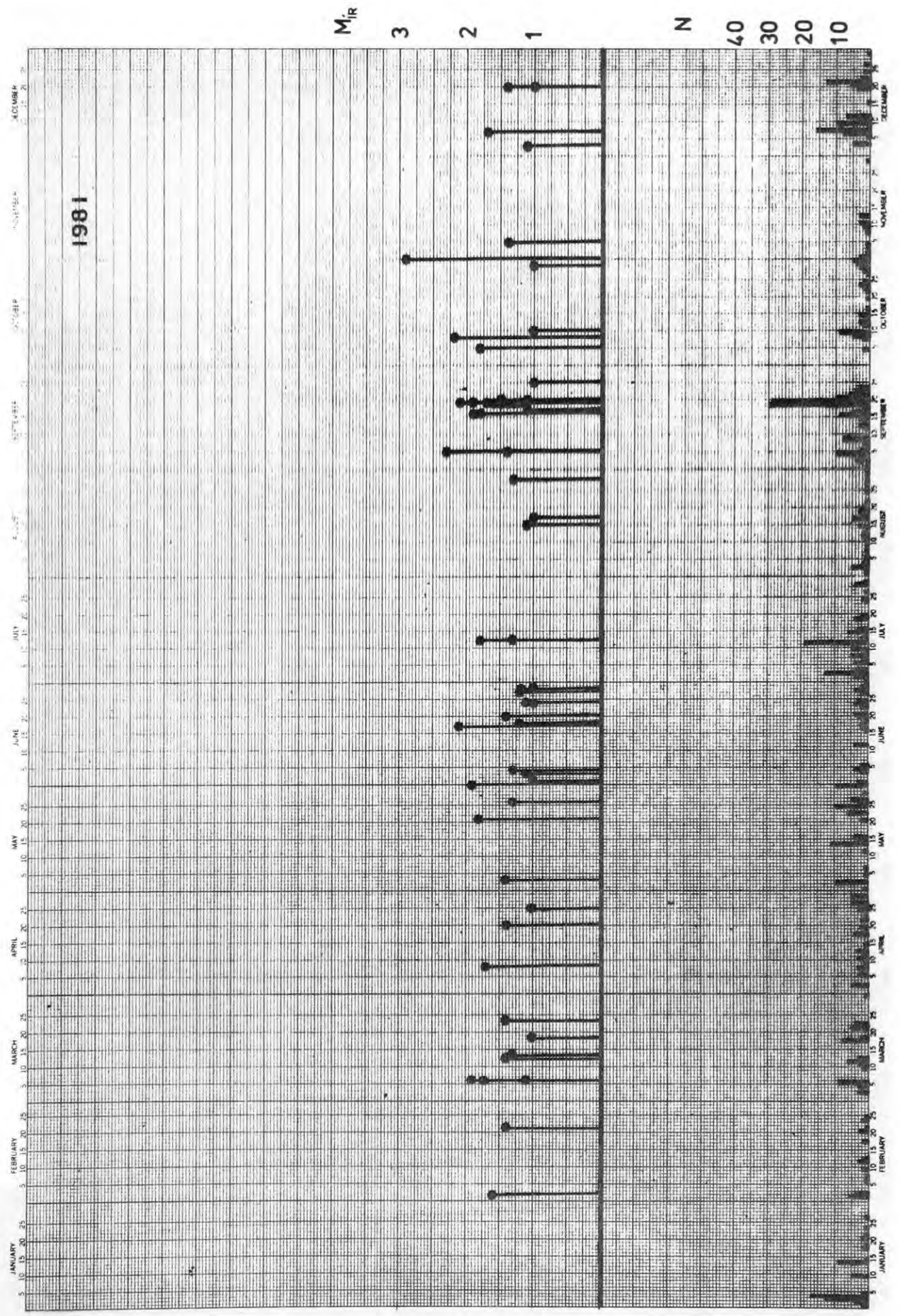

Fig. A5.14 1981

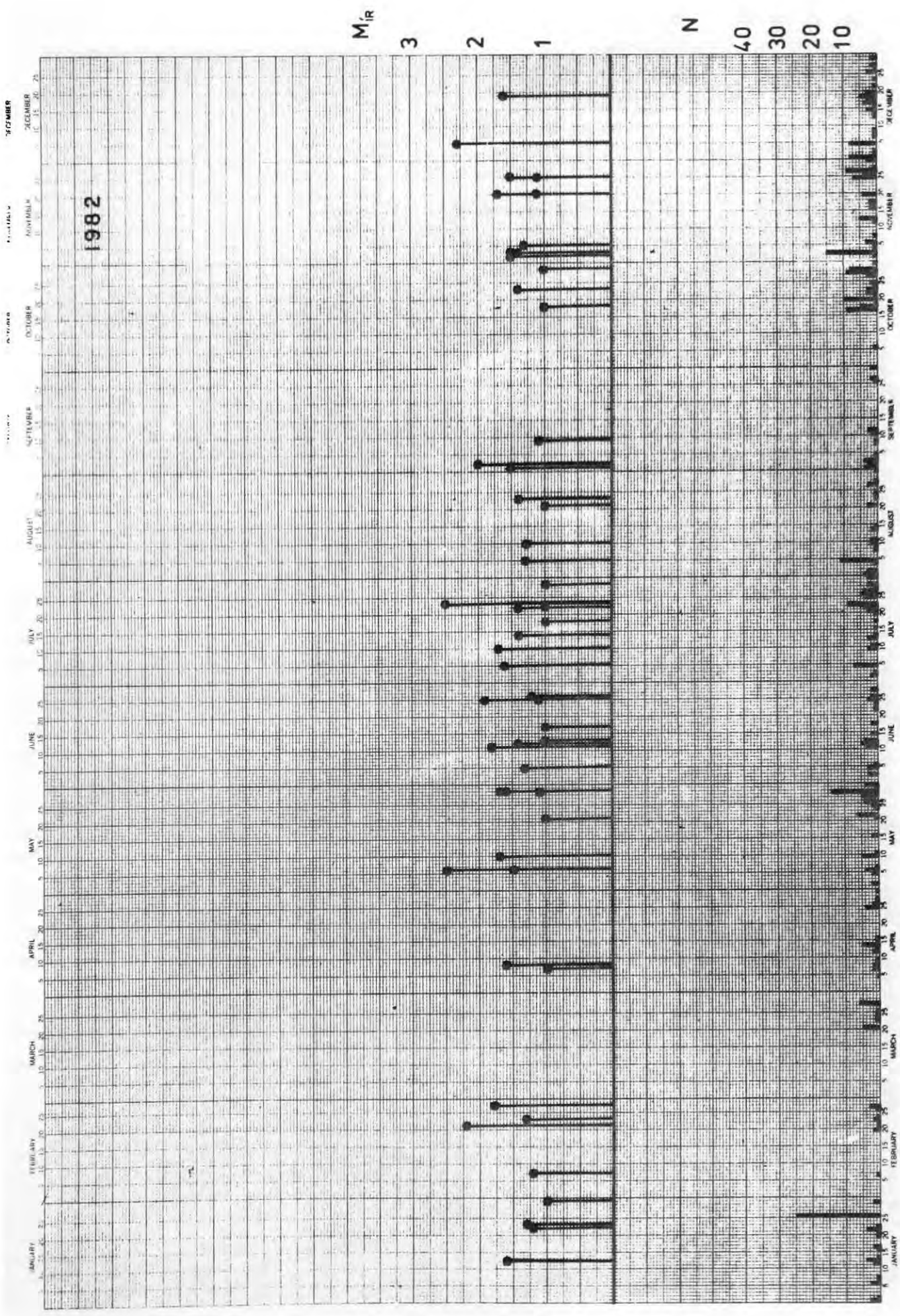

Fig. A5. IR 1982

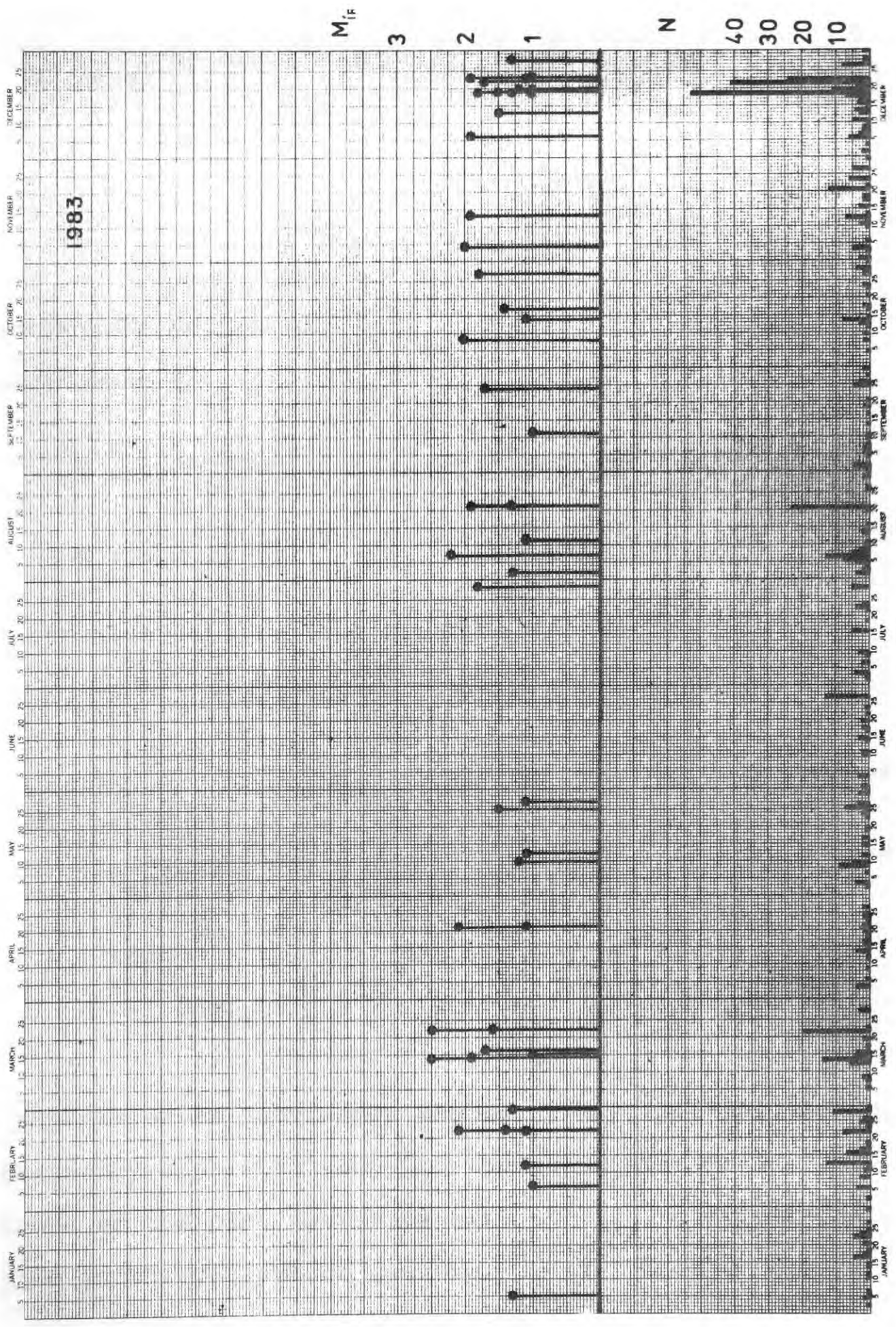

Fig. A5.16 1983

APPENDIX 6

DERIVATION OF THE EXPRESSION DESCRIBING THE FORM OF THE FREQUENCY - MAGNITUDE PLOT OF A COMBINATION OF TWO EARTHQUAKE SETS EXHIBITING DIFFERENT B-VALUES

for earthquake set (a): $\log_{10} N = a - bM$

for earthquake set (b): $\log_{10} N' = a' - b'M$

then $N = 10^{(a-bM)}$ $\qquad N' = 10^{(a'-b'M)}$

$$N + N' = 10^{(a-bM)} + 10^{(a'-b'M)}$$

if earthquake sets (a) and (b) were combined:

$$\log_{10}(N + N') = \log_{10}(10^{(a-bM)} + 10^{(a'-b'M)})$$

$$= \log_{10}[10^{(a-bM)} (1 + 10^{(a'-a)-(b'-b)M})]$$

$$\log_{10}(N + N') = a - bM + \log_{10}(1 + 10^{(a'-a)-(b'-b)M})$$

if $a = a'$, then

$$\log_{10}(N + N') = a - bM + \log_{10}(1 + 10^{(b-b')M})$$

This expression is non-linear and describes the expected form of the frequency-magnitude plot for the composite data set.
The slope of the plot decreases with increasing magnitude i.e. the plot is always upwards concave.

APPENDIX 7

POLARITY PLOTS OF 178 EVENTS LOCATED WITHIN THE HENGILL AREA

For location of place names, see Section 4.3.2.1.

Figs. A7.1 - A7.14 Upper hemisphere plots in stereographic projection. ● : compressions, ○ : dilations, X : nodal arrivals, lines: intersections of the nodal surfaces on the focal sphere. In the cases where these lines cross they are great circles and indicate a double couple solution. Where they are parallel they are small circles and indicate a tensile crack solution.

KLAMBRAGIL 1 OF 3

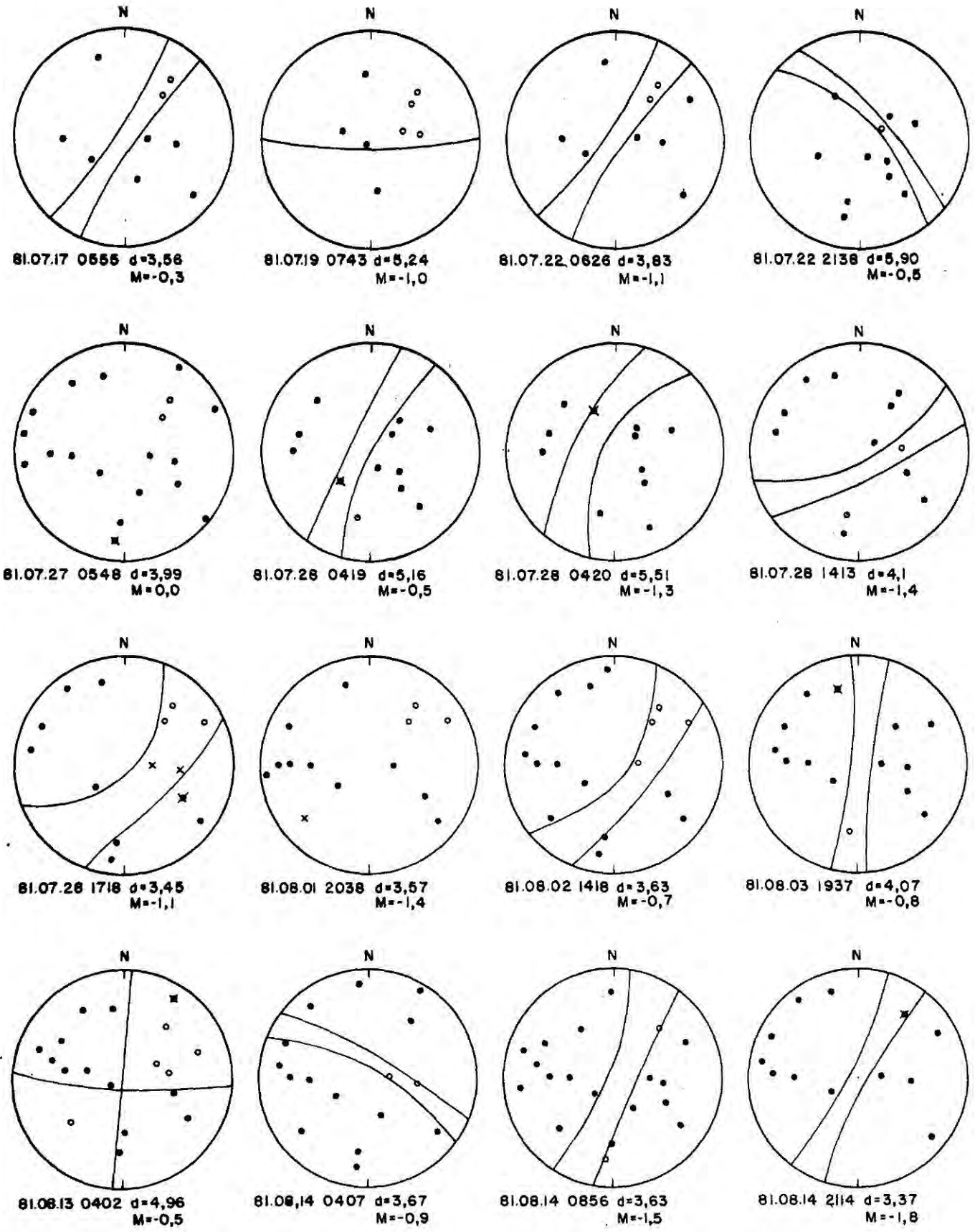

Fig. A7.1 Polarity plots of events from Klambragil, 1 of 3.

KLAMBRAGIL 1 OF 3

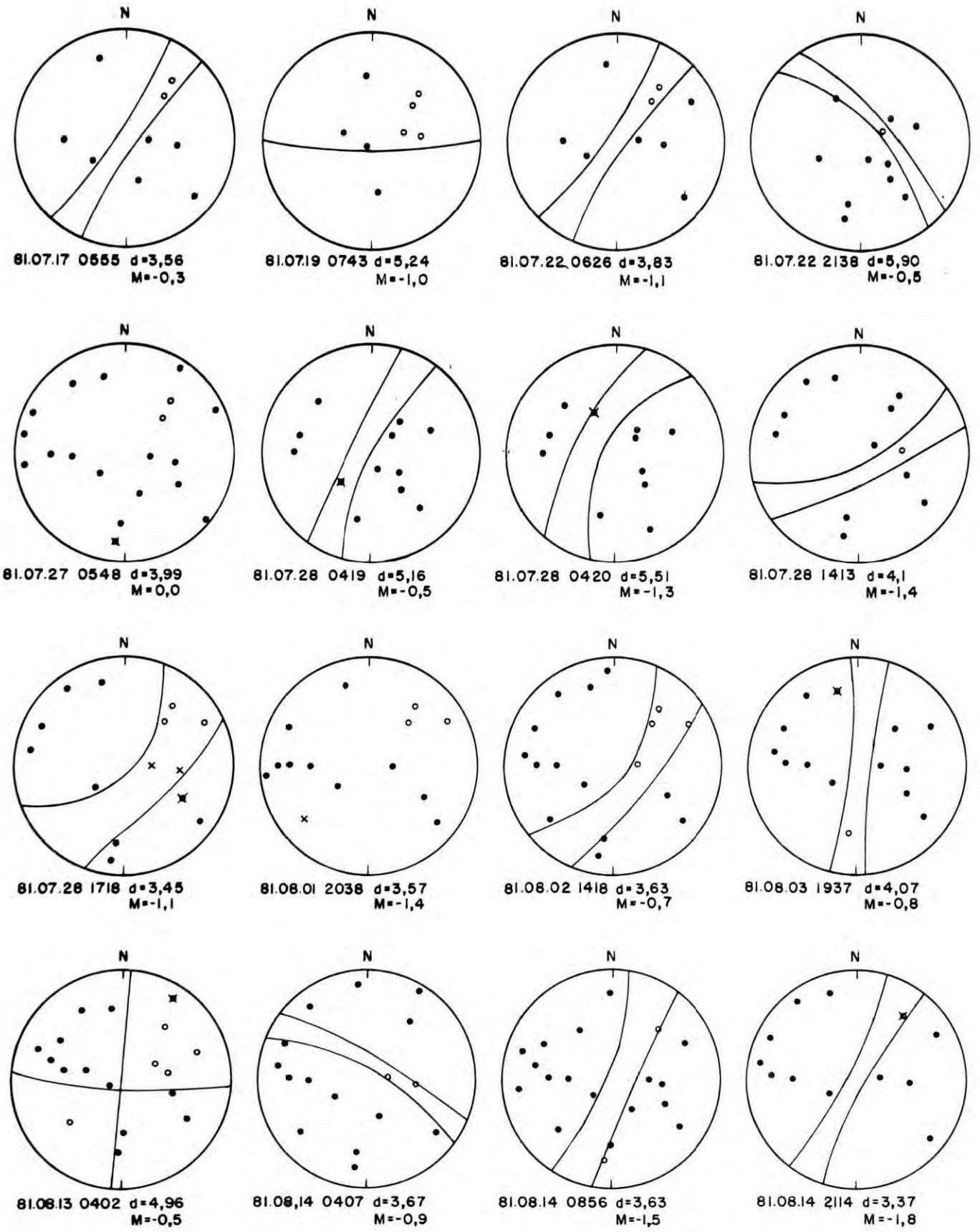

Fig. A7.2 Polarity plots of events from Klambragil, 1 of 3.

JHD-JEO-8716.GRF
84.07.0879. Sy.J.

KLAMBRAGIL 1 OF 3

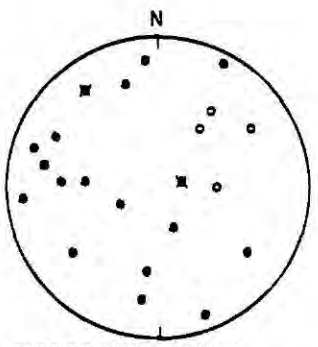

81.09.06 2018 d=4,28
M=0,8

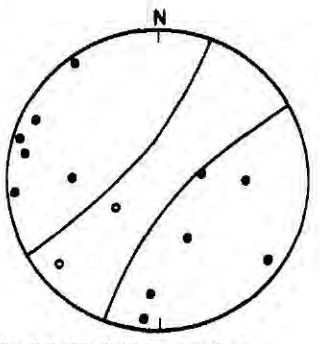

81.09.07 0123 d=3,14
M=-0,1

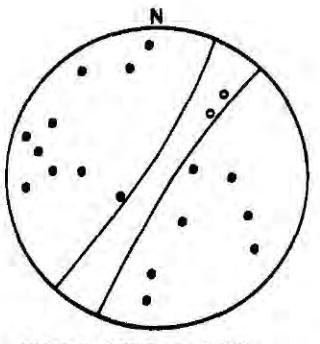

81.09.12 2237 d=3,74
M=-0,3

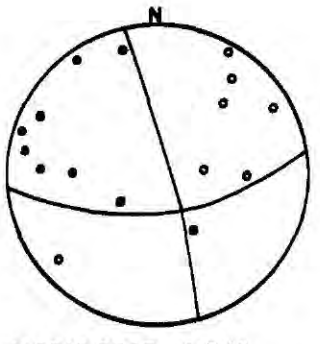

81.09.18 0643 d=3,14
M=-0,4

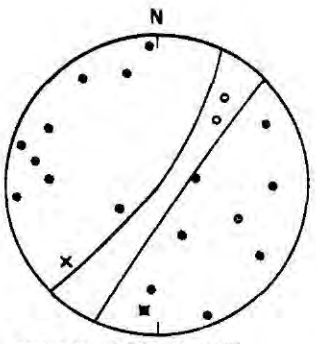

81.09.23 0501 d=3,51
M=0,0

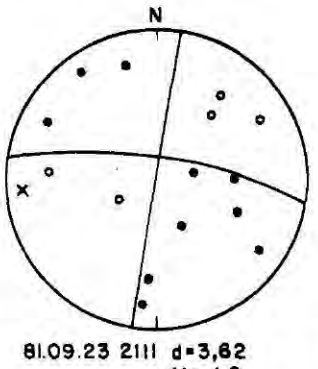

81.09.23 2111 d=3,62
M=-1,2

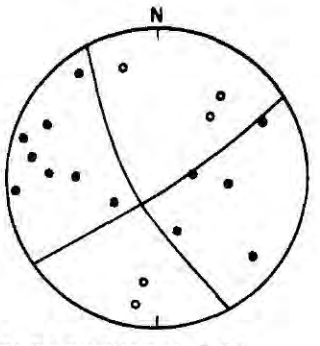

81.09.27. 0156 d=3,55
M=-0,8

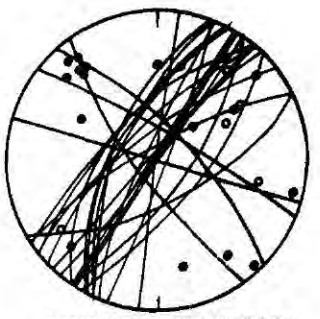

SUMMARY – KLAMBRAGIL

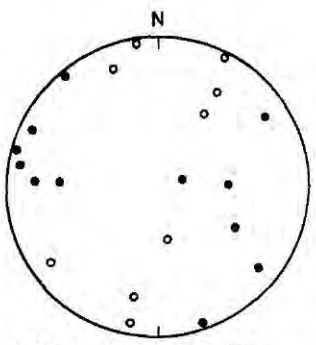

81.09.28 1853 d=3,25
M=1,3

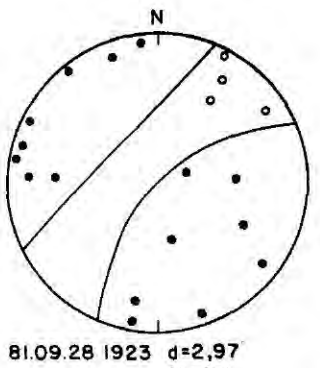

81.09.28 1923 d=2,97
M=0,1

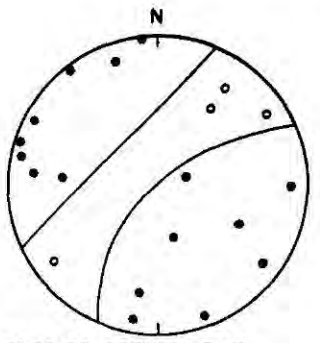

81.09.28 2002 d=3,16
M=-0,5

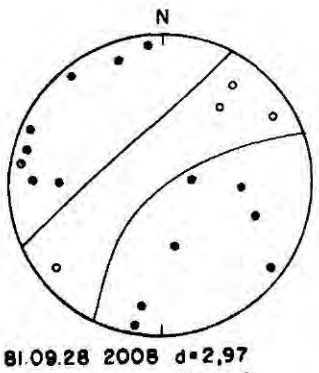

81.09.28 2008 d=2,97
M=-0,6

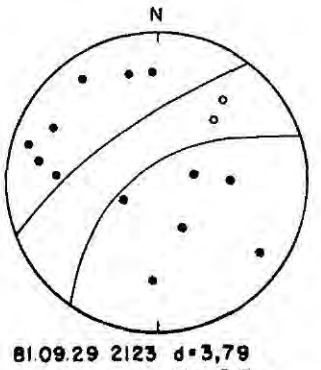

81.09.29 2123 d=3,79
M=-0,7

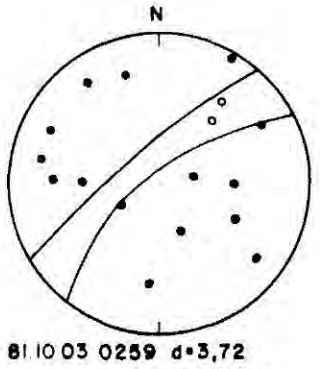

81.10.03 0259 d=3,72
M=-0,8

Fig. A7.3 Polarity plots of events from Klambragil, 1 of 3.

JHD-JED-8716-GRF
84.07.0888.0D

FISSURE SWARM 1 OF 2

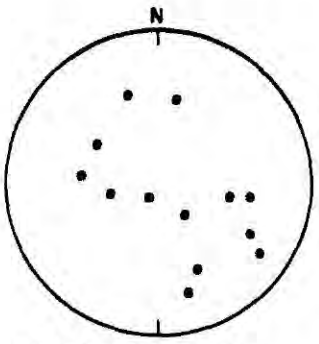

81.07.26 0734 d=4.95
M=-1.0

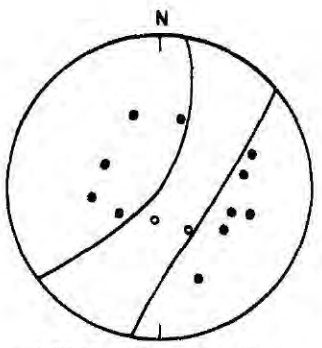

81.07.26. 1958 d=5.29
M=-1.0

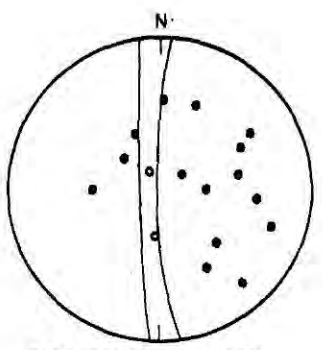

81.08.02 1044 d=6.27
M=-0.4

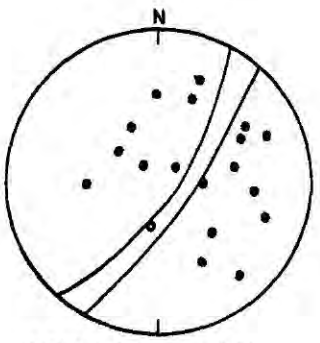

81.08.03 0207 d=6.45
M=0.0

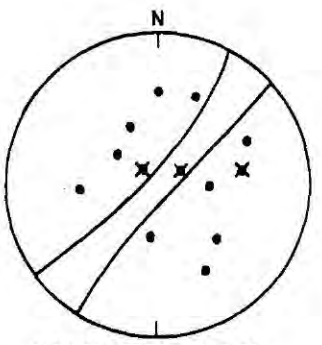

81.08.03. 0320 d=5.70
M=-1.2

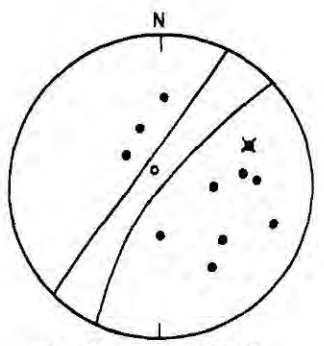

81.08.03 0853 d=6.15
M=-1.7

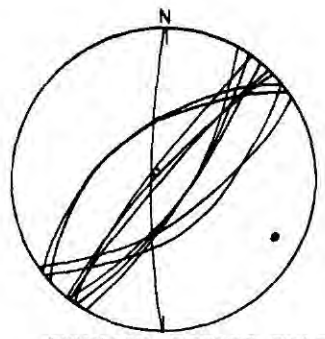

SUMMARY - FISSURE SWARM

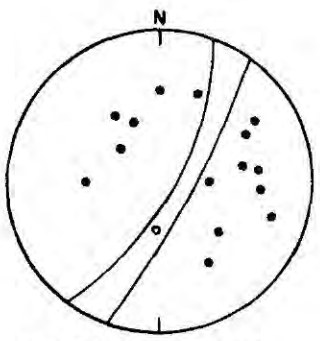

81.08.03 1355 d=5.99
M=-0.6

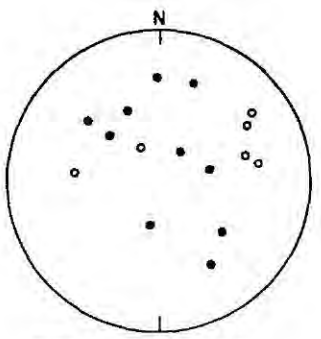

81.09.03 1120 d=5.31
M=-0.7

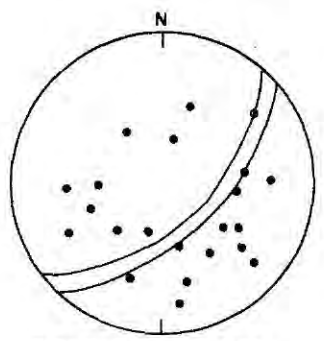

81.09.13 0601 d=5.58
M=0.8

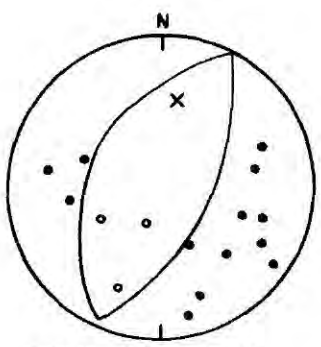

81.09.15. 1504 d=4.08
M=-0.7

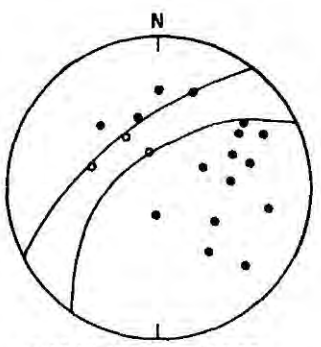

81.09.24 0139 d=6.53
M=-0.5

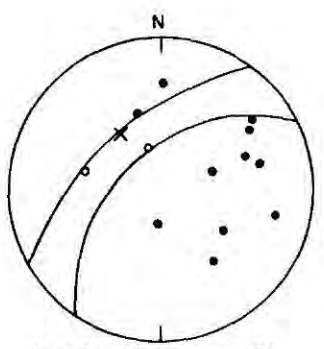

81.09.24 1018 d= 5.76
M=-1.1

Fig. A7.4 Polarity plots of events from the Fissure swarm, 1 of 2.

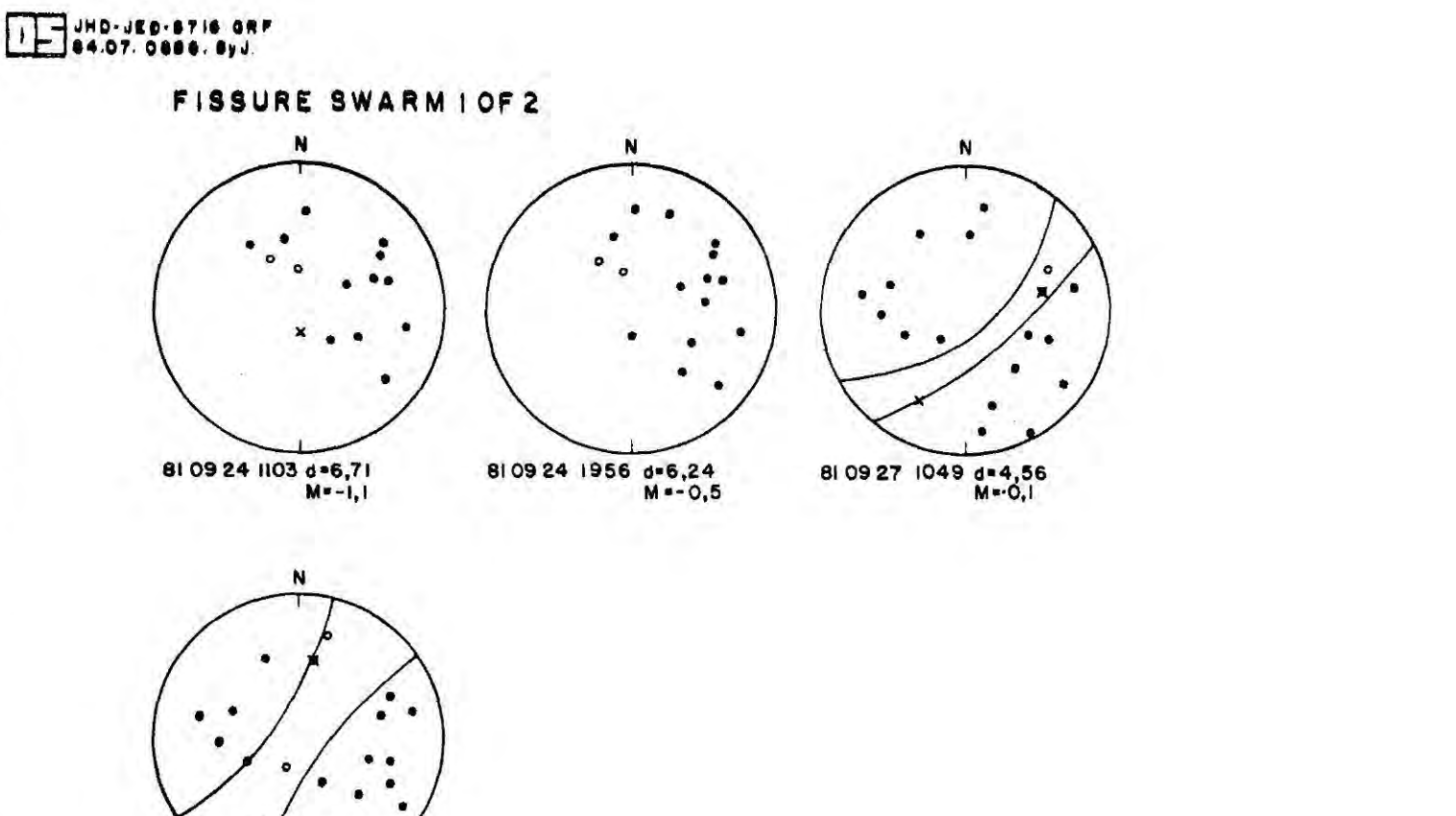

Fig. A7.5 Polarity plots of events from the Fissure swarm, 1 of 2, and Mosfellsheidi.

JHD-JED-8716-GRF
84.07.0887-0D

KYLLISFELL

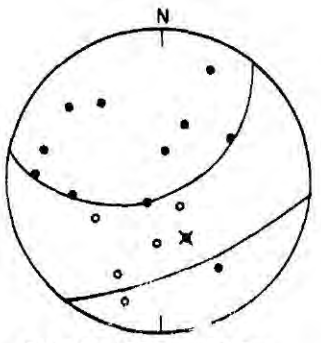

810728 1609 d=4.89
M=-0.2

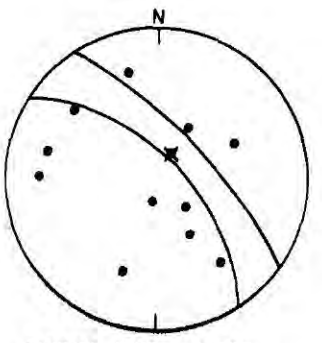

81.08.05 1928 d=4.77
M=-1.3

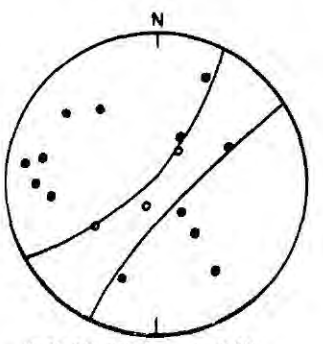

81.08.06 1104 d=4.89
M=0.0

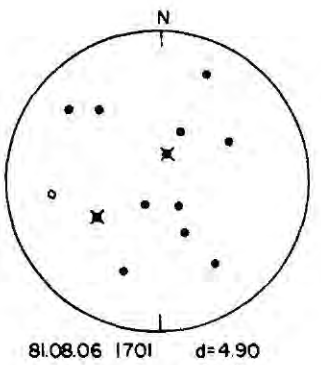

81.08.06 1701 d=4.90
M=-1.1

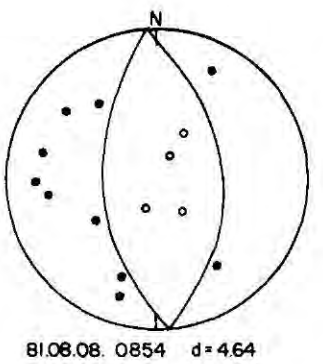

81.08.08. 0854 d=4.64
M=-0.6

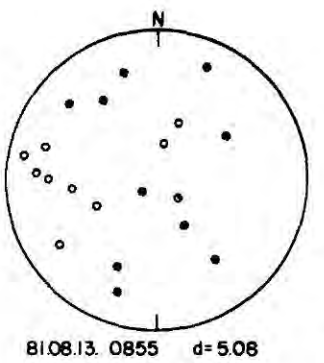

81.08.13. 0855 d=5.08
M=0.5

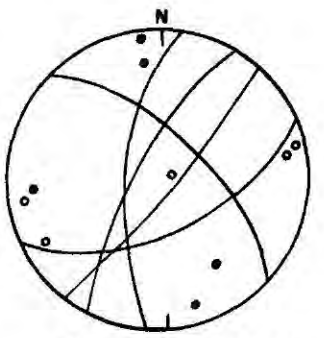

SUMMARY - KYLLISFELL

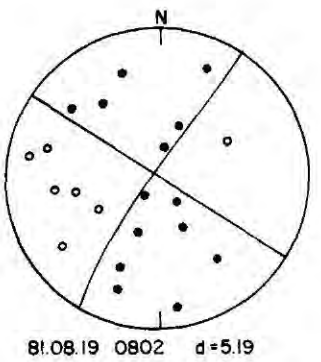

81.08.19 0802 d=5.19
M=0.2

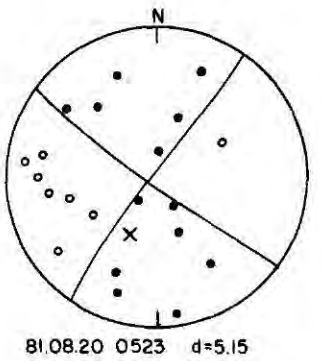

81.08.20 0523 d=5.15
M=0.1

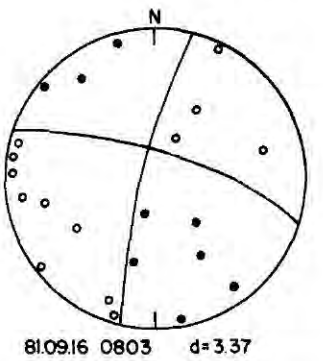

81.09.16 0803 d=3.37
M=-0.1

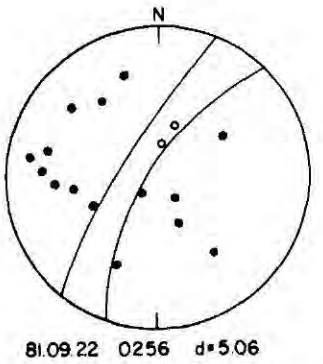

81.09.22 0256 d=5.06
M=-0.8

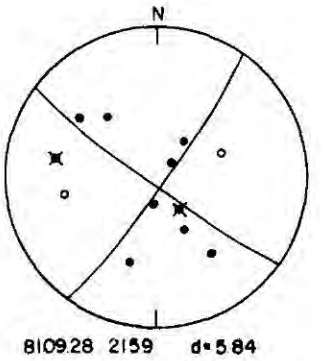

810928 2159 d=5.84
M=-1.0

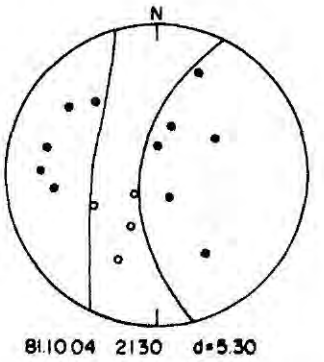

81.10.04 2130 d=5.30
M=1.1

Fig. A7.6 Polarity plots of events from Kyllisfell.

JHD-JED-8716.GRF
84.07.0883 SyJ

NESJAVELLIR

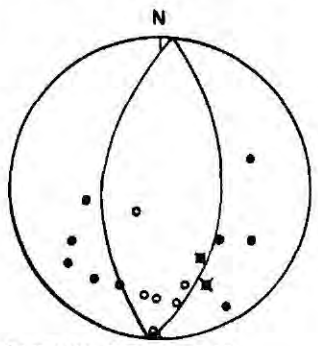

8107 26 0124 d=5,10
M=-0,3

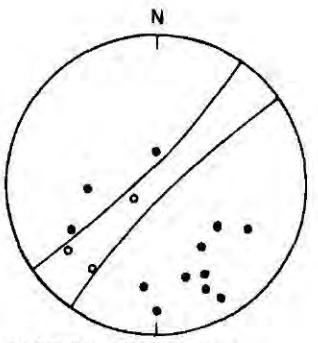

8107 31 1634 d=5,32
M=-0,2

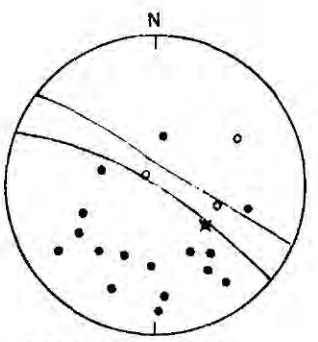

8108 04 2112 d=6,08
M=0,50

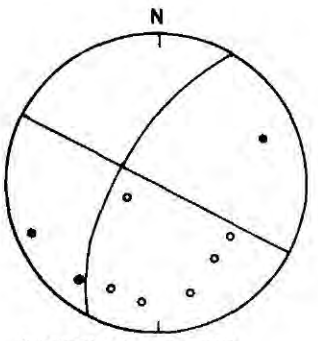

8108 06 1414 d=3,97
M=-1,0

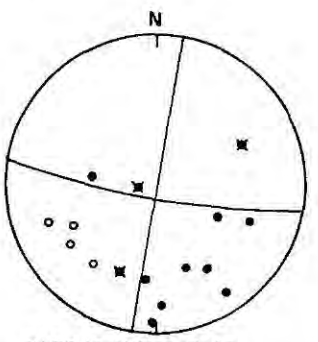

8108 15 1119 d=5,46
M=-0,6

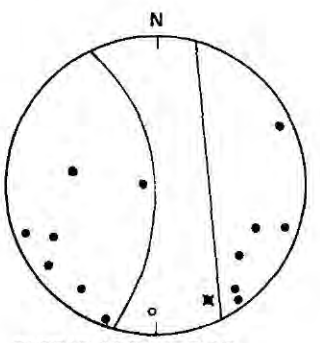

8108 16 1020 d=3,42
M=-0,6

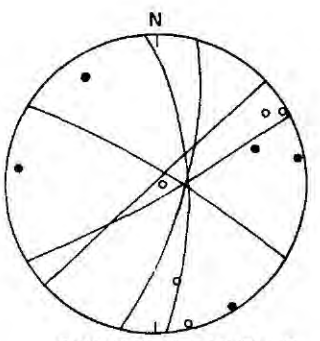

SUMMARY-NESJAVELLIR

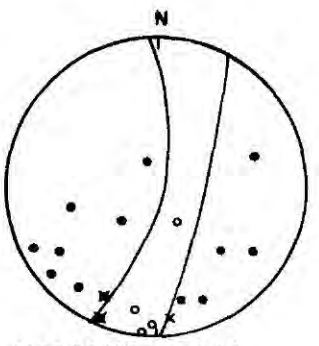

8108 20 1004 d=4,48
M=0,1

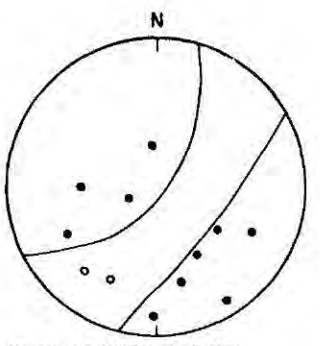

8108 22 0205 d=4,80
M=-1,0

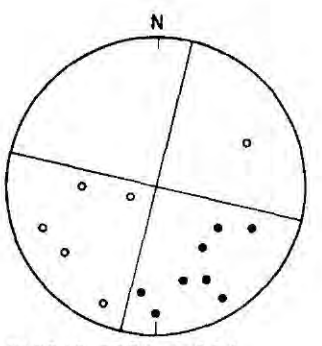

8109 16 2206 d=4,94
M=-0,8

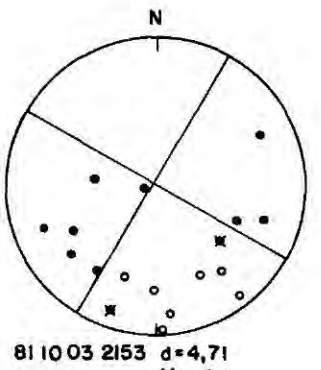

8110 03 2153 d=4,71
M=-0,1

Fig. A7.7 Polarity plots of events from Nesjavellir.

JHD-JED-8716-GRF
84.070889.0D

CLUSTER 1 OF 2

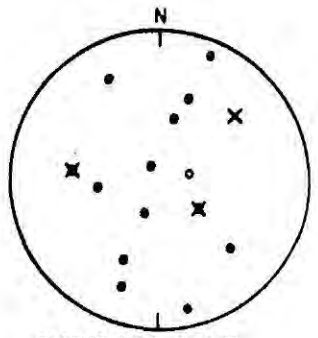

81.07.23. 1147 d=4.41
M=0.1

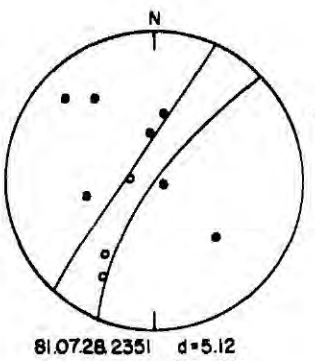

81.07.28.2351 d=5.12
M=-0.8

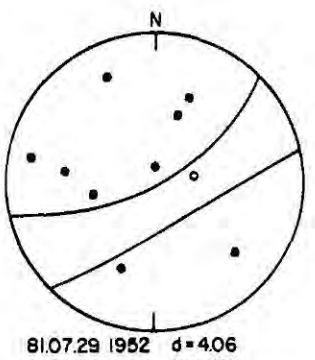

81.07.29 1952 d=4.06
M=-0.9

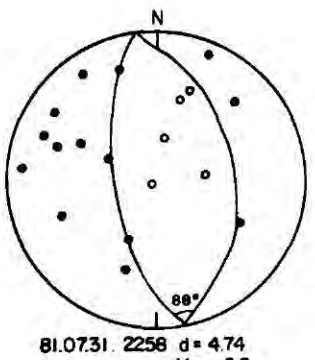

81.07.31. 2258 d=4.74
M=-0.2

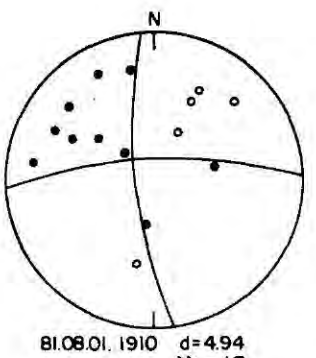

81.08.01. 1910 d=4.94
M=-1.7

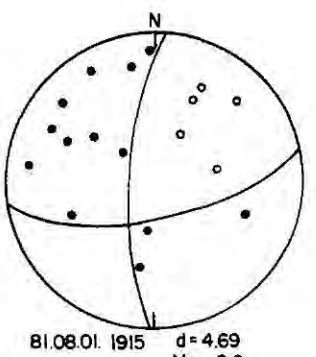

81.08.01. 1915 d=4.69
M=-0.9

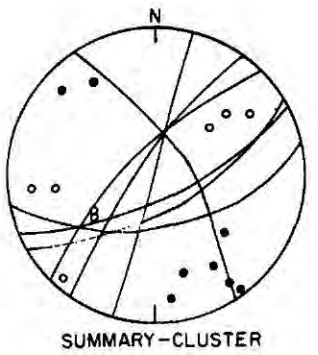

SUMMARY-CLUSTER

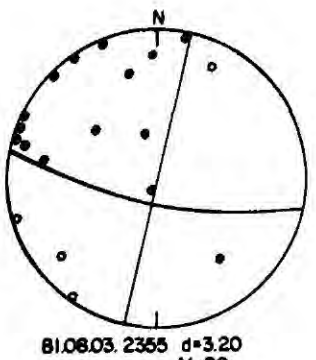

81.08.03. 2355 d=3.20
M=0.0

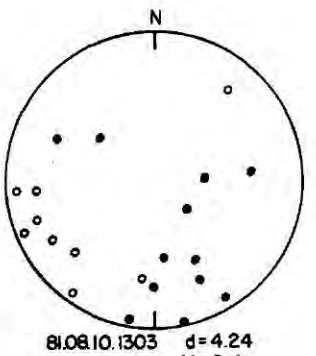

81.08.10.1303 d=4.24
M=0.4

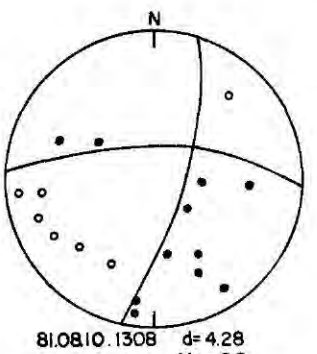

81.08.10.1308 d=4.28
M=-0.2

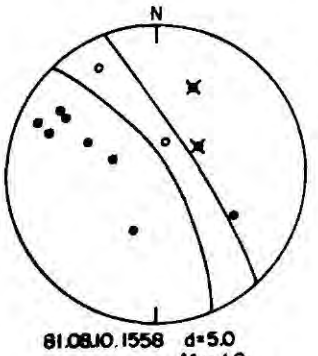

81.08.10.1558 d=5.0
M=-1.0

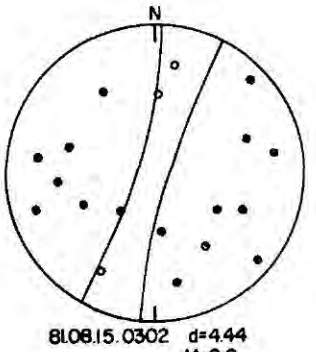

81.08.15.0302 d=4.44
M=0.0

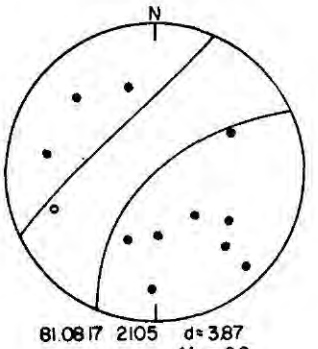

81.08.17 2105 d=3.87
M=-0.8

Fig. A7.8 Polarity plots of events from the central cluster, 1 of 2.

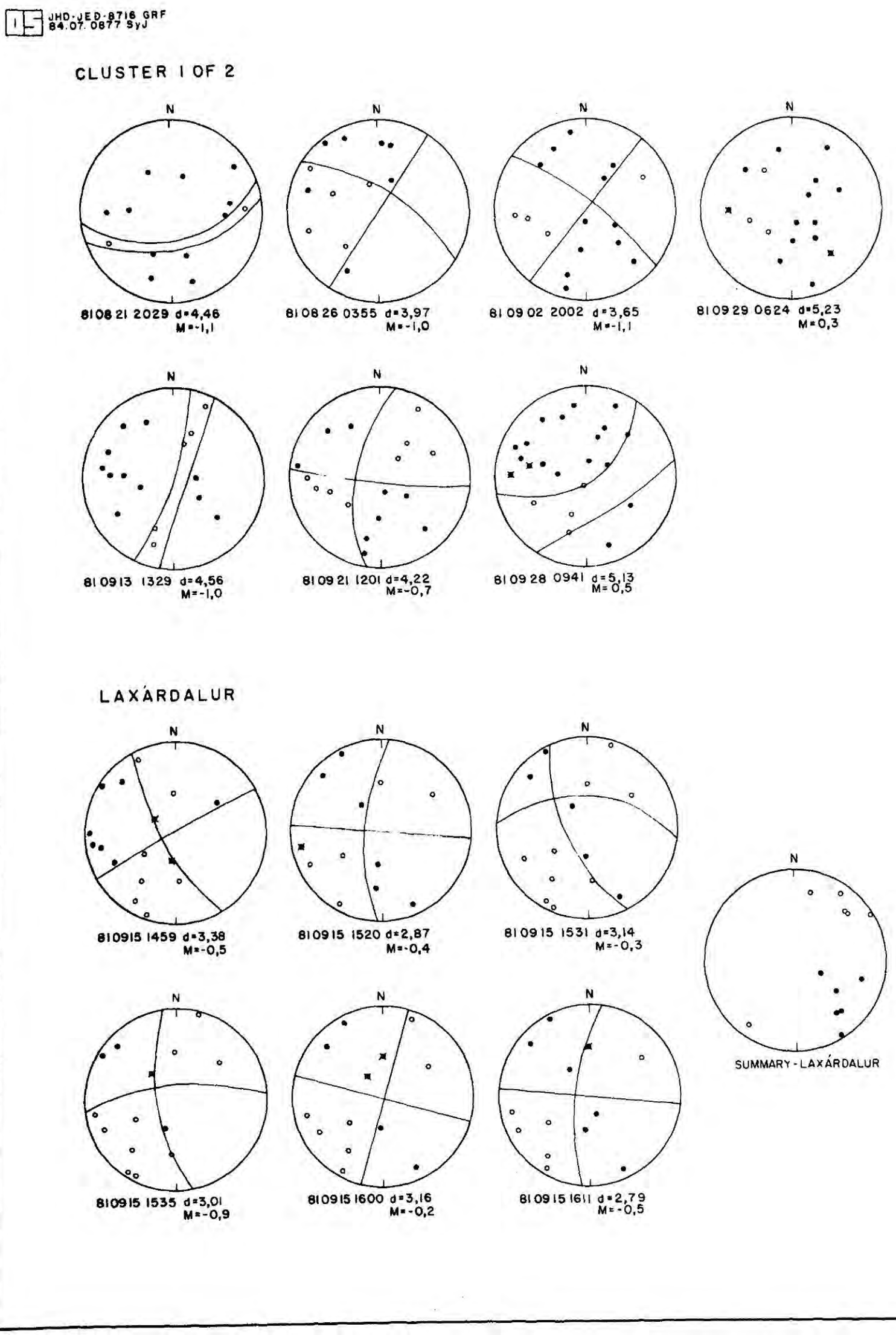

Fig. A7.9 Polarity plots of events from the central cluster, 1 of 2, and Laxardalur.

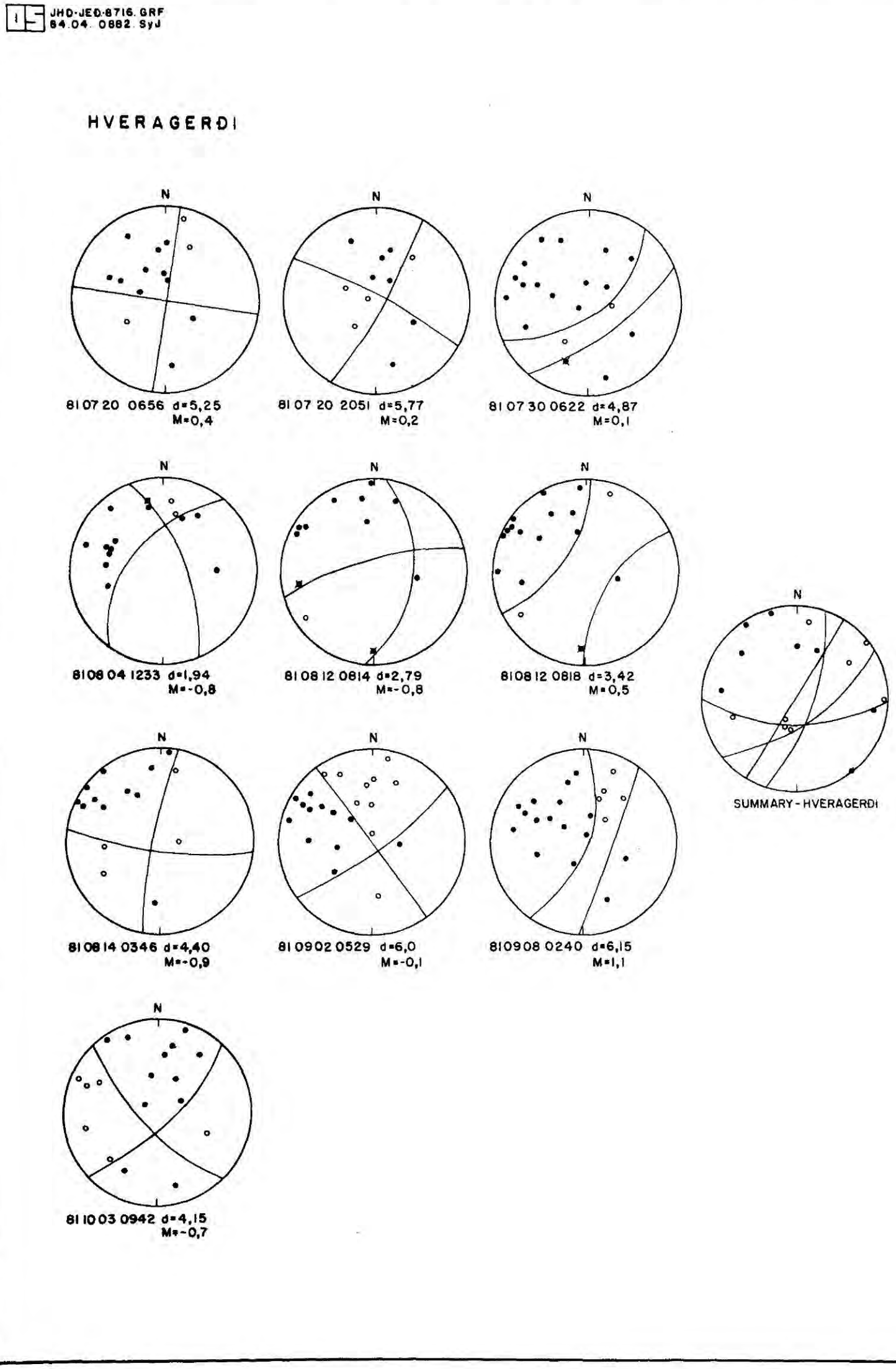

Fig. A7.10 Polarity plots of events from Hveragerdi.

JHD-JED-8716. GRF
84.07. 0885 SyJ

SVÍNAHLÍÐ

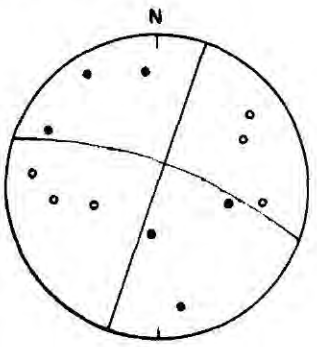

8108 03 0515 d=3,23
M=-1,6

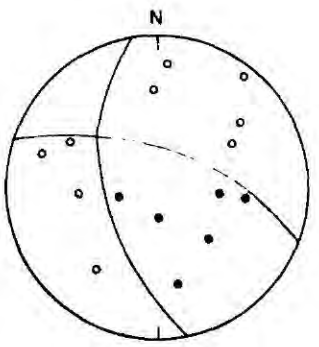

8109 08 1112 d=4,2
M=-1,0

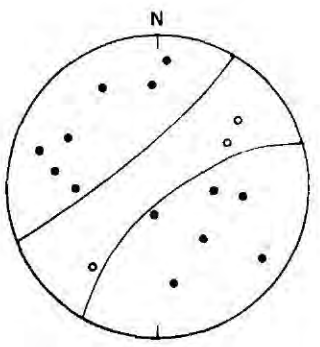

8109 09 1322 d=4,15
M=-0,2

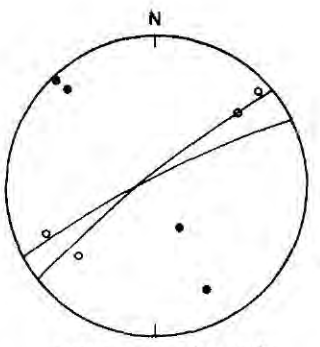

SUMMARY-SVÍNAHLÍÐ

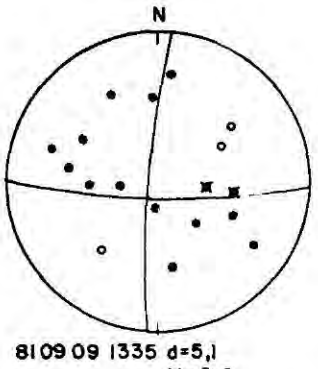

8109 09 1335 d=5,1
M=0,8

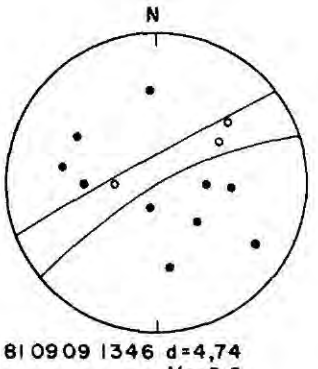

8109 09 1346 d=4,74
M=-0,9

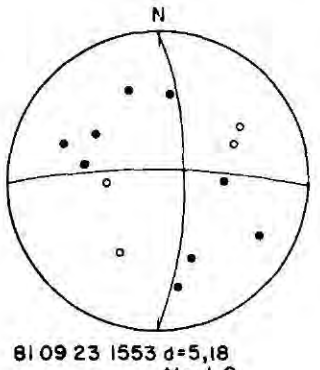

8109 23 1553 d=5,18
M=-1,0

ÓRUSTUHÓLSHRAUN

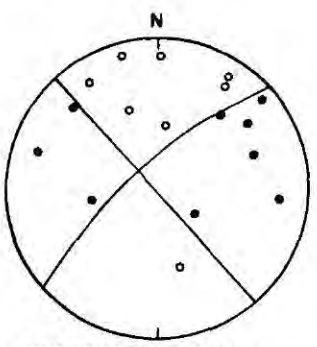

8107 29 1721 d=4,45
M=-0,3

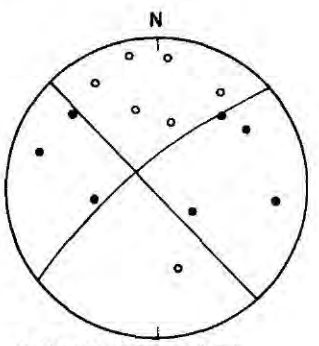

8107 29 1722 d=4,09
M=-0,8

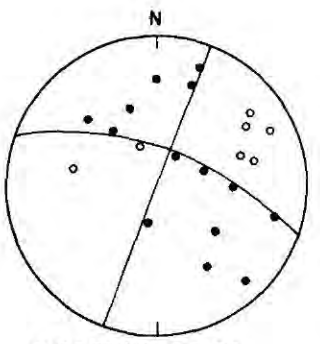

8109 03 1112 d=5,66
M=0,7

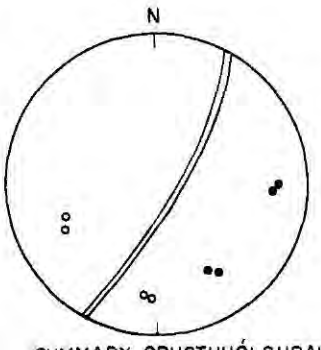

SUMMARY-ORUSTUHÓLSHRAUN

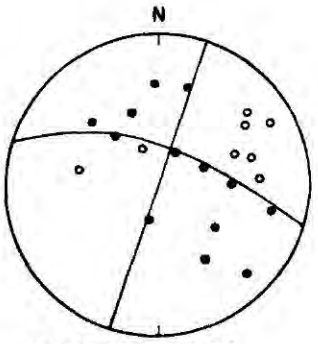

8109 03 1134 d=6,24
M=0,0

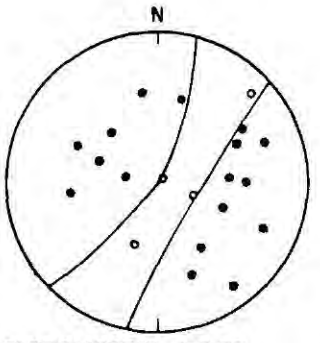

8109 21 1247,13 d=5,77
M=-0.2

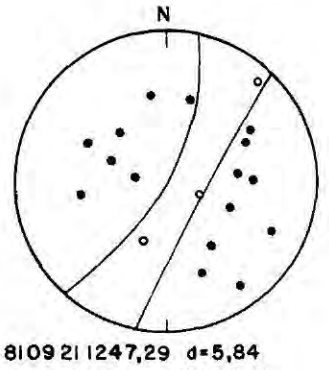

8109 21 1247,29 d=5,84
M=-0,2

Fig. A7.11 Polarity plots of events from Svinahlid and Orustuholshraun.

JHD-JEF-8716.GRF
84.07. 0878. Sy J.

ÖLFUS 1 OF 2

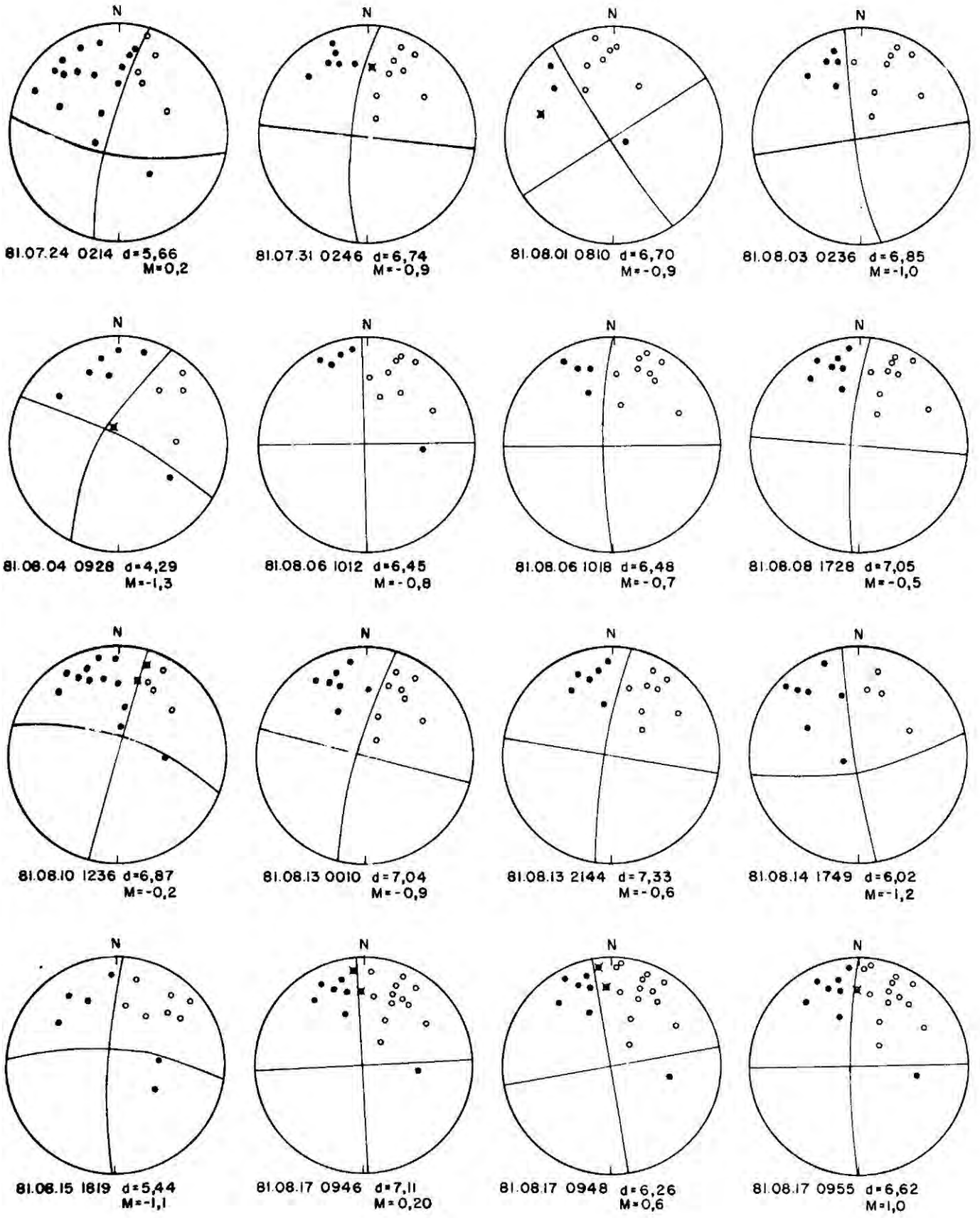

Fig. A7.12 Polarity plots of events from Olfus, 1 of 2.

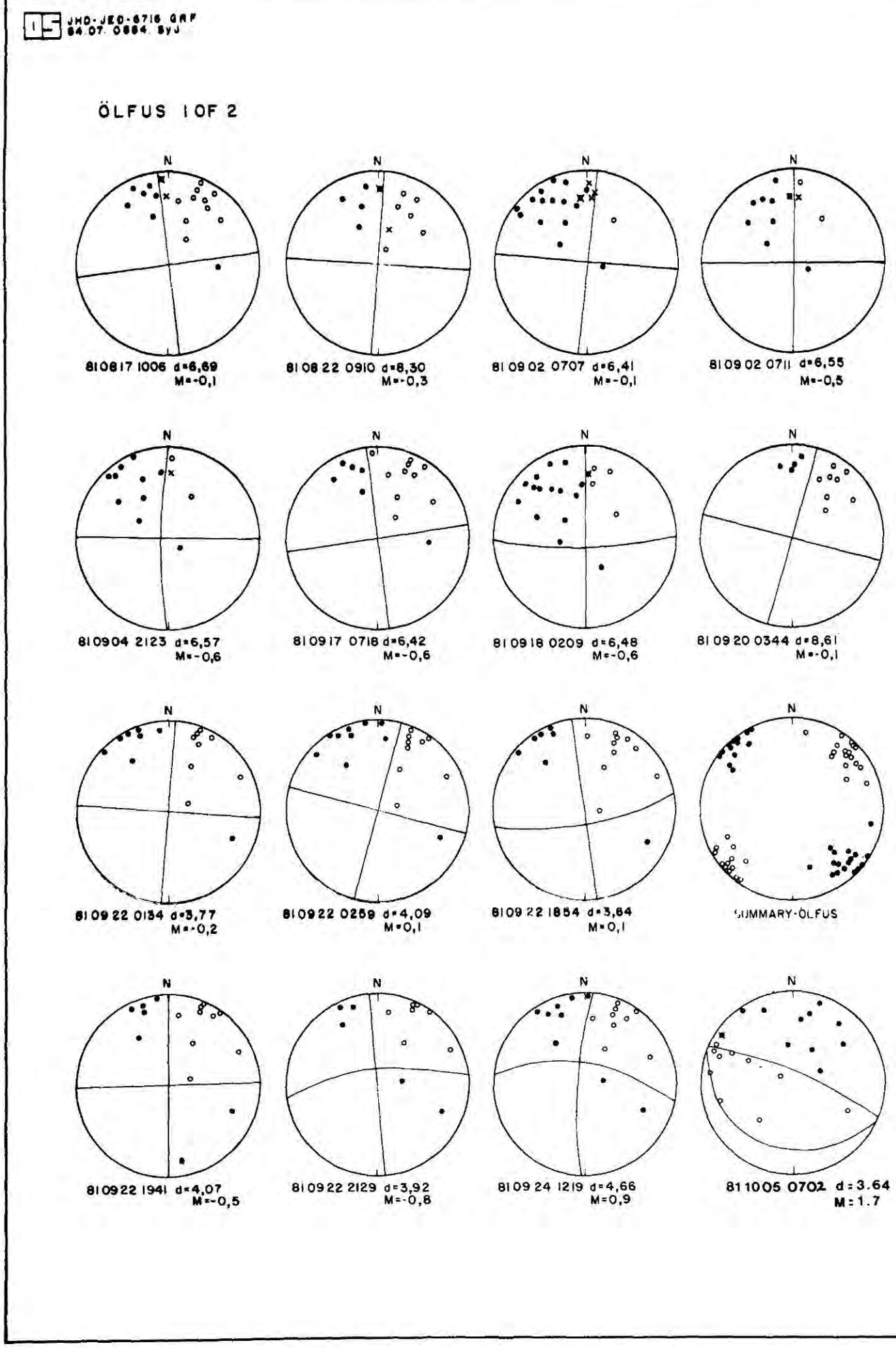

Fig. A7.13 Polarity plots of events from Olfus, 1 of 2.

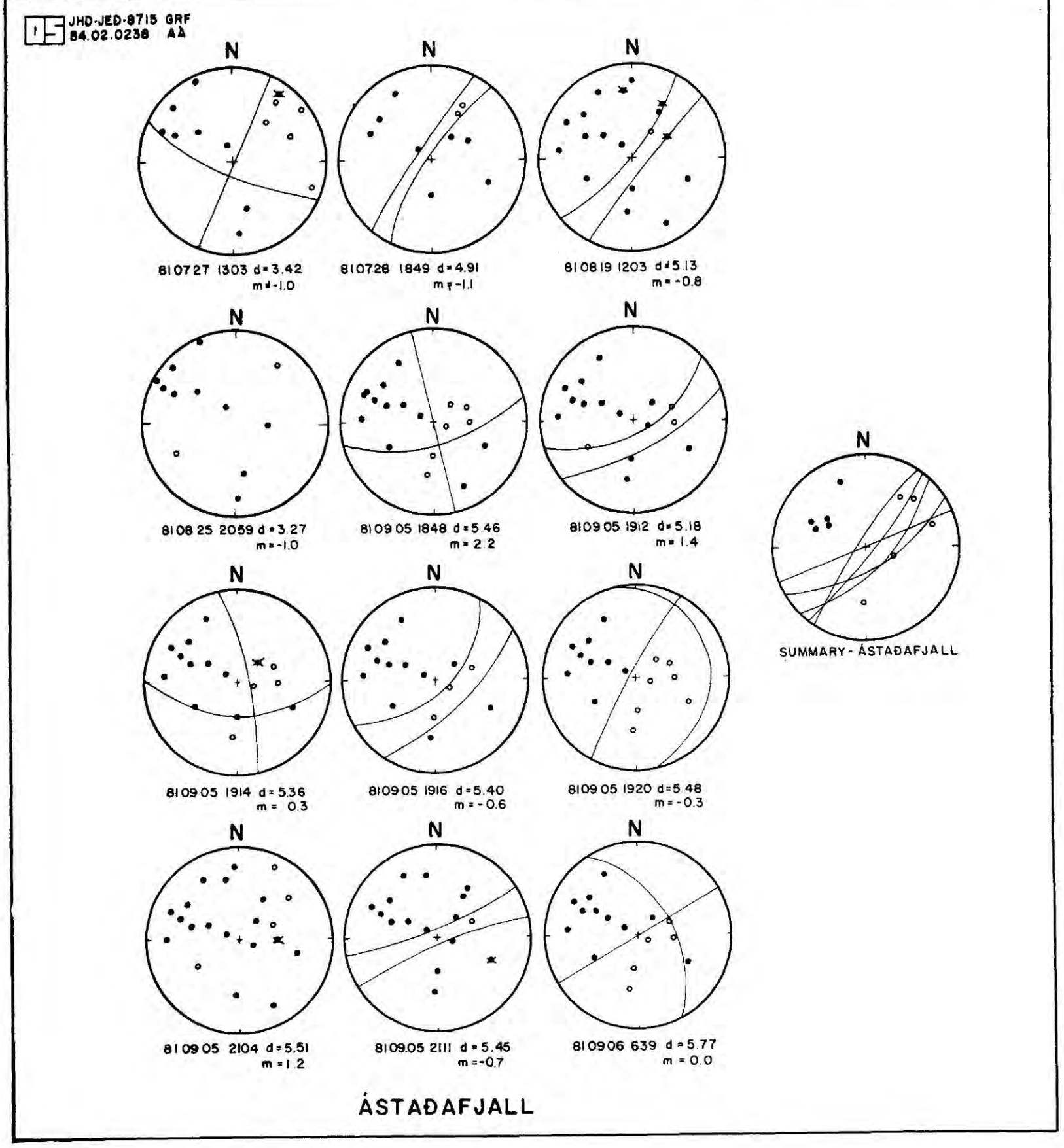

Fig. A7.14 Polarity plots of events from Astadafjall.

APPENDIX 8

POSSIBLE AVENUES OF FURTHER STUDY

As only 2 years were available to process the data collected during the 1981 radio telemetry monitoring project, and because the amount of data collected was far greater than anticipated, a number of possible lines of study were not pursued. These include:

a) Modelling of the teleseismic data by the "Aki inversion" procedure.

b) Modelling of the local and regional explosions by ray tracing or "Aki inversion".

c) Spectral analysis of the explosions, especially the fan shots.

d) Examination of the relative attenuation of P- and S-waves generated by regional earthquakes and recorded at various stations over the network.

e) Simultaneous inversion of local explosions and earthquakes to obtain a 3-dimensional velocity structure for the crust.

f) Inversion of P waveform data of the tensile crack type earthquakes of the geothermal field in order to calculate a best value for their seismic moment density tensors.

g) Mapping of variations in Poissons ratio over the area.

Reprinted from Nature, Vol. 310, No. 5972, pp. 43-45, 5 July 1984

Anomalous focal mechanisms: tensile crack formation on an accreting plate boundary

G. Foulger*† & R. E. Long†

* Science Institute, University of Iceland, Dunhaga 3, Reykjavik, Iceland
† Department of Geological Sciences, University of Durham, Science Laboratories, South Road, Durham DH1 3LE, UK

Conventional double-couple solutions do not satisfactorily account for many small magnitude earthquakes in the Hengill geothermal area in the Neovolcanic Zone of Iceland. The far-field radiation pattern is predominantly compressional but a few dilatational arrivals have been recorded. We prefer the interpretation that these events are due to tensile crack formation at a shallow (1–7 km) depth within a cooling intrusive body. Volume considerations indicate that initial fracturing of the rock is seismic but that subsequent widening proceeds aseismically. Other reports of anomalous radiation patterns from earthquakes on the Mid-Atlantic Ridge describe events of a similar type, that is, exhibiting predominantly compressional radiation patterns and a reduced dilatational field[1–4].

In 1981, an intensive 3-month seismic monitoring project was carried out in the Hengill geothermal area of Iceland (Fig. 1). The project was designed using foreknowledge of the spatial distribution of earthquake activity within the area and its ongoing nature[5]. The crustal structure is well constrained by refraction shooting[6,7] and shots fired within the area during the monitoring project confirmed that the crustal model used is accurate to within 5%. In total, 30 seismometers were operated within 14 km of the centre of the network.

About 140 well-constrained focal mechanism solutions were obtainable for small magnitude earthquakes occurring within the network. Conventional double-couple solutions with orthogonal nodal planes cannot be fitted to half of the events.

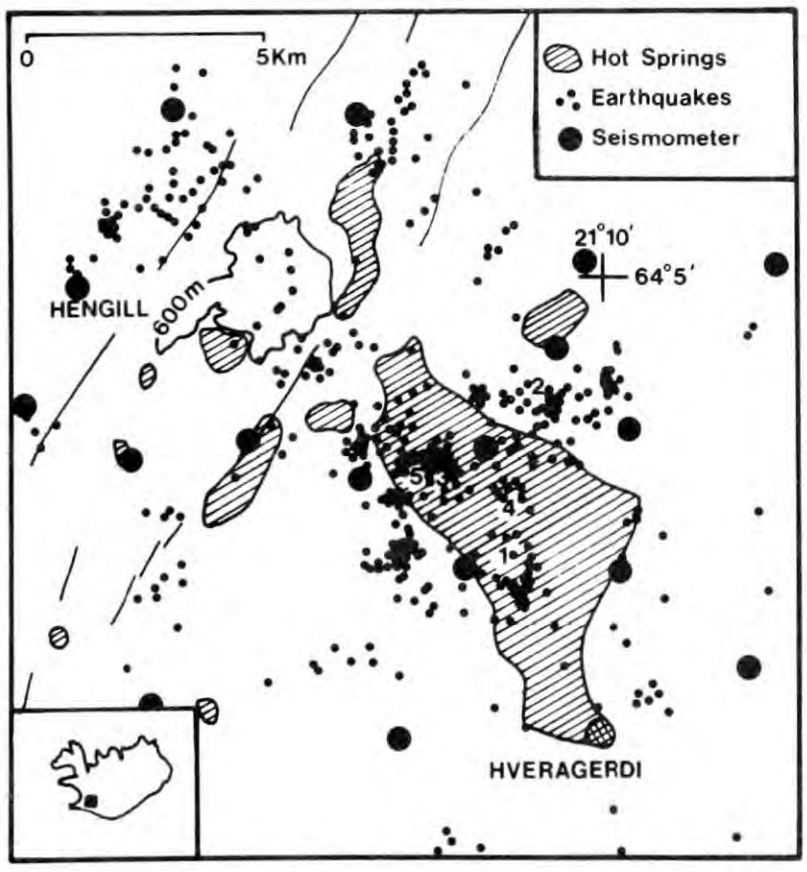

Fig. 1 Hengill central volcano and vicinity, the inset shows its location in Iceland. The map reveals seismic activity during the 3-month recording period, areas of hot springs and outline of fissure swarm transecting the area through Hengill. Of the 30 stations operated, 17 lie within the area shown. 1, 2, Locations of events shown in Fig. 2; 3, 4, 5, locations of events used for composite solution shown in Fig. 2.

Compressional arrivals dominate the focal sphere and dilatational arrivals of normal amplitude project onto the focal sphere in a narrow zone striking about north-east. Two examples and a composite solution are shown in Fig. 2. The dilatational and compressional portions of the focal sphere may be separated by small circles with typical radii of about 80°. Hence the ratio of the principal seismic moments of these events is approximately: $30:-1:-1$.

The predominant component of this mechanism is a linear vector dipole (LVD). The sum of the principal moments is significantly greater than zero, indicating a volume increase. In this respect, the source differs fundamentally from the CLVD source recognized by Julian[8].

We propose that this radiation pattern is generated by the formation of a tensile crack in the presence of a pore fluid, and that this type of fissure formation would be expected to occur in the tensile stress regime of an accreting plate boundary.

The Hengill area forms part of the continuation of the Mid Atlantic Ridge (MAR) onto the Icelandic landmass and has been volcanically active for ~700,000 yr (ref. 9). Originally the volcanic centre lay to the north of the village of Hveragerdi but later moved west and now underlies the central volcano Hengill (Fig. 1). The area is occupied by an extensive and complex geothermal field, which is hottest in the immediate vicinity of Hengill. However, most of the hot springs, and hence the greatest heat loss, occur in the vicinity of the original volcanic centre. A fissure swarm striking at N 25° E transects the area, passing through Hengill. The eruption fissures, and vertical, open fissures contained within it, testify to the tensional nature of the stress regime of the area. The direction of least compressive stress is orientated N 65° W, normal to the fissure swarm[10].

Earthquake activity is continuous. The activity rate is 1 magnitude (M_L)0 event per day. The hypocentres of most of the events cluster in a volume beneath the old volcanic site. Hypocentral depths are mostly within the range 1–7 km (Fig. 3). The pore fluid is thus hydrous at shallow depths but may be magmatic deeper down. In such a regime, the most likely cause of continuous seismicity is contraction cracks in the cooling roots of the extinct volcano.

As a result of continuous heat loss from the surface, the rock cools and contracts. This produces a local tensional stress field that is superimposed on the regional. The total stress field is additionally modified by geothermal processes (for example, boiling in the rock), that influence the pore pressure on a very small scale. Where these processes result in an increase in pore pressure thay may trigger fracture formation.

Failure in this predominantly tensile total stress field results in the formation of roughly vertical tensile cracks orientated about NE–SW.

The formation of a planar tensile crack in an isotropic medium would yield an all-compressive far-field radiation pattern of variable amplitude with respect to the orientation of the crack. The largest amplitude is normal to the crack, and the amplitude minimum traces a great circle on the focal sphere where the crack plane projects onto it. The point force equivalent of such a source may be represented by three mutually orthogonal vector linear dipoles with moments in the ratio: $(\lambda+2\mu):\lambda:\lambda$, where λ and μ are the Lamé elastic modulii[11]. The seismic moment tensor of the Hengill events can be modelled by combining a tensile crack with a spherically symmetrical implosion:

$$[(\lambda+2\mu):\lambda:\lambda]+[-(\lambda+\delta):-(\lambda+\delta):-(\lambda+\delta)]$$
$$=[(2\mu-\delta):-\delta:-\delta]$$

Fluid flow is a slow process compared with the speed at which a fracture forms so at the moment of fissuring, the volume occupied by the fluid in the immediate vicinity of a fracture increases and causes a local pore pressure drop[12]. This sudden pore pressure drop is omnidirectional and generates the dilatational portion of the radiation pattern.

Decreasing pore pressure limits crack propagation and hence probably limits the size of events. The formation of one fracture

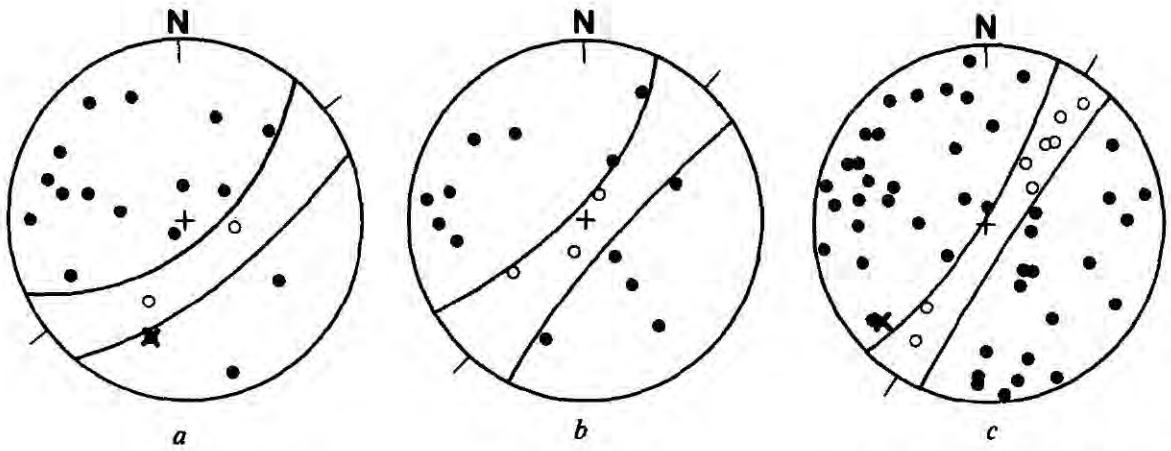

a b c

Fig. 2 P-wave first motions from two non-double couple events and one composite solution. Upper hemisphere plots in stereographic projection. ●, Compressions; ○, dilatations; ×, nodal arrivals; curved lines, small circles of radius θ defining nodal lines of tensile crack solution. *a*, Event 1: depth 4.87 km; $M_L = 0.1$; strike N 53° E; dip = 60°, θ = 78°. *b*, Event 2: depth = 4.99 km; $M_L = 0.0$; strike = N 42° E; dip = 80°; θ = 76°. *c*, Composite solution for three events; strike normalized; dip = 80°; θ = 80°

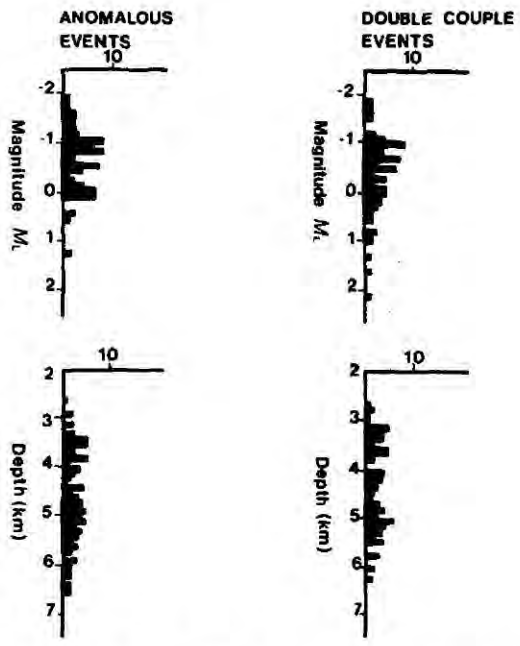

Fig. 3 Magnitudes and depths of events for which good focal mechanism solutions were possible.

causes local changes in the rock medium and stress field, and may trigger a chain reaction. This could explain the 'geothermal swarms' of numerous, very small events observed in many geothermal areas in Iceland.

It is, therefore, a pore pressure drop caused by restricted fluid flow at the moment of fissuring that generates the dilatational part of the radiation field and limits crack growth.

The natural heat loss of the Hengill area is 350 MW (ref. 13). If attributed to a cooling intrusion, the rate of volume contraction may be calculated using the equation:

$$\Delta V = \frac{H\gamma}{C_p \rho}$$

where ΔV is the contraction rate, H is the cooling rate, γ is the coefficient of thermal expansion ($\simeq 16.2 \times 10^{-6}\ K^{-1}$), ρ is the density ($\simeq 3 \times 10^3\ kg\ m^{-3}$) and C_p is the specific heat of basalt at constant pressure ($\simeq 1.3 \times 10^3\ J\ kg^{-1}\ K^{-1}$). Application of this equation to the Hengill area gives a contraction rate of: $\Delta V = 4.5 \times 10^4\ m^3\ yr^{-1}$. An estimate of the total volume of contraction cracks formed seismically may be made and compared with this value. The equations[14,15].

$$\log M_0 = 15.1 + 1.7 M_L$$

$$\log E = 11.8 + 1.5 M_L$$

give estimates of seismic moment and energy release from local magnitudes (M_L). The ratio of principal seismic moments observed for the Hengill events indicates that δ is small. Therefore, they are predominantly linear vector dipole sources and seismic moment may be approximately related to volume by the equation: $M_0 = 2\mu V$, where V is the volume of the crack. Using these equations, the contraction rate within the seismically active volume is estimated to be two orders of magnitude smaller than that calculated for the cooling intrusion. A similar result is obtained if energy is considered.

These calculations demonstrate that the seismicity may be attributed entirely to a cooling volume and that it is likely that much aseismic widening occurs after the initial fracturing.

There have been other reports of anomalous radiation patterns from the MAR and its continuation onto the Icelandic landmass[1–4]. For these events, dilatational arrivals occupy less than half of the focal sphere. Interpreted in terms of source mechanism this also requires a net explosive component. In the case of large, teleseismically recorded events, where lower hemisphere polarity plots are made, explanations for the observed anomalous radiation patterns may readily be found by invoking interference, or path effects where the events are shallow and in areas of active volcanism, where severe crustal inhomogeneity is to be expected[16,17]. However, in the Hengill case we are dealing with shallow earthquakes, upper hemisphere plots and a well constrained crustal structure. Many of the events exhibit extreme non-dipolarity and occur interspersed with double-couple sources. Here it is less easy to explain away the anomalous events as the result of a path effect.

We conclude that the Hengill source mechanism data indicate that at this point on the accreting plate boundary stress is being released by tensile crack formation. These data strongly suggest that such sources can occur in nature in a tensile stress environment. Thus, more credence should be given to the theory that the anomalous radiation patterns reported for MAR earthquakes are due to source effects, particularly an enhanced explosive element leading to volume increase at source, as a result of the crustal accretion process.

Shear source mechanism solutions are commonly fitted to data that are not sufficient to constrain such a solution. The present results suggest that the custom of routinely fitting double-couple solutions to inadequate data should be viewed more critically.

We acknowledge the loan of geostore equipment by the NERC, UK. Financial support was provided by the National Energy Authority, Iceland, and the Municipal Heating Authority, Reykjavik, Iceland. We thank Professor M. H. P. Bott, Dr P. Einarsson and Dr S. McNutt for helpful suggestions.

Received 16 January; accepted 9 May 1984.

1. Sykes, L. R. *J. geophys. Res.* **72**, 2131–2153 (1967).
2. Sykes, L. R. *Bull. Seismol. Soc. Am.* **60**, 1749–1752 (1970).
3. Klein, F. W., Einarsson, P. & Wyss, M. *J. geophys. Res.* **82**, 865–888 (1977).
4. Einarsson, P. *Tectonophysics* **55**, 127–153 (1979).
5. Foulger, G. & Einarsson, P. *J. Geophys.* **47**, 171–175 (1980).
6. Palmason, G. *Crustal Structure of Iceland from Explosion Seismology* (Societas Scientiarum Islandica Publ. 40, 1971).
7. RRISP Working Group *J. Geophys.* **47**, 228–238 (1980).
8. Julian, B. R. *Nature* **303**, 323–325 (1983).
9. Bjornsson, A., Tomasson, J. & Saemundsson, K. *Hengilssvaedid, stada jardhitarannsokna vorid 1974* Orkustofnun Rep. OSJHD 7415 (1974).
10. Haimson, B. C. & Voight, B. *Pageophysics* **115**, 153–190 (1977).
11. Aki, Keiiti & Richards, P. G. *Quantitative Seismology* (Freeman, San Francisco, 1980).
12. Robson, G. R., Barr, K. G. & Luna, L. C. *Nature* **218**, 28–32 (1968).
13. Bodvarsson, G. *J. Engnr Ass. Iceland* **36**, 1–48 (1951).
14. Wyss, M. & Brune, J. N. *J. geophys. Res.* **73**, 4681–4694 (1968).
15. Spottiswoode, S. M. & McGarr, A. *Bull. seismol. Soc. Am.* **65**, 93–112 (1975).
16. Solomon, S. C. & Julian, B. R. *Geophys. J.R. astr. Soc.* **38**, 265–285 (1974).
17. Trehu, A. M., Nabelek, J. L. & Solomon, S. C. *J. geophys. Res.* **86**, 1701–1724 (1981).

Printed in Great Britain by Macmillan Production Ltd., Basingstoke, Hampshire

Geothermics, Vol. 11, No. 4, pp. 259 – 268, 1982.
Printed in Great Britain.

0375 – 6505/82/040259 – 10 $03.00/0
Pergamon Press Ltd.

GEOTHERMAL EXPLORATION AND RESERVOIR MONITORING USING EARTHQUAKES AND THE PASSIVE SEISMIC METHOD

G. FOULGER

Science Institute, University of Iceland, Dunhagi 3, Reykjavík, Iceland

(*Received* 1 *December* 1981; *accepted for publication* 27 *May* 1982)

Abstract—This paper reviews the use of earthquake studies in the field of geothermal exploration. Local, regional and teleseismic events can all provide useful information about a geothermal area on various scales. It is imperative that data collection is conducted in properly designed, realistic experiments. Ground noise is still of limited usefulness as a prospecting tool. The utility of the method cannot yet be assessed because of its undeveloped methodology and the paucity of case histories.

INTRODUCTION

Volcanism, tectonic activity and seismicity often occur side by side. This, in turn, results in the commonly observed association of geothermal areas and seismicity. That the seismicity of a geothermal area is often different from that of the surrounding region was first established in Iceland (Ward *et al.*, 1969; Ward and Björnsson, 1971), and its potential as a prospecting tool quickly pointed out (Ward, 1972).

In the intervening years substantial advances have been made in the development of a methodology. In common with all other geophysical exploratory disciplines, the passive seismic method has both advantages and disadvantages. It can supply information that is unobtainable otherwise, and is most useful when results are reviewed in the light of information obtained by other exploratory methods. The fact that the method has received relatively little attention as a prospecting tool has doubtless much to do with the unconstrained and poorly understood nature of the energy source, which, in the case of local earthquakes, is, in part, a measure of our lack of understanding of geothermal areas. However, interest has increased with the greater keenness in exploiting geothermal resources, and at present ideas and theories are rather more numerous than case histories.

This paper aims at presenting a brief review of the main results obtained by application of the passive seismic method to the field of geothermal prospecting, together with illustrative case histories. A minimum of reference will be made to the voluminous speculation which appears in the literature.

SEISMICITY OF GEOTHERMAL AREAS

Many geothermal areas exhibit a higher background seismicity than their surrounding regions (e.g. Ward *et al.*, 1969; Ward and Björnsson, 1971; Marks *et al.*, 1978; Conant, 1972) whereas others have a similar seismicity to the regional (e.g. Evison *et al.*, 1976; Majer, 1978; Hunt and Latter, 1979) or even define a seismic gap (e.g. Steeples and Pitt, 1976; McEvilly *et al.*, 1978b).

Certain aspects of the seismicity of some seismically active geothermal areas have been related to the regional. For example, the South Iceland zone of destructive historic earthquakes extends into the Hengill geothermal area (Björnsson and Einarsson, 1974). Focal mechanism solutions of earthquakes in The Geysers area, California, are consistent with the regional Coastal Range

tectonics (Bolt *et al.*, 1968). Majer and McEvilly (1979) concluded that in The Geysers area the direction of failure is controlled by regional stress, whilst the rate of failure is controlled by local stress levels.

It may be concluded, therefore, that in many cases the location of a geothermal area coincides with an area where regional stress is being released at a different rate to the surrounding areas. The differences in the seismicity of different geothermal areas may hence reflect differences in the regional tectonics of the areas in question.

For example, the Krafla geothermal area lies within the Northern Volcanic Zone of Iceland, (Björnsson *et al.*, 1977; Björnsson *et al.*, 1979) whereas the Hengill geothermal area lies at a triple junction where the Reykjanes Peninsula, the Western Volcanic Zone and the South Iceland Seismic Zone meet (Foulger and Einarsson, 1980). There is evidence that the Hengill area has displayed fairly continuous seismicity, with events up to magnitude 6, over the last half century, whereas no such seismicity is recorded from the Krafla area (Tryggvason, 1973; Tryggvason, 1978a; 1978b; Tryggvason, 1979). The two areas hence lie in contrasting regional tectonic settings, and display contrasting seismicity patterns. It may be that the ongoing seismicity of the Hengill area is intimately related to the proximity of the South Iceland zone of destructive historic earthquakes.

Variations in the seismicity within a large geothermal area may correspondingly reflect variations in tectonics within the area. For example, Smith *et al.* (1974) interpreted spatial and temporal variations in seismicity in the Yellowstone geothermal area in terms of contrasting crustal structure inside and outside the caldera.

LOCAL EARTHQUAKES

Spatial distribution

The spatial epicentral distribution of local earthquakes and its relation to surface features has provided insight into the geographical distribution of high temperature areas. The positions of high temperature areas on the Reykjanes Peninsula have been correlated with the points where fissure swarms cross the trace of the plate boundary as defined by earthquake epicenters (Klein *et al.*, 1977).

Marks *et al.* (1978) correlated the spatial distribution of microearthquakes in The Geysers area with two pressure sinks in the steam field. A well-defined westward dipping seismic gap between them was interpreted as an unfractured, impermeable barrier separating the two discrete sinks. Denlinger and Bufe (1980) likened the spatial distribution of The Geysers earthquakes to a two-stemmed mushroom occupying the zone of pore pressure decline, fluid withdrawal and negative reservoir dilation.

Microearthquakes located in the Ahuachapan geothermal area were found to define a plane of activity extending down to 6.5 km depth (Fig. 1). The interpretation that this plane of activity defines a fault that allows hot water to circulate to the surface was supported by evidence from borehole data and surface tectonics (Ward and Jacob, 1971).

Combs and Hadley (1977) likewise inferred the presence of a fault passing through the East Mesa geothermal area, California, on the basis of microearthquake locations.

Variations in the pressure and temperature conditions in the crust can also cause variations in seismicity. Laboratory experiments have demonstrated that a mechanism known as "stick-slip", where motion occurs as a series of discrete, rapid slips, occurs most readily at high pressures and low temperatures. This implies that the maximum depth at which earthquakes occur may be temperature dependent, and thereby of possible use as a geothermometer (Brace and Byerlee, 1966; Brace and Byerlee, 1970). Majer (1978) found that depths of microearthquakes beneath Grass Valley, Nevada, were within the range 0 – 8 km, contrasting

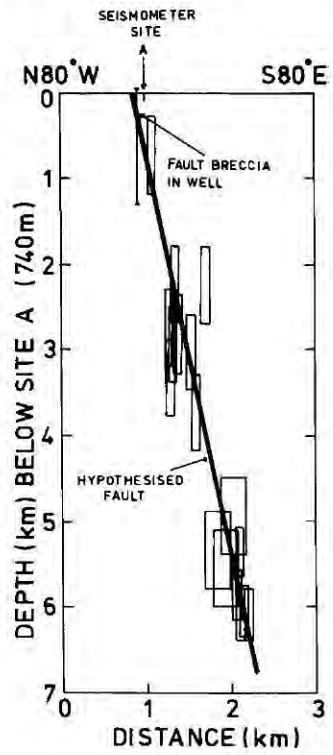

Fig. 1. Earthquake hypocenters projected on a vertical plane striking S80°E through the Ahuachapan geothermal area, 70 km WNW of San Salvador, El Salvador. Rectangles denote approximate precision in location. (Adapted from Ward and Jacob, 1971.)

with the typical 10 – 15 km for the region. This was thought to suggest a broad, shallow high temperature regime. Majer and McEvilly (1979) noted that the maximum depth of earthquakes beneath The Geysers area is 5 km as compared to 11 – 12 km for the surrounding region, and interpreted this as indicating elevated temperatures at 4 – 5 km depth. They also noted that earthquake activity tended to occur at the edges of, and not within, the production zone itself. This was interpreted as indicating relatively high pore pressure gradients at the edges of the field, and low pressure and high temperatures within it. The random distribution of events and lack of event migration was considered to indicate the intensely fractured state of the area and the lack of throughgoing faults.

Walter and Weaver (1980), in a study of the Coso Range, California, found no anomalous hypocentral depth distribution beneath the Coso geothermal field, which they concluded to indicate the absence of liquidus temperatures at shallow depths.

Chronological distribution

Microearthquakes from The Geysers production zones display a relatively high *b* value., i.e. an unusually high preponderance of small magnitude shocks (Marks *et al.*, 1978; Majer and McEvilly, 1979). This implies that the reservoir rocks are in a low stress state. Spectral analysis confirms this. The high *b* value also indicates that the microearthquake activity probably results from crack closing and sliding rather than the propagation of new fractures. It could also be an indication of structural heterogeneity and induced seismicity.

Cavit and Hadley (1980) considered the lack of temporal clustering in events in The Geysers area to indicate that the geothermal wells affected normal seismicity.

Walter and Weaver (1980) found a relatively high *b* value at shallow depths beneath the Coso geothermal area. This was interpreted as indicating short average fault lengths, and less likelihood of a large earthquake occurring within this volume of rock than outside it.

Estimates of Poisson's ratio

Poisson's ratio may be estimated by examining the relative travel times of compressional and shear waves from different microearthquakes to individual stations. Laboratory experiments indicate that dry rocks display a lower Poisson's ratio than wet ones. Somerton (1978) made laboratory measurements of Poisson's ratio in both dry and water-saturated sandstones from the Cerro Prieto (Mexico) geothermal field and obtained values of 0.1 for the dry and 0.3 for the wet samples. Majer and McEvilly (1979) obtained values for Poisson's ratio for The Geysers, by the passive seismic method, and obtained values of 0.15 – 0.2 inside the production zone, and higher values outside it. The low value obtained was thought to reflect steam domination of the reservoir rocks. Low values were also obtained for the Coso Hot Springs area (Combs and Rotstein, 1975) and interpreted as indicating vapour domination.

Studies of water-dominated fields, however, have yielded higher values, typically 0.4, e.g. the East Mesa (California) field (McEvilly *et al.,* 1978b), and the Cerro Prieto (Mexico) field (Majer and McEvilly, 1978a). Estimates of Poisson's ratio, obtained by the passive seismic method, are hence demonstratively useful in indicating degree of water saturation within the reservoir.

Source properties

Studies of the spectra of compressional and shear waves of microearthquakes from The Geysers also yielded exclusive information, especially when supplemented with data obtained from explosion seismology, using the same recording network. An estimate of the volume decrease attributable to seismic failure in the area was found to be much less than that which would be attributable to fluid withdrawal (Majer and McEvilly, 1979). In the absence of aseismic crustal adjustment, the difference must be taken up by re-injection and reservoir recharge.

Evidence of uniform source dimensions (50 m) for these microearthquakes was also obtained, compatible with low pressure and constant permeability and porosity.

Many focal mechanism studies have been done which give information about the strike and dip of active faults, and the direction of movement over the fault plane (e.g. Klein *et al.,* 1973; Majer and McEvilly, 1979).

Seismic attenuation

Information about Q (the quality factor, or the inverse of the attenuation) was also obtained for The Geysers by combining explosion seismological data and data from spectral analyses of microearthquakes. Estimates of Q for both compressional and shear waves were obtained. Variations in Q may be interpreted in terms of variations in the degree of water saturation, pressure, temperature, the presence of gas, partial melting and degree of compositional heterogeneity.

For The Geysers it was found that Q was high at shallow depths within the production zone, and low below it. This is interpreted as a reflection of the low pressure and the low degree of water saturation within the production zone, and higher pressure and degree of saturation below it (Majer and McEvilly, 1979; Kjartansson and Nur, 1981).

At the Cerro Prieto field, spectral analysis of a regional earthquake indicated significant variations in attenuation within the production zone, thought to be associated with subsurface faulting, alteration by precipitation and variations in sediment thickness (Majer and McEvilly, 1978).

At Grass Valley, Nevada, Majer (1978) detected clear high frequency attenuation of both earthquake and explosion generated seismic waves passing through the immediate area of the

hot springs. This was attributed to effects within the upper 1 km of the crust beneath the springs.

At Sierra La Primavera, Mexico, McEvilly *et al.* (1978a) observed substantial differences in the attenuation of body waves of regional events, which they attibuted to the effects of the upper few kilometers of crust, possibly a shallow zone of partially molten material.

In Long Valley Caldera (California), Hill (1976) detected clear high frequency attenuation of explosion generated seismic waves passing at shallow depths beneath a region of hydrothermal alteration and hot spring activity. This could be caused by crustal heterogeneity, or indicate that the system reaches near boiling pressure at the depths penetrated by the seismic energy (Kjartansson and Nur, 1981). Unusually high attenuation of explosion generated seismic waves has also been reported from geothermal areas at Wairakei (Modriniak and Studt, 1959), Broadlands (Hochstein and Hunt, 1970) and Kawerau (Studt, 1958), New Zealand; Matsukawa, Japan (Hayakawa, 1970); and Coso Hot Springs, California (Combs and Jarzabeck, 1977).

Monitoring operations

Earthquakes provide one of the few means for continuous monitoring of the whole field, both before and after production has commenced. With the latter aim in mind, it is very important to commence data collection prior to exploitation so that seismicity during exploitation can be compared to pre-exploitation data.

There are many examples of changes in surface geothermal activity consequent to earthquakes. For example, changes in the eruptive cycle of Old Faithful Geyser, and also effects on hot springs in Yellowstone have been correlated to seismic activity (Rinehart, 1969; Rinehart and Murphy, 1969; Marler, 1964). Dramatic changes in the Geysir area in Haukadalur, Iceland, have been noted on several occasions, accompanying large destructive earthquakes in southern Iceland (Einarsson, 1964).

Significant changes in surface thermal activity have also accompanied earthquake swarms, e.g. in Reykjanes, Iceland (Ward *et al.,* 1969; Tryggvason, 1970) and the Krafla area, Iceland (Björnsson *et al.,* 1977, 1979; Einarsson and Brandsdóttir, 1980). Periodic variations in the discharge and temperature of thermal water in the Kagai hot spring area, Japan, has been correlated to changes in seismic rate within the Matsushiro sequence (Kasuga, 1967).

Data from The Geysers area, California, suggest that microearthquake activity has increased by a factor of 10 in the past 7 years. This has been attributed to accelerated fluid withdrawal and re-injection (Marks *et al.,* 1978; Majer and McEvilly, 1979; Denlinger and Bufe, 1980). The apparent increase in the frequency of large events may also be attributable to the re-injection process. Majer and McEvilly (1979) considered the microearthquakes to indicate regions of expansion of the vapour-dominated zone, and the level of activity to be a measure of the degree of departure from a state of equilibrium. Migration of the active zones may thus indicate migration of the boundaries of the vapour-dominated zone.

REGIONAL EARTHQUAKES

Both regional and local events have been used in several instances to define areas of anomalous shear wave attenuation, interpreted as magma chambers in the crust and upper mantle. Some notable examples are studies done in the Katamai volcanic range, Alaska (Kubota and Berg, 1967; Matumoto, 1971); the Sulphur Springs geothermal region, St. Lucia, West Indies (Aspinall *et al.,* 1976); at Socorro, New Mexico (Sanford *et al.,* 1977a,b); and Krafla, Iceland (Einarsson, 1978).

Spectral analysis of seismic waves of regional earthquakes indicated anomalous *P*-wave attenuation in the East Mesa, California, area, and was presented as evidence for a magma chamber (Combs and Jarzabeck, 1978).

TELESEISMS

Teleseismic techniques can be used to obtain precise information from much greater depths than most conventional geophysical methods. A technique which has been used in geothermal exploration with good results involves accumulating records of distant earthquakes on a relatively dense network of stations over the area under investigation. Delays in the relative arrival times of the *P*-waves are then assessed for each station. The data can be used to estimate the size and position of low velocity bodies in the crust and upper mantle. Assuming that such delays are attributable to hot or partially molten rock, rough estimates of the total heat anomaly may be made.

In the Yellowstone region, delays of up to 2 s were recorded on a dense network, and attributed to a zone of partial melting extending to a depth of 200 – 250 km, with a higher proportion of melt at shallow depths. The *P*-wave velocity within this body was estimated to be about 10% lower than that of the surrounding rocks. This would imply average temperatures of the order of 1000°C within the body (Iyer, 1979; Steeples and Iyer, 1976).

Delays of up to 0.3 s were detected at the Long Valley geothermal area. Analysis of these data revealed that the anomalous body is probably shallower than 25 km, with a velocity contrast in the range 5 – 15%. Steeples and Iyer (1976) found that a spherical body 14 km in diameter with its upper surface at 6 km depth was consistent with these and gravity observations (Fig. 2). The order of magnitude of the teleseismic delays indicated that temperatures within the body are such that some degree of partial melt must be present. The fact that teleseismic shear

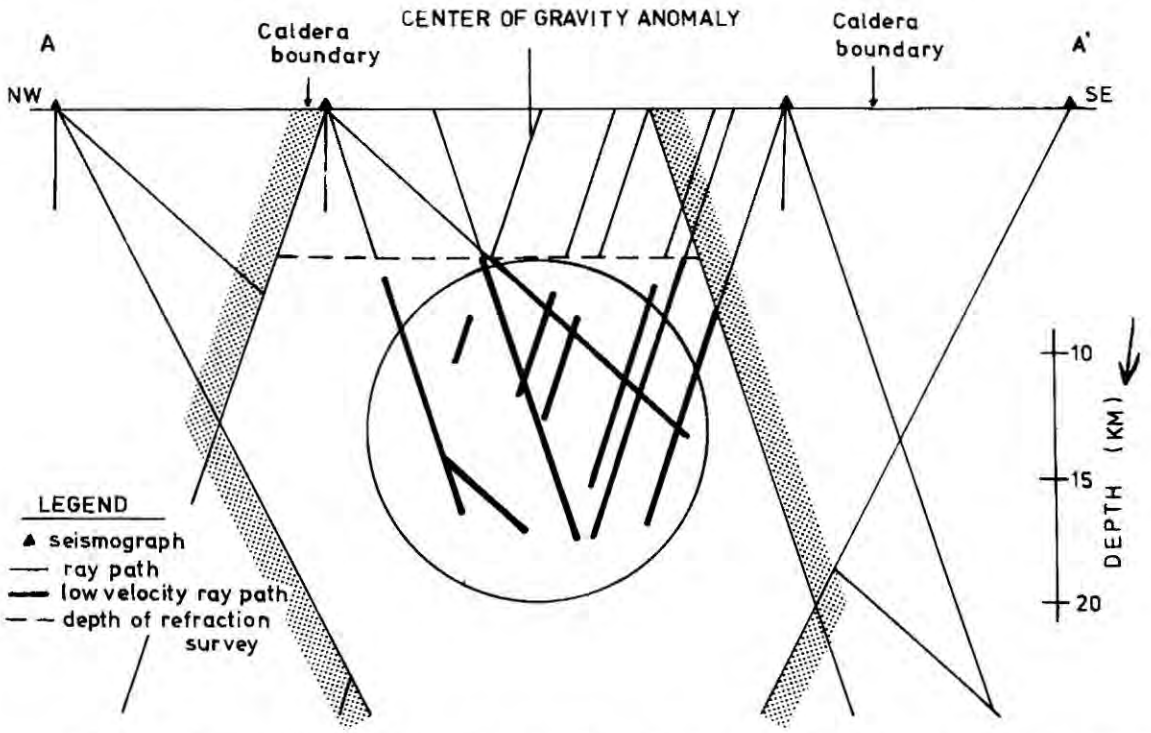

Fig. 2. Sectional view of Long Valley Caldera. Stations within 1 km of section line have been projected on to the section. Model represents velocity contrast of 15% along heavy ray paths. Heavy lines on ray paths are proportional in length to delays detected along respective ray paths. Velocities outside the stippled zone are normal (6.0 km/s) and the effects of the upper 6 km of material (depth penetrated by refraction survey) have been removed. The circle is a sectional view of a sphere 14 km in diameter. A density contrast of 0.18 g/cm³ would produce a 10 mGal gravity anomaly at the surface directly above the center of the sphere. (Adapted from Steeples and Iyer, 1975.)

waves were transmitted indicated, however, that either the molten portion of the body must exist in pockets less than 4 km in diameter (the approximate wavelength of the shear waves), or the body must have sufficient viscosity to transmit shear energy. *S*-waves from local earthquakes were found not to penetrate deep enough to sample the anomalous body.

P-wave delays of more than 1 s have been observed in The Geysers – Clear Lake area. Iyer *et al.* (1979) postulated the existence of a magma chamber with a core of severely molten rock beneath Mt. Hannah, to the NE of The Geysers area, and partially molten rock underlying The Geysers field itself. Both zones extend down to a depth of 20 km or more.

Young and Ward (1978) analysed *P*-waves from over 60 teleseismic events recorded over the Coso Hot Springs, California, and modelled two-dimensional variations in attenuation. In a later study the model was extended to three dimensions (Young and Ward, 1980). Their method involves dividing the rock volume of interest into cells, and calculating the attenuation of each of these. Based on these data a model for the Coso Hot Springs KGRA is proposed with high attenuation at near surface (0 – 5 km), due to 'lossy' lithology or partial fluid saturation; an intermediate fractured zone (5 – 12 km), through which heat is transferred by fluid movement; and a deep zone (12 – 20 km), containing intrusives or magma. A two-dimensional model has also been calculated for The Geysers – Clear Lake field, which indicates a high attenuation zone in a position corresponding to gravity anomalies and *P*-wave travel time residuals (Ward and Young, 1980).

GROUND NOISE

For completeness, some mention of ground noise should be made. The method commonly consists of sampling the ambient ground noise over the surface of the geothermal area with a dense station network. Two main lines of approach are followed.

Firstly, the theory has been proposed that hydrothermal processes within reservoirs (e.g. a phase change) radiate seismic energy. To test this hypothesis noise levels are contoured on the surface in order to delineate noise sources.

Secondly, consideration is taken of the type of elastic wave propagating, and processing then aimed at inverting the propagation characteristics to obtain information about the distribution of medium properties (e.g. seismic velocity and attenuation), and the location of sources.

High levels of ground noise have been detected at many sites in the vicinity of hot springs and geysers, and some evidence presented for the existence of radiating sources at shallow depths. For example, at Grass Valley, Nevada (Liaw and McEvilly, 1979); Long Valley, California (Iyer and Hitchcock, 1976); and Yellowstone National Park (Iyer and Hitchcock, 1974). At Wairakei and Waiotapu, New Zealand, depths of less than 200 m were attributed to noise sources beneath sites of surface activity (Whiteford, 1975). There is also some evidence that geothermal areas with no visible surface expression may not be noise emitters, e.g. East Mesa, California (Iyer and Hitchcock, 1975) and Kurobe, Japan (Ehara and Yuhara, 1978). As yet, no deep subsurface emitter has been located.

Formidable difficulties are associated with the application of this method to geothermal prospecting. The greatest of these are high levels of cultural and meteorological noise interference, laterally variable and unassessable ground amplification (due to variable geology), and poorly constrained crustal models. The lack of station correlation prohibits the location of sources, and powerful surface sources such as hot springs mask weaker seismic waves from buried emitters, so amplitude mapping will only yield information about shallow sources. In order to demonstrate the existence of body waves radiated by deep emitters within geothermal systems, large station arrays and sophisticated processing methods would be necessary.

Analysis of ground noise remains, as yet, a tool of very limited applicability in geothermal prospecting.

FURTHER DEVELOPMENTS

The main points emerging from a review of the use of the passive seismic method as a prospecting tool at present is that there is a paucity of case histories, and no well-developed systematic methodology for the delineation of anomalous portions of the crust, with the possible exception of the treatment of teleseisms. Indeed, results may be contradictory, or ambiguous in the light of parallels drawn with laboratory experiments, or at best difficult to interpret. On the positive side, however, seismic monitoring is cheap, has yielded valuable information about reservoirs in many cases, and can be used to 'see' much deeper than conventional geophysical methods.

When exploration of a prospect commences there is a strong case for conducting a preliminary monitoring experiment using a small number of stations, over as long a period as possible, in order reliably to assess the level, and temporal nature, of local and regional activity. Only then can a more sophisticated experiment be designed on a realistic basis. In areas which have a high seismicity prior to exploitation there is an especially strong case for commencing monitoring early, particularly if injection wells are likely to be used.

To the author's knowledge, The Geysers is the only exploited geothermal area where continuous seismic monitoring and spectral analysis was, and is, being done with a view to modelling the reservoir.

Many questions remain to be answered before the potential utility of the method can be fully assessed, and many more case histories with intensive studies are necessary. The possibility of developing methods to map attenuating areas should be investigated. Spectral analysis, and the calculation of source characteristics could provide an answer to whether the phenomenon of a 'geothermal' earthquake exists. Changes in the rate of seismicity due to production activities should be evaluated, and efforts made to find discriminants between natural and induced earthquakes. Finally, more laboratory work needs to be done to enable the results of seismic studies to be interpreted with a minimum of ambiguity, in terms of reservoir characteristics.

Acknowledgements—My grateful thanks are extended to the following people for reading the manuscript and making many valuable suggestions for its improvement: Sveinbjörn Björnsson, Axel Björnsson, Páll Einarsson, Gudmundur Pálmason and Ernie Majer.

REFERENCES

Aspinall, W. P., Michael, M. O. and Tomblin, J. (1976) Evidence for fluid bodies beneath the Sulphur Springs geothermal region, St. Lucia, West Indies. *Geophys. Res. Lett.* **3**, 87.

Björnsson, S. and Einarsson, P. (1974) Seismicity of Iceland. In *Geodynamics of Iceland and the North Atlantic Area* (Edited by Kristjánsson, L., D.) pp. 225–239. Reidel, Dordrecht, Holland.

Björnsson, A., Johnsen, G., Sigurdsson, S., Thorbergsson, G. and Tryggvason, E. (1979) Rifting of the plate boundary in North Iceland. *J. geophys. Res.* **84**, 3029–3038.

Björnsson, A., Saemundsson, K., Einarsson, P., Tryggvason, E. and Grönvold, K. (1977) Current rifting episode in North Iceland. *Nature, Lond.* **266**, 318–323.

Bolt, B. A., Lomnitz, C. and McEvilly, T.V. (1968) Seismological evidence on the tectonics of central and northern California and the Mendocino escarpment. *Bull. seism. Soc. Am.* **58**, 1725–1767.

Brace, W. F. and Byerlee, J. D. (1966) Stick-slip as a mechanism for earthquakes. *Science* **153**, 990–992.

Brace, W. F. and Byerlee, J. D. (1970) California earthquakes: why only shallow focus? *Science* **168**, 1573–1575.

Cavit, D. S. and Hadley, D. M. (1980) Geothermal earthquakes: temporal and spatial characteristics. *EOS* **61**, 1051.

Combs, J. and Hadley, D. (1977) Microearthquake investigation of the Mesa geothermal anomaly, Imperial Valley, California. *Geophysics* **42**, 17–33.

Combs, J. and Jarzabeck, D. (1977) Preliminary seismic wave attenuation and Poisson's ratio studies at the Coso geothermal area, California: The Coso Geothermal Project. Technical Report, No. 5, Center for Energy Studies, U.T. at Dallas, Richardson, Texas.

Combs, J. and Jarzabeck, D. (1978) Seismic wave attenuation anomalies in the East Mesa geothermal field, Imperial Valley, California: preliminary results. *Geoth. Res. Council, Trans.* **2**, 109–112.

Combs, J. and Rotstein, Y. (1975) Microearthquake studies at the Coso geothermal area, China Lake, California. *Proc. Second U.N. Symp. Develop. Use Geoth. Res., San Francisco, U.S.A.* Library of Congress Catalog Card No. 75-32682, pp. 909 – 916.

Contant, D. A. (1972) A microearthquake survey of geothermal areas in Iceland, 1970. *Earthq. Notes* **43**, 19 – 32.

Denlinger, R. P. and Bufe, C. A. (1980) Seismicity induced by steam production at The Geysers steam field in Northern California. *EOS* **61**, 1051.

Ehara, S. and Yuhara, K. (1978) Seismic noise measurements of some geothermal areas in Japan. *Geotherm. Res. Council, Trans.* **2**, 171 – 172.

Einarsson, P. (1978) *S*-wave shadows in the Krafla caldera in NE-Iceland, evidence for a magma chamber in the crust. *Bull. volcan.* **43**, 1 – 9.

Einarsson, P. and Brandsdóttir, B. (1980) Seismological evidence for lateral magma intrusion during the July 1978 deflation of the Krafla volcano in NE-Iceland. *J. Geophys.* **47**, 160 – 165.

Einarsson, T. (1964) *Geysir í Haukadal. (The Great Geysir in Haukadalur).* The Geysir Committee, Reykjavík, Iceland.

Evison, F. F., Robinson, R. and Arabasz, W. J. (1976) Microearthquakes, geothermal activity and structure, Central North Island, New Zealand. *N.Z. Jl. Geol. Geophys.* **19**, 625 – 637.

Foulger, G. and Einarsson, P. (1980) Recent earthquakes in the Hengill-Hellisheidi area in SW-Iceland. *J. Geophys.* **47**, 171 – 175.

Hayakawa, M. (1970) The study of underground structure and geophysical state in geothermal areas by seismic exploration. *Geothermics Special Issue* 2, 347 – 357.

Hill, D. P. (1976) Structure of Long Valley Caldera, California, from a seismic refraction experiment. *J. geophys. Res.* **81**, 745 – 753.

Hochstein, M. P. and Hunt, T. M. (1970) Seismic, gravity and magnetic studies, Broadlands geothermal field, New Zealand. *Geothermics Special Issue* 2, 333 – 346.

Hunt, T. and Latter, J. H. (1979) Seismic activity near Wairakei geothermal field. *Proc. N.Z. Geotherm. Workshop 1979,* Part 1, 14 – 19.

Iyer, H. M. (1975) Short note: search for geothermal seismic noise in the East Mesa area, Imperial Valley, California. *Geophysics* **40**, 1066 – 1072.

Iyer, H. M. (1979) Deep structure under Yellowstone National Park, U.S.A.: a continental 'hot spot'. *Tectonophysics* **56**, 165 – 197.

Iyer, H. M. and Hitchcock, T. (1974) Seismic noise measurements in Yellowstone National Park. *Geophysics* **39**, 389 – 400.

Iyer, H. M. and Hitchcock, T. (1975) Seismic noise as a geothermal exploration tool: techniques and results. *Proc. 2nd U.N. Symp. Develop. Use Geotherm. Res., San Francisco, U.S.A.* Library of Congress Catalog Card No. 75-32682, pp. 1075 – 1083.

Iyer, H. M. and Hitchcock, T. (1976) Seismic noise survey in Long Valley, California. *J. geophys. Res.* **81**, 821 – 840.

Iyer, H. M., Oppenheimer, D. H. and Hitchcock, T. (1979) Abnormal *P*-wave delays in The Geysers – Clear Lake geothermal area, California. *Science* **204**, 495 – 497.

Kasuga, I. (1967) Aspect on the relation of thermal water and Matsushiro earthquakes in Kagai hotspring area, Nagano prefecture. *J. Geol. (Tokyo)* **76**, 16 – 26.

Kjartansson, E. and Nur, A. (1981) Attenuation due to thermal relaxation in porous rocks. *Geophysics,* in press.

Klein, F. W., Einarsson, P. and Wyss, M. (1973) Microearthquakes on the Mid-Atlantic plate boundary on the Reykjanes Peninsula in Iceland. *J. geophys. Res.* **78**, 5084 – 5099.

Klein, F. W., Einarsson, P. and Wyss, M. (1977) The Reykjanes Peninsula, Iceland, earthquake swarm of September 1972 and its tectonic significance. *J. geophys. Res.* **82**, 865 – 888.

Kubota, S. and Berg, E. (1967) Evidence for magma in the Katmai volcanic range. *Bull. volcan.* **31**, 175 – 214.

Liaw, A. L. and McEvilly, T. V. (1978) Microseisms in geothermal exploration—studies in Grass Valley, Nevada. *Geophysics* **44**, 1097 – 1115.

Lofgren, B. (1978) Monitoring crustal deformation in The Geysers geothermal area, California. U.S.G.S. Open-file Report 78-597, 19 pp.

McEvilly, T. V., Mahood, G. A., Majer, E. L., Schechter, B. and Truesdell, A. H. (1978a) Seismological/geological field study of the Sierra La Primavera geothermal system. Preliminary Report, Department of Geology and Geophysics, Berkeley, California, 13 pp.

McEvilly, T. V., Schechter, B. and Majer, E. L. (1978b) East Mesa seismic study. Annual Report, Earth Sciences Division, Lawrence Berkeley Laboratory, University of California, pp. 26 – 28.

Majer, E. L. (1978) Seismological investigations in geothermal regions. Ph.D. thesis, University of California, Berkeley.

Majer, E. L. and McEvilly, T. V. (1978) Seismological studies at Cerro Prieto. Annual Report, Earth Sciences Division, Lawrence Berkeley Laboratory, University of California, pp. 29 – 33.

Majer, E. L. and McEvilly, T. V. (1979) Seismological investigations at The Geysers geothermal field. *Geophysics* **44**, 246 – 269.

Marks, S. M., Ludwin, R. S., Louie, K. B. and Bufe, C. G. (1978) Seismic monitoring at The Geysers geothermal field, California. U.S.G.S. Open-file report 78-798.

Marler, G. D. (1964) Effects of the Hebgen Lake earthquake of August 17, 1959, on the hot springs of the Firehole Geyser Basin, Yellowstone National Park. U.S.G.S. Professional Paper 435, pp. 185 – 197.

Matumoto, T. (1971) Seismic body waves observed in the vicinity of Mount Katmai, Alaska, and evidence for the existence of molten chambers. *Geol. Soc. Am. Bull.* **82**, 2905 – 2920.

Modriniak, N. and Studt, F. E. (1959) Geological structure and volcanism of the Taup-Tarawera district. *N.Z. Jl. Geol. Geophys.* **2**, 654.

Rinehart, J. S. (1969) Old Faithful performance, 1890 through 1966. *Bull. volcan.* **33**, 153 – 163.

Rinehart, J. S. and Murphy, A. (1969) Observations of pre- and post-earthquake performance of Old Faithful Geyser. *J. geophys. Res.* **74**, 574 – 575.

Sanford, A. R., Mott, R. P., Shuleski, P. J., Rinehart, E. J., Caravella, F. J., Ward, R. M. and Wallace, T. C. (1977a) Geophysical evidence for a magma body in the crust in the vicinity of Socorro, New Mexico. *Am. Geophys. Union Monog.* **20**, 385 – 403.

Sanford, A. R., Rinehart, E. J., Shuleski, P. J. and Johnston, J. A. (1977b) Evidence from microearthquake studies for small magma bodies in the upper crust of the Rio Grande Rift near Socorro, New Mexico. *Trans. Am. Geophys. Union* **58**, 1188 (Abstr.).

Smith, R. B., Shuey, R. T., Freidline, R. O., Otis, R. M. and Alley, L. B. (1974) Yellowstone hotspot: new magnetic and seismic evidence. *Geology* **2**, 451 – 455.

Somerton, W. (1978) Some physical properties of Cerro Prieto cores. *Proc. First Symp. Cerro Prieto Geothermal Field, Baja California, Mexico.* Berkeley, Lawrence Berkeley Laboratory, LBL-7098.

Steeples, D. W. and Iyer, H. M. (1975) Teleseismic *P*-wave delays in geothermal exploration. *Proc. Second U.N. Symp. Develop. Use Geotherm. Res., San Francisco, U.S.A.* Library of Congress Catalog Card No. 75-32682, pp. 1199 – 1205.

Steeples, D. W. and Iyer, H. M. (1976) Low velocity zone under Long Valley as determined from teleseismic events. *J. geophys. Res.* **81**, 849 – 860.

Steeples, D. W. and Pitt, A. M. (1976) Microearthquakes in and near Long Valley, California. *J. geophys. Res.* **81**, 849 – 860.

Studt, F. E. (1958) Geophysical reconnaissance at Kawerau, New Zealand. *N.Z. Jl. Geol. Geophys.* **1**, 219 – 246.

Tryggvason, E. (1970) Surface deformation and fault displacement associated with an earthquake swarm in Iceland. *J. geophys. Res.*, **75**, 4407 – 4422.

Tryggvason, E. (1973) Seismicity, earthquake swarms and plate boundaries in the Iceland region. *Bull. seismol. Soc. Am.* **63**, 1327 – 1348.

Tryggvason, E. (1978a) Jarðskjálftar á Íslandi 1930 – 1939. (The seismicity of Iceland 1930 – 1939.) Science Institute, Reykjavík, Report RH-78-21, 92 pp.

Tryggvason, E. (1978b) Jarðskjálftar á Íslandi 1940 – 1949. (The seismicity of Iceland 1940 – 1949.) Science Institute, Reykjavík, Report RH-78-22, 51 pp.

Tryggvason, E. (1979) Jarðskjálftar á Íslandi 1950 – 1959. (The seismicity of Iceland 1950 – 1959.) Science Institute, Reykjavík, Report RH-79-06, 90 pp.

Walter, A. W. and Weaver, C. S. (1980) Seismicity of the Coso Range, California. *J. geophys. Res.* **85**, 2441 – 2458.

Ward, P. L. (1972) Microearthquakes: prospecting tool and possible hazard in the development of geothermal resources. *Geothermics* **1**, 3 – 12.

Ward, P. L. and Björnsson, S. (1971) Microearthquakes, swarms and the geothermal areas of Iceland. *J. geophys. Res.* **76**, 3953 – 3982.

Ward, P. L. and Jacob, K. H. (1971) Microearthquakes in the Ahuachapan geothermal field, El Salvador, Central America. *Science* **173**, 328 – 330.

Ward, P. L., Pálmason, G. and Drake, C. L. (1969) Microearthquakes and the Mid-Atlantic Ridge in Iceland. *J. geophys. Res.* **74**, 665 – 684.

Ward, R. W. and Young, C-Y (1980) Mapping seismic attenuation within geothermal systems using teleseisms with application to The Geysers – Clear Lake region. *J. geophys. Res.* **85**, 5227 – 5236.

Whiteford, P. C. (1975) Studies of the propagation and source location of geothermal seismic noise. *Proc. Second U.N. Symp. Develop. Use Geotherm. Res., San Francisco, U.S.A.* Library of Congress Catalog Card No. 75-32682, pp. 1263 – 1271.

Young, C-Y. and Ward, R. W. (1978) 2-*D* inversion of seismic attenuation observations in Coso Hot Springs, KGRA. *Geotherm. Res. Council, Trans.* **2**, 743 – 746.

Young, C-Y. and Ward, R. W. (1980) Three-dimensional Q^{-1} model of the Coso Hot Springs known geothermal resource. *J. geophys. Res.* **85**, 2459 – 2470.